UNIVERSITY OF
TECHNOLOGY SYDNEY

Bio-driven control system for the rehabilitation hand device: a new approach

By
Khairul Anam

Submitted in fulfilment of the requirement for the degree of Doctor of Philosophy

Supervisor: Assoc. Prof. Adel Al-Jumaily

School of Electrical, Mechanical and Mechatronic Systems
Faculty of Engineering and Information Technology
University of Technology, Sydney (UTS)

January 2016

Certificate of Original Authorship

I, Khairul Anam, certify that the work in this thesis has not previously been submitted for a degree nor has it been submitted as part of requirements for a degree except as fully acknowledged within the text.

I also certify that the thesis has been written by me. Any help that I have received in my research work and the preparation of the thesis itself has been acknowledged.

In addition, I certify that all information sources and literature used are indicated in the thesis.

Signature of Student:

Date: 8 January 2016

This page is intentionally left blank

Acknowledgment

First and foremost, my sincere thanks to God, Allah Al-Mighty, who endowed me to complete my PhD study.

I would like to express my deep gratitude to my principal supervisor, **Associate Professor Dr. Adel Al-Jumaily** for all his support, help, guidance, understanding, discussions, ideas, patience, and chances given to me to work with him during my PhD study.

I would also like to thank **Dr. Rami Khushaba** and **Dr. Ali H Al-Timemy** who generously supported me with the EMG datasets and valuable discussions.

I would like to extend further my genuine appreciations to **Dr. Ananda Modan Sanagavarapu** and **Dr. Steve Ling** for giving me the chance of working as a casual academic at UTS.

I wish to acknowledge the PhD scholarship provided by the Directorate General of Higher Education (DGHE), the Republic of Indonesia that has supported my study for four years.

I am sincerely grateful to the Vice Chancellor's Postgraduate Research Student Conference Funding and the Faculty of Engineering and Information Technology (FEIT) travel funding committees for their generous financial support for my conference trips.

I would also like to express my deep thanks to the Centre for Islamic Dakwah and Education (CIDE) committee who invited me to be an imam of Al-Hijrah Mosque during my stay in Sydney and gave me a wonderful trip to the Holy cities, Mecca and Medina, to perform the Islamic pilgrimage/Hajj.

I am very keen to express my appreciation to Tanvir Anwar, Dr. Yashar Maali, Dr. Muhammad Khalid, Dr. Yee Mon Aung, Sahar, Gadeh, Marwah, Dr. Van Linh Nguyen, Dr. Delwar, Dr. Nuryani, Sonki Prasetya, Dessi Wanda, Muhammad Anshar, Dwi Linna Suswardany, and all the people that I could not mention, for help, support and kindly relationship during my PhD life.

Table of Contents

List of Figures

List of Tables

This page is intentionally left blank

List of Abbreviations

AR	:	Autoregressive
AW-ELM	:	Adaptive wavelet extreme learning machine
ELM	:	Extreme learning machine
EMG	:	Electromyography
FFNN	:	Feed forward neural network
FFT	:	Fast Fourier transform
kNN	:	k nearest neighbourhood
LDA	:	Linear discriminant analysis
Lin-ELM	:	Linear extreme Learning Machine
MES	:	Myoelectric signal
ML	:	Multilayer perceptron
M-PR	:	Myoelectric pattern recognition
OFNDA	:	Orthogonal fuzzy neighbourhood discriminant analysis
OS-ELM	:	Online sequential extreme learning machine
OS-ELM-R	:	Online sequential extreme learning machine with rejection
PCA	:	Principal component analysis
Poly-ELM	:	Polynomial extreme learning machine
RBF-ELM	:	Radial basis function extreme learning machine
RBF-ELM-R	:	Radial basis function extreme learning machine with rejection
SLin-ELM	:	Swarm linear extreme learning machine
SPoly-ELM	:	Swarm polynomial extreme learning machine
SRBF-ELM	:	Swarm radial basis function extreme learning machine
SRDA	:	Spectral regression discriminant analysis
SR-ELM	:	Spectral regression extreme learning machine
SVM	:	Support vector machine
SW-RBF-ELM	:	Swarm wavelet radial basis function extreme learning machine
TD	:	Time domain
W-ELM	:	Wavelet extreme learning machine
LIBSVM	:	Library support vector machine

MAV	:	Mean absolute value
MAVS	:	Mean absolute value slope
ZC	:	Zero crossing
SSC	:	Slope sign changes
WL	:	Waveform length
RMS	:	Root mean square
MNF	:	Mean frequency features
MDF	:	Median frequency

Abstract

The myoelectric pattern recognition (M-PR) for hand rehabilitation devices has shown its efficacy in the laboratory environment. However, the performance of the M-PR in the clinical application is very poor. There is a big gap between the success of the laboratory experiment and the clinical application. The researchers found that the major cause of the gap was the robustness of the M-PR. Many aspects influence the robustness of the M-PR including the limb position, skin humidity, muscle fatigue, improvement in the muscle function, electrode shifts, and other clinical reasons. The aim of this thesis is to introduce novel M-PRs dealing with the robustness issues in real-time implementation. The goal was accomplished through the following actions.

1. Developing a new M-PR that can work well on the amputees and non-amputees. The proposed M-PR consists of time-domain and autoregressive features (TD-AR), spectral regression discriminant analysis (SRDA) as a feature reducer, and radial basis function extreme learning (RBF-ELM) as a classifier. The experimental results showed that the proposed system was able to detect the user's intention with accuracy of roughly 99% on the able-bodied subjects and around 98% on the trans-radial amputees using six EMG channels.

2. Introducing new classifiers. The first classifier is adaptive wavelet extreme machine learning (AW-ELM). AW-ELM is the node-based ELM that can adapt to the changes that occur in the input. In general, AW-ELM could classify ten finger movements from two EMG channels with a good accuracy of 94.84 %. The second classifier is swarm radial basis extreme learning machine (SRBF-ELM). SRBF-ELM is a hybridization of particle swarm optimization (PSO) and the kernel-based ELM. The role of PSO is to optimize the kernel parameters. The last classifier is swarm wavelet extreme learning machine (SW-RBF-ELM). The role of the wavelet is to avoid PSO being trapped in local optima. The experiments have been done on the healthy subjects and amputees for both, SRBF-ELM and SW-RBF-ELM. On the healthy subjects, the accuracy of SW-RBF-ELM is 95.62 % while SRBF-ELM is 95.53 %. On the amputees, the SW-RBF-ELM achieved the average accuracy of 94.27 %, while SRBF-ELM produced the average accuracy of 92.55 %.

3. Developing a new feature projection and feature reduction called spectral regression extreme learning (SR-ELM). SR-ELM can enhance the class separability of the features to improve the classification performance. The experimental results showed that SR-ELM can work well on different classifiers and various numbers of classes with an average accuracy ranging from 95.67 % to 86.73 %

4. Developing a robust M-PR by involving the transient state of EMG signal along with the steady state of it in the real-time experiment. The classification accuracy is 90.46 % and 89.19 % on the offline and online classification, respectively.

5. Introducing a new myoelectric controller for the exoskeleton hand. The myoelectric controller consists of two main parts: the myoelectric pattern recognition (M-PR) and myoelectric non-pattern recognition (M-non-PR). In the system, RBF-ELM-R (radial basis extreme learning machine with a rejection mechanism) represents the M-PR, and the proportional controller represents the M-non-PR. The power actuated to the linear motors is proportional to the amplitude of the EMG signals. The experimental results showed that, in the offline experiment of 10 classes, the accuracy is around 90 % and 92 % for RBF-ELM and RBF-ELM-R, respectively. In the online experiment, the accuracy is about 89.22 % and 89.73 % for RBF-ELM and RBF-ELM-R, respectively.

6. Introducing an adaptive mechanism to the M-PR to adapt to changes in the characteristic of the electromyography (EMG) signal. The thesis proposes a new M-PR with online sequential extreme learning machine (OS-ELM) and OS-ELM with rejection (OS-ELM-R). The experimental results showed that the accuracy is around 89 % and 91 % for OS-ELM and OS-ELM-R on the first-day experiment.

CHAPTER 1
Introduction

Bio-signal control systems based on surface electromyography (EMG) signal for the hand rehabilitation such as a hand prosthetic and exoskeleton hand have shown success in the laboratory environment. However, the acceptance rate of the rehabilitation device on the clinical application is very low. The gap between two sides, laboratory and real-time environment should be removed or at least reduced to some extent. The research in this thesis will address this issue. As an introduction, this chapter will begin with the background of this doctoral research. The next two sections will discuss the problem statements and the objectives of the research. The contributions and the organisation of this thesis will be presented afterward. The last section will provide some publications produced during the doctoral study.

1.1   Background

Many countries in the world have a significant number of people with a disability. The result of the Survey of Disability, Ageing and Carers (SDAC) in 2009 showed that four million people in Australia (18.5%) have a disability (Ewing, 2010). In the USA, 18.4 % or 54.4 million people are in some of level disability, and 12 % are in a severe disability (Brault, 2008). The same situation happens in Britain. Over 10 million disabled people live in Britain (Farmer & Macleod, 2011). All of them are human being, and they have the same right as others to participate in a normal life. Therefore, many efforts have been made to provide many facilities to accommodate the disabled person needs in public areas. Globally, The world health organisation (WHO) encouraged its members to consider this issue seriously and made a report to evaluate how seriously these members are addressing this problem (WHO, 2001). Those actions raise hopes for a bright future for disabled people around the globe.

The World Health Organisation (WHO) defines disability as "a great number of different functional limitations occurring in any population in any country of the world. People may be disabled by physical, intellectual or sensory impairment, medical conditions or mental illness. Such impairments, conditions or illnesses may be permanent or transitory in nature"(WHO, 2001). Based on SDAC, disability is defined as any limitation, restriction or impairment, which restricts everyday activities and has lasted or is likely to last for at least six months. This definition was set for SDAC purpose only. In the result of SDAC, the incidence of disability was classified into two groups, a disability caused by mental or behavioural disorders and by physical conditions. Over fifteen per cent of Australians had physical disabilities and the rest, about 3.4 % of them have mental disabilities (Ewing, 2010). Therefore, the physical disabilities have received more attention to be solved because they are in the majority. However, both of these types of disabilities need a different kind of therapy. The type of therapies will depend on the sort of disability and the conditions causing them.

For recovering the ability of movement, rehabilitation is the best way to improve the condition of most clients. World Health Organization defines the term "rehabilitation "as a process aimed at enabling persons with disabilities to reach and maintain their optimal physical, sensory, intellectual, psychiatric and/or social functional levels, thus providing them with the tools to change their lives towards a higher level of independence. Rehabilitation may include measures to provide and/or restore functions, or compensate for the loss or absence of a function or a functional limitation. It includes a wide range of measures and activities from more basic and general rehabilitation to goal-oriented activities, for instance, vocational rehabilitation. The rehabilitation process does not, however, involve initial medical care (WHO, 2001). In other words, rehabilitation aims to return the patient's physical, sensory, intellectual and mental capabilities that were lost because of injury, illness, and disease, and to help the patient to compensate for weakness that cannot be treated medically (Akdoğan & Adli, 2011).

A hand disability is one of the most frequent disability problems that occur in the community. The hand disability can be caused by either amputation or motor function problem. The development of the perfect technology for hand rehabilitation is a challenging task. Various cutting-edge technologies have been developed to deal with the hand rehabilitation. For hand amputees, Touch Bionics Limited has introduced a revolutionary prosthetic hand named i-limb (TouchBionics, 2007). The i-limb looks like

a natural hand, and it is designed in such a way that it conforms around the shape of the object being grasped. The i-limb prosthetic hand has five fingers so that it can perform a large number of finger configurations. Another example of a bionic hand that is available in the market is a bebionic hand (TouchBionics, Accessed in 2015) by RSLSteeper (E. Scheme & Englehart, 2011). Thus, the hardware robotic hands that mimic the hand in the shape and functionality are available. These sophisticated prosthetic hands need a sophisticated control system that can be applied in the real-time application. In addition, the control system should work in agreement with a human's desire to enhance the convenience of the wearer.

In addition to the prosthetic hand, a rehabilitation device for recovering motor function has been developed recently. An example of the commercial rehabilitation devices is Hand of Hope from Rehab-robotics company (Hu *et al.*, 2013). The Hand of Hope is an exoskeleton hand robot designed to help people after stroke and train their impaired hand function. Interestingly, this device is able to detect the user's intention from the user's muscle using electromyography (EMG) signal. Hu *et al.* (2013) shows the efficacy of EMG as a control source of the robot. However, the device can detect the user's intention for opening and closing hand only. In reality, the motor function in the hand involves many movements encompassing individual and combined finger movements.

Dealing with user's intention using myoelectric signal is a challenging task, yet it gives many benefits. One of the major benefits is to create a smooth interaction between the human and the rehabilitation device. This interaction will enable the device as a natural extension of the human body. This mechanism can be done by capturing the message caught by muscles from the human brain and then conveying it to drive the device after processing with an appropriate method.

EMG that records myoelectric signals from muscle activity has been widely used to detect the user's intension beforehand (Roche *et al.*, 2014). The EMG electrodes are located in the human's limb either in an invasive or non-invasive way. The majority of people do not like to plant electrodes inside the body. Most people prefer to use surface EMG (sEMG) instead. However, the sEMG has several drawbacks such as the crosstalk problem from other muscles and the robustness issue. In addition, it is difficult to obtain a myoelectric signal from deeper muscles. As a result, myoelectric signal processing using sEMG is not easy to deal with.

Another issue emerges dealing with muscles driving the finger movements. The extrinsic muscles that move the flexion, extension, abduction and adduction of digits are mostly not located in superficial layer, but in the middle (flexor digitorum superficialis muscle) and deep layer (flexor digitorum profundus muscle). Therefore, surface EMG will not provide the precise signal from the intended muscles. Fortunately, extension muscle is located in the superficial layer (extensor digitorium). Another problem exists due to the skeletal muscles of a human's body. For instance, one muscle is responsible for moving all fingers either individually or in combination. Of course, this fact increases the difficulty of myoelectric control for hand or more specifically, finger rehabilitation.

EMG signal for user's intention detection can be implemented in two ways: non-pattern recognition based and pattern recognition based. EMG-based non-pattern recognition (EMG-based non-PR) or myoelectric non-pattern recognition (M-non-PR) has been used widely in current exoskeleton hand to drive a movement or to take no action, based on the level of EMG signals. This control system can work on a maximum of two movements only, which are mostly hand opening and hand closing. In fact, the finger should be able to move in many motions, not only two motions.

On the other hand, EMG-based pattern recognition (EMG-based PR) or myoelectric pattern recognition (M-PR) can deal with many limb movements. M-PR has been implemented in the finger motion recognitions for decades, and it shows the benefits over EMG-based non-pattern recognition. Uchida *et al.* (1992) extracted fast Fourier transform (FFT) features from two electromyography (EMG) channels. Using feed-forward neural networks (FF-NN), they were able to classify five-finger movements with the accuracy of 86%. The classical problems of the FF-NN, which needs a heuristic architecture process and takes much time, were the main shortcomings of this recognition system. Similar to Uchida *et al.*, Tsenov *et al.* (2006) developed a recognition system of finger movement using multilayer perceptron (MLP). MLP classified four finger movements using time-domain (TD) features extraction and achieved the accuracy of 93% using 2 EMG channels and 98% using four EMG channels.

Instead of MLP, Cipriani *et al.* (2011) utilized k-nearest neighbour (kNN) as a classifier. The M-PR extracted features from 9 EMG channels using TD features acquired from five able-bodied and amputee subjects. The recognition system was implemented online and was able to classify seven finger movements with the accuracy of around 79

% on the amputee subjects and about 89% on the non-amputee subjects. The controller delay time was fast, approximately 50 ms, yet the accuracy was poor.

Besides MLP/FF-NNs and kNN, the support vector machine (SVM), which is powerful and used extensively in many areas (R. N Khushaba *et al.*, 2012; Oskoei & Huosheng, 2008), was also employed. R. N Khushaba *et al.* (2012) utilized the SVM to classify ten finger movements consisting of individual and combined movements. The M-PR extracted features using TD and autoregressive (AR) features from 2 EMG channels and then reduced the features dimension using linear discriminant analysis (LDA). Their system succeeded in obtaining accuracy of approximately 92% in the offline classification and about 90% in the online classification. In terms of accuracy, Khushaba *et al.*'s recognition system was promising, but the system contains a natural shortcoming of SVM in dealing with the multi-classification problem. In general, at least, the recognition system should use m SVMs to deal with m movement classes. Inevitably, this will add to the processing time of the system.

The most recent study of a pattern-recognition system on finger movement classification was undertaken by Al-Timemy *et al.* (2013). The developed system extracted features from six EMG channels using TD, and AR features. Before being fed to the classifier, the features were reduced using orthogonal fuzzy neighbourhood discriminant analysis (OFNDA) (R. N. Khushaba *et al.*, 2010). Finally, linear discriminant analysis (LDA) was used to classify 12 and 15 movement classes on six amputees and ten able-bodied subjects, respectively. The system succeeded in achieving an average accuracy of around 98% on the able-bodied subjects and approximately 90% on the amputee subjects. However, there was a significant gap in the performance between the able-bodied and amputee subjects.

Until now, the success of M-PR for finger motion recognition is very promising and exciting. However, there is a big gap between the success of the laboratory environment and the clinical application. Farina *et al.* (2014) found that the major cause of the gap is related to the robustness of M-PR in the clinical applications. The performance of M-PR degrades when it works in the clinical applications.

Ning *et al.* (2012) gave reasons that have hampered the clinical application of M-PR. They found that the existing M-PRs worked on limited limb movements. M-PR should provide a simultaneous and proportional controller that can handle the multi degrees of freedoms. The second reason for the failure of M-PR in the clinical application is the M-

PRs do not have sensory feedback. Therefore, the user could not feel the real existence of the device. Another factor is the inability of M-PR to adapt to the changes of EMG signal characteristic. EMG signals can change easily due to many factors such as electrode shift, the humidity of the skin, the improvement in the muscle function and other clinical factors. The last, the existing M-PRs do not integrate with sensor modalities, so M-PR could not work on the complex actions.

1.2   Problem statement

Myoelectric controller or EMG-based controllers have been implemented in the hand rehabilitation devices either in the prosthetic or exoskeleton hand for decades. Myoelectric controller in a prosthetic hand is usually implemented using myoelectric pattern recognition (M-PR). The implementation of M-PR for the hand rehabilitation device is related to finger motion recognition. Tenore *et al.* (2009) found that the performance of M-PR on amputee and non-amputee is not significantly different for individual finger recognition. However, Al-Timemy *et al.* (2013) showed that there was a significant gap of M-PR on amputee and non-amputee when M-PR classified individual and combined finger movements together. This fact raises questions in relation to a way to reduce the performance gap of M-PR on the amputee and non-amputee in classifying complex finger movements.

The users prefer to utilize a small number of channels. However, this will decrease the performance of M-PR as proven by Al-Timemy *et al.* (2013). To compensate the accuracy degradation, the enhancement in the recognition performance should be made. L.J. Hargrove *et al.* (2007) found that the recognition performance depends on the classifiers and the features. The problems exist in relation to ways to improve the performance of the classifiers and enhance the feature representation for the myoelectric pattern recognition using two EMG channels.

Few researchers developed a myoelectric pattern recognition (M-PR) using two channels. R. N Khushaba *et al.* (2012) are an example. They classified ten finger movements using two EMG channels in both offline and online experiment with the accuracy of about 92 % and 89 % on the offline and online classification, respectively. Unfortunately, their M-PR neglected the transient state of EMG signals. In addition, the real-time experiment was tested on one subject only. Therefore, the robustness of the M-PR in the real-time experiment is questioned. Thus, another issue arises about improving

the performance of M-PR for complex finger movements using two EMG channels in the real-time application.

Myoelectric pattern recognition frequently attains very good performance in the laboratory experiment. However, the performance degrades sharply when it is applied to the real-time application. One of the reasons is because the system is trained with limited number of movements 10 or 15 finger movements, for instance. In reality, a human's finger can do an unlimited number of movements. The majority of current M-PRs for finger recognitions could not handle this problem. Thus, other problems emerge in relation to the method to anticipate and ignore the movements that are not included in the training stage.

The performance of myoelectric pattern recognition (M-PR) decreases due to changes in EMG signal. For instance, 2-cm electrode shift can downgrade the performance of the M-PR up to 25 – 30 % (Young *et al.*, 2012). Furthermore, different environment of experiment may change the characteristic of EMG signals. For example, the experiment done today will have different setups with the experiment the day after or maybe a couple of days after it. This fact raises issues about the M-PR that can adapt to changes in EMG signals.

The majority of exoskeleton hands employ EMG signals for actuating simple movement such as opening hand and closing hand. Wege and Zimmermann (2007) developed a blind source separation to decompose the individual finger motions from 10 EMG channels. The goal was to increase the number of movements that could be handled by the myoelectric controller. However, the report indicates that they have not succeeded yet in doing so. Thus, a problem appears in relation to improving the number of movements that the exoskeleton hand can perform and its efficacy in the real time application.

1.3 Objectives

Considering problems associated with the myoelectric controller in the hand rehabilitation device, the main purpose of this research is to introduce novel myoelectric controllers for a hand rehabilitation device that can deal with issues appearing in the real-time application.

The main purpose of this research is supported by specific research objectives, which are:

1. Develop an accurate myoelectric pattern recognition (M-PR) system that can work well in amputee and non-amputee subjects.

2. Develop novel classifiers for acquiring effective, fast and powerful methods to classify finger movements using two EMG channels.

3. Develop a novel feature projection / dimensionality reduction to improve the feature representations in the M-PR. This method is needed to reduce the features dimension and produce a small number of features that have high-class separability.

4. Develop robust myoelectric pattern recognition for individual and combined finger movements using two channels over some subjects for real-time application.

5. Develop a novel myoelectric pattern recognition that can reject the movements that are not included in the training stage. This is needed to increase the robustness of the myoelectric pattern recognition in the real-time application

6. Develop a novel myoelectric pattern recognition (M-PR) that can adapt to changes in EMG signal characteristic. This method is needed to produce a M-PR that has stable performance regardless of changes in the environment

7. Develop a novel myoelectric controller for the exoskeleton hand. The controller is needed to enable the exoskeleton hand to work with individual and combined finger movements.

1.4 Contribution of the doctoral thesis

This thesis contributes to knowledge theoretically and practically. The following are the main contributions from the work presented in this thesis:

- The thesis develops novel myoelectric pattern recognition (M-PR) systems for recognizing individual and combined finger movements that can work well with the amputees and non-amputees. The proposed recognition system, which is an integration of SRDA and RBF-ELM, attained the accuracy of approximately 99% on able-bodied subjects and around 98% on the amputee subjects using six EMG channels when working on 15 and 12 finger movements, respectively. This contribution will be discussed in detail in Chapter 3. However, using less number of EMG channels can enhance the comfort of the subject as long as the accuracy is still good. R. N Khushaba *et al.* (2012) showed that the M-PR with two EMG channels could achieve the accuracy of up to about 92 %. Therefore, the experiments

conducted in following chapters will employ two EMG channels instead of six channels. The majority of the contents in Chapter 3 has been submitted in the Journal of Neural Networks, the official journal of the International Neural network society published in Elsevier. The title of the paper is *Evaluation of Extreme Learning Machine for Classification of Individual and Combined Finger Movements using Electromyography on Amputees and Non-amputees*.

- Chapter 3 shows that the performance of the node-based ELM is less than the kernel-based ELM, especially with RBF-ELM. **The second section of Chapter 4**, proposes the innovation in the node-based ELM to improve the performance of the node-based ELM. It constitutes an adaptive extreme learning machine (AW-ELM). AW-ELM has been tested on EMG dataset (in the M-PR case) and the UCI machine-learning repository. On the M-PR case, the integration of SRDA and AW-ELM achieved the accuracy of 94.84 % using two EMG channels. The results is better than the accuracy attained by R. N Khushaba *et al.* (2012), which is about 92% when recognizing the finger movements using two EMG channels. In addition, AW-ELM is comparable to RBF-ELM and other well-known classifiers such as SVM, LDA, and kNN. As for UCI machine learning datasets, AW-ELM can work on a wide range of datasets. For the general case, AW-ELM offers some advantages over wavelet neural networks (WNN) and wavelet extreme learning (W-ELM). On WNN, AW-ELM offers fast training but comparable performance to WNN. Furthermore, on W-ELM, AW-ELM removes the initialization stages that should be performed in WNN and W-ELM. In summary, the aim to improve the node-based ELM AW-ELM was achieved. The content of this contribution has been presented at The 21st International Conference on Neural Information Processing (ICONIP) 2014 and was published in Neural Information Processing Vol. 8834 as a book section. The paper's title is *adaptive wavelet extreme learning machine (AW-ELM) for index finger recognition using two-channel electromyography (Khairul Anam & Al-Jumaily, 2014a)*.

- Development of a dimensionality reduction algorithm is the next contribution of this thesis. Spectral regression extreme learning machine (SR-ELM) is proposed to improve the performance of spectral regression discriminate analysis (SRDA). SR-ELM has been tested on the EMG dataset and the UCI machine-learning repository. On the myoelectric finger motion recognition using two EMG channels, SR-ELM outperforms SRDA. However, SR-ELM and SRDA are comparable when they work

on a wide range of datasets from UCI machine learning datasets. **Chapter 4** Section 4.3 discusses this contribution. SR-ELM on myoelectric pattern recognition has been presented at the 7th International IEEE/EMBS Conference on Neural Engineering (NER), 2015. The paper entitled a *novel extreme learning machine for dimensionality reduction on finger movement classification using sEMG* was published online on IEEE Explore (K. Anam & A. Al-Jumaily, 2015).

- The efficacy of the kernel-based ELM depends on the kernel parameters. Therefore, these parameters should be optimized properly. This thesis contributes to developing a new way to optimize kernel-based-ELM using particle swarm optimization (PSO). This leads to some new extreme learning machine designs such as swarm-radial-basis-ELM (SRBF-ELM), swarm-linear ELM (SLIN-ELM), and swarm-polynomial ELM (SPOLY-ELM). Using only two EMG channels, the proposed myoelectric pattern recognition using the integration of SRDA and SRBF-ELM achieved an accuracy of about 94 % using two EMG channels. Chapter 4 Section 4.1 will address this contribution. This contribution was presented in the 2014 Middle East Conference on Biomedical Engineering (MECBME). The paper entitled *Swarm-based extreme learning machine for finger movement recognition* was published online on the IEEE Explore (Khairul Anam & Al-Jumaily, 2014b).

- Some enhancements have been done to improve previously proposed method to overcome the problem of PSO, which is easy to be trapped in local optima. Thus, a new ELM, swarm wavelet radial basis ELM (SW-RBF-ELM) is proposed. The experimental results showed that the integration of SRDA and SW-RBF-ELM could enhance the performance of M-PR. The accuracy is around 95 % and 94 % for able-bodied subjects and amputees, respectively, using two EMG channels. Chapter 4 Section 4.2 will discuss this contribution in detail. The idea of this contribution was presented at the 36th Annual International Conference of the IEEE Engineering in Medicine and Biology Society (EMBC) 2014. The paper entitled *Swarm-wavelet based extreme learning machine for finger movement classification on trans-radial amputees* was published online on the IEEE Explore.

- The real-time myoelectric pattern recognition on individual and combined finger movements using only two EMG channels has been developed and tested on eight able-bodied subjects. The achievement of this method is that it involves the transient and steady state in both the experiments, offline and online. Most M-PRs avoid

including the transient state because it can downgrade the performance of the M-PR. Even so, the experiments in this thesis achieved a high accuracy of 90.46 % and 89.19 % on the offline and online classification, respectively. **Chapter 5** Section 5.2 addresses this contribution. The initial results of this chapter has been presented in International Congress on Neurotechnology, Electronics and Informatics (NEUROTECHNIX) 2014 (K Anam & Al-jumaily, 2013).

- A novel myoelectric controller that consists of myoelectric pattern recognition with rejection mechanism and the proportional controller has been designed and tested on the exoskeleton hand. The myoelectric controller enables the exoskeleton to move five individual fingers and five combined fingers. A single subject participated in the experiment and repeated the exercises four times. The M-PR achieved an accuracy of 89.72%. The contribution in this section lies in two things. The first contribution lies in the motion rejection. The motion rejection enables the M-PR to focus on the movements that were included in the training stage and reject movements that were not involved in the training. This mechanism improves the robustness of the myoelectric controller. The second contribution lies on the capability of the exoskeleton hand dealing with more than two movements. Chapter 5 Section 5.3 discusses this contribution.

- The performance of myoelectric pattern recognition (M-PR) will decrease if it is used for long use, for days or months, due to its inability to adapt to changes that occur in EMG signals. This thesis proposes an adaptation mechanism in M-PR, by employing online sequential extreme learning machine (OS-ELM). Not only that, a motion rejection is included as well. The experimental results show a stable performance of M-PR over three different days of experiments. This section will be discussed in **Chapter 5** Section 5.4. This contribution has been presented at the 37th Annual International Conference of the IEEE Engineering in Medicine and Biology Society (EMBC) 2015. The paper entitled *a robust myoelectric pattern recognition using online sequential extreme learning machine for finger movement classification* was published online on IEEE Explore (Khairul Anam & Adel Al-Jumaily, 2015).

1.5 Organization of the thesis

The thesis contains six chapters, appendix, and references The contents are organized sequentially from one chapter until the references.

- Chapter I presents the introduction.

- Chapter II presents the literature reviews.

- Chapter III presents extreme learning machine-based classification of finger movements using surface electromyography for amputees and non-amputees

- Chapter IV discusses some novel methods of ELM-Based Classification for myoelectric finger recognition using two EMG channels

- Chapter V presents some efforts toward robust myoelectric pattern recognition for real-time finger movement classification

- Chapter VI presents summary, conclusion, and future work

1.6   Publication outcomes of the doctoral research

The publications published during the doctoral studies are as follows:

Submitted Journal

- **Anam, K**, Al-Jumaily, A," Evaluation of Extreme Learning Machine for Classification of Individual and Combined Finger Movements using Electromyography on Amputees and Non-amputees", *Neural Networks. The first revision*

- **Anam, K**, Al-Jumaily, A," Improved Myoelectric Control System Using Rejection-Based Extreme Learning Machine for a Hand Exoskeleton" IEEE Transaction on Industrial Electronics

Journal:

- **Anam, K**., Al Jumaily, A., Maali, Y., (2014). Index finger motion recognition using self-advice support vector machine. *International Journal on Smart Sensing and Intelligent Systems*, 7(2), 644-657.

Book section:

- Anwar, T., **Anam, K**, Al-Jumaily, A (2015). EMG Signal Based Knee Joint Angle Estimation of Flexion and Extension with Extreme Learning Machine (ELM) for Enhancement of Patient-Robotic Exoskeleton Interaction. Neural Information Processing (Vol. 9489, pp. 583-590): Springer International Publishing

- **Anam, K.**, & Al-Jumaily, A. (2014). Adaptive Wavelet Extreme Learning Machine (AW-ELM) for Index Finger Recognition Using Two-Channel

Electromyography. In C. Loo, K. Yap, K. Wong, A. Teoh & K. Huang (Eds.), Neural Information Processing (Vol. 8834, pp. 471-478): Springer International Publishing.

Conference:

- **Anam, K**. and A. Al-Jumaily (2015). *A robust myoelectric pattern recognition using online sequential extreme learning machine for finger movement classification*. 37th Annual International Conference of the IEEE Engineering in Medicine and Biology Society (EMBC), Milan, Italy

- **Anam, K**., & Al-Jumaily, A. (2015, 22-24 April 2015). *A novel extreme learning machine for dimensionality reduction on finger movement classification using sEMG*. Paper presented at the 7th International IEEE/EMBS Conference on Neural Engineering (NER), Montpellier, France

- Yee Mon, A., **Anam, K**., & Al-Jumaily, A. (2015, 22-24 April 2015). *Continuous prediction of shoulder joint angle in real-time.* Paper presented at the 7th International IEEE/EMBS Conference on Neural Engineering (NER), Montpellier, France

- **Anam, K.**, & Al-Jumaily, A. (2014, 26-30 Aug. 2014). *Swarm-wavelet based extreme learning machine for finger* movement *classification on transradial amputees.* Paper presented at the 2014 36th Annual International Conference of the IEEE Engineering in Medicine and Biology Society (EMBC), Chicago, USA

- Aung, Y. M., Al-Jumaily, A., & **Anam, K**. (2014). A novel upper limb rehabilitation system with self-driven virtual arm illusion. The 2014 36th Annual International Conference of the IEEE. Engineering in Medicine and Biology Society (EMBC), Chicago, USA

- **Anam, K.**, & Al-Jumaily, A. A. (2014, 17-20 Feb. 2014). *Swarm-based extreme learning machine for finger movement recognition.* Paper presented at the 2014 Middle East Conference on Biomedical Engineering (MECBME), Doha, Qatar.

- **Anam, K.**, & Al-Jumaily, A. (2013). Real-time Classification of Finger Movements using Two-channel Surface Electromyography. Proceedings of the International Congress on Neurotechnology, Electronics and Informatics (NEUROTECHNIX), Portugal

- **Anam, K**., Khushaba, R. N., & Al-Jumaily, A. (2013, Aug). *Two-channel surface electromyography for individual and combined finger movements.* Paper presented at the Proc. 35th Ann. Int. Conf. IEEE-EMBS Eng. Med. Biol. Soc.

- **Anam, K.**, & Al-Jumaily, A. A. (2012). Active exoskeleton control systems: State of the art. *Procedia Engineering, 41*, 988-994.

Publication to support other works

- Masood, A., Al-Jumaily, A., & **Anam, K**. (2015, 22-24 April 2015). *Self-supervised learning model for skin cancer diagnosis*. Paper presented at the 7th International IEEE/EMBS Conference on Neural Engineering (NER), Montpellier, France

- Masood, A., Al-Jumaily, A., & **Anam, K**. (2014). Texture Analysis Based Automated Decision Support System for Classification of Skin Cancer Using SA-SVM. In C. Loo, K. Yap, K. Wong, A. Teoh & K. Huang (Eds.), Neural Information Processing (Vol. 8835, pp. 101-109): Springer International Publishing.

- Mahmoud, M. K. A., Al-Jumaily, A., Maali, Y., & **Anam, K**. (2013). Classification of Malignant Melanoma and Benign Nevi from Skin Lesions Based on Support Vector Machine. Paper presented at the 2013 Fifth International Conference on Computational Intelligence, Modelling and Simulation (CIMSim).

CHAPTER 2
Literature review

2.1 Introduction

This chapter covers an essential theory of the anatomy of the hand to understand the hand structure that the rehabilitation device hand will work on. Then, it is followed by the muscles involved in the digit movements. A basic knowledge about the biological concept of electromyography (EMG) or myoelectric signal (MES) will be presented in the following section. Furthermore, different myoelectric controller methods will be addressed as well. Afterward, the chapter presents a literature review on the hand rehabilitation devices utilizing EMG/MES as the control source. Finally, the chapter will highlight the shortcomings of the existing myoelectric controller that this thesis aims to overcome.

2.2 The hand anatomy and bio-signal

2.2.1 The hand anatomy

The anatomy of the hand is needed to understand the structure of the hand and the related muscles so that the controller for the hand rehabilitation device is designed properly. Firstly, this section discusses the bones and joints of the hand. The muscles driving the hand are discussed afterward.

2.2.1.1 Bones and joints

The bones of hand have multiple articulations to the eight carpal bones that form the wrist (Figure 2.1). The eight carpal bones are grouped into the proximal and distal row. The bones in the proximal row from radius to ulna are the scaphoid, lunate and triquetrum. These bones are mobile bones. As for the rest of the bones, which are in the distal row, they are the trapezium, trapezoid, capitate, and hamate (Nordin & Frankel, 2012). The bones in the distal row fit tightly against each other. These bones become the root of the hand and the digits (Heo *et al.*, 2012).

The thumb and fingers are the main components of the hand. The thumb is composed of one metacarpal and two phalanges while each finger is composed of one metacarpal and three phalanges. The finger rays are numbered and named from the radial to ulnar side: I(thumb), II (index finger), III (middle finger), IV (ring finger) and V (little finger). Each finger ray proximally articulates with a carpal bone. This articulation forms the carpometacarpal (CMC) joint. The next joint in each ray is the metatarsophalangeal (MCP) joint. The MCP joint connects the metacarpal bone to the proximal phalanx. The interphalangeal (IP) joint links the phalanges of the fingers. In each finger, they are two IP joints: a proximal (PIP) and a distal (DIP) interphalangeal joints. As for the thumb, it has only one IP joint. In total, there are 19 bones and 14 joints in the hand, as shown in Figure 2.1.
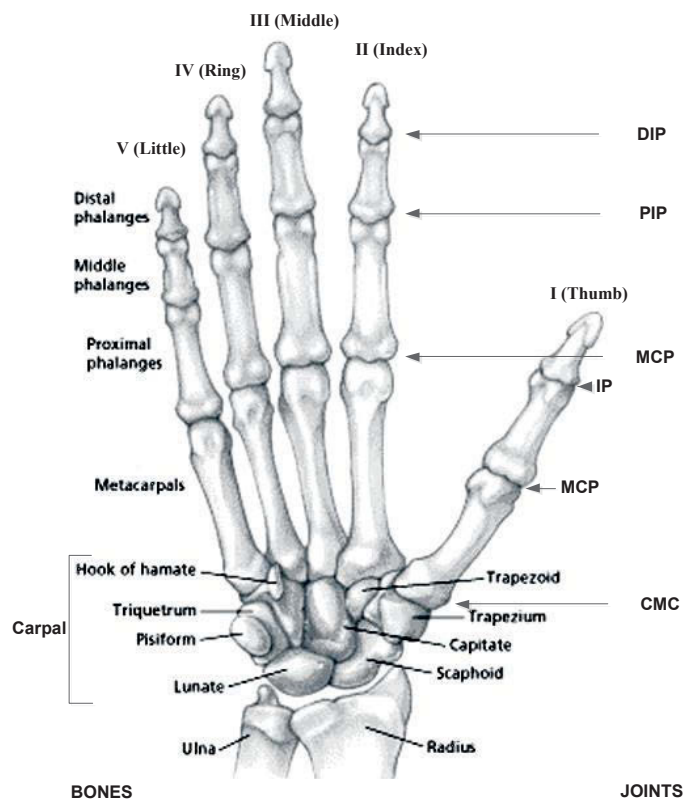
Figure 2.1 Right hand, proximal view (Doyle & Botte, 2002)

The shape variation of the joints of the thumb and the fingers results in the variation of the degree of freedom at these joints. The unique orientation and configuration of the CMC joint of the thumb give the digit large mobility and great flexibility (Nordin & Frankel, 2012). The second (the index finger) and the third (the middle finger) CMC joints are an immobile unit of the hand because they are connected to the trapezoid and capitate bone that are immobile bones. The fourth (the ring finger) and the fifth (the little finger)

16

CMC joint are able to move 10 º to 15 º and 20 º to 30 º of flexion and extension, respectively.

The MCP joints of the four fingers are unicondylar diarthrodial joints, providing three degrees of freedom: flexion-extension, abduction-adduction, and slight pronation-supination. The range of flexion of the MCP joints is from zero to approximately 90 º (Figure 2.2), but it differs among the fingers. For example, the fifth finger is able to move until 95 º while the second finger can move until 70 º only. Likewise, the extension movement beyond zero position varies among the fingers.
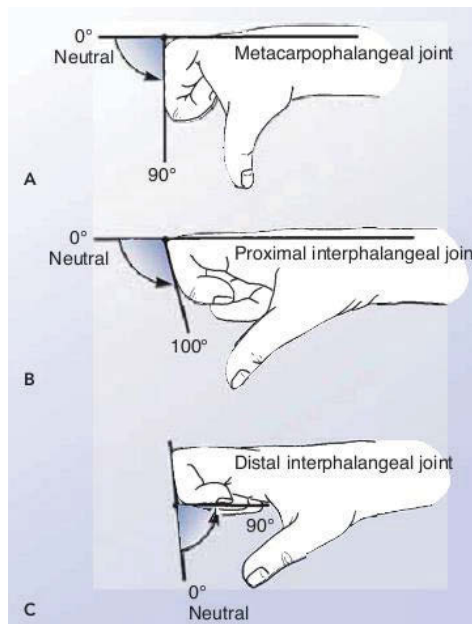
Figure 2.2 Flexion of three joint of the fingers. A. Flexion of the MCP joint. B. Flexion of the PIP joint. C. Flexion of DIP joint (Nordin & Frankel, 2012)

The PIP and DIP joints of the fingers are bicondylar hinge joints allowing only flexion-extension motion. The range of flexion in the PIP joints measured from zero position is maximum 110º or more. Zero position is measured when the finger is in the plane of the hand. In the DIP joints, the range of flexion is approximately 9 º.

The CMC joint of the thumb is a saddle joint allowing the thumb metacarpal to move in a wide range of motion in two degrees of freedom: flexion-extension and abduction-adduction. The MCP joint of the thumb is similar to the MCP joints of the fingers. The range of flexion from zero position varies from person to person from 30 º to 90 º; extension from zero position is about 15 º (Nordin & Frankel, 2012). The IP joint of the thumb is similar to the distal joint of the fingers.

2.2.1.2 *Muscles*

The coordination of the extrinsic and intrinsic muscles contributes in performing dexterous movements of the hand. The term extrinsic shows that the muscle is mostly located outside the hand. They originate from the arm and forearm and end up within the hand. These muscles control the flexion and the extensions of the digits. Different from the extrinsic muscles, the intrinsic muscles are located inside the hand. They can perform independent actions of each digit (Heo *et al.*, 2012).

According to the functionality, the extrinsic muscles are mostly classified into flexor and extensor muscles. The flexor muscles lay on several layers starting from a superficial layer to a deeper one, as shown in Figure 2.3. According to Muscolino (2014), there are three muscles that move the digits. Two muscles are located in the middle layer: flexor digitorum superficialis (**FDS**) and flexor policis longus (**FPL**), and one muscle is located in the deepest layer: flexor digitorum profundus (**FDP**). Similarly, the extensor muscles are located in some regions from the superficial to deeper layer, as shown in Figure 2.4. Four muscles are responsible for the extensions of the digits: extensor digitorum **(ED)**, extensor digiti minimi **(EDM),** extensor pollicis longus **(EPL)**, and extensor indicis **(EI)**. Table 2.1 presents the function of the muscles mentioned above.
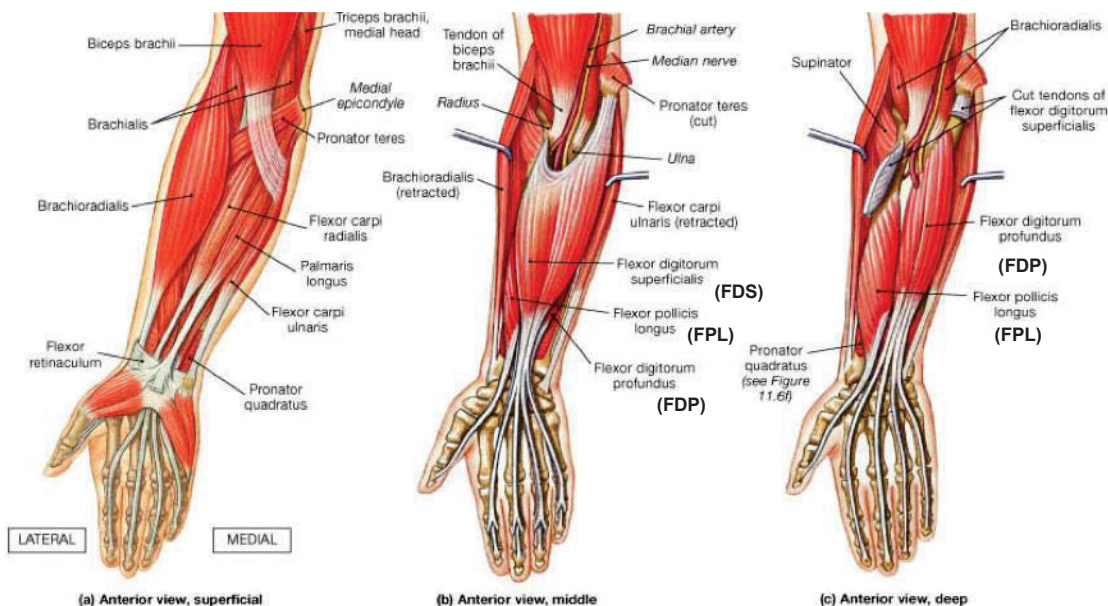
Figure 2.3 Flexor Muscles (Marieb, 2009)
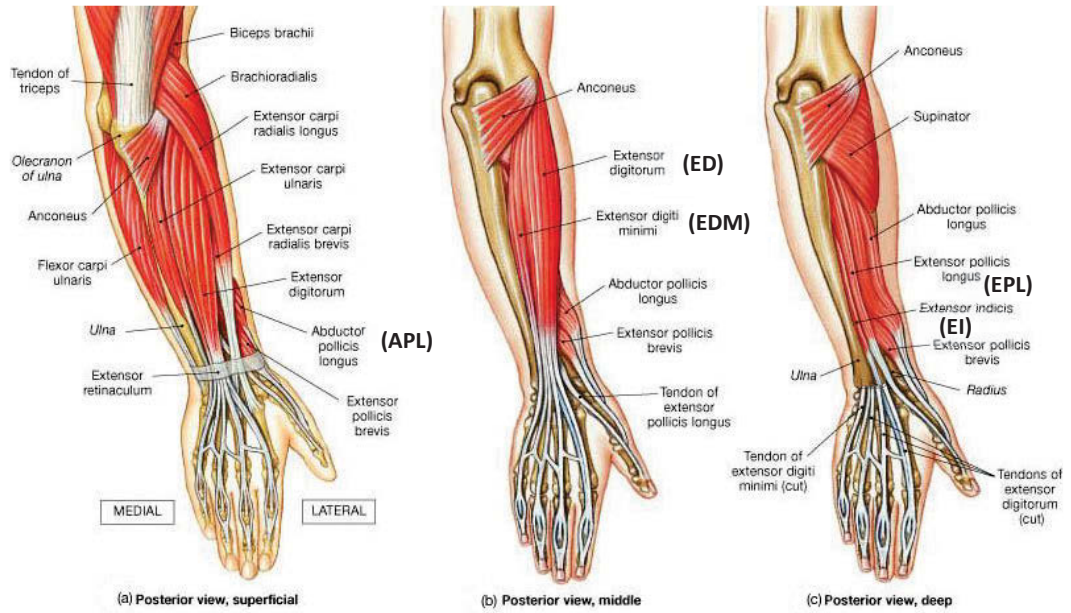
Figure 2.4 Extensor muscles (Marieb, 2009)

Table 2.1 Extrinsic muscles for digit movements (Muscolino, 2014)

Muscle	Action
Flexor digitorum superficialis **(FDS)**	1. Flexion of the second to fifth fingers at PIP joint, and MCP joint. 2. Flexion of the hand at the wrist joint
Flexor digitorum profundus **(FDP)**	1. Flexion of the second to fifth fingers at DIP, PIP, and MCP joints 2. Flexion of the hand at the wrist joint
Flexor policis longus **(FPL)**	1. Flexion of the thumb at the CMC, MCP and IP joints, and adduction at the CMC joint. 2. Flexion of the hand at the wrist joint
Extensor digitorum **(ED)**	1. Extension of the second to fifth fingers at the MCP, PIP, and DIP joints 2. Extension of the hand at the wrist joint
Extensor digiti minimi **(EDM)**	1. Extension of the little finger at the MCP, PIP, and DIP joints 2. Extension of the hand at the wrist joint
Abductor pollicis longus **(APL)**	1. Abduction of the thumb at the CMC joint 2. Extension of the thumb at the CMC joint
Extensor pollicis longus **(EPL)**	Extension of the thumb at the CMC, MCP, and IP joints
Extensor indicis **(EI)**	1. Extends the index finger at the MCP, PIP, and DIP joints 2. Extends the hand at the wrist joint

2.2.2   Electromyography as a bio-signal

The extrinsic and intrinsic muscles drive the fingers and the thumb. These muscles generate electrical signals called electromyography (EMG) or myoelectric signal (MES). This section will discuss the anatomy and physiology of the muscle contraction. The

19

characteristic of the EMG signals and the method to record this signal are presented afterward.

2.2.2.1   *Anatomy and physiology of muscle contraction*

Electromyography is a process of the detection, analysis, and use of the electrical signal that originates from contracting muscles (C. De Luca, 2006). The signal is called an electromyogram (EMG) or myoelectric signal (MES) (R. Khushaba, 2010). Figure 2.5 shows the generation of the EMG signal.

The generation of the electric signal in the muscle relates to the concept of a motor unit (MU). The concept of MU in the central nervous system (CNS) is simply presented in Figure 2.5. The CNS is arranged in a hierarchical style. The human cortex produces signals that have a powerful influence on the motoneurons of the spinal cord. A motor unit (MU) consists of a motoneuron in the spinal cord. Because the motorneuron is activated, the muscle fibres are innervated. The number of MUs per muscle may range from approximately 100 to 1000 or more for small hand muscle to large limb muscle. Furthermore, the force generation of MUs varies greatly until 100-fold or more difference (Moritani *et al.*, 2005).
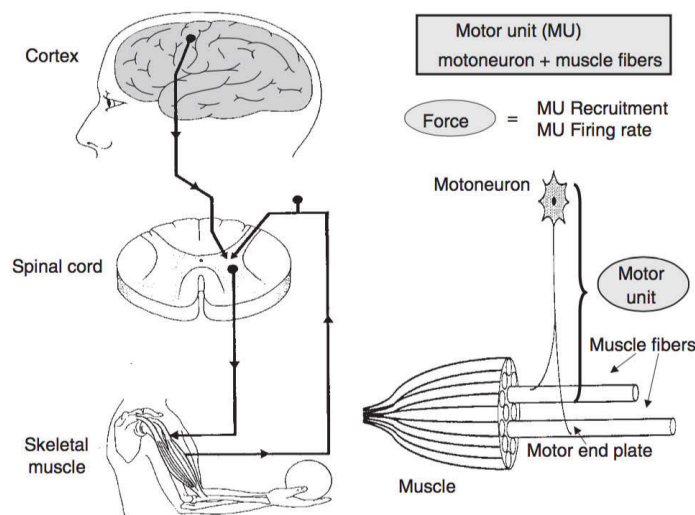
Figure 2.5 The basic motor control mechanism (Moritani *et al.*, 2005)

2.2.2.2   *The characteristics of the electromyography signal*

The EMG signal is a stochastic or random signal whose amplitude can range from 0 to 1.5 mV (root mean square) or 0 to 10 mV (peak-to-peak). The energy above the electrical noise level is in the range of frequency 0 – 500 Hz and the dominant energy of the noise is in the range of 50-150 Hz (C. J. De Luca, 2002). The noise may emanate from many sources such as inherent noise in the electronic components, motion artefacts, the

inherent instability of the signal, and ambient noise. The energy under the noise level is not reasonable for analysis. Figure 2.6 shows the example of EMG signal and its power or energy collected from the Tibialis anterior muscle during constant force isometric contraction at 50% of voluntary maximum.
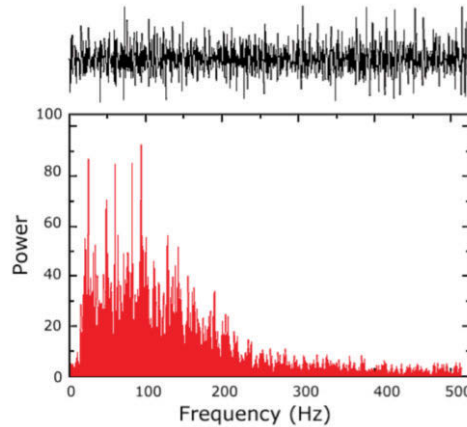
Figure 2.6 The example of the EMG signal (top) and its energy (bottom) (C. J. De Luca, 2002)

2.2.2.3   *The detection of EMG signal*

The EMG signal may be collected in two ways, either invasive or non-invasive. L.J. Hargrove *et al.* (2007) shows that the control system using surface EMG is not too much different from invasive one. For further discussion, this thesis considers only surface EMG. Surface EMG electrodes are located on the subject's skin, as described in Figure 2.7. Meanwhile, Figure 2.8 describes the stages in the acquisition of the EMG signal. The source of EMG or myoelectric signal is the motor unit action potential (MUAP), the action potential generated by each of the motor units activated during a contraction. The populations of motor units activated are asynchronous to allow smooth movements. The electrodes pick up the conducted signals generated by all activities involved (Criswell, 2010).
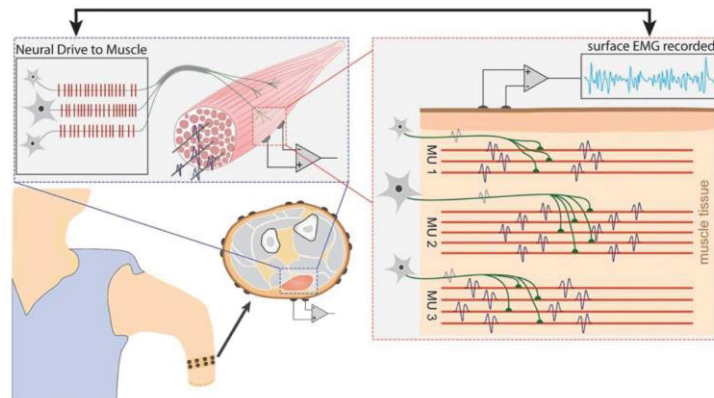
Figure 2.7 EMG signal generation and collection (Farina *et al.*, 2014)
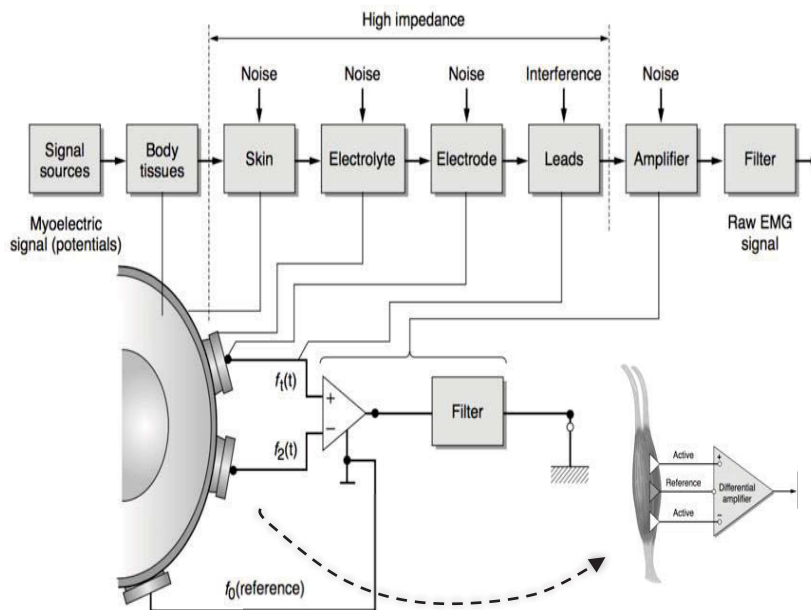
Figure 2.8 Data instrumentation of the EMG signal (Criswell, 2010)

The noise may happen in all steps of the signal acquisition, as shown in Figure 2.8. In fact, it is desirable to collect the EMG signal containing the maximum amount of information and the minimum amount of noise contamination. One way to overcome the noise existence, especially from the power line radiation (50 or 60 Hz), is to use a differential amplifier from two electrodes sites (C. J. De Luca, 2002). In the differential amplification concepts, the electronic circuit will remove the common signal of two electrode sites and amplify the difference. The common signal represents any signal that originates far away from the detection sites whereas the difference represents the immediate vicinity of the detection surfaces. Thus, the local EMG signals will be amplified, and the distant power line noise will be removed.

The noise caused by motion artefacts most probably happen during the data recording. There are two main sources of this noise: one from the cable movement linking the electrode to the amplifier, and the other from the junction of the detection surface of the electrode and the skin. The energy of the noise is in the frequency range from 0 to 20 Hz. These noise sources can be attenuated by proper design of the electronic circuits.

2.3 Myoelectric control system

The EMG signal can be used in the control system of the hand rehabilitation devices either in EMG-based pattern recognition or non-pattern recognition system (Gopura *et al.*, 2013). The EMG-based pattern recognition (EMG-PR) or myoelectric pattern

recognition (M-PR) consists of several steps, as shown in Figure 2.9. The goal of M-PR is to recognise and classify the EMG patterns into classes or limb movements. On the other hand, the EMG-based non-pattern recognition (EMG-non-PR) system does not classify any limb movement (Figure 2.10). It may estimate human physical parameters such as the angle of the elbow or the force exerted by the hand according to the EMG signals collected. Moreover, the EMG-non-PR may use EMG signals as a threshold control system or proportional control system. The following sections will explain M-PR and EMG-non-PR in detail.
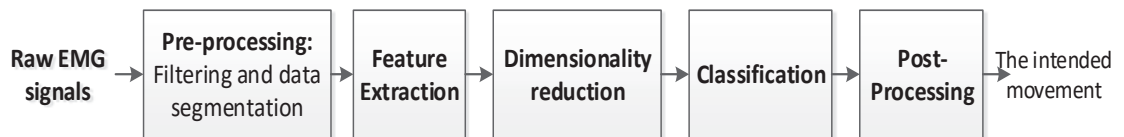
Figure 2.9 The myoelectric pattern recognition system
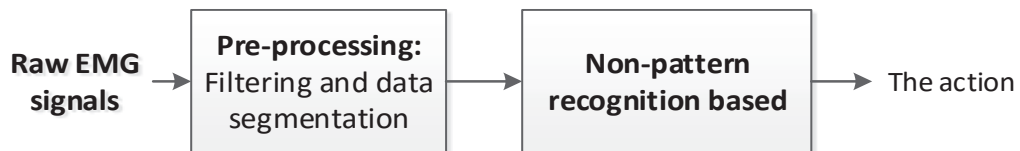
Figure 2.10 The EMG-based non-pattern recognition

2.3.1   Myoelectric pattern recognition (M-PR)

This section addresses the stages of myoelectric pattern recognition (M-PR) in detail by describing each component of M-PR as presented in Figure 2.9.

2.3.1.1   Pre-processing

- **Filtering**

The aim of filtering is to reduce the unwanted noises. We can apply a band-pass filter between 20-500 Hz. The filter can have the upper bandwidth cut-off of 400 Hz if a stricter filter is needed. The power line noise 50 Hz or 60 Hz may be removed using a notch filter of 50 or 60 Hz. However, the filter possibly removes the information of the EMG signal. Therefore, it is not advisable to use the notch filter. Instead, the differential amplification is used.

- **Data segmentation**

The classification process lasts for a certain period called a window. In this window, the system extracts valuable information from the row of myoelectric signals. This information is called a feature. The quality of features greatly determines the performance

of the finger recognition system (L.J. Hargrove *et al.*, 2007). The feature is extracted in a data sequence bounded in this time slot or window. Based on the data in this window, the whole stages of the recognition system are performed.

(a)   (b)
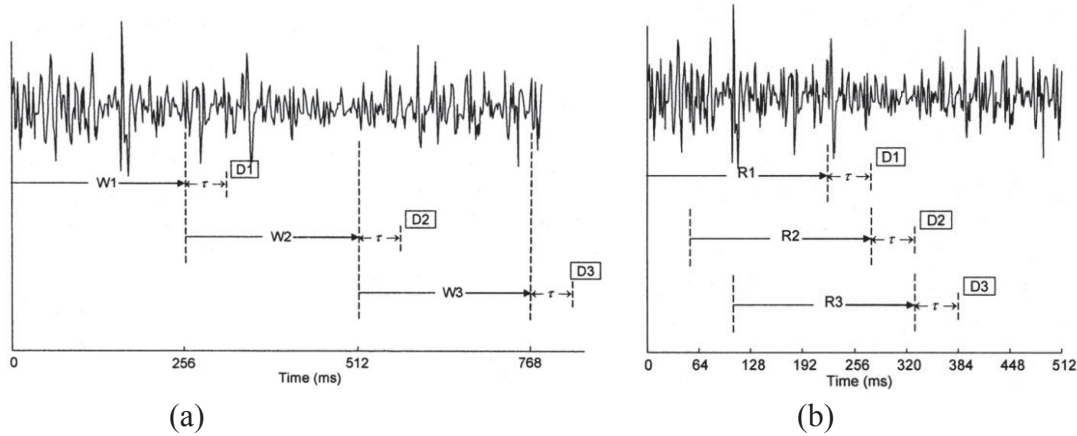
**Figure 2.11 The data segmentation: disjoint windowing (a) and
overlapped windowing (b) (Kevin Englehart & Hudgins, 2003)**

In general, the data or signal can be segmented in two ways: either as a disjoint or overlapped windowing (Kevin Englehart & Hudgins, 2003; Oskoei & Huosheng, 2008), as shown in Figure 2.11. The disjoint windowing is only associated with the window length. On the other hand, the overlapped windowing is associated with the window length and window increment. The window increment is a period between two consecutive windows. In general, the disjoint windowing is overlapped windowing in a condition where the window increment is equal to the window length.

- **Transient and steady-state response**

Transient and steady state of the EMG signals is one of the common issues in the area of myoelectric pattern recognition. Transient state of myoelectric signals is related to a signal state when a person produces a contraction from rest while the steady state of the myoelectric signal indicates the signal state when the person maintains the contraction in a certain level (R. Khushaba, 2010). Hudgins *et al.* (1993) were the first researchers who employed both the transient and the steady state of the myoelectric signals in experiments. Kevin Englehart *et al.* (2001) found that the classification performance of the steady state outperforms that of the transient state. Therefore, to increase the accuracy, the majority of the myoelectric control only considers the steady state response. However, the system that only considers steady state response in the training stage will not be robust with changes that present in the real-time application.

- **Controller delay**

The controller delay is a period required to acquire the myoelectric signal and process the acquired signal to produce an output. The first part is known as a segment length while the second is the processing time of the myoelectric controller. Hudgins *et al.* (1993) suggested that the controller time should be less than 300 ms to ensure the myoelectric controller responds to the user's command in a quick and accurate manner. Furthermore, T. R. Farrell and Weir (2007) have different suggestions based on their experiments. They recommended an optimal controller delay that lies between 100 and 175 ms for the average users and between 100 and 125 ms for the 90th percentile users. To combine both results, we can say that the acceptable controller delay is less than 300 ms while the optimal controller delay lies between 100 and 175 ms.

2.3.1.2   *Feature extraction*

The next step of the myoelectric pattern recognition after pre-processing is the feature extraction. The feature extraction is a process that converts patterns to features. In the case of EMG signals, it means a process that converts the pattern of EMG signals, in particular, segments to a set of features that contains salient features of the signals (R. Khushaba, 2010).

Boostani and Moradi (2003) suggested some conditions that the features should have. Firstly, the feature should have maximum class separability to ensure the misclassification rate is as low as possible. The second condition is robustness. The robustness means that the feature space can preserve its class separability in a noisy and real-time environment. The last condition is the complexity of the features should be kept as low as possible to be easily implemented in the real-time environment with reasonable hardware. Another interesting fact in the feature extraction is a feature may be not relevant individually, but it becomes relevant when it joins other features (Oskoei & Huosheng, 2008).

In general, the feature extraction in EMG signal consists of three groups: time domain features, frequency domain features and time-frequency domain or time-scale domain (Phinyomark *et al.*, 2012). The following sections will describe each group in detail.

- **Time domain (TD) features**

Time domain features have been used widely in EMG pattern recognition system (Al-Timemy *et al.*, 2013; L.J. Hargrove *et al.*, 2007; Oskoei & Huosheng, 2008). The advantages of the TD features are quick, easy implementation, low computational

complexity and having good performance in low noise environment (Phinyomark *et al.*, 2012). However, it has a major disadvantage in dealing with non-stationary signals such EMG signals. This thesis will provide some of most used TD features.

1. **Mean absolute value (MAV)**

MAV is an average of the absolute value of the amplitude of the EMG signal in a particular segment. It is defined as:

$$MAV = \frac{1}{N}\sum_{k=1}^{N}|x_k| \qquad \textbf{2.1}$$

2. **Mean absolute value slope (MAVS)**

MAVS is a difference between the current MAV and the previous one (Hudgins *et al.*, 1993), as defined as:

$$MAVS = MAV_{k+1} - MAV_k \qquad \textbf{2.2}$$

3. **Zero crossings (ZC)**

Zero crossing is a feature obtained by counting the number of times the signals crosses the zero (Hudgins *et al.*, 1993). A threshold is included to attenuate the noise about the zero crossing. It is defined as:

$$ZC = \sum_{k=1}^{N} z_k, \quad z_k = \begin{cases} 1 & x_k x_{k+1} < 0 \text{ and } |x_k - x_{k+1}| \geq threshold \\ 0 & else \end{cases} \qquad \textbf{2.3}$$

4. **Slope sign changes (SSC)**

Slope sign changes is a feature that counts the number of times the slope of the signal changes its sign (Hudgins *et al.*, 1993). It is defined as:

$$SSC = \sum_{k=1}^{N} z_k, \quad z_k = \begin{cases} 1 & \begin{aligned} &\left(x_k > x_{k-1} \text{ and } x_k > x_{k-1}\right) \text{ or} \\ &\left(x_k < x_{k-1} \text{ and } x_k < x_{k-1}\right) \text{ and} \\ &|x_k - x_{k+1}| \geq threshold \text{ or} \\ &|x_k - x_{k-1}| \geq threshold \end{aligned} \\ 0 & else \end{cases} \qquad \textbf{2.4}$$

5. **Waveform length (WL)**

Waveform length is a feature of the cumulative length of the EMG signal over a segment.

$$WL = \sum_{k=1}^{N}|x_k - x_{k-1}| \qquad \textbf{2.5}$$

6. Root mean square (RMS)

Root mean square is a square root of the mean of the squares of a segment. In the EMG signals, it is an amplitude modulated Gaussian random process that relates to constant force and non-fatiguing contraction (Phinyomark *et al.*, 2012). RMS can be calculated as:

$$RMS = \frac{1}{N}\sum_{k=1}^{N} x_k^2 \qquad \textbf{2.6}$$

7. Autoregressive (AR) features

The myoelectric signal is a non-stationary signal. However, it can be regarded as a stationary Gaussian process in a short time or a segment (Zecca *et al.*, 2002). Therefore, the EMG signal can modelled as:

$$x_k = \sum_{i=1}^{m} a_k x_{k-i}, \qquad AR = a_k \quad m^{th}\ order\ AR\ model \qquad \textbf{2.7}$$

8. Hjorth parameters

Hjorth proposed three time-domain features for EEG activity: activity, mobility, and complexity. These features can be extended to the EMG signals as well (Mouzé-Amady & Horwat, 1996) (R. N Khushaba *et al.*, 2012). The formulation of the features is as follow.

$$Activity\colon m_0 = var(x(t)) \qquad \textbf{2.8}$$

$$Mobility\colon m_1 = \sqrt{\frac{m_0\left(\frac{dx(t)}{dt}\right)}{m_0(x(t))}} \qquad \textbf{2.9}$$

$$Complexity\colon m_2 = \frac{m_1\left(\frac{dx(t)}{dt}\right)}{m_1(x(t))} \qquad \textbf{2.10}$$

- **Frequency domain (FD) features**

Frequency or spectral domain features are frequently used in fatigue analysis. The features are mostly obtained from power spectral density (PSD).

1. Mean frequency (MNF)

Mean frequency is an average frequency that is obtained from the sum of the product of the frequency and its power spectrum divided by the total sum of the power spectrum, as defined by:

$$MNF = \sum_{k=1}^{N} f_k P_k \Big/ \sum_{k=1}^{N} P_k \qquad \textbf{2.11}$$

where f_k is the frequency of the spectrum and P_k is the power spectrum at frequency f_k.

2. Median frequency (MDF)

MDF is the frequency when the power spectrum is divided into two regions with equal amplitudes. It is formulated as:

$$\sum_{k=1}^{MDF} P_k = \sum_{k=MDF}^{N} P_k = \frac{1}{2}\sum_{k=1}^{N} P_k \qquad \textbf{2.12}$$

- **Time-frequency domain**

Time-frequency (TFD) domain features provide more accurate description of the physical phenomenon than the time domain and frequency domain features separately. The reason is that TFD can localize the energy of the EMG signals both in time and in frequency (K. Englehart *et al.*, 1999). However, the TFD transformation needs heavy computation; somehow, it will not be reasonable for real-time application.

Kevin Englehart *et al.* (2001) tested three different TFD features in the myoelectric pattern recognition system. It included short-time Fourier transform (STFT), wavelet transform (WT) and wavelet packet transform (WPT). They are different in how they partition the time-frequency plane, as shown in Figure 2.12. The STFT has a fixed tilling while the WT has a variable tilling. In the WT, the aspect ratio of the tilling is proportional to the centre frequency. As for WPT, it has an adaptable tilling, which can be the best for most application. However, it is computationally heavy and time costly.
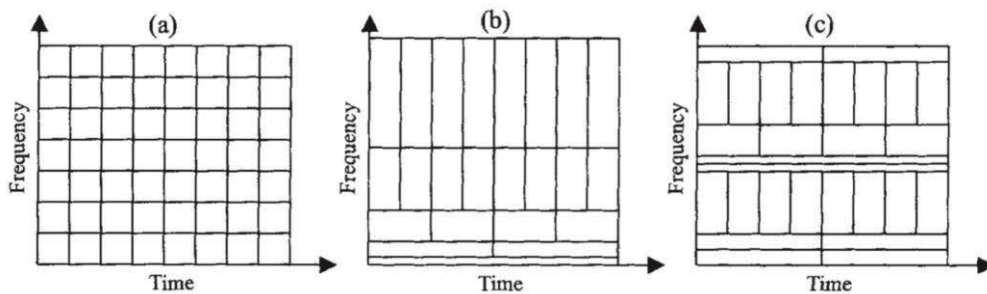
Figure 2.12 The time-frequency tilling of three different TFD features: a. SFFT b. WT and c. WPT (Kevin Englehart *et al.*, 2001)

2.3.1.3 Dimensionality Reduction

Features extracted from all EMG channels are joined to form a large feature set. As a result, the dimension of the feature set is large and should be reduced without compromising the main features. In general, there are two methods of dimensionality reductions: feature selection (FS) and feature projection (FP) (K. Englehart *et al.*, 1999). The FS tries to reduce the dimension of the input feature space by selecting a subset of

features from the original features. On the other hand, the FP reduces the dimension of the feature space by transforming the original feature space to a new feature space with smaller dimension. In the EMG signals cases, the feature projection is more favourable than the feature selection due to the large variance of the EMG signals K. Englehart *et al.* (1999). The projection-based method can consolidate the information contained in EMG signals more effectively than the selection-based method (R. N. Khushaba *et al.*, 2010). K. Englehart *et al.* (1999) proved it in their experiment. In the following section, this thesis will focus on the feature projection only. In other words, the term of a dimensionality reduction refers to the feature projection.

The feature projection can be classified into an unsupervised and supervised method. The unsupervised method simply projects the feature space into a new space without any class information. Principle component analysis (PCA) (Martínez & Kak, 2001) is an example. On the other hand, the supervised method includes the class knowledge into the projection. Linear discriminant analysis (LDA) (D. Cai *et al.*, 2008) is as an instance. Inevitably, the class inclusion can enhance the accuracy of the myoelectric pattern recognition (Al-Timemy *et al.*, 2013). One of the drawbacks of the LDA is a singularity problem that happens when the number of classes is larger than the number of samples. Some methods have been proposed to overcome the singularity problem. Examples are uncorrelated LDA (ULDA) (Ye *et al.*, 2006), spectral regression discriminant analysis (SRDA) (D. Cai *et al.*, 2008), and orthogonal fuzzy neighbourhood discriminant analysis (OFNDA) (R. N. Khushaba *et al.*, 2010).

Furthermore, the feature projection can also be grouped into linear and non-linear feature projection. PCA and LDA are examples of the linear feature projection. As for the non-linear method, the non-linear version of PCA is as an example. It is a kernel PCA that employ a kernel instead of a linear function in the process. Another example of the non-linear method is a neural-network based feature projection such as unsupervised extreme learning machine (USELM) and Autoencoder (Hinton & Salakhutdinov, 2006).

2.3.1.3.1   Principle component analysis (PCA)

The main aim of principle component analysis (PCA) is to compress the size of the dataset by extracting the most important information and maintaining only this important information (Abdi & Williams, 2010). To achieve this goal, PCA calculates principal components computed from the linear combination of the original data.

Let consider a feature set $X = \{x_1, \cdots, x_N\}$ in which N is the number of samples and $\mathbf{x}$ is a matrix with t-dimensional space. PCA can be used to find a linear transformation that transform t-dimensional space of features onto m-dimensional space of features. Let $\mathbf{P}$ represents the linear transformation that maps the features from t to m-dimensional space with $m \ll t$. Then, the new features $y_i \in \Re^m$ are defined by:

$$y_i = \mathbf{P}^T \mathbf{x}_i \quad i = 1, \dots, N$$ 2.13

where $\mathbf{x}_i \in \Re^t$ and $\mathbf{P}$ consists of columns that are the eigenvectors $\mathbf{e}_i$. The eigenvalues are computed by solving the singular value decomposition (SVD):

$$\lambda_i \mathbf{e}_i = \mathbf{Q}\mathbf{e}_i$$ 2.14

$$\mathbf{Q} = \mathbf{X}\mathbf{X}^T$$ 2.15

where Q is the covariance matrix and λ_i is the eigenvalue associated with the eigenvector $\mathbf{e}_i$.

2.3.1.3.2 Linear discriminant analysis (LDA)

The main goal of the linear discriminant is to search for vectors that best discriminate among classes instead of searching for those that best describe the feature data (Martínez & Kak, 2001). In other words, the goal of LDA is to maximize the *between-class* scatter matrix while minimizing the *within-class* scatter matrix. The within-class scatter matrix is given by:

$$S_w = \sum_{j=1}^{c} \sum_{i=1}^{N_j} \left(\mathbf{x}_i^j - \mu_j\right)\left(\mathbf{x}_i^j - \mu_j\right)^T$$ 2.16

where x_i^j is the ith sample of class j, μ_j is the mean of the class j, c is the number of classes and N_j is the number of samples in class j. The *between-class* scatter matrix is defined by:

$$S_b = \sum_{j=1}^{c} \left(\mu_j - \mu\right)\left(\mu_j - \mu\right)^T$$ 2.17

One way to achieve the goal of LDA is by maximizing the objective function of LDA, as given by:

$$\mathbf{a}^* = \arg \max_a \frac{\mathbf{a}^T S_b \mathbf{a}}{\mathbf{a}^T S_w \mathbf{a}}$$ 2.18

If the matrix S_w is non-singular, then the objective function will be a maximum when the column vectors of the projection matrix P are the eigenvectors of $S_w^{-1}S_b$. As a note, there are at most *c-1* non-zero generalized eigenvectors. In order words, the dimension of the new features will be at a most *c-1* number of features.

The singularity problem that exists in the LDA raises various methods to overcome it for example by employing PCA before LDA (PCA+LDA) or utilizing SVD before LDA (D. Cai *et al.*, 2008). In addition, different concepts were also used such as spectral regression (SR) that results in the spectral regression discriminant analysis (SRDA) (D. Cai *et al.*, 2008) or fuzzy logic that yields orthogonal fuzzy neighbourhood discriminant analysis (OFNDA) (R. N. Khushaba *et al.*, 2010).

2.3.1.3.3   Spectral regression discriminant analysis

SRDA is an improvement of LDA, which is better than LDA in the computational aspect and the ability to cope with a large dataset (D. Cai *et al.*, 2008). Let eigen problem of LDA be

$$\overline{X}W\overline{X}^{T}a = \lambda\overline{X}\overline{X}^{T}a \qquad \textbf{2.19}$$

where $\overline{X}$ (1 x c) is centred data matrix, W is eigenvector matrix (*m* x *m*), λ = eigenvalue, a = transformation vector, c = the number of classes, and m = the number of total training data points. Modification of the Eq. 2.19 gives:

$$W\overline{y} = \lambda\overline{y} \qquad \textbf{2.20}$$

where

$$\overline{X}^{T}a = \overline{y} \qquad \textbf{2.21}$$

The solution of LDA problem by SRDA is to get *y* by solving Eq. 2.21 and then use the *y* obtained to find *a*. To solve *a*, the least square sense could be employed by using:

$$a = \arg\min_{a} \sum_{i=1}^{m}\left(a^{T}\overline{x}_{i} - \overline{y}_{i}\right)^{2} \qquad \textbf{2.22}$$

Regularize least square problem of SRDA, we get:

$$a = \arg\min_{a} \sum_{i=1}^{m}\left(\left(\overline{X}^{T}a - \overline{y}\right)^{T}\left(\overline{X}^{T}a - \overline{y}\right) + \alpha a^{T}a\right) \qquad \textbf{2.23}$$

Derivative of Eq. 2.23 gives:

$$\left(\overline{X}\overline{X}^{T} + \alpha I\right) = \overline{X}\overline{y} \qquad \textbf{2.24}$$

$$\Rightarrow a = \left(\overline{X}\overline{X}^T + \alpha I \right)^{-1} \overline{X}\overline{y} \qquad\qquad \textbf{2.25}$$

2.3.1.4   *Classification*

The classifier is one of the main components of the myoelectric pattern recognition (M-PR) system. It classifies the extracted and reduced features into particular classes. In the early stage of M-PR system, multilayer perceptron (MLP) (Tsenov *et al.*, 2006) or feed-forward neural networks (FNN) was frequently used as a classifier (Hiraiwa *et al.*, 1989). The FNNs is a powerful classifier, but the training process is time-consuming. Therefore, some researchers preferred using linear discriminant analysis (LDA) than MLP because LDA is fast and performs as accurately as FNNs (L.J. Hargrove *et al.*, 2007). In addition to MLP and LDA, a few researchers employed k-nearest neighbour (kNN) (Cipriani *et al.*, 2011) and hidden markov model (HMM) (A. D. Chan & Englehart, 2005).

Recently, support vector machine (SVM), which is used in many applications, promises better performance than LDA, FNNs, k-nearest neighbour (kNN) as long as the SVM parameters are optimized properly (R. N Khushaba *et al.*, 2012). However, SVM is originally developed for binary classification. The recognition system should use several SVMs to deal with multi-class classification. Inevitably, this will add to the processing time of the system. Recently, a new machine learning originated from the artificial neural network was proposed and called extreme learning machine (ELM) (G. B. Huang *et al.*, 2012). Not like FNNs, ELM omits iterative learning and does not need to tune the hidden-node parameters. Nevertheless, ELM is superior to F-NNs (G. B. Huang *et al.*, 2012). G. B. Huang *et al.* (2012) have introduced two kinds ELM, the kernel-based ELM and node-based ELM. The kernel-based ELM behaves like SVM in which the performance is extremely dependant on the parameters of the kernel.

2.3.1.4.1   **Extreme learning machine (ELM)**

G. B. Huang *et al.* (2012) introduced extreme learning machine (ELM) as a generalization of single-hidden-layer feed-forward networks (SLFNs) that avoids iterative tuning in the determination of weights in both the hidden and output weights. Especially for the hidden layer, the weight is independent of the training data. Moreover, in training mode, the aim of the ELM is to reach the smallest training error and the smallest norm of output weights, which is different from the traditional learning algorithm of SLFNs. Using least square method, eventually the output weight can be calculated by

applying Moore-Penrose inverse to the matrix of the hidden layer output. As a result, the training speed is much faster compared to normal SLFNs.

Randomization in the weight of artificial neural networks is not a new idea. Pao and Takefji (1992) proposed the randomness in an artificial neural network prior to the work of Huang. Firstly, they proposed a functional-link net (FLN). FLN is originally an SLFN whose hidden layer is pulled back and added to the input layer. As a result, the dimension of the new input is the dimension of the original input plus the dimension of the hidden layer, and it does not have the hidden layer anymore. A special case of FLN is a randomization of FLN named a random vector functional-link net (RVFLN) (Pao *et al.*, 1994). In the RVFLN, the weights of the hidden layer that have been moved to the input layer are determined randomly. The learning goal is to train the output weight by considering the new input using quadratic optimization. If the matrix inverse using a pseudo-inverse is feasible, the output weight can be calculated instantly.

Generally speaking, RVFLN and ELM have similarity in the randomization of the weight of the hidden layer and in some cases in the output weight as well. However, firstly, they are different in the structure. ELM preserves the architecture of SLFN while RVFLN changes its architecture by removing the hidden layer to the input layer. Secondly, RVFLN is a new type of artificial neural networks with its own learning while ELM is a type of learning for SLFN. Lastly, the preservation of the architecture of ELM gives benefits to ELM. For instance, the replacement of kernel system to the hidden layer node produces a kernel based ELM.

2.3.1.4.2 Basic concept of ELM

The basic concept of ELM is as follows. Essentially, it is single feed-forward networks as shown in Figure 2.13.
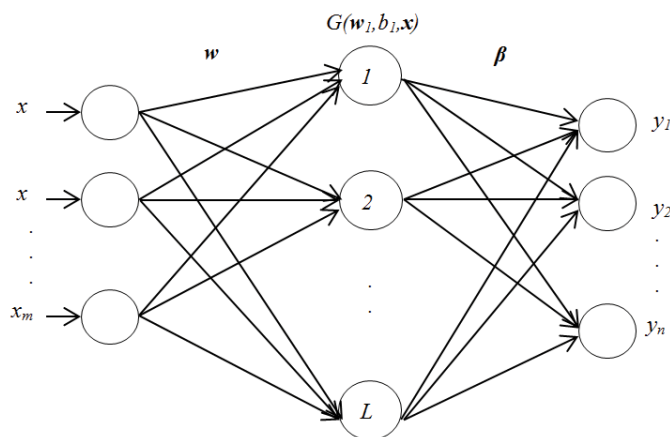
Figure 2.13 Single feed-forward networks for extreme learning machine

For N samples (x_j, y_j) where input $x_j = [x_{j1}, x_{j2}, ..., x_{jm}]^T \in R^m$ and target $y_j = [y_{j1}, y_{j2}, ..., y_{jn}]^T \in R^n$, the output of a standard SLFN with L hidden neurons is

$$f_j(x) = \sum_{i=1}^{L} \beta_j g(w_i.x_j + b_i) = G\beta \quad j = 1, ..., N \qquad \textbf{2.26}$$

where $w_i = [w_{i1}, w_{i2}, ..., w_{im}]^T$ denotes the vector of the weight linking the ith hidden neuron and the input neurons, $\beta_j = [\beta_{j1}, \beta_{j2}, ..., \beta_{jL}]^T$ defines the weight vector of the ith hidden neuron and the output neuron, b_i is the threshold of the ith hidden neuron and g(x) is the activation function of the hidden node. The right part of (Eq. 2.26) is the compact form of the SLFN output where G is the hidden layer output matrix:

$$G = \begin{bmatrix} g(w_1.x_1 + b_1) & \cdots & g(w_L.x_1 + b_L) \\ \vdots & \ddots & \vdots \\ g(w_1.x_N + b_1) & \cdots & g(w_L.x_N + b_L) \end{bmatrix}_{NxL} \qquad \textbf{2.27}$$

and

$$\beta = \begin{bmatrix} \beta_1^T \\ \vdots \\ \beta_1^T \end{bmatrix} \qquad \textbf{2.28}$$

Different from SLFNs, the aim of the ELM is not only to minimize the training error but also to minimize the norm of the output weights, that is:

$$\min_{w_i, b_i, \beta} : \|G(w_1, ..., w_L, b_1, ..., b_L)\beta - T\|^2 \qquad \textbf{2.29}$$

where T is the target.

$$T = \begin{bmatrix} y_1^T \\ \vdots \\ y_N^T \end{bmatrix}_{Nxn} \qquad \textbf{2.30}$$

In the ELM, the input weights w_i and biases b_i are assigned randomly. Thus Eq. **2.29** becomes:

$$\min_{\beta} : \|G\beta - T\|^2 \qquad \textbf{2.31}$$

The least-square solution of Eq. 2.31 with minimum norm is indicated by:

$$\beta = G^\dagger T \qquad \textbf{2.32}$$

where $G^\dagger$ is the Moore–Penrose generalized inverse of the matrix G.

Based on Eq. 2.31, the formulation the optimization of the ELM training is as follows.

$$Minimize: L_{P_{ELM}} = \frac{1}{2}\|\boldsymbol{\beta}\|^2 + C\frac{1}{2}\sum_{i=1}^{N}\|\boldsymbol{\xi}_i\|^2 \qquad \text{2.33}$$

$$Subject\ to: g(\mathbf{x}_i)\boldsymbol{\beta} = \mathbf{t}_i^T - \boldsymbol{\xi}_i^T \qquad i = 1, \dots,$$

where $\boldsymbol{\xi}_i^T = [\xi_{i,1}, \dots, \xi_{i,n}]$ is the vector of output error m with respect to input $\mathbf{x}_i$.

Based on the Karush-Khun-Tucker (KKT) theorem (Fletcher, 2013), the training of ELM is the solution of the dual optimization problem of Eq. 2.33. Hence:

$$L_{D_{ELM}} = \frac{1}{2}\|\boldsymbol{\beta}\|^2 + C\frac{1}{2}\sum_{i=1}^{N}\|\boldsymbol{\xi}_i\|^2 - \sum_{i=1}^{N}\sum_{j=1}^{n}\alpha_{i,j}\big(g(\mathbf{x_i})\boldsymbol{\beta}_j - t_{i,j} + \xi_{i,j}\big) \qquad \text{2.34}$$

where $\boldsymbol{\beta}_j$ is the output weight connecting the hidden layer and the jth output node and $\boldsymbol{\beta}_j = [\beta_1, \dots, \beta_n]$. Differentiation of Eq. 2.34 will give:

$$\frac{\partial L_{D_{ELM}}}{\partial \boldsymbol{\beta}_j} = 0 \rightarrow \boldsymbol{\beta}_j = \sum_{j=1}^{N}\alpha_{i,j}g(\mathbf{x}_i)^{\mathrm{T}} \rightarrow \boldsymbol{\beta} = \mathbf{G}^T\boldsymbol{\alpha} \qquad \text{2.35}$$

$$\frac{\partial L_{D_{ELM}}}{\partial \xi_i} = 0 \rightarrow \boldsymbol{\alpha}_i = C\xi_i \qquad \text{2.36}$$

$$\frac{\partial L_{D_{ELM}}}{\partial \boldsymbol{\alpha}_i} = 0 \rightarrow \mathbf{g}(\mathbf{x}_i)\boldsymbol{\beta} - t_i^T + \xi_i^T = 0 \qquad \text{2.37}$$

where $\boldsymbol{\alpha}_i = [\alpha_{i,1}, \dots, \alpha_{i,n}]$ and $\boldsymbol{\alpha} = [\boldsymbol{\alpha}_1, \dots, \boldsymbol{\alpha}_N]$.

By substituting Eq. 2.36 and 2.37 to Eq. 2.35, we obtain:

$$\left(\frac{1}{C} + \mathbf{G}\mathbf{G}^T\right)\boldsymbol{\alpha} = \mathbf{T} \qquad \text{2.38}$$

where

$$\mathbf{T} = \begin{bmatrix} \mathbf{t}_1^{\mathrm{T}} \\ \vdots \\ \mathbf{t}_N^{\mathrm{T}} \end{bmatrix} = \begin{bmatrix} t_{11} & \cdots & t_{1n} \\ \vdots & \vdots & \vdots \\ t_{N1} & \cdots & t_{Nn} \end{bmatrix} \qquad \text{2.39}$$

Substituting Eq. 2.38 to Eq. 2.32 produces:

$$\boldsymbol{\beta} = \mathbf{G}^T\left(\frac{1}{C} + \mathbf{G}\mathbf{G}^T\right)\mathbf{T} \qquad \text{2.40}$$

where C is a user-specified parameter. Eventually, the output functions of SLFN in 2.26 could be modified to be:

$$f(\mathbf{x}) = \mathbf{g}(\mathbf{x})\boldsymbol{\beta} = \mathbf{g}(\mathbf{x})\mathbf{G}^T\left(\frac{1}{C} + \mathbf{G}\mathbf{G}^T\right)^{-1}\mathbf{T} \qquad \text{2.41}$$

If the training data is very large, as it has been proven in (G. B. Huang *et al.*, 2012), the output of the ELM becomes

$$f(\mathbf{x}) = g(\mathbf{x})\boldsymbol{\beta} = g(\mathbf{x})\mathbf{G}^T \left(\frac{1}{C} + \mathbf{G}\mathbf{G}^T\right)^{-1} \mathbf{G}^T \mathbf{T} \qquad \text{2.42}$$

where C is a user-specified parameter and g(x) is a feature mapping (hidden layer output vector) which can be:

$$\mathbf{g}(x) = [\mathbf{Q}(\mathbf{w}_1, b_1, \mathbf{x}) \quad \cdots \quad \mathbf{Q}(\mathbf{w}, b_1, \mathbf{x})] \qquad \text{2.43}$$

where Q is a non-linear piecewise continuous function, such as a sigmoid, hard limit, Gaussian, and multi-quadratic functions. The mathematical formula of those functions can be as follows.

1. Gaussian function

$$\mathbf{Q}(\mathbf{w}, b, \mathbf{x}) = exp(-b\|\mathbf{x} - \mathbf{w}\|^2) \qquad \text{2.44}$$

2. Sigmoid function

$$\mathbf{Q}(\mathbf{w}, b, \mathbf{x}) = \frac{1}{1 + exp(-(\mathbf{w}.\mathbf{x} + b))} \qquad \text{2.45}$$

3. Hard-limit function

$$\mathbf{Q}(\mathbf{w}, b, \mathbf{x}) = \begin{cases} 1, & if\ (\mathbf{w}.\mathbf{x} - b) \geq 0 \\ 0, & otherwise \end{cases} \qquad \text{2.46}$$

4. Multi-quadratic function

$$\mathbf{Q}(\mathbf{w}, b, \mathbf{x}) = (\|\mathbf{x} - \mathbf{w}\|^2 + b^2)^{1/2} \qquad \text{2.47}$$

2.3.1.4.3   Kernel-based ELM

In ELM, the feature mapping in the hidden layer g(x) can be replaced by a kernel function. Kernel matrix for ELM is defined as follows:

$$\Omega_{ELM} = \mathbf{G}\mathbf{G}^T : \Omega_{ELM\ i,j} = g(\mathbf{x}_i).g(\mathbf{x}_j) = K(\mathbf{x}_i, \mathbf{x}_j) \qquad \text{2.48}$$

Then, Eq. 2.41 would be:

$$f(\mathbf{x}) = g(\mathbf{x})\mathbf{G}^T \left(\frac{\mathbf{I}}{C} + \mathbf{G}\mathbf{G}^T\right)^{-1} \mathbf{T}$$

$$\text{2.49}$$

$$f(\mathbf{x}) = \begin{bmatrix} K(\mathbf{x},\mathbf{x}_1) \\ \vdots \\ K(\mathbf{x},\mathbf{x}_N) \end{bmatrix}^T \left(\frac{\mathbf{I}}{C} + \Omega_{ELM}\right)^{-1} \mathbf{T}$$

where and K is a kernel function as shown in Eq. 2.50 –2.52.

$$\text{Radial basis function: } K(\mathbf{x}_i, \mathbf{x}_j) = \exp(-\gamma\|x_i - x_j\|) \qquad \text{2.50}$$

$$\text{Linear: } K(\mathbf{x}_i, \mathbf{x}_j) = \mathbf{x}_i.\mathbf{x}_j \qquad \text{2.51}$$

$$\text{Polynomial: } K(\mathbf{x}_i, \mathbf{x}_j) = (\mathbf{x}_i . \mathbf{x}_j + 1)^d \qquad \qquad \textbf{2.52}$$

2.3.1.5   *Post-processing*

The aim of post-processing is to smoothen and refine the classification results. The majority vote (Kevin Englehart *et al.*, 2003) is one of the most frequent methods in this area. It utilizes the results from the present state and *n* previous states and makes a new classification result based on the class that appears most frequently. This procedure produces the finger movement class that removes fake misclassifications. However, the number of *n* votes will increase the delay time taken to generate the class output as mentioned in (T. Farrell & Weir, 2008). Besides, we should make sure that the delay time will not exceed the optimal delay time of real-time application in the range of 100 – 125 ms as recommended by T. R. Farrell and Weir (2007) or acceptable time delay recommended by Kevin Englehart *et al.* (2001), which is 300 ms.

2.3.2   Myoelectric non-pattern recognition (M-non- PR) system

The previous sections have discussed the myoelectric pattern recognition (M-PR). In this section, the myoelectric non-pattern recognition (M-non-PR) will be addressed. The M-non-PR system has similar steps as the M-PR except in the classification stage. The M-non-PR does not have it. Instead, it has different processes. Among examples of EMG-based non-pattern recognition are the threshold myoelectric control, proportional myoelectric control, simultaneous and propositional myoelectric control and finite state machine (FSM) control (Oskoei & Huosheng, 2007).

2.3.2.1   *The threshold myoelectric control*

The threshold myoelectric control is a control system that utilizes a threshold value from the contraction level of EMG signal as a control source to activate or deactivate an action. It is also known as a binary on/off myoelectric control because the threshold value determines the on or off state of the assistive device (Simon *et al.*, 2011). The early stage of EMG controller in the prosthetic device employed this controller (Popov, 1965). Besides, the majority of the current exoskeleton hands utilize the threshold controller instead of EMG based pattern recognition (Ho *et al.*, 2011; Mulas *et al.*, 2005).

2.3.2.2   Finite state machine

Finite state machine control consists of some states that the device should perform. The switching between states can be triggered by a timer or based on the level contraction of the EMG signals (Fougner *et al.*, 2012; Oskoei & Huosheng, 2007).

2.3.2.3   The proportional myoelectric control

The proportional myoelectric control gives a more advanced control scheme than the threshold myoelectric control. In this myoelectric control, the control signal for the rehabilitation device is proportional to the contraction level of the EMG signal. The control system utilizes the EMG signal to estimate a specific physical parameter such as force or angle. Afterward, the control system treats those biofeedback values as the target that the device should achieve. Figure 2.14 shows an example of the proportional controller.
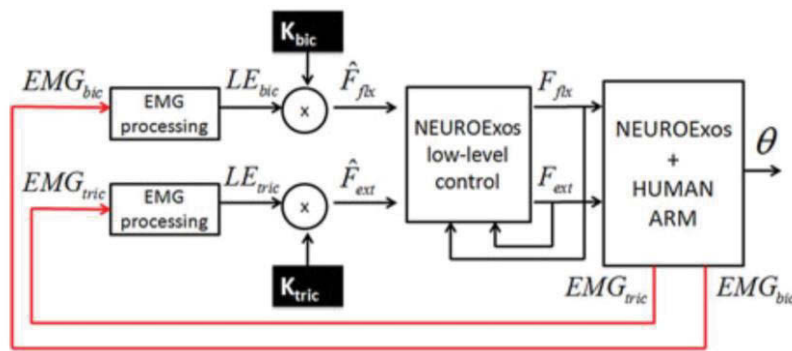
Figure 2.14 The proportional myoelectric control of Neuroexos exoskeleton (Lenzi *et al.*, 2012)

2.3.2.4   The simultaneous and proportional myoelectric control

The simultaneous and propositional myoelectric control is more advanced than the proportional one. This control system controls all joints proportionally and simultaneously from the EMG signal. To train the system, the amputees need a help form their healthy hand to produce target movement, as shown in Figure 2.15. The control system should estimate all physical parameters recorded from the raw EMG signal. Therefore, this control system is also known as regression based myoelectric system (Farina *et al.*, 2014).
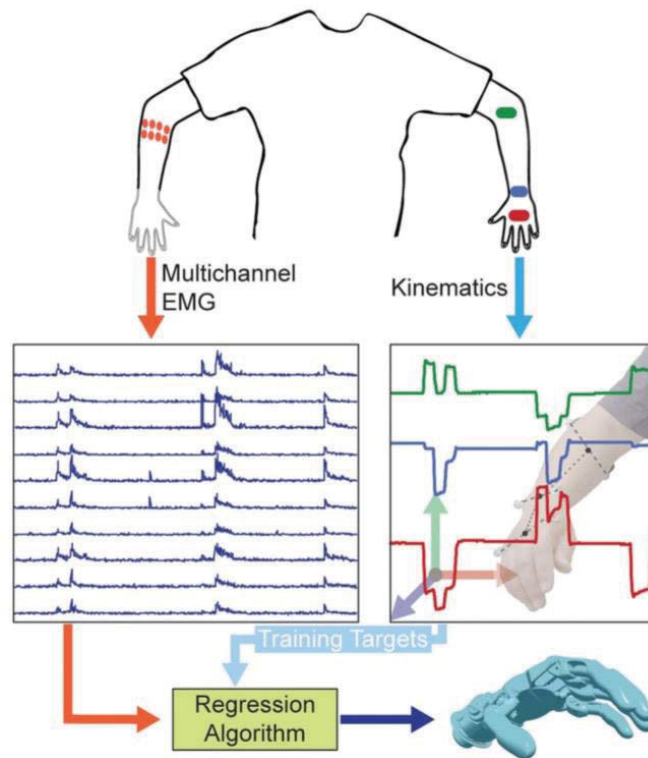
Figure 2.15 Regression based myoelectric control (Farina *et al.*, 2014)

2.4   EMG signal for hand rehabilitation devices

This thesis investigates the use of EMG signal in hand rehabilitation devices. The hand rehabilitation device considered in this thesis is a wearable robot including the prosthetic and orthotic hand devices. The prosthetic hand device is a wearable hand robot that can replace the missing hand and have the functionality of the hand replaced. Nowadays, few dexterous and commercial prosthetic hands are available. For instance, i-limb ultra by Touch Bionic. Inc and a bebionic (TouchBionics, Accessed in 2015) hand by RSLSteeper (E. Scheme & Englehart, 2011) (Figure 2.16). Furthermore, a few low-cost prosthetic hands are available as well. They are prosthetic hands from www.openbionic.org (Kontoudis *et al.*, 2014) (Figure 2.16c) and www.openhandproject.org (Figure 2.16d).

The second rehabilitation hand device discussed in this thesis is the orthotic hand. Different form the prosthetic hand, the orthotic hand resembles the user's hand. It augments or assists the hand to perform some activities. The orthotic hand is often known as an exoskeleton hand and it is a part of an active exoskeleton (Khairul Anam & Al-Jumaily, 2012). Figure 2.17 shows a "hand of hope", a commercial exoskeleton hand by rehab-robotics (http://www.rehab-robotics.com/).
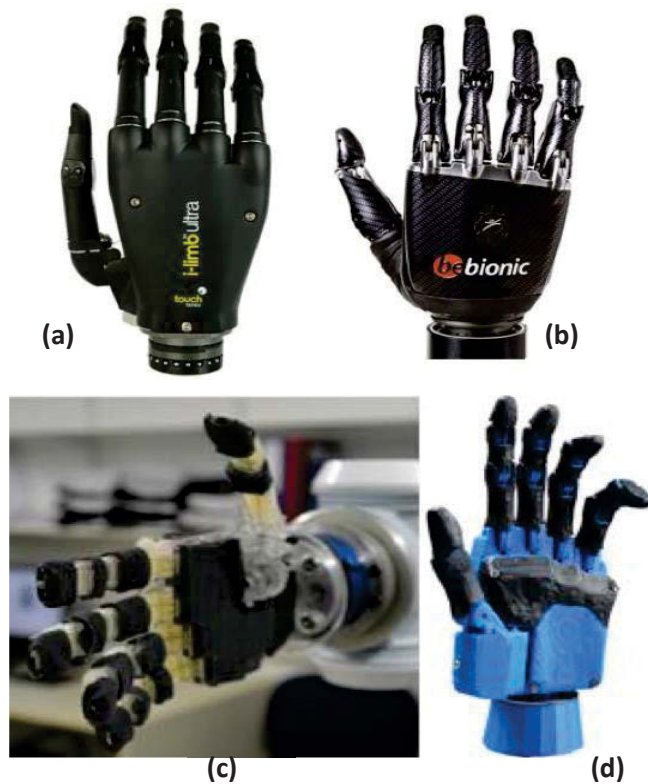
Figure 2.16 The high-cost prosthetic hands : i-limb ultra (a) and bebionic (b) and the low-cost prosthetic hands: openbionic's hand (c) and openhandproject's hand (d)
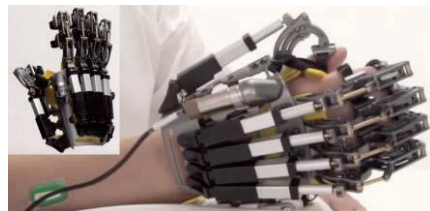
Figure 2.17 The hand of hope: a commercial exoskeleton hand

This section presents a discussion on the use of EMG in the prosthetic and exoskeleton hand. The discussion will be started with the EMG-based prosthetic hand and then followed by the EMG-based exoskeleton hand.

2.4.1 EMG-based prosthetic hand

This sub-section provides a review of prosthetic hands controlled by EMG signal. The discussion is focused on the hand movement excluding the arm movements such as shoulder, elbow and wrist movements.

2.4.1.1 The Russian EMG controlled hand

Historically, Rieter was the first person who developed an EMG controlled hand in 1948 (Jacobson *et al.*, 1982). In 1957, B Popov, a Russian researcher, began to develop a bioelectricity controlled prosthetic hand (Popov, 1965), as shown in Figure 2.18. The

40

possibility of the use of bioelectricity for controlling a prosthetic was initiated in (Battye *et al.*, 1955). This prosthetic is designated for the upper extremity. The electrodes were located in the stump. There are two movements: grasp and release. The EMG signals were collected from two opposing muscles. The hand will grasp if the exerted voltage of the flexion muscle exceeds 30-40 mV. To release or open the hand, the system will detect the opposing flexing muscle. If the recorded voltage was more than the threshold value, then the hand will open. The prosthetic hand is controlled with a threshold control system. This is a very basic myoelectric control system.
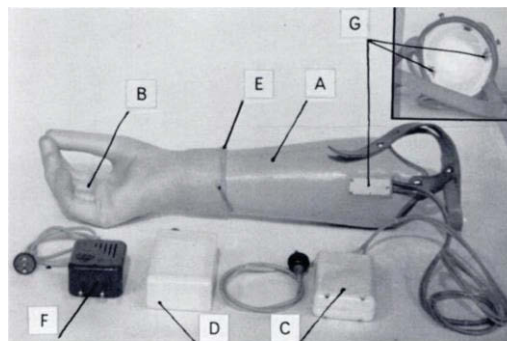
FIG. 1
The prosthesis. A=laminated plastic casing. B=hand containing drive mechanism. C=amplifier. D=feed unit which supplies power to the electric motor in the hand. E=cosmetic glove. F=battery charger. G=current-tapping device (also seen inside prosthesis in inset).

Figure 2.18 The Russian EMG controlled hand (Popov, 1965)

2.4.1.2 Suzuki 's system (Suzuki & Suematsu, 1969)

In 1969, Suzuki and Suematsu (1969) developed a more complex control system using EMG signals. They called it pattern recognition of multichannel myoelectric signals. The system classified seven kinds of hand motions using a spatial pattern collected from three EMG channels on the forearm. The system learned the pattern or the classes using the learning discrimination mechanism (Suzuki & Suematsu, 1969). Compared to the Russian EMG controller, the EMG controller is more advanced. The indication is shown by involving more motions and employing a learning mechanism to learn the pattern of EMG signals.

2.4.1.3 Uchida's system (Uchida et al., 1992)

Hiraiwa *et al.* (1989) employed a single channel EMG to classify five hand motions. They utilized the neural network to analyse and classify the EMG pattern to control a prosthetic hand. The work of Hiraiwa was continued and developed by Uchida *et al.* (1992) to deal with multichannel EMG. In their work, the electrodes were located on the forearm especially on the flexor digitorium superficialis (FDS) muscle. Five motions involved were the flexion of all fingers (A), the flexion of the index finger (B), the flexion

of the middle finger (M), the flexion of the thumb (T) and relaxation of all fingers (N). Signal was collected for 20 sec of a particular motion. They extracted fast Fourier transform (FFT) features from two electromyography (EMG) channels. The FFT of the EMG signals became the inputs of the feed-forward neural networks (FF-NN).

Using only one channel, they were able to classify five-finger movements with an accuracy of 67%. In the case of 2 EMG channels, by adding another electrode on the extensor digitorium muscle, they could improve the accuracy up to 86%. Furthermore, in order to adapt to dynamical finger movements, they conducted an additional experiment by estimating the angles of finger joints, as shown Figure 2.19. The target angles were collected from the glove worn on the hand where the electrodes were located. The results were the root mean square error that was less than 25 degrees.
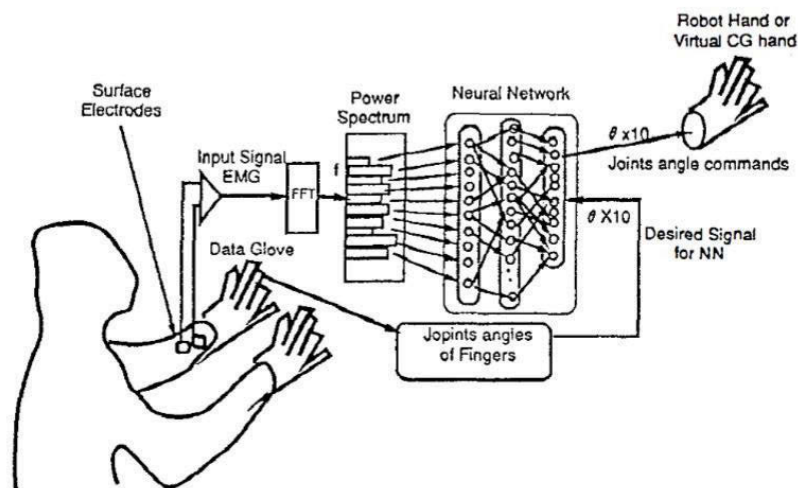
Figure 2.19 Myoelectric pattern recognition for a prosthetic hand using FFT and Artifical neural network (Uchida *et al.*, 1992)

2.4.1.4   *Tsenov's system (Tsenov et al., 2006)*

Similar to Uchida *et al.* (1992), Tsenov *et al.* (2006) developed a recognition system of finger movement using multilayer perceptron (MLP). MLP classified four finger movements: thumb, pointer, middle and hand closure. The electrodes were located on two groups of muscles, planaris longus (PL) and extensor digitorum(ED). They extracted time-domain (TD) features from EMG signals and put them on the input of the MLP. In the offline experiment, they achieved an accuracy of 93% using two EMG channels and 98% using four EMG channels. Meanwhile, in the online classification, the system showed a promising performance by making 30 errors of 250 tested movements.

2.4.1.5   Tenore's system (Tenore et al., 2009)

Tenore *et al.* (2009), researchers from John Hopkins University developed a pattern recognition system using EMG signals to decode individual finger movements. The movements consisted of the flexion and extension of all individual fingers and the middle, ring, little fingers as a group. There are 12 classes involved in the experiment. The work involved five able-bodied subjects and one transradial amputee.

Thirty-two electrodes were located in the forearm of the subject. They were divided into five different levels comprising of 32, 28, 24, 19, and 12 electrodes, as shown in Figure 2.20. The EMG pattern recognition system comprised some stages. The first stage is filtering. The EMG signals were bandpass filtered between 10 and 500 Hz. Then the EMG signals were segmented using sliding time windows of 200 ms every 25 ms. The system employed time domain (TD) feature extraction to extract features from EMG signals including the mean of the absolute value (MAV), variance, waveform length (WL), and Willson amplitude (W). Feed-forward multilayer perceptrons (MLPs) classified the features into twelve classes.
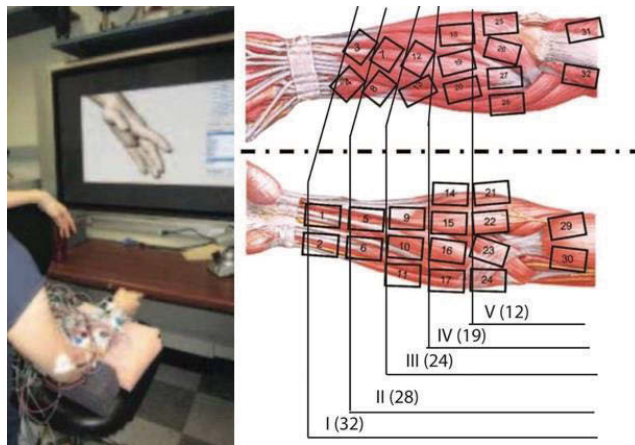
Figure 2.20 The experimental procedure (left) and the electrode positions (right) (Tenore et al., 2009)

The experiments results show that the system achieved a high level of classification accuracy (approximately 90 %). Another interesting result was that the accuracy between the able-bodied subjects and the transradial amputee was not significantly different.

2.4.1.6   Cipriani

Cipriani *et al.* (2011) developed EMG pattern recognition for a prosthetic hand. Different from the previous researcher who employed MLPs or ANN, they utilized k-nearest neighbour (kNN). The system extracted features from nine EMG channels using TD features acquired from five able-bodied and amputee subjects. There are seven hand

movements classified including thumb flexion (A), index finger flexion (B), thumb opposition (C) middle, ring, and little finger flexion (D), long fingers flexion (E), tri-digital grasp (F) and lateral grip/key grip (G), as shown in Figure 2.21.
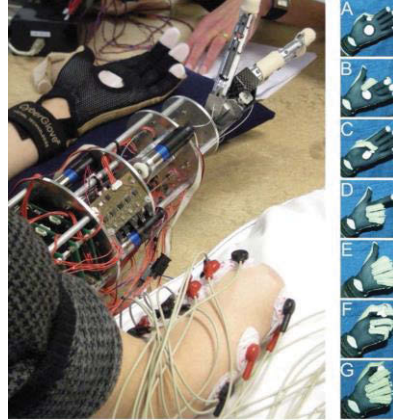
Figure 2.21 The EMG pattern recognition of Cipriani (Cipriani *et al.*, 2011)

The experiment involved 10 participants, five trans-radial amputees, and five able-bodied subjects. Eight bipolar EMG electrodes were placed on the right arm of participants or the residual limbs. For both amputees and able-bodied subjects, six electrodes were put on superficial flexor muscles, and the last two were placed on superficial extensor muscles.

The recognition system was implemented online and able to classify seven finger movements with the accuracy of around 79 % on the amputee subjects and about 89% on the non-amputee subjects.

2.4.1.7 *Khushaba*

R. N Khushaba *et al.* (2012) developed a new EMG pattern recognition system for finger movements using support vector machine (SVM) (Oskoei & Huosheng, 2008). There are ten finger movements involved, as shown in Figure 2.22. Those movements consist of the individual and combined finger movements consisting of the flexion of each of the individuated fingers, i.e., Thumb (T), Index (I), Middle (M), Ring (R), Little (L) and the pinching of combined Thumb–Index (T–I), Thumb–Middle (T–M), Thumb–Ring (T–R), Thumb–Little (T–L), and eventually the hand close (HC).
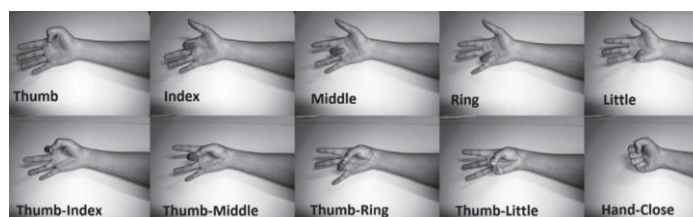
Figure 2.22 Ten finger movement involved in the experiment

The myoelectric pattern recognition employed in the experiment comprised some stages, as shown in Figure 2.23. There were eight healthy subjects involved. In the data collection, the subjects performed a finger posture, which was started from a relaxation state and then this was followed by holding a certain posture for 5 s. The subject repeated the same movement six times with 3 to 5 s resting period between trials. The collected data from six trials were divided into two groups, the training data, and the testing data. The four trials were used as the training data and the remaining trials were used as test data.
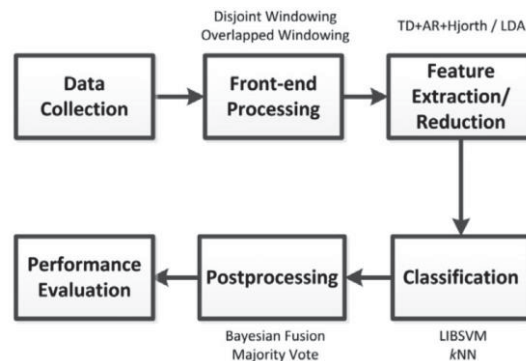
Figure 2.23 The stages of the EMG pattern recognition

Different sets of time-domain features were used (Tkach *et al.*, 2010). There were six time-domain features involved, i.e. number of zero crossings (ZC), waveform length (WL), slope sign changes (SSC), Hjorth time domain parameters (HTD), sample skewness (SS), and autoregressive (AR) model parameters. Then, the dimension of the extracted features was reduced using linear discriminant analysis (LDA).

The experimental results indicated that the system achieved an accuracy of approximately 92% in the offline classification and about 90% in the online classification. Regarding accuracy, Khushaba *et al.*'s recognition system was promising, but the system contains a natural shortcoming of SVM in dealing with the multi-classification problem. At least, the recognition system should use *m* SVMs to deal with *m* movement classes. Inevitably, this will add to the processing time of the system.

2.4.1.8 *Al-Timemy*

The most recent study of a pattern-recognition system on finger movement classification was undertaken by Al-Timemy *et al.* (2013). They investigated several schemes for the EMG pattern recognition, as shown in Figure 2.24. The developed system extracted features from six up to twelve EMG channels using TD and AR features. There were four combinations of dimensionality reductions and classifiers employed. They are

principal component analysis (PCA)-linear discriminant analysis (LDA), PCA-SVM, orthogonal fuzzy neighbourhood discriminant analysis (R. N. Khushaba *et al.*, 2010) (OFNDA)-LDA and OFNDA-SVM. Those systems classified 12 and 15 movement classes on six amputees and ten able-bodied subjects, respectively.
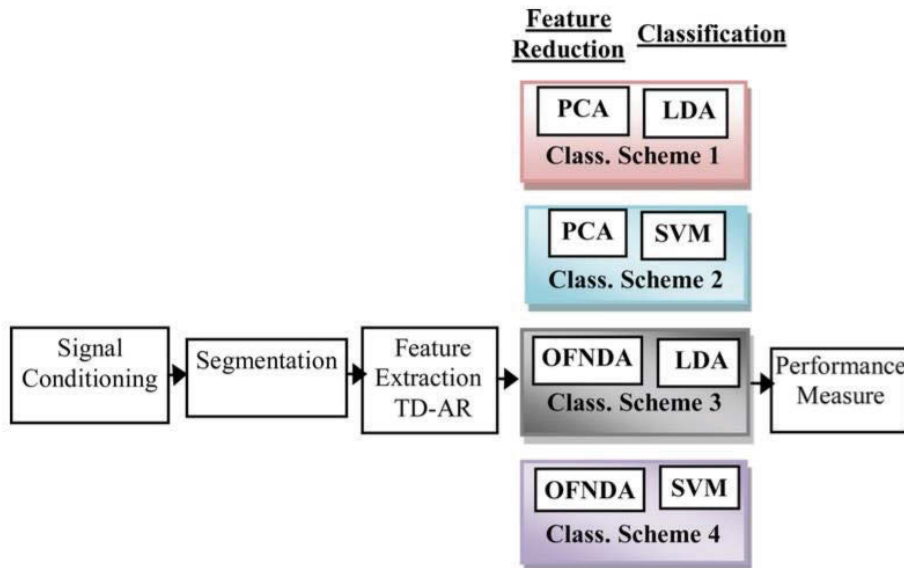
Figure 2.24 Various schemes of the myoelectric pattern recognition investigated

The most accurate of the four combinations was the system with OFNDA-LDA. The system succeeded in achieving an average accuracy of around 98% on the able-bodied subjects and approximately 90% on the amputee subjects. However, there was a significant accuracy gap between the able-bodied and amputee subjects.

2.4.2   EMG-based exoskeleton hand

This section presents a review on the current EMG-based exoskeleton hand.

2.4.2.1   *Mulas's exoskeleton (Mulas et al., 2005)*

Mulas's exoskeleton is a exoskeleton hand that is designed for the hand recovery of a patient after a stroke or other motor diseases, as depicted in Figure 2.25. The EMG signals obtained from the subject's forearm are used to predict the user's intention to perform a certain task or activity. The exoskeleton is composed of a glove with plastic support to guide the fingers to accomplish a natural movement and avoid getting an excessive load on the tips. It is actuated by two electric motors that are hitec servos HS-8-5BB. One actuator is used to flex the thumb while the other is used to flex the four fingers simultaneously. Two springs on the dorsal side were put in to allow extension movements.
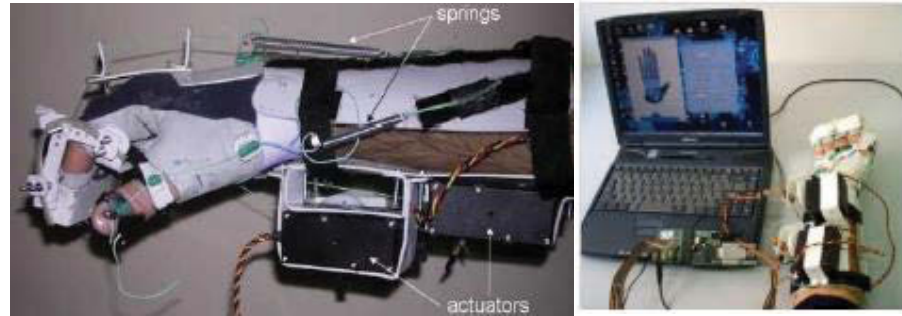
Figure 2.25 The Mulas's exoskeleton hand

The main controller runs on the personal computer (PC) using MALTAB. The PC obtains the user's intention from the EMG signals acquired from two electrodes that capture the signals from the Flexor Digitorum Superficialis and the Flexor Flexor Pollicis Longus as shown in Figure 2.26. Then the output control from the PC was fed to the microcontroller to control the finger movements according to the intended position. In the hierarchical structure, the microcontroller behaves as a low-level controller while the PC behaves as a high-level controller.
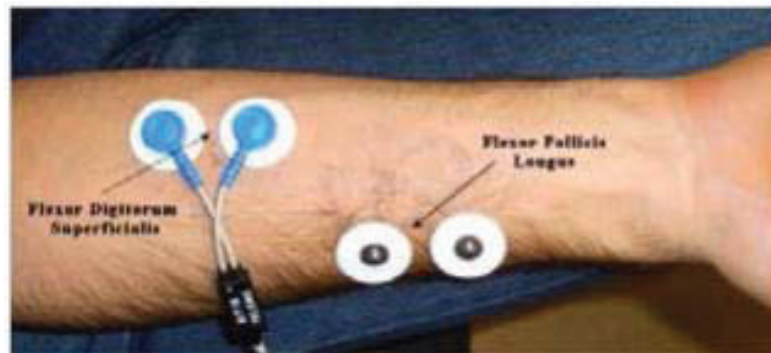
Figure 2.26 The placement of the electrodes

The EMG signals were sampled at 500 Hz and rectified and filtered using the second-order filter. The threshold of 50 mV was applied to the rectified EMG signal to distinguish the real electrical activity from the noise. If the signals exceed the threshold value, the actuator will start to flex the fingers of the exoskeleton. The speed of the finger movements depends on the angle of the fingers that goes to zero when the finger fully flexed and proportionally increases while the fingers are opening.

Some shortcomings could be noticed from this exoskeleton. Firstly, the four fingers are controlled simultaneously. The individual finger should be able to be controlled separately to allow more comprehensive therapy. Even the finger combination movement should be involved to achieve better therapies. In other words, the control system only deals with a simple functional task and it is not able to work on more complex movements.

2.4.2.2   Wege's exoskeleton hand (Wege & Zimmermann, 2007)

This exoskeleton hand was developed to support the rehabilitation process for the patient after a stroke or hand injuries. It has four degrees of freedom in each finger, the flexion and extension of the metacarpophalangeal (MCP) joint, proximal interphalangeal (PIP) joint, and distal interphalangeal (DIP) joint; and abduction/adduction in the MCP joint, as depicted in Figure 2.27. The thumb can move in four degrees of freedom. The carpometacarpal joint (CM) is supported in flexion/extension and abduction/adduction movement, metacarpophalangeal (MC), and the interphalangeal (IP) joint are supported in their flexion movement. Therefore, in total, it supports up to 20 finger joints.
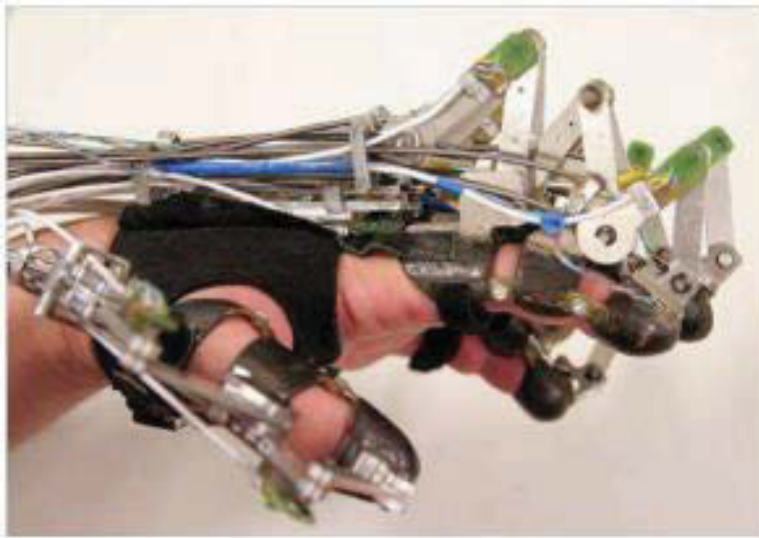
Figure 2.27 The wege's exoskeleton hand

The system is equipped with some sensors such as hall sensors to measure joint angles, optical encoders to measure angles of motor axes, and force sensors to measure the force between human and machine. These force sensors were placed between the finger attachments and the levers. Other sensors are surface Electromyography sensors at the forearm. Electromyography (EMG) electrodes can measure the electrical activity in the skin of up to sixteen muscles. The control system of the hand is described in Figure 2.28.
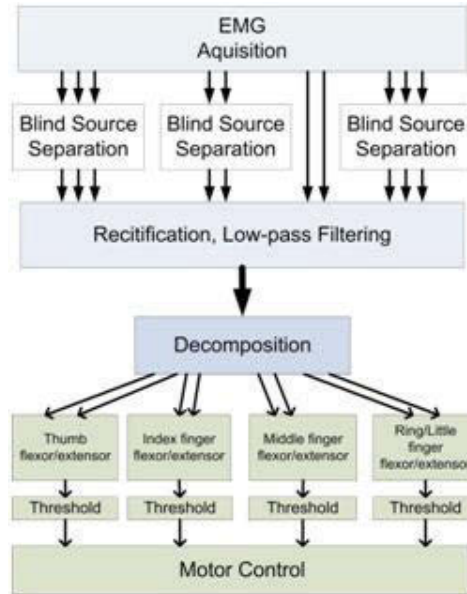
Figure 2.28 Control diagram of the Wege's exoskeleton

This exoskeleton hand employed the blind source separation, as shown in Figure 2.28, to separate the information contained in the high-density surface EMG signals at the forearm into several signals related to specific finger movement. Ten electrodes were located in the forearm, as shown in Figure 2.29, such that it acquired the signals from:

- Flexor digitorium superficialis which is responsible for finger flexion at MCP and PIP joints
- Flexor policis longus which is partly responsible for the flexion of the thumb
- Extensor digitorum which is responsible for the extension of all digits
- Extensor pollicis which is responsible for the extension of the thumb
- Extensor indicis which is only responsible for the extension of the index finger.

Figure 2.29 The electrode placement for the wege's exoskeleton hand

Some drawbacks are apparent in this exoskeleton. The control scheme is not very practical (as mentioned by the authors) because of the following reasons. Firstly, the placement of the electrodes was the major issue and was critical. In addition, the wrist should be fixed to avoid any wrist movement including pronation and supination. Secondly, the blind source separation was not working properly. More EMG sensors were needed to achieve a more promising blind separation result.

2.4.2.3 Tong's exoskeleton (Ho et al., 2011)

This exoskeleton was designed as a hand robotic training device to help people after stroke to train their impaired hand function. This device is able to detect the user's intention from the user's muscles in the hand opening and closing training. The exoskeleton's structure fits the different finger lengths and aligns the virtual centre of rotation of the metacarpophalangeal (MCP) and the proximal interphalangeal (PIP) as shown in the Figure 2.30 and Figure 2.31. It consists of 5 linear actuators, the palm support platform, and 2 degrees of freedom that are able to rotate 55 degrees and 65 degree range of motion for the MCP and PIP, respectively.
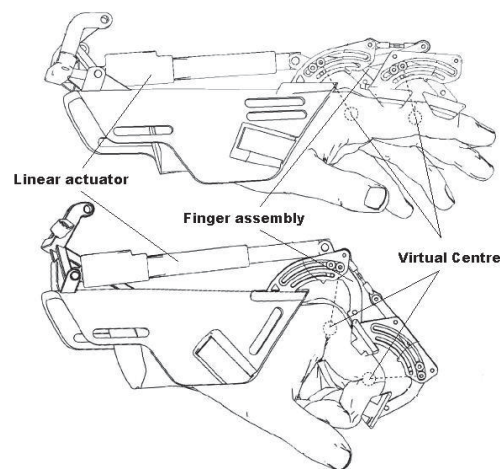
Figure 2.30 Mechanical design of Tong's exoskeleton hand
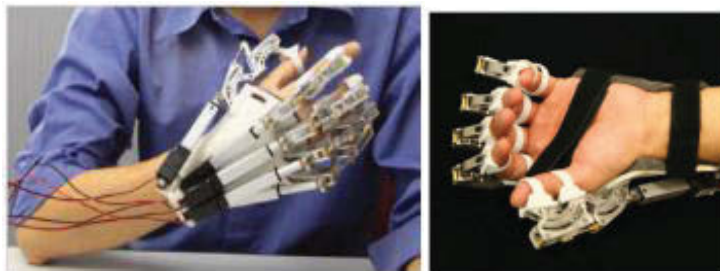
Figure 2.31 The Tong's exoskeleton hand

The embedded controller is built to accompany the hand module that drives the linear actuator and detect the user's intention by interpreting the surface EMG signals that are acquired from the abductor pollicis brevis (APB) and the extensor digitorum (ED) from the impaired hand, as shown in Figure 2.32. The signals from APB and ED that were sampled at 1 kHz were used to predict the hand closing and hand opening task respectively. The embedded controller was equipped with a wireless module to enable the therapist to configure the exoskeleton and the training module.
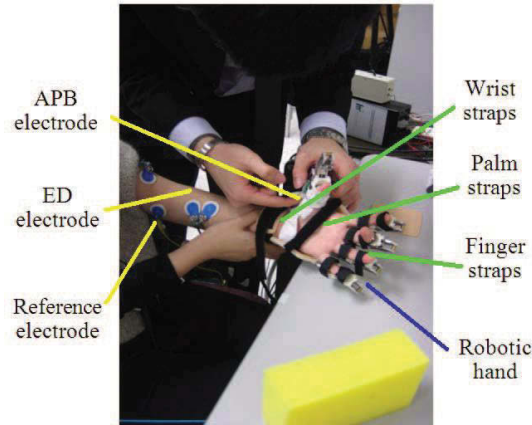
Figure 2.32 The electrode placement for the Tong's exoskeleton hand

The training module in this exoskeleton was an EMG-triggered training mode. The hand opening and the hand closing action were obtained by applying the threshold of 20 % of the maximum voluntary contraction (MVC) from the APB and ED muscle respectively. When the hand closing intention was detected, the hand started closing until the EMG muscle from the APB muscle exceeded the 20 % of its MVC value. Likewise, the exoskeleton hand opened the hand when the EMG signals from the ED exceeded the 20 % of its MVC value.

Different control systems were implemented on this exoskeleton (Tong *et al.*, 2010) such as the continuous passive motion (CPM), the EMG-triggered motion (TRIG), the continuous EMG-driven motion (CONT), and the Free-running mode (FREE). In the CPM mode, the hand opening or closing tasks were passively done and did not require any voluntary effort from the user.

In the TRIG mode, the hand opening and the hand closing action were initiated when the measured EMG signals were above the threshold of 20 % of the maximum voluntary contraction (MVC) from the APB and ED muscle respectively. When the hand closing intention was detected, the hand started closing until the EMG muscle from the APB muscle exceeded the 20 % of its MVC value. Likewise, the exoskeleton hand opened the hand when the EMG signals from the ED exceeded the 20 % of its MVC value.

In the CONT mode, the user's effort is needed to complete the full range of the function task because the exoskeleton hand performs the task step by step. If it is the hand closing, for example, the exoskeleton will close the hand step by step every time the measured EMG signal from the APB is above the threshold.

Meanwhile, the FREE mode is implemented on the user who has better motor control and coordination. The strength of EMG signal from APD and ED will be compared to

initiate the functional motion task. If the APB is stronger than the ED, then a hand closing is initiated. On the other hand, if the ED is stronger than the APB, then a hand opening is initiated. Therefore, this mode enables the user to use their own intentions in doing the functional tasks.

The diversity of the EMG control modes in this exoskeleton improves the efficacy of its implementation. However, a significant drawback still exists. All fingers are actuated and moved simultaneously. Even though it is comprised of 5 linear actuators for each finger, the control strategies did not allow each finger to move individually.

2.4.2.4 *Ngeo's finger exoskeleton (Ngeo et al., 2013)*

This finger exoskeleton is constructed of a four-bar linkage structure that is able to actuate the movement at MCP, PIP and DIP joints, as depicted in Figure 2.33. The Arduino Mega micro-controller was used to control the movement of the exoskeleton based on the motor command obtained from the processed EMG signals. The surface EMG from the Flexor Digitorum Superficialis (FDS), Flexor Digitorum Profundus (FDP), Extensor Digitorium (ED) and Extensor Indicies (EI) muscles were acquired and processed to predict the motor intention of the continuously moving fingers that was represented by the angle of the index finger.
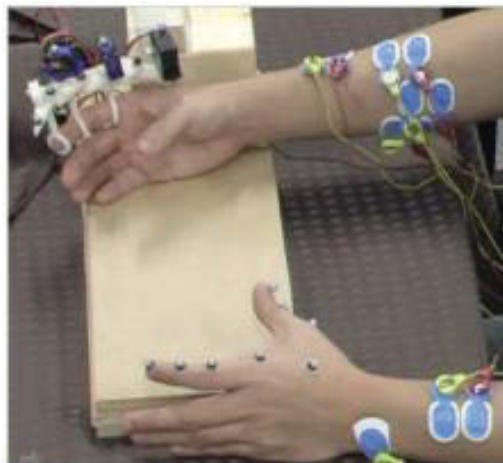
Figure 2.33 Finger exoskeleton

Each surface EMG signal was converted to a muscle activation by using the so-called EMG-to-muscle activation model proposed by Buchanan *et al.* (2004). The muscle activations from each muscle were fed to the artificial neural network (ANN) to predict the intended finger joint angle. The feed-forward neural networks composed of three layers: an input layer with four nodes from four targeted muscles, a single hidden layer and a single linear output with 3 to 6 nodes, were used.

The experimental result was good and promising even though it was only tested on a healthy subject. The drawback of this system is obviously working on one finger only. The complexity and density of the muscles in the forearm have not been considered yet. Another example of EMG controller for index finger was proposed by Khairul Anam *et al.* (2014)

2.5 Summary

Basic theory of the physiology of the hand, the muscle controlling the hand and the electric signal generated by the muscle activities have been presented in detail in this chapter. In addition, this chapter addressed different methods used to take benefit of the bio-signals of muscles or electromyography or myoelectric signal on different hand rehabilitation devices.

Myoelectric pattern recognition (M-PR) for finger movement is used in most current prosthetic hands. The major issue emerging in the M-PR for a prosthetic hand is the big gap between the real success of the laboratory experiments and the clinical applications. Farina *et al.* (2014) noted that the primary causes of the gap are related to the robustness of M-PR in the clinical applications. Ning *et al.* (2012) explained that the robustness of M-PR can be achieved by fulfilling four conditions. Firstly, major M-PRs should provide the simultaneous and proportional controller that can handle multi-degrees of freedom. Secondly, M-PR has to have sensory feedback. Thirdly, M-PR should adapt to the changes of EMG signal characteristic, and the last, M-PR should integrate with sensor modalities to allow complex actions.

As for the exoskeleton hand, myoelectric non-pattern recognition (M-non-PR) is widely used instead of M-PR. Most of the exoskeleton hands employ a myoelectric threshold controller. As a result, the hand or finger actions involved are very limited. Most of them are the hand opening and hand closing only. In reality, the finger movements are not limited to two of those actions only. The exoskeleton hand should consider more finger motions instead of just two fingers.

The research conducted in this thesis will consider the robustness issue in M-PR. The limitation of myoelectric control in the exoskeleton hand will be discussed as well. In myoelectric pattern recognition (M-PR), this thesis proposes various methods to improve the performance of M-PR by proposing classifiers and a feature projection method that will be discussed in **Chapter 3** and **Chapter 4**. Meanwhile, **Chapter 5** provides efforts

to improve the robustness of M-PR by developing an M-PR that adapts to the changes of the characteristic of EMG signals. Furthermore, this thesis develops a new myoelectric controller for an exoskeleton hand that could work on five individual fingers and five-finger combinations, as will be discussed in **Chapter 5**.

The main metric to measure the success of the M-PR in the laboratory and clinical application is either an error or accuracy of the classification result. These measurements (error or accuracy) is used to judge the efficacy of the proposed M-PR as an attempt to reduce the gap between the laboratory experiment and clinical application. To the best of the author's knowledge, the majority of researchers have used this metric for years. Nevertheless, there is little improvement in the error metric by proposing incorrect active decisions instead of using wrong decision only, as proposed by E. J. Scheme *et al.* (2011). Therefore, the error or accuracy are the primary measurement used to verify the efficacy of the M-PR. This thesis employs accuracy as the primary metric to measure the efficacy of all proposed methods.

CHAPTER 3

Extreme Learning Machine-Based Classification of Finger Movements Using Surface Electromyography

3.1 Introduction

The main aim of the research in this doctoral thesis is to develop a robust myoelectric controller for a hand rehabilitation device in a real-time application. Before considering real-time implementation, the research investigates a novel myoelectric pattern recognition that is highly accurate and can work well in amputees and non-amputees.

In this chapter, the proposed myoelectric pattern recognition system will be based on the state-of-the-art of the pattern recognition system. The success of myoelectric pattern recognition mostly depends on two factors, i.e. feature, and classification. In the feature extraction, the focus will be on finding the best feature set of time domain features and autoregressive features. As for the classification, the investigation will be on the efficacy, and feasibility of single layer feedforward networks (SLFNs) named extreme learning machine (ELM) as a classifier in the myoelectric pattern recognition system. Therefore, Chapter 3 will focus on the classifier and features as it has been introduced at the end of Chapter 2.

Some experiments will be involved to figure out the optimal myoelectric pattern recognition for finger movements. Following the state-of-the-art of myoelectric pattern recognition system, this chapter will be started with the discussion of the proposed recognition system as discussed in **section 3.2**. Then, the experiments and the results are discussed in **section 3.3**. Finally, this chapter will end with discussion and summary in **section 3.4** and **section 3.5**, respectively.

The contribution of this chapter is in providing an accurate and optimal M-PR system for recognizing complex finger movements consisting of individual and combined finger movements that can work well on amputees and non-amputees.

3.2 Evaluation of ELM-based myoelectric finger recognition for amputees and non-amputees

In this section, the classification of the finger movements utilizes a state-of-the-art of pattern recognition system for myoelectric (MES) or electromyography (EMG) signals as shown in Figure 3.1. The following sections will describe the stages involved in the figure. In addition, this section will involve different kinds of ELM. In general, there are two groups of ELM based on the structure of the network, the node-based ELM, and kernel-based ELM. This chapter will discuss two node-based ELMs (sigmoid ELM and radial basis ELM), and three kernel-based ELMs (linear ELM, polynomial ELM and radial-basis-function ELM). Moreover, this chapter will compare the performance of ELMs with other famous classifiers such as the SVM, least square SVM (LS-SVM), linear discriminant analysis (LDA), and k-nearest neighbour (KNN).
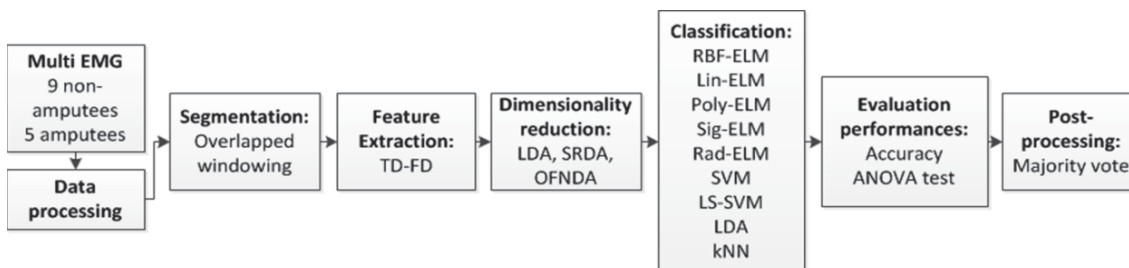
Figure 3.1 The proposed pattern recognition for classifying finger movements

3.2.1 Data acquisition and processing

3.2.1.1 Subjects

EMG signals employed in this proposed system were collected by Al-Timemy *et al.* (2013). Nine able-bodied subjects, six males and three females aged 21–35 years and five traumatic below-elbow amputees aged 25–35 years participated in the data collection. Table 3.1 presents the demographics of the amputees. The electromyography signals came from twelve pairs of self-adhesive Ag-AgCl electrodes forming twelve EMG channels that were located on the right forearms of the intact-limbed subjects. Meantime, the amputees used eleven electrode pairs placed on the forearms by considering different levels of trans-radial amputation. Figure 3.2 depicts the placement of the electrodes.

56

Table 3.1. Demographics of the amputees involved in the experiment

ID	Age (year)	Missing hand	Dominant hand	Stump length (cm)	Stump circumference (cm)	Time since amputation (year)
A1	25	Left	Right	13	27	4
A2	33	Left	Right	18	24	6
A3	27	Left	Right	16	23	4
A4	35	Left	Right	23	26	8
A5	29	Left	Right	24	26	7

Non-amputee subject   Amputee subject
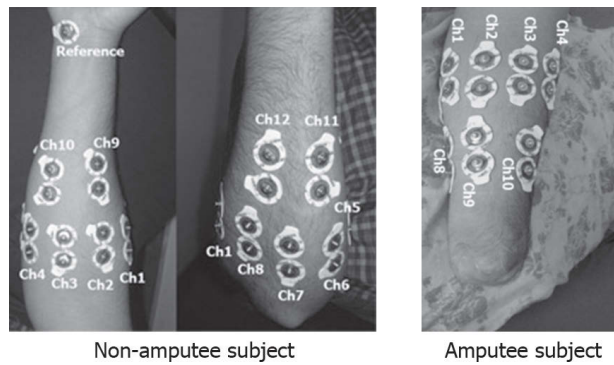
Figure 3.2 Electrode's position of an intact-limbed subject and an amputee subject

3.2.1.2 Acquisition Device

A custom-built multichannel EMG acquisition device developed by Al-Timemy *et al.* (2013) was used to record the EMG signals. It consists of a 1000-gain factor amplifier for each channel and two analogue filters (a fourth-order Butterworth low-pass filter with cut-off frequency of 450 Hz and a second-order Butterworth high-pass filter with cut-off frequency of 10 Hz). Also, it is equipped with a USB data acquisition device (National Instruments USB-6210) with a sample rate of 2000 Hz and 16-bit resolution. Furthermore, the device has two digital filters, a pass-band frequency 20–450 Hz and a fifth-order Butterworth notch filter at 50 Hz. The acquired EMG signals were displayed and stored in the PC(personal computer) using National Instruments LABVIEW. The EMG signals collected were down-sampled to 1000 Hz.

3.2.1.3 Acquisition Protocol

The non-amputee subjects were instructed to perform fifteen (15) actual finger movements. As for the amputee subjects, they were asked to imagine moving their fingers representing twelve (12) finger movements. The fifteen finger movements consisted of eleven individual finger movements, three combined ones, and one rest state. Different from the able-bodied subjects, the amputee subjects were asked to perform eleven (11) individual finger movements, as on the able-bodied subjects, and one rest state (R). The

individual finger movements comprise a thumb abduction (Ta), thumb flexion (Tf), index flexion (If), and middle flexion (Mf). Then ring flexion (Rf), and little flexion (Lf). Moreover, it involved thumb extension (Te), index extension (Ie), middle extension (Me), ring extension (Re), and little extension (Le). As for the combined movements, they consisted of little and ring flexion (LRf), index, middle and ring flexion (IMRf), and middle, ring and little flexion (IMRLf). The normal subjects performed these combined movements only.

During the data recording, the users were sitting on a chair in front of a personal computer. The subjects put their arms on a pillow and produced distinct finger movements subsequently. They had a rest of 5-10 seconds between two consecutive movements. The final movement took 8–12 seconds for normal-limbed subjects and 5–10 seconds for amputees. As a note, Amputees A1 and A2 performed movements of 3–4 seconds shorter than the rest of the amputees. Moreover, each movement was repeated six times. All trials in a movement were combined and labeled with a class related to the movement.

3.2.1.4   The Channel Number

The number of channels utilized in myoelectric pattern recognition influences the performance of the system. This subsection would like to investigate its influence and observe the feasibility of using fewer channels for finger movement recognition. In this chapter, the electrode locations were positioned on the limb in such a way that the number of electrodes on extension and flexion muscles is the same or similar. This method is similar to symmetrical channel reduction used in (L.J. Hargrove *et al.*, 2007). Other techniques can be utilized to choose the best channel combination when considering channel reduction. Examples are the straightforward exhaustive search algorithm (Li *et al.*, 2010) which explores all possible electrode combinations, and the channel elimination (Al-Timemy *et al.*, 2013) which eliminates the least contribution channel in each elimination iteration.

3.2.1.5   Data Segmentation

In general, the data or signal can be segmented in two ways: either as a disjoint or overlapped windowing. The disjoint windowing only associates with the window length. On the other hand, the overlapped windowing is associated with the window length and window increment. The window increment is a period between two consecutive windows. In general, the disjoint windowing is overlapped windowing in a condition where the

window increment is equal to the window length. Also, the window increment should not be more than the window length (Oskoei & Huosheng, 2008). Moreover, it should not be greater than the total time of the recognition system (Oskoei & Huosheng, 2007).

The determination of window length should consider the optimal delay time of a myoelectric control system (MCS), as defined by Farrell and Weir (T. Farrell & Weir, 2008) as:

$$D = \frac{1}{2}T_{wl} + \frac{n}{2}T_{inc} + \tau \qquad \qquad 3.1$$

where D is the MCS delay time, and T_{wl} is the length of the window. Meanwhile T_{inc} is the increment of the window, n is the number of votes in the post-processing stage and τ is the processing time taken by a pattern-recognition system.

In addition to the segmentation method, the features are extracted from the signal on the steady state of the muscle contraction excluding the transient state. The classification process on the transient state necessitates muscle contraction from the rest state. In fact, in a real-time application, the switching happens from one movement to another, not from the rest state. Moreover, Kevin Englehart *et al.* (2001) found that the classification performance of the steady state outperforms that of the transient state. However, ignoring the transient state will reduce the robustness of the pattern recognition.

3.2.2 Feature Extraction

Time domain (TD) and autoregressive (AR) features provide a robust feature set for an EMG signal recognition system (L.J. Hargrove *et al.*, 2007; Tkach *et al.*, 2010). A single TD feature does not offer enough features for the classifier to identify the intended movement properly (Oskoei & Huosheng, 2008). Therefore, the combination of several TDs and AR should be considered in designing an effective classification system.

This chapter combines a new feature set consisted of SSC (slope sign changes), ZC (zero crossing), WL (waveform length), HTD (Hjorth time-domain parameters), SS (sample skewness), MAV (mean absolute value), MAVS (mean absolute value slope), RMS (root mean square), and sixth order of autoregressive model (AR6). The new feature set was tested on ten different window lengths. Then, its performance was compared to other well-known feature sets, such as the feature set of Hudgin (MAV+MAVS+SSC+ZC+WL) (Hudgins *et al.*, 1993), Englehart (MAV+ZC+SSC+WL) (Kevin Englehart & Hudgins, 2003), Khushaba (SSC+ZC+WL+HTD+SKW+

AR5+MAV) (R. N Khushaba *et al.*, 2012) and Hargrove (MAV+MAVS+SSC+ ZC+Wl+RMS+AR5) (L.J. Hargrove *et al.*, 2007). As for the theoretical explanation of these features, the reader can refer to **section 2.3.1.2.**

3.2.3　Dimensionality Reduction

All features extracted from all EMG channels are concatenated to form a large feature set. As a result, the dimension of the feature set is enormous and needs to be reduced without compromising the information contained in the original features. To reduce the feature dimension, the experiments in this chapter employed supervised feature projections that is linear discriminant analysis (LDA) (Fukunaga, 2013). Besides, this chapter employed the extension of LDA, which are spectral regression discriminant analysis (SRDA) (D. Cai *et al.*, 2008), and orthogonal fuzzy neighbourhood discriminant analysis (OFNDA) (R. N. Khushaba *et al.*, 2010). In LDA, the feature sets are reduced and projected to *c-1* features where *c* is the number of classes. As for the basic theory, the reader can refer to **section 2.3.1.3**.

3.2.4　Classification using Extreme Learning Machine (ELM)

This work investigates the performance of extreme learning machine (ELM) (see section 2.3.1.4.1 for the ELM's theory) in finger movement classification. In general, the ELM can be divided into two groups, node-based ELM and kernel-based ELM. They are different in the feature mapping. The node-based ELM utilizes hidden layer nodes to map the features while the kernel-based ELM employs the kernel function. The work in this chapter used a sigmoid-additive hidden node (Sig-ELM) and a multi-quadratic radial-basis-function hidden node (Rad-ELM) for the node-based ELM. As for the kernel-based ELM, the work employed linear (Lin-EM), polynomial (Poly-ELM), and RBF kernels (RBF-ELM).

Some experiments were performed to compare classification performances among different types of ELMs with respect to the classification accuracy. Besides, comparison with other well-known classifiers, such as the SVM, LS-SVM, kNN and LDA, was also carried out. Also, except for kNN and LDA, the SVM, and the kernel-based ELM require parameter optimization. The RBF kernel, for example, consists of the cost parameter C and kernel parameter γ. G. B. Huang *et al.* (2012) noted that the combination of (C,γ) greatly affects the performance of the SVM and ELM.

In this work, the parameter adjustments were selected using a coarse grid-search method (Chang & Lin, 2011). The parameter ranges of C and γ are mostly dissimilar between one classifier and another. For the SVM and LS-SVM, the C and γ ranges were the same, that is $(2^{-9}, 2^{-8},\ldots, 2^9, 2^{10})$. Meanwhile, the parameter ranges of the other kernel-based ELMs were as follows: the linear kernel $C = (2^{-4}, 2^{-3}, \ldots, 2^4, 2^5)$; the polynomial kernel $C = (2^{-4}, 2^{-3}, \ldots, 2^4, 2^5)$ and $d = (2^{-5}, 2^{-4}, \ldots, 2^8, 2^9)$, and the RBF kernel $C = (2^{-9}, 2^{-8}, \ldots, 2^9, 2^{10})$ and $\gamma = (2^{-19}, 2^{-18}, \ldots, 2^7, 2^8)$.

Different from the kernel-based ELM, the non-kernel-based ELM does not strictly depend on specific parameters. In the ELM, the hidden layer parameters were randomly generated based on uniform distribution. Nevertheless, the user needs to select C and the number of hidden layers L. Fortunately, the combination of (L,C) does not affect the generalization performance as long as the number of hidden nodes L is large enough (G. B. Huang *et al.*, 2012). In this work, L = 2000 was chosen. As for the range parameter of C, it was varied among $(2^{-9}, 2^{-8},\ldots, 2^{29}, 2^{30})$, and it was selected using the coarse grid search method.

In the offline mode, the classification employs the aforementioned optimal parameters. The classification process was verified using a four-fold cross-validation in all experiments. The accuracy formulated in Eq. **3.2** was used to measure the performance of the classifier in recognizing the finger movements. Furthermore, the analysis of variance test (ANOVA) was used to statistically examine the significance of the proposed system.

$$Accuracy = \frac{Number\ of\ correct\ samples}{Total\ number\ of\ testing\ samples}\ x\ 100\ \% \qquad 3.2$$

3.2.5   Post-processing

The myoelectric pattern recognition (M-PR) system can employ a majority vote to refine the classification result and reduce the misclassification rate. However, the use of the majority vote produces delay time that should be kept under the acceptable delay which is 300 ms (Kevin Englehart & Hudgins, 2003). Alternatively, the M-PR can design the system to comply with the optimal delay of the myoelectric control system, which is 100-125 ms for the 90-percent of users or 100-175 ms for the average users (T. R. Farrell & Weir, 2007). In this work, the optimal number of *n* votes was determined by varying the number of *n* from 0 to the maximum allowable *n* that can be calculated using:

$$n_{max} = \frac{2}{T_{inc}} \left(D_{max} - \frac{1}{2} T_{wl} - \tau \right)$$

<div align="right">3.3</div>

where n_{max} = n maximum votes, T_{inc} = window increment (ms), T_{wl} = window length (ms), τ = processing time taken to generate the output (ms), and D_{max} = maximum delay time (ms).

3.2.6   Simulation Environment

The collected data were huge and took much time and computing power to process. Therefore, the pattern-recognition systems of the finger movements on the non-amputee and amputee subjects were carried out using a high-performance computer with a nine core Intel Xeon, 3.47-GHz CPU with 94.5-GB RAM running MATLAB 8.20 64-bit. The recognition system code was implemented in m-file MATLAB. The codes involved some libraries from myoelectric toolbox (A. D. C. Chan & Green, 2007), BioSig toolbox (Schlogl & Brunner, 2008), and the ELM source code (G. B. Huang *et al.*, 2012). Meanwhile, the codes of other classifiers for comparisons, such as LDA, the SVM, LS-SVM, and kNN, were obtained from the MATLAB package.

3.3   Experiments and Results

In this section, the results of several experiments are presented and analysed. The first part is the examination of the number of channels. A four-fold cross-validation method was used to validate the classification performance in all experiments.

3.3.1   The Number of channels

This section aims to investigate the classification performance based on the number of channels from one up to twelve (12) channels across nine normal-limbed subjects. It also investigates the performance of an eleven-channel experiment across five amputees. The goal is to classify fifteen (15) and twelve (12) finger movements from nine normal-limbed subjects and five amputees, respectively. In this section, the myoelectric pattern recognition (M-PR) system employed Khusaba's feature set (SSC+ZC+WL+HTD+SKW+AR5+MAV) (R. N Khushaba *et al.*, 2012) with 200 ms window length shifted by 50 ms window increment. SRDA (spectral regression discriminant analysis) is used to reduce the feature dimension while RBF-ELM (ELM with radial basis kernel) is used as the classifier. No post-processing was involved after

classification. The classification performances are assessed using average classification accuracy as described in Figure 3.3.

Figure 3.3 shows the performance comparison of the channel-number experiments across nine non-amputee subjects and five amputee subjects. The figure presents an interesting finding in the non-amputee subjects. The accuracy is very low when the system employed the small channel numbers, but it increased rapidly as the channel number rose up to six channels. Interestingly, the accuracy stayed constant at roughly 98 % on the number of channels more than six. Similarly, on the amputee subjects, the accuracy swiftly increased up to six channels at about 96%. However, it increased insignificantly on the number of channels more than six and reached the maximum accuracy when using 11 channels at roughly 97%
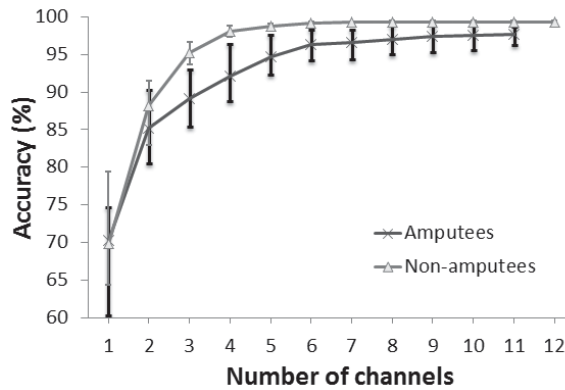
Figure 3.3 Accuracy of the number of channel experiments across nine able-bodied subjects and five amputees using four-fold cross validation

A statistical test using one-way ANOVA with a significance level set at $p = 0.05$ was conducted on the classification accuracy across all subjects. It shows that on the non-amputee and amputee people, the accuracy of six-channel trial and more than six-channel trials are not significantly different ($p > 0.05$). Based on these results, the subsequent experiments will explore the classification performances of the six-channel case and 11-channel case for the non-amputee and amputee subjects.

3.3.2 Window Length

The goal of this experiment is to find the optimal window length for finger classification by varying the window length from 50 to 500 milliseconds (ms) with fixed window increment of 50 ms. In this trial, the M-PR system employed six EMG channels from able-bodied and amputee subjects. Besides, the work utilized the feature set of Khushaba (SSC+ZC+WL+HTD+SKW+AR5+MAV) (R. N Khushaba *et al.*, 2012). The dimension of the extracted features was reduced using SRDA. RBF-ELM was utilized to

identify ten finger movements. No post-processing was involved after classification. The experiment results are presented in Figure 3.4.

Figure 3.4 shows that the average accuracy increases as the window length increases. Thus, the experiment using maximum window length achieves the best accuracy. However, the maximum window length does not always determine it as the optimum window length. Smith *et al.* (2011) advised that the optimal window length should be between 150 ms and 250 ms. As shown in Figure 3.4, in this range, the average accuracy is 96 – 98% and 92 – 94% in non-amputee and amputee subjects, respectively.
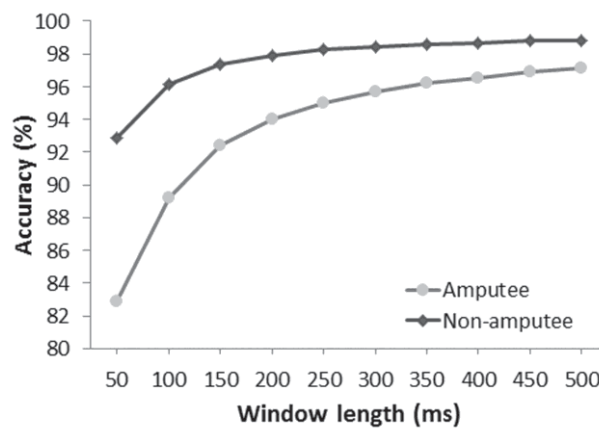
Figure 3.4 Average classification accuracy across 10 different window lengths

The window length and the window increment along with the processing time of the recognition system influence the delay time of the myoelectric control system (MCS), as shown in Eq. **3.1**. T. R. Farrell and Weir (2007) urged that the optimal delay time should be between 100 – 125 ms. Figure 3.5 shows the processing time of the system. The longest processing time is 2.2 ms when the window length is 500 ms. By considering the Farrel's suggestions and the maximum processing time, there are many allowable combinations of window length and window increments. If the longest window, which is 200 ms in Figure 3.4, is chosen then using Eq. **3.1** the window increment is 25 ms.
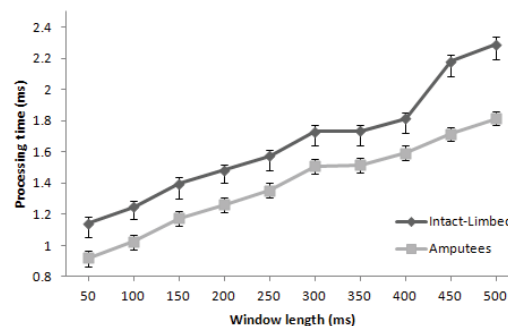
Figure 3.5 Averaged processing time of the finger recognition

3.3.3   Feature Extraction

There are six feature sets examined in this work. Six-order autoregressive (AR6) and Hjorth Time Domain (HTD) parameters are the first and second feature set. Other feature sets are combinations of features introduced and employed by researchers, and they are named according to the researchers proposing it. Hudgins's feature set consists of MAV, MAVS, ZC, SSC, and WL. Englehart's set excludes MAVS from Hudgins set. Meanwhile, Hargrove's set is composed of Hudgins's set plus AR6 and RMS. Different from Hargrove's set, Khusaba's set is constructed from Englehart's set plus HTD, SS, and AR. This work introduces a new combination of features, which is a concatenation of Hargrove's and Khusaba's set. It comprises MAV, MAVS, ZC, SSC, SS, WL, RMS, AR6, and HTD that forms 16 features in each channel. The experimental results are shown in Figure 3.6 and Table 3.2.

(a)   (b)
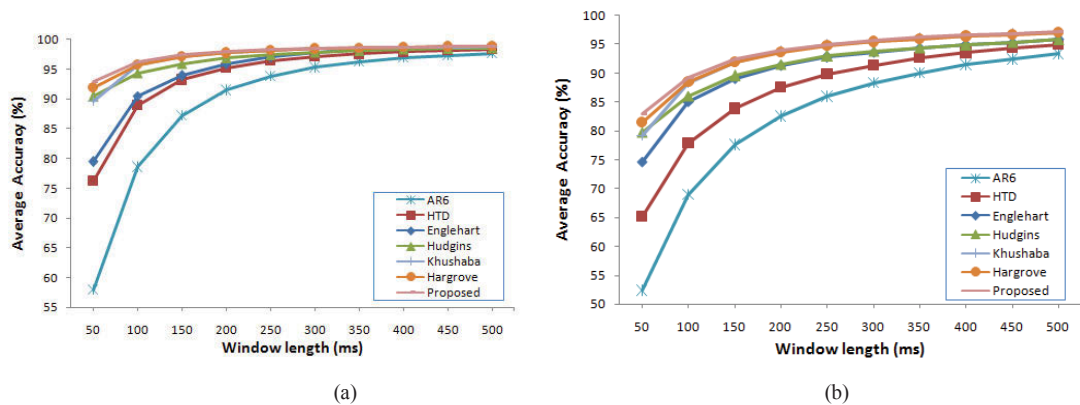
Figure 3.6 Average classification accuracy of different feature extraction on nine able-limbed subjects (a) and five amputee subjects (b) using 4-fold cross validation

Figure 3.6 presents the accuracy of different feature sets across window lengths from 50 to 500 ms on nine able-bodied subjects (a) and five amputee subjects (b). All feature sets have similar behaviour i.e. the accuracy increases along with the increase of the window length. In the able-bodied subjects, the individual feature sets including AR6 (six-order Autoregressive) and HTD (Hjorth parameters) are less accurate than the combined feature sets. This fact supports the results of Oskoei and Huosheng (2008) that a single features is less accurate than a combination one. Among combined feature sets, the proposed feature is significantly better than some other methods but does not change too much from two other methods (Hargrove's and Khushaba's feature) for different window lengths.

Table 3.2 Averaged classification accuracy of the system using different features across all subjects using four-cross validation

Features(#)	Amputee (%)	Intact-limbed (%)	Time (ms)
AR6 (#6)	82.29±12.99	89.25 ± 12.48	0.27 ± 0.07
HTD (#3)	87.12±9.38	93.90 ± 6.86	0.17 ± 0.01
Englehart (#4) (Kevin Englehart & Hudgins, 2003)	90.74±6.53	94.89 ± 6.03	0.52 ± 0.20
Hudgins (#5) (Hudgins *et al.*, 1993)	91.43±5.08	96.60 ± 2.55	0.58 ± 0.19
Khushaba (#14) (R. N Khushaba *et al.*, 2012)	93.01±5.57	97.16 ± 2.82	1.14 ± 0.28
Hargrove (#12) (L.J. Hargrove *et al.*, 2007)	93.19±4.86	97.39 ± 2.15	0.94 ± 0.26
This thesis (#16)	93.60±4.48	97.59 ± 1.86	1.39 ± 0.33

In contrast, on the amputee subjects, the proposed feature set is far more accurate than other sets except Khushaba's and Hargrove's set. Those two sets are as accurate as the proposed one. Statistical test using one-way ANOVA with $p = 0.05$ showed that there are no significant differences between them ($p > 0.05$). Nonetheless, the proposed one still outperforms the others as shown in Table 3.2. As for the time, the processing time of the proposed one and Khushaba's set is not significantly different ($p > 0.05$). However, the time difference is significant compared to Hargrove's set ($p < 0.05$).

3.3.4 Feature Reduction

Three dimensionality reduction methods were examined in this experiment. The primary goal was to investigate the performance of different types of LDA variances i.e. original LDA (linear discriminant analysis), SRDA (spectral regression discriminant analysis) and OFNDA (orthogonal fuzzy neighbourhood discriminant analysis). As mentioned in section 3.3.3, the feature set used in this experiment comprises MAV, MAVS, ZC, SSC, SS, WL, RMS, AR6, and HTD. It produces 16 features in each channel. In other words, the feature set produced 96 (16x6) features of the six-channel EMG signals and 176 (16x11) features of the 11-channel EMG. The dimensionality reduction methods reduced these features into 14 and 11 features of the non-amputee and amputee subjects, respectively. No majority vote was used after RBF-ELM classifier. The results are depicted in Figure 3.7 and Figure 3.8.

Figure 3.7 indicates that on the amputee subjects, the recognition system using SRDA outperformed LDA and OFNDA for both cases, the six-channel and 11-channel cases.

On the other hand, on the able-bodied subjects, OFNDA is the most accurate method of the six-channel trials, while LDA is the best method in the 11-channel experiments. Besides, in all cases, standard deviations of the performance of OFNDA are large compared to the other two. In other words, its performance varies across different subjects, especially on the amputee subjects. OFNDA seems to be less stable than the other two methods.
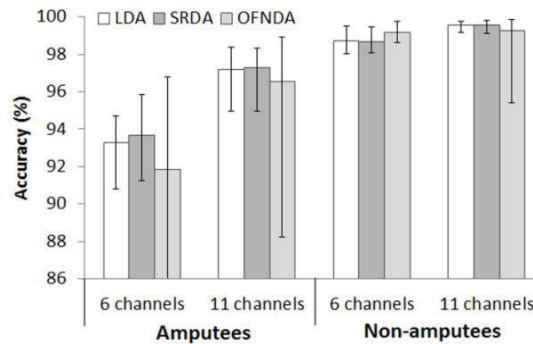
Figure 3.7 Averaged classification accuracy of different reduction dimensionality methods across nine and five non-amputee and amputee subjects, respectively

In terms of processing time of three methods tested, SRDA is the fastest method (Figure 3.8). In contrast, the longest processing time was OFNDA. Another interesting finding is in the comparison of LDA and SRDA. In the 6-channel amputee, the time difference between LDA and SRDA is not significant; however, it becomes double on the 11-channel amputee. A similar trend occurred in the non-amputee subjects. The LDA's reduction time is roughly twice of the SRDA's reduction time in 11-channel non-amputees. Therefore, based on these results, SRDA is the best option for the dimensionality reduction.
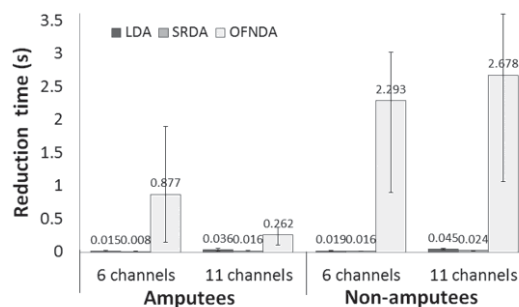
Figure 3.8 Averaged reduction time of different reduction dimensionality methods across nine and five non-amputee and amputee subjects respectively

3.3.5 Majority Vote

This subsection examines one of the post-processing methods called a majority vote. This experiment was done to observe the optimal vote number for the classification

enhancement. The majority vote can smoothen and enhance the classification results, as explained in **section 3.2.5**. In this experiment, the M-PR system employs SRDA to reduce the feature dimension and RBF-ELM to classify the finger movements. In addition, the number of votes tested is from one until six votes. Figure 3.9 presents the results.
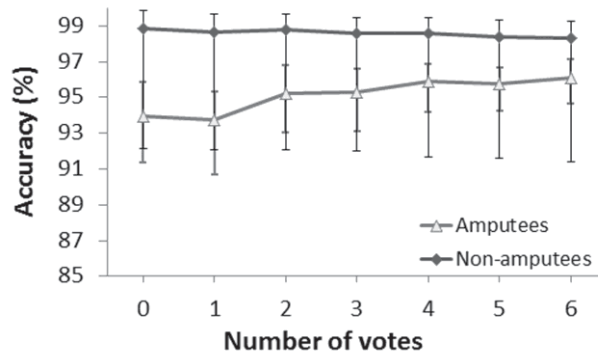
Figure 3.9 The results of the majority vote experiment using RBF-ELM classifer validated by four-fold cross validation

The figure shows that, in amputee subjects, the greater the number of the votes, the more accurate the system. On the other hand, in the non-amputee subjects, an opposite trend occurred, the greater the number of the votes, the less accurate the system. Therefore, no-majority vote is the best option for the able-bodied subjects, but on the contrary, six votes is the best vote number for the amputee subjects.

As shown in Eq. 3.3, the majority vote increases the delay time of a pattern recognition system. In the literature, there are two delay times. Firstly, it is the acceptable delay time proposed by Kevin Englehart and Hudgins (2003). It should be less than 300 ms. The second one is the optimal delay time proposed by T. R. Farrell and Weir (2007), which is 100 - 125 ms. As discussed in **section 3.3.2**, the window length is 200 ms and the window increment is 25 ms. If it is desired that the delay time should comply with the optimum delay time then, by using Eq. 3.3, then the number of votes is one. In Figure 3.9, the no-majority vote was better than the one-majority vote. Therefore, no majority vote was the best option for the next experiments.

3.3.6   Classification

In this section, the performances of various types of ELM for finger movement classification on amputee and able-bodied subjects are investigated. As presented in **section 3.2.4**, ELM consists of two types, the node ELM and kernel-based ELM. The M-PR system in the experiments utilized two node ELMs: a sigmoid-additive hidden-node (Sig-ELM) and multi-quadratic RBF hidden-node (Rad-ELM). As for the kernel-based

ELM, the work employed three kernel-based ELMs: linear (Lin-ELM), polynomial (Poly-ELM), and RBF kernels (RBF-ELM). Furthermore, the performances of these ELMs were compared with other famous classifiers such as sequential minimal optimization SVM (SM-SVM), least-square SVM (LS-SVM), LDA, and kNN. Moreover, multi-class SVM problem is implemented using one-against-all (OAA). The kernel-based ELM and SVM need the optimal kernel parameters to have good performance. Table 3.3 presents the optimized parameters of some classifiers computed using a grid search method.

Table 3.3 The optimum parameters of the classifiers used in the experiment

Classifier	C	γ	d	L
Sig-ELM	2^{30}	-	-	2000
Rad-ELM	2^{24}	-	-	2000
Lin-ELM	2^{-1}	-	-	-
Poly-ELM	2^{-1}	-	2^{6}	-
RBF-ELM	2^{6}	2^{-10}	-	-
SVM	2^{2}	2^{0}	-	-
LS-SVM	2^{10}	2^{0}	-	-

Besides relying on the optimized parameters, the experiments in the following section consider all results done previously. The system will classify 15 finger motion classes of the able-bodied subjects and 12 finger movement classes of the amputees. The proposed system employs nine feature extraction methods (MAV, MAVS, ZC, SSC, SS, WL, RMS, AR6, and HTD) that constitute sixteen (16) features per channel. They are extracted using overlapping windowing with the window length of 200 ms and window increment of 25 ms.

Furthermore, the system is applied to two channel groups, i.e., six-channel and 11-channel group that produces 96 features and 176 features, respectively. Then, SRDA (see **section 3.3.4**) is used to reduce the feature's dimension into 14 and 11 features of the able-bodied and amputee subjects, respectively. Finally, ELM classifiers are utilized to classify and recognize the finger movement classes without using majority vote. As a note, the recognition systems for amputee and non-amputee subjects are alike in structure, composition and parameters. A trial using only two channels will be investigated at the end of experiments.

3.3.6.1 *ELM Performances*

In this experiment, five types of ELM consisting of two non-kernel based ELMs (Sig-ELM and Rad-ELM) and three kernel-based ELMs (Lin-ELM, Poly-ELM, and RBF-ELM) are examined. The results are described in Figure 3.10. Figure 3.10 shows that, on

the amputee subjects, RBF-ELM outperforms other classifiers in two cases, a six-channel case by average accuracy of 98.55 % and an 11-channel case by the average accuracy of 99.50 %. The worst classifier is Lin-ELM especially in the 6-channel condition with average accuracy of 90%.
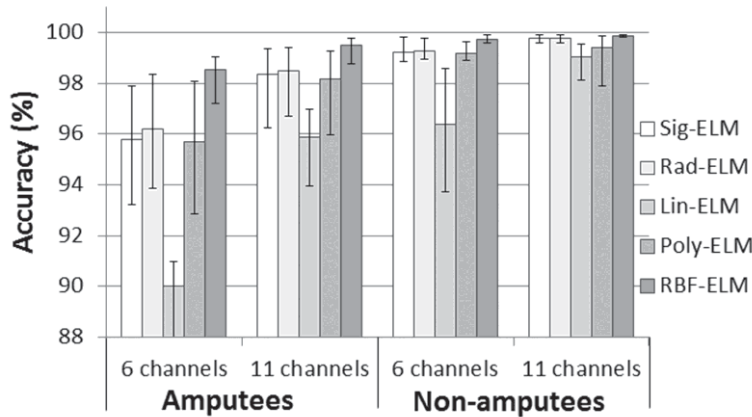
Figure 3.10 Average accuracy of various ELMs across five amputees and nine able-bodied subjects using four-fold cross validation

Furthermore, RBF-ELM is the only classifier that achieved average accuracy more than 98% in the 6-channel experiment. On the contrary, in the 11-channel trial, all classifiers attained average accuracy higher than 98 % except Lin-ELM. Likewise, on the non-amputee subjects, RBF-ELM is superior to other ELMs. It achieved classification accuracy up to 99.71 % on the 6-channel case and 99.88% on the 11-channel case. Interestingly, all classifiers exceeded the average accuracy of 98 % in both cases, 6-channel and 11-channel cases except Lin-ELM. It can be concluded that RBF-ELM is the best classifier on both the amputee and non-amputee subjects. The significance of RBF-ELM over other classifiers is also indicated by the results of ANOVA test as shown in Table 3.4.

Table 3.4 *p*-values from a pair-wise comparison of various ELM classifiers on Five Amputee Subjects

	6-channel condition				11-channel condition			
	Non-kernel		Kernel		Non-kernel		Kernel	
	Rad-ELM	Lin-ELM	Poly-ELM	RBF-ELM	Rad-ELM	Lin-ELM	Poly-ELM	RBF-ELM
Sig-ELM	0.726	0.000	0.927	0.015	0.821	0.011	0.823	0.080
Rad-ELM		0.000	0.668	0.026		0.006	0.650	0.089
Lin-ELM			0.001	0.000			0.019	0.000
Poly-ELM				0.017				0.060

A one-way ANOVA test with a significance level set at p = 0.05 was applied to the amputee subjects. Table 3.4 shows the results of ANOVA test for the amputee subjects. The result indicates that when using six channels, the accuracy of RBF-ELM was significantly different from other ELM classifiers (p = 0.015). However, in the 11-channel experiment, there was no significant difference in the classification accuracy between RBF-ELM and other classifiers (p = 0.076) except Lin-ELM (p=0.19e-3). Moreover, the ANOVA test on the non-amputee subjects (Table 3.5) highlights that RBF-ELM was statistically superior to other ELM classifiers (p<0.001). In addition, Sig-ELM, Rad-ELM, and Poly-ELM significantly obtained no different accuracy (p>0.05). In general, these facts confirm the classification superiority of RBF-ELM over other ELM classifiers.

Table 3.5 *p*-values from a pair-wise comparison of various ELM classifiers on Nine Able-bodied Subjects

	6-channel condition				11-channel condition			
	Non-kernel		Kernel		Non-kernel		Kernel	
	Rad-ELM	Lin-ELM	Poly-ELM	RBF-ELM	Rad-ELM	Lin-ELM	Poly-ELM	RBF-ELM
Sig-ELM	0.902	0.000	0.673	0.000	0.857	0.000	0.073	0.018
Rad-ELM		0.000	0.570	0.000		0.000	0.067	0.024
Lin-ELM			0.000	0.000		1.000	0.206	0.000
Poly-ELM				0.000		0.206	1.000	0.024

Figure 3.11 shows the average classification accuracy of RBF-ELM on five amputee subjects in two conditions: six channels and 11 channels. The recognition system using RBF-ELM was capable of classifying the 12 finger movements by a minimum average accuracy of more than 97%. However, the classifier underwent some difficulties in identifying signals from the amputee subjects, especially for the subject A4. Based on the demographic data in Table 3.1, the subject A4 has been a hand amputee for eight years. S/he might have a difficulty in imagining the intended finger movements due to the length of time of the amputee condition. Meantime, the subject A1 and A3 who have been hand amputees for four years performed well in imagining finger movements so that their signals were more detectable than others.
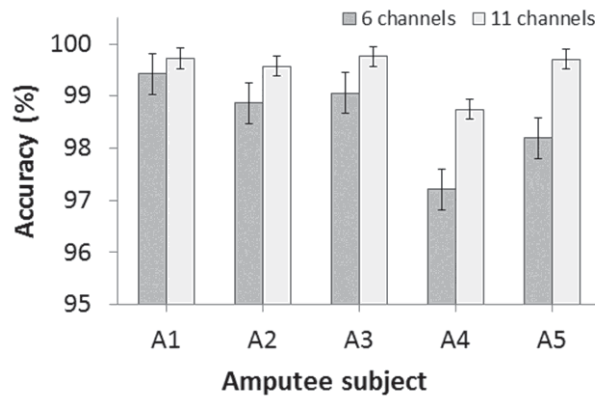
Figure 3.11 Average classification accuracy of RBF-ELM on five-amputee subjects using four-cross validation

Different from Figure 3.11, Figure 3.12 presents the classification accuracy of RBF-ELM in recognizing the intended classes of the five amputee subjects. The finger movements performed by the amputees here are not the actual movements. They imagined the finger movements representing 12 finger movements aided by their healthy hands. The figure shows that RBF-ELM could classify all classes correctly with average accuracies of more than 96% on the six-channel and 98% on the 11-channel experiments. The easiest finger movement was the rest condition while little extension (Le) and ring extension (Re) movements were the most difficult movements to identify. Furthermore, middle extension (Me) and index extension (Ie) movements were the next two consecutive intricate movements. Interestingly, most of the complicated movements were the extension movements, while flexion movements were relatively easily recognized. To analyse the misclassified classes, we can observe the confusion matrix plot presented in Figure 3.13. It seems that Le was identified as Re and vice versa. Besides, Me was recognized as Le.
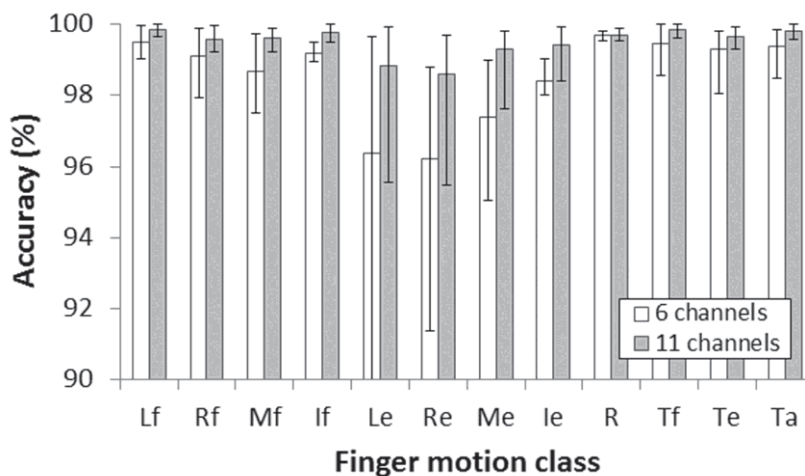
Figure 3.12 Average classification accuracy of RBF-ELM on 12 finger movement classes over five amputee subjects.

72
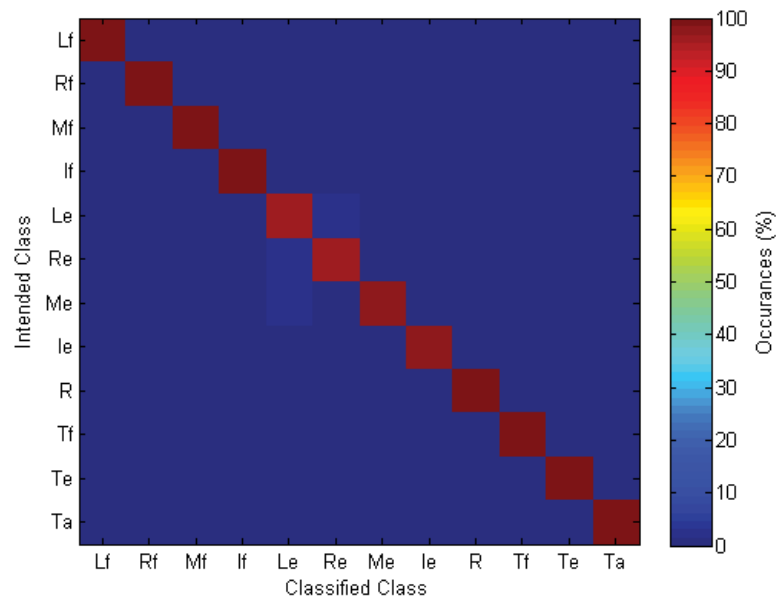
Figure 3.13 Average confusion matrix plot of six-channel RBF-ELM on five amputee subjects

As for the non-amputee subjects, the average accuracy of RBF-ELM on individual subjects is depicted in Figure 3.14. RBF-ELM succeeded in recognizing 15 classes across nine subjects by average accuracy of more than 99 % in 6-channel and 11-channel cases. The most accurate classification occurs in subject 4 in which the accuracy is comparatively the same, on 6-channel and 11-channel experiments. Obviously, 11-channel trials are more accurate than 6-channel trials.
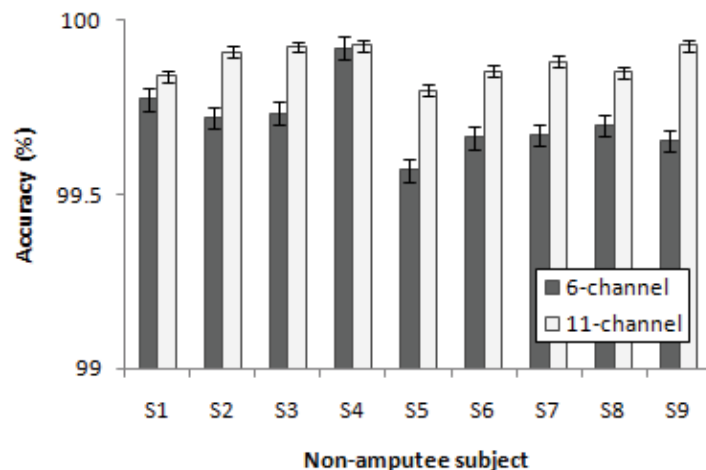
Figure 3.14 Average classification accuracy of RBF-ELM on nine able-bodied subjects
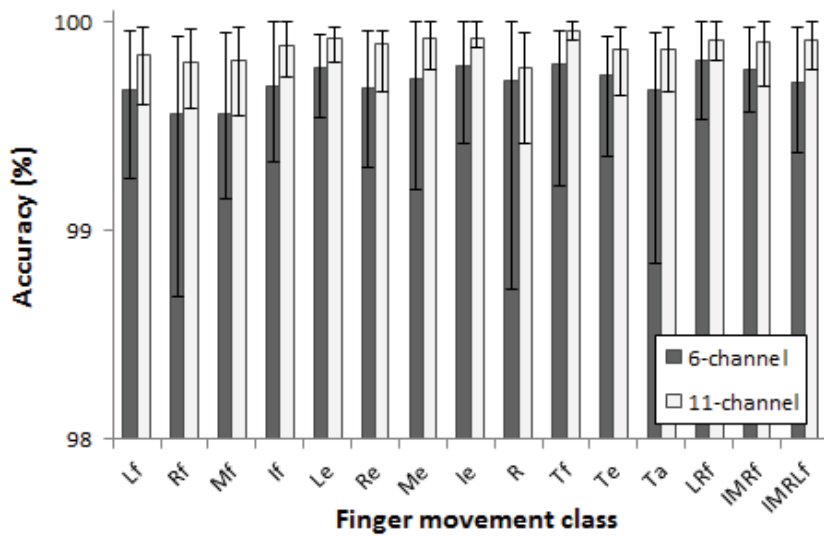
Figure 3.15 Average classification accuracy of RBF-ELM on 15 finger motion over nine non-amputee subjects

In addition to the classification performances of subjects, the performance of finger motion recognition is analysed. On able-bodied subjects, depicted in Figure 3.15, the system can classify all classes by the average accuracy of more than 99%. However, on the ring flexion (Rf), rest (R) and thumb abduction (Ta), the accuracies are diverse and they descend to less than 99 % in the 6-channel case. Overall, RBF-ELM accurately recognizes 15 classes with the accuracy of more than 98 %.

To investigate misclassified classes, the plot of the confusion matrix of the classification results is presented in Figure 3.16. Figure 3.16 shows interesting results. The difference between the misclassified data is not clear because the average errors are extremely small and relatively similar. Therefore, it confirms that RBF-ELM's performance is clearly outperforms the other classifiers.
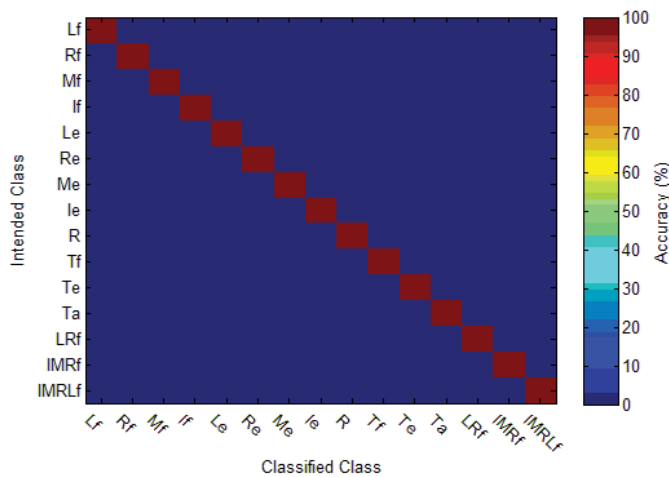
Figure 3.16 Average confusion matrix plot of six-channel RBF-ELM on nine non-amputee subjects

3.3.6.2 ELM and other classifiers

In this section, the performance of ELM is compared to other well-known classifiers to verify its performance in recognizing finger motions over amputee and non-amputee subjects. This work compared ELM with some known classifiers such as SM-SVM, LS-SVM, LDA, and kNN. The structure of the recognition system for these two subject groups is alike. In this comparison, ELM is represented by RBF-ELM. The results are described in Figure 3.17.

The figure indicates that the accuracy of RBF-ELM has a higher value than the others in all conditions. On six-channel amputee subjects, RBF-ELM was the most accurate classifier. It was far superior to LDA and kNN, but it was slightly better than the SVM family, SM-SVM and LS-SVM. Likewise, in the 11-channel case, RBF-ELM achieved the best accuracy, but the accuracy gap was not as large as in the six-channel experiments.
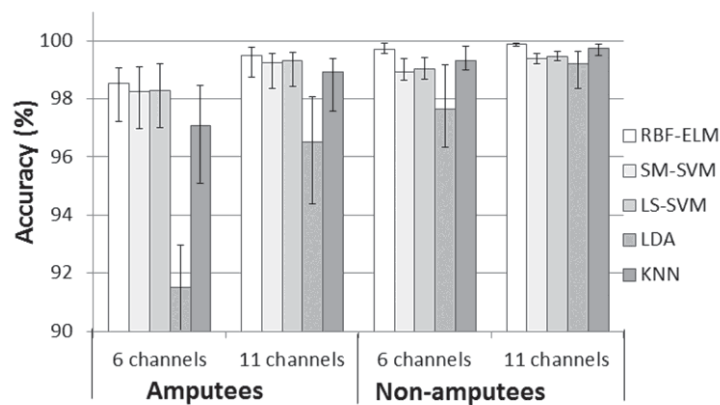
Figure 3.17 Average accuracy comparison between RBF-ELM and other famous classifiers

Similar to the amputee subjects, the accuracy of RBF-ELM on the non-amputee subjects exceeded that of other classifiers. Different from 6-channel amputee results, the average accuracies of 6-channel trial on non-amputee subjects are close to each other except for LDA. On the other hand, the accuracies are relatively the same for the 11-channel cases including LDA. It seems that the more complex the data involved, the closer the accuracy of classifiers. The superiority of RBF-ELM is more noticeable by considering ANOVA test as presented in Table 3.6 and Table 3.7 which shows p-values of ANOVA pair-wise test of various classifiers across five amputee subjects. It indicates that on the amputee subjects, the accuracy of RBF-ELM was significantly different from LDA ($p = 0.001$) but it was not significantly different to other rest classifiers ($p > 0.05$). Meanwhile, different results occurred to the able-bodied subjects, as depicted in Table 3.7. In all cases, six-channel and 11-channel, RBF-ELM attained accuracy, which was

significantly different from the other classifiers (p = 0.001). This fact means that RBF-ELM was clearly superior to the other classifiers in recognizing 15 finger movement classes.

Table 3.6 *p*-values from a pair-wise comparison of different classifiers on five amputee subjects

	6 channels				11 channels			
	SM-SVM	LS-SVM	LDA	KNN	SM-SVM	LS-SVM	LDA	KNN
RBF-ELM	0.577	0.665	0.000	0.067	0.429	0.539	0.001	0.178

Table 3.7 *p*-values from a pair-wise comparison of different classifiers on nine non-amputee subjects

	6 channels				11 channels			
	SM-SVM	LS-SVM	LDA	KNN	SM-SVM	LS-SVM	LDA	KNN
RBF-ELM	0.000	0.000	0.000	0.000	0.000	0.000	0.000	0.008

The comparison of ELM and other familiar classifiers was undertaken not only in terms of accuracy but also in the training time as shown in Table 3.8 and Table 3.9. For the amputee subjects, the fastest training time was LDA followed by kNN. As for the ELM, the training time was far quicker than the SVM family, SM-SVM, and LS-SVM, but slower than LDA and kNN. As for the non-amputee subjects, because they have more data, their training time is slower. Interestingly, the time difference between the kernel-based and node-based ELM is very noticeable in the non-amputee cases. The kernel-based ELM consumed much more training time than the node-based ELM. This fact confirms the benefit of the node ELM in which the calculation of output weight can be modified to deal with extensive data (see Eq. 2.42 in **section 2.3.1.4.2**).

Table 3.8 Training time of amputee subjects

Classifier	Six-channel		11-channel	
	Mean (ms)	Std	Mean (ms)	Std
Sig-ELM	4.293	2.159	4.351	2.190
Rad-ELM	4.301	2.118	4.261	2.115
Lin-ELM	4.643	5.073	4.635	5.064
Poly-ELM	5.214	5.567	5.194	5.550
RBF-ELM	5.581	6.005	5.556	5.958
SM-SVM	66.402	88.639	54.973	69.084
LS-SVM	86.339	73.602	86.921	74.398
LDA	0.012	0.005	0.010	0.004
KNN	0.785	0.689	0.782	0.690

Table 3.9 Training time of non-amputee subjects

Classifier	Six-channel		11-channel	
	Mean (ms)	Std	Mean (ms)	Std
Sig-ELM	7.338	1.355	7.362	1.343
Rad-ELM	7.417	1.337	7.346	1.291
Lin-ELM	17.318	7.441	17.272	7.443
Poly-ELM	18.956	8.019	18.881	7.995
RBF-ELM	19.876	8.409	19.829	8.301
SM-SVM	324.064	233.388	249.582	173.228
LS-SVM	241.715	76.175	242.684	76.531
LDA	0.031	0.006	0.026	0.007
KNN	2.656	0.885	2.658	0.887

In addition to the training time, the testing time is presented as well, as shown in Table 3.10 and Table 3.11.

Table 3.10 indicates that the testing time of the kernel and non-kernel ELM is very close in the amputee subjects. However, in the non-amputee subjects, the testing time of kernel-based ELM is about double that of amputee subjects (Table 3.11). In comparison with SVM, the testing time of ELM's family is far quicker than that of SVM's family in both, the amputees and non-amputees. Overall, the performance of ELM's family for finger classification is comparable to SVM's family in terms of accuracy but superior to SVM's family in terms of the processing time. However, the processing time of ELM is not comparable to those of LDA and kNN. LDA and kNN consumed much shorter time than ELM's family. Nevertheless, the processing time of ELM is still reasonable for the real-time application.

Table 3.10 Testing Time of amputee subjects

Classifier	Six-channel		11-channel	
	Mean (ms)	Std	Mean (ms)	Std
Sig-ELM	1.493	0.088	1.530	0.105
Rad-ELM	1.500	0.097	1.505	0.085
Lin-ELM	1.387	0.944	1.183	0.960
Poly-ELM	1.559	1.014	1.341	1.038
RBF-ELM	1.668	1.094	1.435	1.112
SM-SVM	20.127	15.659	15.416	12.941
LS-SVM	26.907	10.802	24.825	11.671
LDA	0.004	0.001	0.004	0.001
KNN	0.243	0.107	0.220	0.112

Table 3.11 Testing Time of non-amputee subjects

Classifier	Six-channel		11-channel	
	Mean (ms)	Std	Mean (ms)	Std
Sig-ELM	1.350	0.045	1.354	0.020
Rad-ELM	1.366	0.035	1.354	0.037
Lin-ELM	3.024	0.929	3.015	0.931
Poly-ELM	3.314	0.991	3.300	0.988
RBF-ELM	3.476	1.033	3.469	1.019
SM-SVM	54.275	34.476	42.036	25.307
LS-SVM	43.208	6.986	43.381	7.022
LDA	0.006	0.001	0.005	0.001
KNN	0.473	0.088	0.473	0.088

3.4 Discussion

This chapter aims to build an accurate and optimum pattern recognition system using different variations of ELM for finger movement classification on amputees and non-amputees. To achieve such a system, the chapter investigated every part of the state-of-the-art pattern-recognition system. Selecting the window length and window increment of the data segmentation started the finding of the optimal system. The experimental results show that a 200-ms window length and a 25-ms window increment are the optimum choices for the pattern-recognition system that comply with the optimal time delay suggested by T. R. Farrell and Weir (2007). These segmentation parameters may result in a pattern-recognition system that is ready for real-time application.

In the feature extraction method, this work introduced a new feature set. The proposed feature set mainly comprises Hargrove's features plus SS (sample skewness) and HTD (Hjorth time domain) parameters (see **section 3.2.2** and **3.3.3**). This additional feature set was able to provide more informative features for the classifier. The classification accuracy of the new feature set was higher than Hargrove's features, especially for the amputee subjects (Table 3.2).

As for the dimensionality reduction method, the results supported the claim D. Cai *et al.* (2008) and our published work (Khairul Anam *et al.*, 2013) that SRDA is faster than LDA. LDA took more time in reducing the dimension of 6-channel features than SRDA, but the time difference between the two is not significant ($p > 0.05$). However, the processing time of LDA is much longer than that of SRDA when reducing the dimension of 11-channel features ($p < 0.05$). As for OFNDA (R. N. Khushaba *et al.*, 2010), its

reduction time is large enough, and it is not comparable to SRDA or even LDA. The processing time of OFNDA is long because OFNDA consists of two stages: principal components analysis (PCA) and fuzzy discriminant analysis (FNDA). PCA in OFNDA is needed to overcome the singularity problem in FNDA.

Unlike the processing time, the accuracy of the system using SRDA is similar to LDA and OFNDA ($p > 0.05$). Probably, this finding can be used to make a comment on the outcomes of Al-Timemy *et al.*'s work (Al-Timemy *et al.*, 2013). Their work, which employed the same data as used in this chapter, utilized ONFDA as a dimensionality reduction and LDA as a classifier. As a note, LDA can be used as either a dimensionality reduction or a classifier. On the six-channel experiment, OFNDA+LDA was able to achieve a high accuracy of about 98 % on the able-bodied subjects, but it showed a lower accuracy on the amputee subjects with the accuracy of about 90%. Comparing their results and the results in this chapter, the proposed recognition system, which utilizes SRDA+ELM, attained the accuracy of approximately 99% on the able-bodied subjects and around 98% on the amputee subjects. Because ONFDA and SRDA have similar performances in terms of accuracy, the inaccuracy of Al-Timemy *et al.*'s work on the amputee subjects was probably caused by LDA as a classifier. This assumption is supported by the results in Figure 3.17, which informs the shortcoming of LDA as a classifier.

The utilization of SRDA as a dimensionality reduction method is important in constructing a recognition system that is powerful and fast. The experimental results show that SRDA is equivalent to other LDA variances, but it is superior to others in terms of speed. SRDA should be better than one of the well-known methods, PCA. Martínez and Kak (2001) proved that LDA outperform PCA especially for large data as being used in this work.

Finally, the discussion of the classifier's performances is presented. The experimental results confirm that the ELM (extreme learning machine) was capable of classifying the EMG signal of the non-amputee and amputee subjects. Among the different types of ELM, the kernel-based ELM with RBF kernel outperformed other types of ELM. This finding supports the results of G. B. Huang *et al.* (2012) that, on some cases, RBF-ELM achieved better accuracy than the node-based ELM: sigmoid-additive node (Sig-ELM) and the radial basis node ELM (Rad-ELM). However, the experimental results show that

the kernel-based ELM needs more processing time than the non-kernel-based ELM, especially on the large data as shown in Table 3.8 and Table 3.9.

The large data problem on the node-based ELM has been solved by G. B. Huang *et al.* (2012) but it is still unsolved on the kernel-based ELM. They had manipulated the output of node-based ELM (see Eq. 2.42 in **section 2.3.1.4.2**) in such a way that the dimension of a feature-mapping matrix has L x L order, instead of N x N as in the kernel-based ELM (see Eq. 2.49 in **section 2.3.1.4.3**). L is the number of hidden nodes, and N is the training data number. In fact, for a large feature, the number of L is far smaller than N. As a result, the training time of the node-based ELM is faster than the kernel-based ELM because the node-based ELM deals with L x L order instead of N x N order.

The comparison of the ELM, which is represented by RBF-ELM, and with other well-known classifiers, confirms that the ELM is comparable with the famous SVM even though there is no iterative learning on the ELM's weight. The superiority of the ELM over the SVM is more noteworthy if the processing time of the classifiers is considered. It is true that the ELM was not the fastest classifier tested in this work. LDA was the fastest one, yet LDA was the least accurate classifier. kNN was faster than the ELM, but its performance was still under that of the ELM especially RBF-ELM. In addition, the fact that the ELM is far superior to LDA especially with small channel numbers disapproves the statement of (L. J. Hargrove *et al.*, 2010) on the classification process. They stated that classification is a trivial process as long as the feature set and the dimensionality reduction are chosen properly.

To evaluate the proposed system, some works related to the finger movement identification are presented in Table 3.12. The table does not always indicate that the system developed here is the best one because the situation, experimental setup and other considerations may be different application to application. However, it can be used to measure the performance of the proposed system. Overall, this work exhibited the most accurate system. Another interesting finding is that the accuracy gap of the non-amputee and amputee subjects was not very large. In the six-channel experiments, the accuracy difference of RBF-ELM on the amputee subjects and non-amputee subjects was 0.95%.

Table 3.12 Comparison of Various Research on Finger Movement Recognition

Work	Nch	Finger Class	Accuracy (%)	Subjects	Mode
Tenore et al. (Tenore *et al.*, 2009)	19	10 Id & 2 Cm	93.4	5 H 1 A	OF
	19	10 Id & 2 Cm	87.80	1 A	OF
	19	10 Id	92.83	1 A	OF
	8	7 Id & 1 Cm	89.00	5 H	OL
Cipriani et al. (Cipriani *et al.*, 2011)	8	7 Id & 1 Cm	79.00	5A	OL
	2	5 Id & 5 Cm	92.00	8 H	OF
Khushaba et al. (R. N Khushaba *et al.*, 2012)	2	5 Id & 5 Cm	90.00	1H	OL
Al-Timemy et al. (Al-Timemy *et al.*, 2013)	6	12 Id & 3 Cm	98.55	10 H	OF
	6	12 Id	90.57	6 A	OF
	6	12 Id & 3 Cm	99.50	9H	OF
This proposed method	6	12 Id	98.55	5A	OF

Nch = Number of channels, Id = Individual finger movements, Cm = Combined Finger movements, H = Healthy Subjects, A = Amputees, OF= Offline classification, OL = Online Classification

3.5 Summary

All components in this recognition system were determined using experimental procedures. As a result, a powerful classification system that can work well on able-bodied and amputee subjects had been achieved. However, this work only studies the offline classification system. In fact, the system was designed to be ready for real-time application. The system recognition produced here fulfils three conditions for a real-time recognition system (Kevin Englehart & Hudgins, 2003). Its performance was highly accurate; it was able to detect the user's intention with accuracy of roughly 99% on the able-bodied subjects and around 98% on the trans-radial amputees using six EMG channels. In addition, it has easy interface for direct control so that it relieves the user's mental difficulties in wearing the hand rehabilitation device. Finally, it meets the optimal delay time for a real application in the range 100–125 ms.

Different ELM classifiers have been tested in this work. This work presents, on average, the kernel-based ELM is better than the node-based ELM. An attempt to enhance the performance of the node-based ELM should be carried out. One weakness of the node-

based ELM is that the input weight was determined arbitrarily and free from the training data so that the ELM produced is not optimum for a specific case. Therefore, optimization of the node-based ELM should be undertaken. Developments, such as the evolutionary extreme learning machine (E-ELM) (Zhu *et al.*, 2005) and the dynamic extreme learning (D-ELM) (Zhang *et al.*, 2013) can be implemented for finger movement classification.

In summary, this chapter presented the detailed investigation of the implementation of different types of ELM for the myoelectric pattern recognition system. This process results in a recognition system, which is fast, accurate, and easy to develop to classify 15 and 12 finger movements on nine able-bodied subjects and five amputee subjects, respectively. The proposed system introduced a new feature set comprising MAVS, ZC, SSC, SS, WL, RMS, AR6, and HTD forming 16 features per channel. The EMG signal is segmented using a 200-ms sliding window with a 25-ms shift. The extracted features are concatenated to yield a large feature. The combined feature dimension is reduced using SRDA, a swift version of LDA. Then the reduced features are fed to the ELM to be identified and classified into the intended class. By using the best ELM classifier, RBF-ELM, the pattern recognition system achieved the accuracy of 98.55% on the amputee subjects and 99.5% on the able-bodied subjects using six EMG channels.

Furthermore, this thesis found that the node-based ELM is not as good as the kernel-based ELM in many cases. Therefore, the next chapter will discuss the way to improve the performance of the node-based ELM. Another thing that should be addressed is about the optimization of RBF-ELM. The performance of RBF-ELM greatly depends on the selection of its parameters. Therefore, in the next chapter will discuss few methods to optimize the parameters of RBF-ELM.

CHAPTER 4

Novel ELM-Based Classifications for myoelectric finger recognition using two EMG channels

4.1   Introduction

Extreme Learning Machine (ELM) has shown its benefit as a classifier in the myoelectric pattern recognition system, as shown in Chapter 3. However, it has some shortcomings as have been highlighted in chapter 3 sections 3.5. Firstly, the feature has significant influence in the myoelectric pattern recognition system. Therefore, improvement in the feature representation should be made to enhance the classification performance. Another issue exists in the node based ELM. The performance of the node based ELM is not as good as the kernel based ELM, especially when using two EMG channels. As for the kernel-based ELM, the kernel parameters should be determined properly to attain a high classification performance. Therefore, parameter optimization is needed.

This chapter will address these three issues. Firstly, this thesis proposes a novel ELM called adaptive wavelet extreme learning machine (AW-ELM). AW-ELM is a node-based ELM that uses wavelet function in the activation function. Interestingly, the shape of the wavelet function can change according to the characteristic of the input. The implementation of AW-ELM in the myoelectric pattern recognition system and some benchmark datasets will be presented in **section 4.2.5**. AW-ELM and its implementation to myoelectric pattern recognition (M-PR) is the second contribution of the thesis.

In the feature side, this thesis proposes a new feature projection that is expected to increases the class separability of the features. This chapter introduces spectral regression extreme learning machine (SR-ELM). **Section 4.3** will present the basic concept of SR-ELM and its implementation in the myoelectric pattern recognition for finger movement and in some benchmark datasets. This is the third contribution of the thesis.

As for the kernel-based ELM, this thesis proposes an optimization of the kernel based ELM using particle swarm optimization (PSO), as will be discussed in **section 4.4**. In some situations, PSO tends to be trapped in local minima. As a result, the solution of the PSO is not global anymore. To overcome this problem, we investigate the enhancement of PSO by injecting a wavelet mutation in the PSO process. Thus, this thesis proposes a hybridization wavelet-PSO and ELM for the myoelectric pattern recognition. This hybridization will be discussed in **section 4.5**. The optimization of PSO and wavelet-PSO for the parameters of the kernel-based ELM is the fourth and fifth contribution of the thesis.

Furthermore, all experiments conducted in this chapter employed two EMG channels only. R. N Khushaba *et al.* (2012) employed two EMG channels to recognize individual and combined finger with the accuracy of about 92% and 89 % on the offline and online classification, respectively. Therefore, the performance of the system with two EMG channels may be reasonable enough as an effort to enhance the comfort of the user wearing the hand rehabilitation device.

In summary, in this chapter, the thesis presents four contributions. The first and the second are AW-ELM and SR-ELM for classification and for feature projection or dimensionality reduction, respectively. The third and fourth contribution is the parameter optimization of the kernel based ELM using PSO and wavelet-PSO.

4.2 Performance evaluation of adaptive wavelet extreme learning machine (AW-ELM)

The experimental results in Chapter 3 show that, in general, the performance of the node-based ELM is less than that of the kernel-based ELM. The thesis proposes a new node-based ELM to enhance the performance of the node-based ELM in the myoelectric pattern recognition (M-PR) for finger movement classification. Firstly, the background of AW-ELM will be presented in **section** 4.2.1. The theory of wavelet ELM and adaptive wavelet-ELM will come after it. The experimental results on EMG datasets for finger motion classification will be presented in the following section. The experiments on the benchmark dataset from UCI machine-learning repository will be conducted as well as the examination of the performance of AW-ELM for a wide range of applications.

4.2.1   Background

A wavelet neural network (WNN) is a special case of a feed-forward neural network whose activation function is a wavelet function (Zhou *et al.*, 2004). It has been applied to many applications (Cao *et al.*, 2010). Furthermore, Subasi *et al.* (2006) extended the application of WNN to EMG based pattern recognition. This indicates that WNN is a promising classifier for the myoelectric finger motion recognition. However, the learning of WNN relies on the gradient descent algorithm. The drawbacks of the gradient descent method such as long training time and ease of being trapped to local minima have hampered the implementation of WNN in the real-time application (Lin & Tsai, 2008).

To improve the performance of WNN, Ling *et al.* (2008) proposed variable translation wavelet neural network (VTWNN). VTWNM is a type of WNN in which the translation parameter of the wavelet function is varied according to the variation of input. To train the weight of VTWNN, Ling *et al.* implemented a hybrid particle swarm optimization wavelet mutation (HPSOWM). The experimental results showed that VTWNN performed better than WNN and feed-forward neural network. However, the training procedure of the VTWNN using the extension of PSO is complex and time-consuming.

On the other hand, an extreme learning machine (ELM) was introduced to train single-hidden layer feed-forward networks (SLFNs) resulting in a system which is fast and able to avoid a local minima (G. B. Huang *et al.*, 2012). The learning mechanism of ELM can be extended to train WNN. The combination of ELM and WNN can be conducted by simply replacing the activation function of ELM with wavelets (Cao *et al.*, 2010; Salih *et al.*, 2013). This is the simplest unification of both networks as has been done by Salih *et al.* (2013). Cao *et al.* (2010) introduced a new combination of these two algorithms by proposing a composite function of WNN with ELM. In this method, they implemented two activation functions, a wavelet function and a piece-wise function that are done in order.

Another new unification of ELM and WNN was proposed by Javed *et al.* (2014) who proposed a summation wavelet extreme learning machine (SW-ELM). In the same way as Cao *et al.* (2010), they utilized two activation functions but employed them in different ways. These two activation functions were done in parallel and their outputs were averaged to be the output of the hidden nodes.

This section proposes a new integration of ELM and WNN. Instead of using original WNN, the proposed method extends VTWNN into the structure of ELM. In order words,

ELM is used to train the weight of VTWNN. Thus, the proposed method is called adaptive wavelet extreme learning machine (AW-ELM). Different from VTWNN in that its weights are trained using HPSOWM, AW-ELM has random weight in the hidden layer. As for the weights of the output layer, they are determined analytically.

According to WNN structure, the proposed system utilizes a wavelet function as the activation function in the hidden node. However, the activation functions are not fixed but they are adjusted taking regard to the changing in the input. The sigmoid function is used to process the input information and produce translation parameters of the wavelets in relation to the hidden node.

This section implemented wavelet extreme learning machine (W-ELM) and the proposed one, adaptive wavelet extreme learning machine (AW-ELM) to the myoelectric pattern recognition system. The goal is to classify the finger motions from the surface Electromyography signal (EMG) extracted from two-channel sources on the forearm. In addition, classification performance of AW-ELM will be compared with W-ELM, ELM with sigmoid function (SIG-ELM), radial basis kernel ELM (RBF-ELM) and other well-known classifiers such as SVM (support vector machine), LDA (linear discriminant analysis) and kNN (k-nearest neighbour).

The main contribution of this section is the AW-ELM and its application for finger motion classifications. Furthermore, to promote broader applications of AW-ELM, the AW-ELM is applied to various classification problems using the benchmark dataset from UCI Machine learning repository.

4.2.2 Wavelet extreme learning machine (W-ELM)

W-ELM is a wavelet neural network that has a single hidden layer; the weights in the hidden layer and output layer are trained using extreme learning machine. W-ELM can be considered as a special case of extreme learning machine in that its activation function is a wavelet. The output function of W-ELM for arbitrary samples $(x_k, t_k) \in \mathbf{R}^n \times \mathbf{R}^o$ with M hidden nodes is

$$f_i^k(\mathbf{x}) = \sum_{j=1}^{M} V_{ij} \psi_{a_j b_j}(w_j, c_j, \mathbf{x}_k) \quad i = 1, 2, ..., O \qquad 4.1$$

where

$$\psi_{a_j b_j}(x) = \frac{1}{\sqrt{a_j}} \psi \left(\frac{x - b_j}{a_j} \right), \qquad j = 1, 2, ..., M \qquad 4.2$$

in which a_j and b_j are dilatation and translation parameters of the wavelet, respectively. Initialization of dilatation and translation parameters, a_j and b_j, in WELM is an important issue. The initialization should consider the input information in order to let the time domain of the wavelet cover the input domain. According to Zhou *et al.* (2004), suppose the input vector x_k has the domain $[x_{kmin}, x_{kmax}]$, t^* and σ^* are the centre and the radius of the mother wavelet $\psi_{a_i b_i}$, then domain of $\psi_{a_i b_i}$ is given by:

$$[b_j + a_j(t^* - \sigma^*) , b_j + a_j(t^* + \sigma^*)] \tag{4.3}$$

Meanwhile, the input information range for ith hidden layer can be calculated as:

$$\left[\sum_{i=1}^{N} w_{ji} x_{i\min} , \sum_{i=1}^{N} w_{ji} x_{i\max} \right] \tag{4.4}$$

where w_{ji} is the weight connecting the jth hidden layer to the ith input. The wavelet can cover the input space if:

$$b_j + a_j(t^* - \sigma^*) = \sum_{i=1}^{N} w_{ji} x_{i\min} \tag{4.5}$$

and

$$b_j + a_j(t^* + \sigma^*) = \sum_{i=1}^{N} w_{ji} x_{i\max} \tag{4.6}$$

From Eq. **4.5** and **4.6**, a_i and b_i are formulated as as:

$$a_j = \frac{1}{2\sigma^*} \left(\sum_{i=1}^{N} w_{ji} x_{i\max} - \sum_{i=1}^{N} w_{ji} x_{i\min} \right) \tag{4.7}$$

$$b_j = \frac{1}{2\sigma^*} \left(\sum_{i=1}^{N} w_{ji} x_{i\max}(\sigma^* - t^*) + \sum_{i=1}^{N} w_{ji} x_{i\min}(\sigma^* + t^*) \right) \tag{4.8}$$

4.2.3 Adaptive wavelet extreme learning machine (AW-ELM)

4.2.3.1 *Theory*

This subsection will explain the theory of the proposed AW-ELM. Figure 4.1 depicts the diagram of the proposed method. If M is the number of hidden node and N is the number of input, then the input of the hidden layer P_j is given by:

$$P_j(x) = \sum_{i=1}^{N} x_i . w_{ji} + c_j \qquad j = 1, 2, ..., M \tag{4.9}$$

where x_i are the input variables, w_{ji} are the weights of the connection between ith input and jth hidden nodes, and c_j denotes the bias of jth hidden layer.
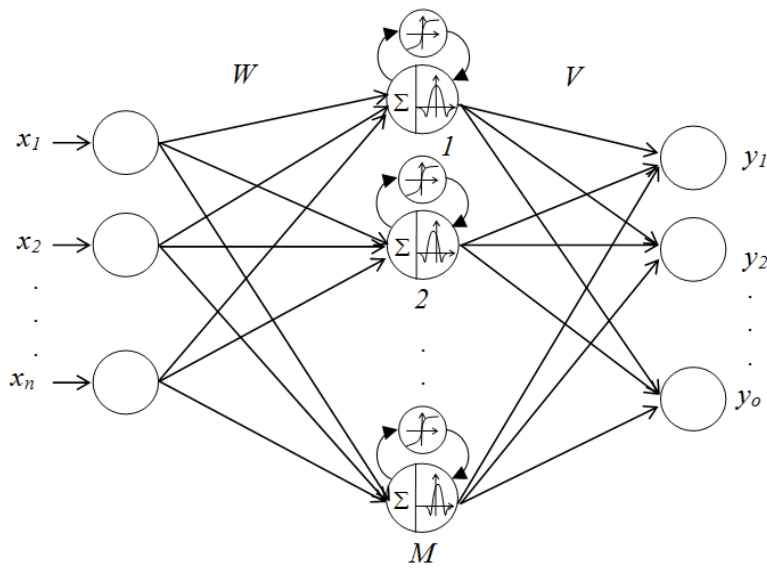
Figure 4.1 The proposed adaptive wavelet extreme learning machine

Using Eq. **4.9**, the output of the hidden node is given by:

$$\psi_{a_j b_j}(P_j(x)) = \psi\left(\frac{P_j(x) - b_j}{a_j}\right), \qquad j = 1, 2, ..., M \qquad 4.10$$

Following the selection of Ling *et al.* (2008), in the experiment, the dilatation parameter a_j is equal to j, so:

$$\psi_{a_j b_j}(P_j(x)) = \psi\left(\frac{P_j(x) - b_j}{j}\right), \qquad j = 1, 2, ..., M \qquad 4.11$$

In this proposed work, the Mexican Hat function (Ling *et al.*, 2008) is used as the mother wavelet $\psi_{a_i b_i}$ as described in Figure 4.2. It is defined as

$$\psi(x) = e^{-x^2/2}(1 - x^2) \qquad 4.12$$
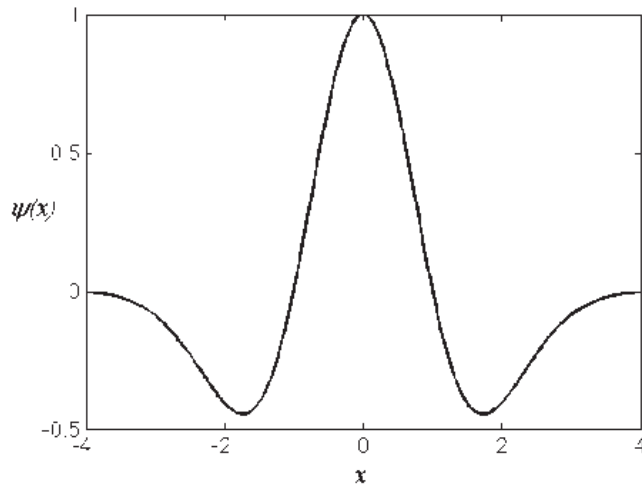
Figure 4.2 The mother wavelet of the Mexican hat

Therefore, the wavelet activation function of AW-ELM is:

$$\psi_{a_j b_j}(P_j) = e^{-0.5\left(\frac{P_j - b_j}{j}\right)^2}\left(1 - \left(\frac{P_j - b_j}{j}\right)^2\right) \qquad 4.13$$

In this proposed AW-ELM, the translation parameters b_j are varied according to the input information and driven by a nonlinear function as shown in Figure 4.3 and defined by :

$$b_j = f(P_j) \qquad 4.14$$

where

$$f(P_j) = \frac{2}{1 + e^{-P_j}} - 1 \qquad 4.15$$
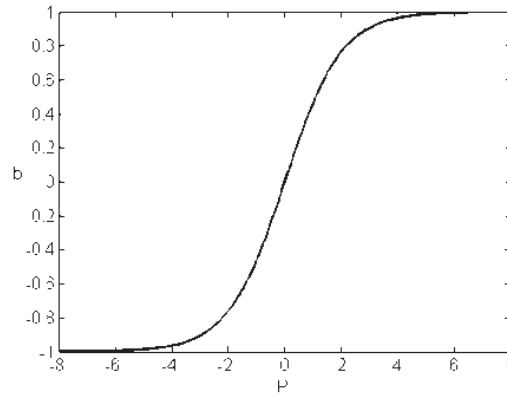
Figure 4.3 A nonlinear function to produce b_j

In the wavelet, the dilatation parameter a_j and translation parameter b_j have different roles. The dilatation parameter a_j determines the shape of the wavelet function. The less the dilatation parameter a_j is, the narrower the shape of the wavelet function is. On the other hand, the translation parameter b_j determines the position of the wavelet function in the direction of x-axis. If b is less than 0, then the wavelet function lies on the left side of y-axis. On the contrary, if b is more than 0, then the wavelet function exists on the right of the y-axis. Thus, b that is equal to zero will make the wavelet function in the middle of xy-plane.

In Eq. **4.13**, the dilatation parameter a_j is replaced by j and b_j is determined by the sigmoid function in Eq. **4.15**. It means that the parameters initialization of a_j and b_j are not needed at all, as in Eq. **4.2**. This is one of the benefits of the proposed system. Actually, it is done by computing parameter b_j according to the changes in the input. The initialization of wavelet parameters is necessary for WNN and W-ELM. Avoiding this

step in AW-ELM is one of the significant improvements in the wavelet neural network family.

Eventually, a new structure of an adaptive W-ELM is constructed and it is presented in Figure 4.1. In the figure, a small circle on the top of each hidden node is used to adjust the b parameters in order to change the shape of the wavelet. Thus, the output of AW-ELM is:

$$f_i^k(\mathbf{x}) = \sum_{j=1}^{M} V_{ij} \psi_{a_j b j}(w_j, c_j, \mathbf{x}_k) = \sum_{j=1}^{M} V_{ij} \psi_{a_j b_j}(P_j(\mathbf{x}_k)) \quad i = 1, 2, ..., O \quad 4.16$$

4.2.3.2 *The learning algorithm of AW-ELM*

For the desired output:

$$\mathrm{D} = (\boldsymbol{d}_1^T \quad \boldsymbol{d}_2^T \quad ... \quad \boldsymbol{d}_L^T)_{LxO} \qquad 4.17$$

The AW-ELM described in Eq. **4.16** can be written as a linear system as follows:

$$\mathbf{HV} = \mathbf{D} \qquad 4.18$$

where

$$\mathrm{H} = \begin{bmatrix} \psi_{a_1 b_1}(P_1(\mathbf{x}_1)) & \cdots & \psi_{a_M b_M}(P_M(\mathbf{x}_1)) \\ \vdots & \vdots & \vdots \\ \psi_{a_1 b_1}(P_1(\mathbf{x}_L)) & \vdots & \psi_{a_M b_M}(P_M(\mathbf{x}_L)) \end{bmatrix}_{LxM} \qquad 4.19$$

$$\mathrm{V} = (\boldsymbol{v}_1^T \quad \boldsymbol{v}_2^T \quad \cdots \quad \boldsymbol{v}_O^T)_{MxO}^T \qquad 4.20$$

V can be obtained by solving the least-square solution of **4.18**, and is given by:

$$\hat{\mathbf{V}} = \mathbf{H}^\dagger \mathbf{D} \qquad 4.21$$

The training algorithm of AW-ELM can be implemented as follows.

Given a training set $\aleph = \{(\boldsymbol{x}_k, \boldsymbol{t}_k) \mid \boldsymbol{x}_k \in \boldsymbol{R}^n, \boldsymbol{t}_k \in \boldsymbol{R}^o, k = 1, 2 ..., L\}$, the hidden node output function $\psi_{ai,bi}(\boldsymbol{w}, \boldsymbol{c}; \boldsymbol{x})$ and the hidden node number M, then

1. Randomly assign vector matrix $\boldsymbol{W}$ and bias c
2. Calculate the input hidden layer P_j in Eq. **4.9**
3. Calculate b_j in Eq. **4.14** and **4.15**
4. Calculate the hidden layer output **H** in Eq. **4.19**
5. Calculate the output weight $\hat{V}$ in Eq. **4.21**.

4.2.4   Experimental setup

The experiments to test the performance of AW-ELM were conducted by following the state-of-the-art of pattern recognition system as shown in Figure 4.4.
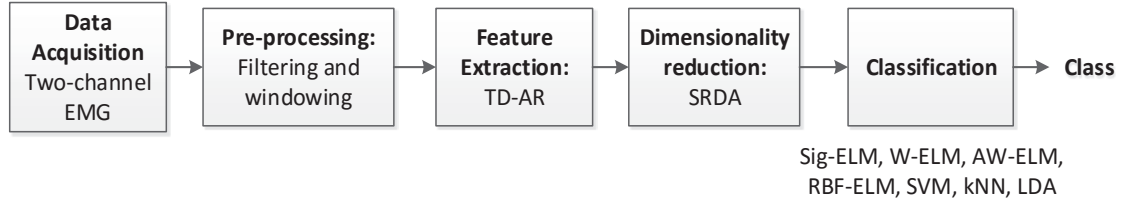
Figure 4.4 Myoelectric finger classification using AW-ELM and other classifiers

Each stage of the processes in Figure 4.4 will be discussed in detail. The EMG signals were acquired from eight subjects. The filtering and windowing were applied to the collected data before being extracted using a time domain feature set and autoregressive model (AR). To reduce the dimension of the features, SRDA was employed. The theory of SRDA was presented in Chapter 2 **section 2.3.1.3.3**. The experimental results in Chapter 3 section 3.3.4 show that SRDA is powerful and fast. Therefore, the myoelectric pattern recognition (M-PR) system chose SRDA for dimensionality reduction. In the classification stage, the performance of AW-ELM will be compared with the other node-based ELMs and other well-known classifiers such as RBF-ELM, SVM, LDA, and kNN. The experimental results of AW-ELM on EMG signals are presented in **section 4.2.5**. The experiments on benchmarks datasets were also performed to test the performance of AW-ELM in a broad range of datasets. Eventually, the last section, which is the conclusion, will end the discussion about AW-ELM.

4.2.4.1   Experimental procedures

The data in this work were acquired from eight subjects, two females and six males aged 24-60 years old. All subjects were normally limbed with no muscle disorders. To avoid the effect of movement position on EMG signals,each subject's arm was supported and fixed at a certain position (R. N Khushaba *et al.*, 2012).

The FlexComp Infiniti™ System from Thought Technology was used to acquire signals from two EMG MyoScan™ T9503M sensors which were put on the subject's forearm, as seen in Figure 4.5. The acquired EMG signals were amplified to a total gain of 1000 and sampled at 2000 Hz.
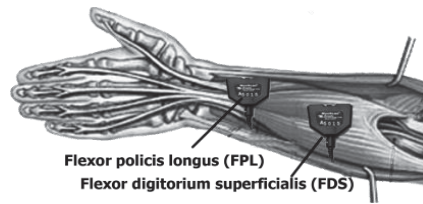
Figure 4.5 The placement of the electrodes

The collected EMG signals were processed in the Matlab 2012b installed in the Intel Core i5 3.1 GHz desktop computer with 4 GB RAM running on Windows 7 operating system. A band-pass filter filters the signals in the frequency range between 20 and 500 Hz. In addition to the band-pass filter, a notch filter was used as well to remove the 50 Hz line interference. Finally, the EMG signals were down-sampled to 1000 Hz to reduce the data size.

Figure 4.6 shows ten classes of the individual and combined finger movements consisting of a flexion of individual fingers, i.e., Thumb (T), Index (I), Middle (M), Ring (R), Little (L) and the pinching of combined Thumb–Index (T–I), Thumb–Middle (T–M), Thumb–Ring (T–R), Thumb–Little (T–L), and the hand close (HC).
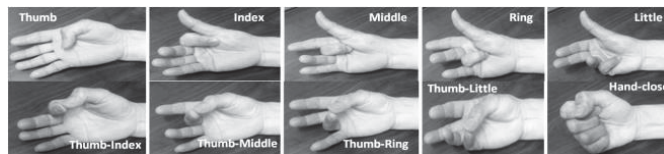
Figure 4.6 Ten different finger movements

The classification was performed based on the data from the data acquisition. In this stage, the subjects were asked to perform a certain posture of finger movement for 5 s and then take a rest for 5 s. Each movement was repeated six times. Therefore, there are 5000 x 6 = 30000 data for each class or in total, the number of data is 30,000 x 10 classes = 300,000/channel. There are two channels, so the number of data as a whole is 600,000. The data collected were divided into training data and testing data using 3-fold cross validation.

4.2.4.2 Feature Extraction

The experiments in this subsection employed a feature set resulted in the chapter 3 **section 3.3.3**. The feature set consists of waveform length (WL), slope sign changes (SSC), number of zero crossings (ZCC), sample skewness (SS), mean absolute value (MAV), mean absolute value slope (MAVS) and root mean square (RMS). In addition, some parameters from Hjorth time domain Parameters (HTD) and autoregressive (AR) model parameters were included. This feature set produces 16 x 2 channels = 32 features.

All features were extracted using myoelectric toolbox (A. D. C. Chan & Green, 2007) and Biosig toolbox (Schlogl & Brunner, 2008). The AR model parameters have been proven to be stable and robust to the electrode location shift and the change of signal level (Tkach *et al.*, 2010).

All features were concatenated and reduced using SRDA. SRDA is an extension of LDA, which can deal with a singularity and a large data set. The window length of 100 ms was applied to the signal to comply with the real-time application, along with a 100-ms increment. The M-PR system only considered the steady state of the EMG signal and remove the transient part of the signal, as recommend by Kevin Englehart *et al.* (2001).

4.2.4.3   *Majority Vote*

To smooth the classification results, the majority vote (A. D. C. Chan & Green, 2007) was applied in some experiments. It employs the results from the *n* present state and *m* previous states and makes a new classification result based on the class that comes out most frequently. In this research, $n = 0$ and $m = 4$ were used.

4.2.5   Experiments and Results

This section applied W-ELM and AW-ELM to two different groups of datasets. The first dataset is the EMG dataset for myoelectric finger motion recognition. The second dataset is a dataset of UCI machine learning repository.

4.2.5.1   *Experiments on myoelectric finger motion recognition*

Various experiments were done to examine the performance of AW-ELM in the myoelectric pattern recognition (M-PR). The first experiment was the experiment performed by varying the number of nodes in the hidden layers. The performance of AW-ELM was compared with other node-based ELM such as wavelet extreme learning machine (W-ELM) and sigmoid extreme learning machine (Sig-ELM). The second experiment is the comparison of AW-ELM and other well-known classifiers such as support vector machine (SVM), kernel-based ELM represented by radial basis function ELM (RBF-ELM), linear discriminant analysis (LDA), and k-nearest neighbour (kNN). Some analyses were given in each experiment.

4.2.5.1.1   AW-ELM and other node based ELM

This subsection examined three node-based ELMs: W-ELM, AW-ELM and sigmoid extreme learning machine (Sig-ELM). The number of hidden nodes varied from 50 up to 500. Four-fold cross validation was used to verify the validity of classification result. For segmentation, the work employed overlap windowing with the window length of 200 ms

along with a 25 increment. Furthermore, post-processing method is not used in the experiments. The M-PR system only considers the state steady of the EMG signal and remove the transient state of the signal. Figure 4.7 and Table 4.1 shows the classification results.
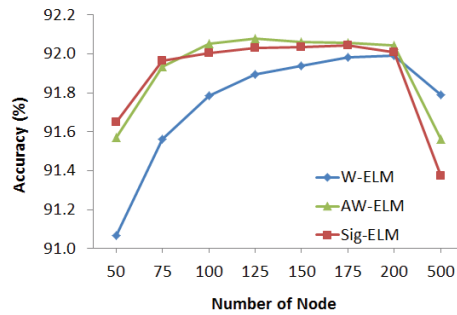
Figure 4.7 The classification accuracy of three node base ELM across eight subjects using 4-fold cross validation

Figure 4.7 and Table 4.1 indicate that the accuracy of AW-ELM was higher than W-ELM in all cases, except for the hidden node number of 500. Likewise, the AW-ELM performance is better than Sig-ELM in all hidden-node numbers except for the hidden node number of 50 and 75. In these two hidden numbers, the Sig-ELM achieved better accuracy than AW-ELM. Overall, in most cases, the adaptation of the wavelet function using a sigmoid function in AW-ELM could enhance the performance of the original wavelet extreme learning machine. Moreover, it is better than Sig-ELM. In the network structure, AW-ELM consists of two activation functions: a sigmoid and wavelet function. The role of the sigmoid function is to reshape the wavelet function in accordance with the changes in the input state. Therefore, AW-ELM performed better than W-ELM and Sig-ELM. In addition, Table 4.1 provides the number of nodes for each classifier in myoelectric finger motion recognition. The optimal number for each classifier is 200 nodes for W-ELM, 125 nodes for AW-ELM and 175 for Sig-ELM.

Table 4.1 The average classification accuracy of AW-ELM across eight subjects using four-fold cross validation compared with W-ELM and Sig-ELM

# Hidden Node	Accuracy (%)		
	W-ELM	**AW-ELM**	**Sig-ELM**
50	91.07 ± 0.17	91.57 ± 0.08	**91.65 ± 0.08**
75	91.56 ± 0.14	91.93 ± 0.14	**91.97 ± 0.10**
100	91.79 ± 0.10	**92.05 ± 0.09**	92.01 ± 0.08
125	91.90 ± 0.08	**92.08 ± 0.09**	92.03 ± 0.10
150	91.94 ± 0.11	**92.06 ± 0.10**	92.04 ± 0.10
175	91.98 ± 0.09	**92.06 ± 0.09**	92.04 ± 0.08
200	91.99 ± 0.08	**92.04 ± 0.08**	92.01 ± 0.06
500	**91.79 ± 0.08**	91.56 ± 0.06	91.37 ± 0.06

In terms of processing time, the ELM using a sigmoid function (Sig-ELM) took less time than W-ELM and AW-ELM, in the training and testing trials, as depicted in Figure 4.8 and Table 4.2. Figure 4.8 shows that the larger the number of the hidden nodes, the longer the time difference between AW-ELM and Sig-ELM. Likewise, in the testing time, AW-ELM is the slowest classifier. The adaptive mechanism in AW-ELM adds to the processing time in both the training and testing trials.
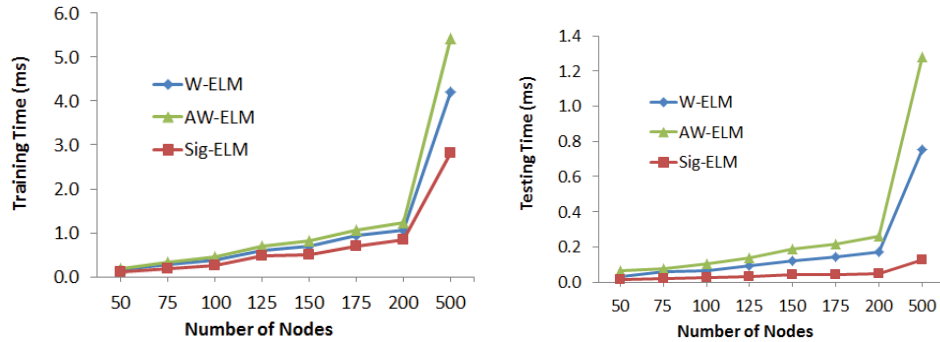
Figure 4.8 The training time (LEFT) and testing time (RIGHT) of the node-based ELMs

Table 4.2 Processing time of different ELM classifiers

#Hidden Node	Training Time (s)			Testing Time (s)		
	W-ELM	AW-ELM	Sig-ELM	W-ELM	AW-ELM	Sig-ELM
50	0.16 ± 0.01	0.19 ± 0.02	0.12 ± 0.00	0.03 ± 0.00	0.06 ± 0.00	0.01 ± 0.00
75	0.28 ± 0.01	0.33 ± 0.01	0.19 ± 0.00	0.06 ± 0.01	0.07 ± 0.00	0.02 ± 0.00
100	0.38 ± 0.02	0.45 ± 0.02	0.27 ± 0.01	0.07 ± 0.00	0.10 ± 0.00	0.02 ± 0.00
125	0.59 ± 0.05	0.70 ± 0.06	0.48 ± 0.07	0.09 ± 0.00	0.14 ± 0.00	0.03 ± 0.00
150	0.71 ± 0.01	0.81 ± 0.01	0.51 ± 0.01	0.12 ± 0.00	0.19 ± 0.01	0.04 ± 0.00
175	0.93 ± 0.06	1.06 ± 0.05	0.69 ± 0.05	0.14 ± 0.00	0.22 ± 0.00	0.04 ± 0.00
200	1.07 ± 0.08	1.22 ± 0.05	0.85 ± 0.06	0.17 ± 0.00	0.26 ± 0.00	0.05 ± 0.00
500	4.20 ± 0.08	5.42 ± 0.08	2.82 ± 0.10	0.75 ± 0.01	1.28 ± 0.01	0.12 ± 0.00

The one-way ANOVA test was done to evaluate the significance of the performance of AW-ELM compared to W-ELM and Sig-ELM, as presented in Table 4.3. Confidence level of the ANOVA test was set at $p = 0.05$. Table 4.3 shows that p-values on the comparison of AW-ELM and W-ELM are less than 0.05. In other words, the improvement of AW-ELM on W-ELM is statistically significant. As for AW-ELM and Sig-ELM, in general, their performances are significantly different except in a few situations. For instance, when using 50 hidden nodes, the accuracy of Sig-ELM is better than AW-ELM; the accuracy gap is statistically significant. However, when using hidden node number 100 or 500, the AW-ELM is better than Sig-ELM and the difference is statistically significant. As for the rest of hidden node numbers, AW-ELM is better than Sig-ELM but the difference is not significant. Overall, AW-ELM is the best classifier among the tested classifier for finger movement recognition.

Table 4.3 The p-value of anova test on the classification accuracy between AW-ELM and other tested classifiers

#Hidden Node	*p*-value	
	AW-ELM & W-ELM	**AW-ELM & Sig-ELM**
50	0.0000	0.0000
75	0.0000	0.1283
100	0.0000	0.0006
125	0.0000	0.0610
150	0.0000	0.3477
175	0.0021	0.5746
200	0.0098	0.0552
500	0.0000	0.0000

4.2.5.1.2   AW-ELM and other well-known classifiers

The experiments were conducted to examine the performance of AW-ELM in recognizing ten finger movements and compare the results with other well-known classifiers. The EMG signal was segmented using the adjoining window with 100 ms of window length and incremented every 100 ms. Four famous classifiers besides AW-ELM involved in this experiment: the kernel based ELM with radial basis function (RBF-ELM), support vector machine (SVM), linear discriminant analysis (LDA) and k-nearest neighbour (kNN). Majority vote with four previous votes refined the classification results. To get the best classification performance, parameters of the classifier were determined using a grid-search method. Table 4.4 presents the optimal parameters for each classifier. Figure 4.9 depicts the performance of AW-ELM compared to other well-known classifiers. A 3-fold cross validation is used to validate the classification performance.

Table 4.4 The parameters of classifier involved in the experiment

Classifier	C	γ	d	#nodes	k
AW-ELM	-	-	-	120	-
RBF-ELM	2^0	2^{-5}	-	-	-
SVM	2^8	2^7	-	-	-
kNN	-	-	-	-	10

Figure 4.9 shows that all classifiers can classify ten finger motions with good accuracy. The best classifier is RBF-ELM. It is the best on most of the eight subjects except subjects S2 and S8. The second best is kNN. As for AW-ELM, its performance is as good as SVM. The least accurate classifier is LDA that occurred in all subjects expect subject S2; even LDA is the most accurate system on this subject. Table 4.5 provide clear information about the accuracy of each classifier that confirms the aforementioned conclusions.
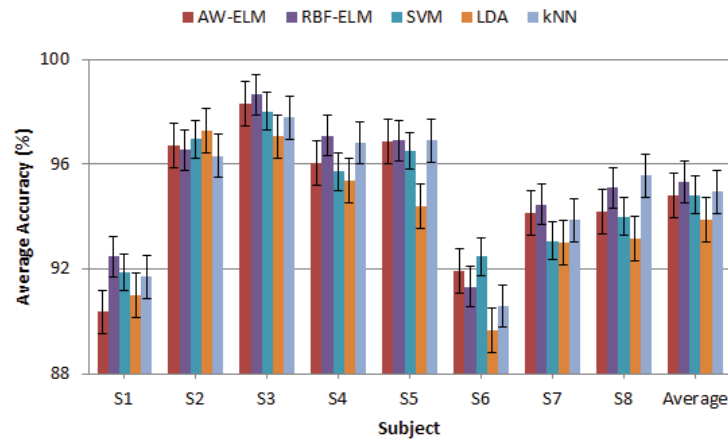
Figure 4.9 The performance of AW-ELM and well-known classifiers in recognizing 10 finger motions on eight different subjects using 3-fold cross validation

Table 4.5 The average accuracy of different classifiers for myoelectric finger motion classification using 3-fold cross validation

Classifier	Accuracy (%)	Training time (ms)	Testing time (ms)
AW-ELM	94.84 ± 2.54	450 ± 62	94 ± 20
RBF-ELM	**$\underline{95.33 \pm 2.48}$**	136 ± 2	50 ± 1
SVM	94.83 ± 2.27	2395 ± 110	97 ± 5
LDA	93.87 ± 2.71	**$\underline{6 \pm 3}$**	**$\underline{4 \pm 1}$**
kNN	94.95 ± 2.63	55 ± 14	33 ± 3

Even though RBF-ELM is superior to other classifier, ANOVA test result on AW-ELM and RBF-ELM indicates the accuracy gap between the two classifiers is not significant (p>0.05), as described in Table 4.6. Similarly, ANOVA test on AW-ELM and SVM shows that their performance difference is not significant including the comparison with LDA and kNN. In summary, the performance of AW-ELM is comparable to other well-known classifiers.

Table 4.6 *p*-value of AW-ELM and other famous classifiers

AW-ELM vs. →	RBF-ELM	SVM	LDA	KNN
***p*-value**	0.667	0.961	0.509	0.894

The goal of the myoelectric recognition in this section is to classify ten finger motions. Therefore, the evaluation of the performance of AW-ELM was performed. Figure 4.10 shows the results. The figure indicates that AW-ELM is the most accurate classifiers in three movements (T-I, T-L, and HC), and it is among the best classifiers in two movements (M and R). Nevertheless, the figure provides the information that AW-ELM is the worst one on little (L) and thumb-ring (T-R) finger movements. Furthermore, all

classifiers can recognize the ring finger movement (R) properly while they could not classify the combination of thumb and ring finger motion (T-R) correctly; even the accuracy of the T-R is the worst. Overall, AW-ELM is a promising classifier for myoelectric finger motion recognition, and it is comparable to most used classifiers used in the myoelectric pattern recognition field such as SVM, LDA and kNN.
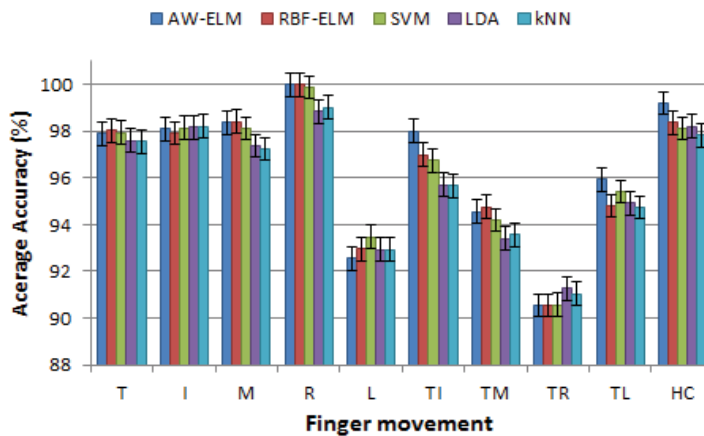
Figure 4.10 The performance of AW-ELM and other classifiers in classifying ten finger movements across eight subjects using 3-fold cross validation

Table 4.7 describes the confusion matrix of the accuracy of AW-ELM. Through this table, we can observe the misclassified movement made by certain movement. For instance, the movement TR (thumb and ring) is the most misclassified, followed by HC (hand-close) and then TI, TL and the least is TM. Furthermore, the movement L (little finger) is misclassified to almost all movements except to T, M, and I. Nevertheless, overall performances indicate the AW-ELM can recognize ten finger motions using only two EMG channels.

Table 4.7 The confusion matrix of accuracy of AW-ELM in classifying ten finger movements across eight subjects using 3-fold cross validation

		Classified									
		T	I	M	R	L	TI	TM	TR	TL	HC
Intended	T	97.89	0.00	0.00	0.00	0.35	0.35	0.00	0.00	0.00	1.41
	I	0.00	98.09	0.00	0.00	0.00	1.91	0.00	0.00	0.00	0.00
	M	0.00	0.17	98.36	0.00	0.00	0.00	1.47	0.00	0.00	0.00
	R	0.00	0.00	0.00	100.00	0.00	0.00	0.00	0.00	0.00	0.00
	L	0.00	0.00	0.00	1.76	92.56	1.51	0.87	1.39	1.39	0.52
	TI	0.69	0.07	0.00	0.00	0.64	98.02	0.35	0.00	0.22	0.00
	TM	0.00	1.34	0.02	0.00	1.51	2.41	94.54	0.00	0.17	0.00
	TR	0.00	0.00	0.00	0.00	0.00	1.86	1.18	90.54	1.35	5.07
	TL	0.97	0.00	0.00	0.00	0.94	2.16	0.00	0.00	95.93	0.00
	HC	0.80	0.00	0.00	0.00	0.00	0.00	0.00	0.00	0.00	99.20

4.2.5.2   Experiments on UCI datasets

AW-ELM has been proven able to classify ten finger movements consisting of five individual fingers and five combined fingers. In this section, the experiments were carried out to investigate the performance of AW-ELM on the benchmark datasets that are available online on the UCI machine learning website. The validation of the experiments is based on the size of the data. The 5-fold cross-validation was implemented on small and medium size data while the 3-fold cross-validation was applied to the large size data. Special for large size data, the work did not randomize the data. Instead, the work just divided the data into three groups and then applied the cross-validation.

Table 4.8 Data specification for benchmarking

Dataset	Group	# data	# features	#classes
Iris	Small size	150	4	3
Glass		214	9	6
Vehicle	Medium size	846	18	4
Vowel		990	10	11
Satimage	Large size	6435	36	6
Letter		20000	16	26
Shuttle		58000	9	7

The experiments in this section involved seven different classifiers: W-ELM, AW-ELM, Sig-ELM (sigmoid ELM), RBF-ELM (kernel based ELM), LIBSVM, LDA and kNN. Before conducting the experiment, the parameters that affect the performance of the classifier were optimized. For instance, LIBSVM with radial basis kernel relies on regulation parameter C and gamma. A grid-search method was used to select the optimum number of nodes in the node based ELM. As for C and gamma in RBF-ELM and LIBSVM, the optimal parameters was taken from (G. B. Huang *et al.*, 2012) because this research used the same data and same classifiers as in (G. B. Huang *et al.*, 2012). Table 4.9 provides all parameters used in the experiment. Table 4.10 presents the experimental results.

Table 4.10 shows that AW-ELM could perform moderately across seven different datasets. The comparison of AW-ELM and W-ELM shows that both classifiers are comparable. One-way ANOVA test shown in Table 4.11 explains that the accuracy gap between them is not significant ($p > 0.05$). It means that they are comparable. As for SIG-ELM, the accuracy of AW-ELM is significantly better than SIG-ELM only in "Letter" dataset while the rest of them are not significantly different ($p < 0.05$).

Table 4.9 The optimal parameters used by each classifier in the UCI dataset experiments

Dataset	# Nodes			RBF		SVM		kNN
	W-ELM	AW-ELM	SIG-ELM	C	gamma	C	gamma	k
Iris	30	30	20	1	1	1	0.25	10
Glass	30	30	20	32	1	1	0.25	10
Vehicle	190	170	210	64	8	2^{14}	4	10
Vowel	290	350	440	32	0.5	1	1	10
Letter	970	980	920	8	0.25	2^{10}	2^{-4}	10
Satimage	740	640	770	16	0.25	1	1	10
Shuttle	900	500	970	2^{20}	2^{-10}	2^{10}	0.25	10

Table 4.10 The accuracy of seven classifiers on various data using 5-fold cross validation for small and medium size data and 3-fold cross validation for large size data

Dataset	Accuracy (%)						
	W-ELM	AW-ELM	SIG-ELM	RBF-ELM	LIBSVM	LDA	kNN
Iris	96.00	96.67	96.67	96.67	96.67	**<u>98.00</u>**	96.00
Glass	65.03	65.38	66.29	**<u>69.23</u>**	63.48	57.50	63.98
Vehicle	82.50	81.68	80.61	**<u>84.17</u>**	71.51	78.47	70.21
Vowel	94.44	93.54	93.84	**<u>94.65</u>**	91.21	60.81	84.75
Satimage	87.35	87.26	87.99	**<u>90.57</u>**	89.91	82.70	88.66
Letter	62.78	62.65	61.99	**<u>69.96</u>**	46.56	33.01	67.31
Shuttle	99.74	99.57	99.72	**<u>99.90</u>**	98.59	85.30	99.81

Table 4.11 One way ANOVA test results on the comparison of AW-ELM and other classifiers (the black box shows p < 0.05)

	p-value					
AW-ELM -->	W-ELM	SIG-ELM	RBF-ELM	LIBSVM	LDA	kNN
Iris	0.771	1.000	1.000	1.000	0.524	0.809
Glass	0.942	0.835	0.377	0.682	0.075	0.755
Vehicle	0.585	0.424	0.080	0.000	0.121	0.000
Vowel	0.432	0.807	0.354	0.064	0.000	0.005
Satimage	0.999	0.980	0.922	0.934	0.885	0.966
Letter	0.765	0.043	0.000	0.000	0.000	0.000
Shuttle	0.996	0.997	0.993	0.980	0.679	0.995

Furthermore, Table 4.10 and Table 4.11 indicate that RBF-ELM is the most accurate classifier across seven datasets except the "Iris" dataset. Nevertheless, the accuracy of AW-ELM is comparable to RBF-ELM in all datasets (p > 0.05) except in "Letter" dataset (p < 0.05). Moreover, AW-ELM has the same performance as LIBSVM except on Vehicle and Letter datasets in which AW-ELM is better. For the rest of the classifiers, Table 4.10 and Table 4.11 show that AW-ELM is significantly better than LDA in two datasets: Vowel and Letter. Moreover, AW-ELM is better than kNN in Vowel dataset

while kNN is better than AW-ELM in Letter datasets ($p < 0.05$). Overall, AW-ELM is comparable to RBF-ELM and LIBSVM and slightly better than LDA and kNN in most of datasets.

In addition to the classification performance, the processing time of classifiers is one of the discussion objectives. Table 4.12 presents the training time while Table 4.13 provides the testing time. Table 4.12 shows that the training time of AW-ELM is one of the slowest classifiers, compared to other classifier over all datasets. It becomes worse when AW-ELM works on big data like "Letter" dataset. The AW-ELM is the slowest classifier taking around 40 s to learn Letter datasets. However, an anomaly occurred when AW-ELM worked on Shuttle datasets. AW-ELM took around 33 s, faster than W-ELM, SIG-ELM even much faster than RBF-ELM that took 123 s. Similar results happen on the testing time. This happened because AW-ELM used lower number of nodes than SIG-ELM or W-ELM when working on the Shuttle dataset.

Table 4.12 The training time of seven classifiers on various data using 5-fold cross validation for small and medium size data and 3-fold cross validation for large size data

Dataset	Training Time (ms)						
	W-ELM	AW-ELM	SIG-ELM	RBF-ELM	LIBSVM	LDA	kNN
Iris	45.20	48.33	41.33	3.51	0.00	15.61	38.53
Glass	69.53	68.40	31.93	1.81	2.00	1.83	9.62
Vehicle	403.13	353.67	438.13	16.03	56.00	2.76	40.11
Vowel	776.00	1,014.80	1,334.67	20.95	30.00	4.82	28.72
Satimage	6,412.22	6,236.67	5,436.33	562.04	723.33	49.07	799.55
Letter	29,202.20	40,664.33	17,541.87	11,442.31	20,140.00	72.39	4,618.73
Shuttle	62,114.33	33,069.22	47,162.44	123,161.44	10,820.00	49.54	1,472.41

Table 4.13 The testing time of seven classifiers on various data using 5-fold cross validation for small and medium size data and 3-fold cross validation for large size data

Dataset	Testing time (ms)						
	W-ELM	AW-ELM	SIG-ELM	RBF-ELM	LIBSVM	LDA	kNN
Iris	10.00	16.27	6.47	0.99	0.00	1.74	6.28
Glass	10.73	17.20	6.60	0.46	2.00	1.47	5.80
Vehicle	38.07	46.00	28.07	2.47	56.00	1.88	9.88
Vowel	51.40	72.67	34.47	3.69	30.00	2.93	12.43
Satimage	709.00	1,082.00	134.67	112.45	723.33	14.85	375.33
Letter	2,391.53	4,751.87	276.87	873.45	20,140.00	28.72	1,177.10
Shuttle	11,241.89	8,536.11	1,001.22	10,101.54	10,820.00	36.02	786.39

One thing that is not normal on LIBSVM; the training time and the processing time of LIBSVM is the same while the other classifiers took a shorter testing time than training

time. The fastest classifier is LDA, which took only around 72 ms on Letter dataset and about 49 ms on Shuttle dataset. Overall, the training time of AW-ELM is slow but it can be compensated by using less number of nodes with comparable performance to other classifiers.

4.2.6   Conclusion

This section presents the implementation of wavelet extreme learning machine (W-ELM) and proposed adaptive wavelet extreme learning machine (AW-ELM) for finger motion recognition using EMG signals. In general, AW-ELM could classify ten finger movements with a good accuracy of 94.84 %. It is even comparable to the well-known classifiers RBF-ELM, SVM, LDA, and kNN. Therefore, AW-ELM could enhance the performance of the node-based ELM.

The research in this section did not compare the performance of AW-ELM with WNN or even VTWNN. However, by comparing AW-ELM to SVM, LDA, and kNN, the results will not be much different with the direct comparison of AW-ELM and WNN or VTWNN especially for myoelectric pattern recognition system (Kevin Englehart *et al.*, 2001).

W-ELM and the proposed one, AW-ELM are better that WNN in terms of training processing time, undoubtedly, because AW-ELM omits the iterative training procedure that is used in WNN. Although no iterative learning, AW-ELM is comparable to most well-known classifiers such as RBF-ELM, SVM, LDA and kNN. The implementation of W-ELM and AW-ELM for myoelectric finger motion recognition is **one of the thesis contributions**.

Another contribution that is proposed in this section is AW-ELM itself. The benefit of AW-ELM over W-ELM exists on omitting wavelet parameters initialization. Not like W-ELM that needs parameter initialization on the wavelet function, AW-ELM is free from that initialization. The benefit of initialization is to setup the range of mother wavelet in the range of input. It means we should know the input characteristic from the beginning. On the other hand, AW-ELM does not need initialization. Instead, it utilizes the internal mechanism to learn the range of input by varying the translation parameter of the wavelet activation function. Even Cao *et al.* (2010) who proposed composite function wavelet neural network with extreme learning machine (CFWNN-ELM) still needs initialization of wavelet parameters. Therefore, this is the contribution of AW-ELM.

In addition to the myoelectric finger motion classification, AW-ELM has been implemented in a wide range classification problem using UCI machine learning datasets.

The experimental results show that AW-ELM could work on a wide range of datasets from small size to large size data. AW-ELM is comparable to W-ELM in all datasets, and it is better than SIG-ELM on Letter datasets. Moreover, AW-ELM attained better accuracy than LDA in Vowel and Letter datasets while the other datasets shows the same performance as LDA. Comparison with RBF-ELM indicates that AW-ELM is comparable to RBF-ELM except on Letter dataset. On this dataset, RBF-ELM is better than AW-ELM.

Other results show that AW-ELM has the same performance as LIBSVM except on Vehicle and Letter datasets in which AW-ELM is better. Finally, the comparison with kNN shows that AW-ELM is better than kNN on Vowel dataset while kNN is better than AW-ELM on Letter dataset. Overall, AW-ELM is a promising classifier for many classification applications, especially for myoelectric pattern recognition.

4.3 Performance evaluation of spectral regression extreme learning machine (SR-ELM)

The previous section proposed a new ELM classifier, which is called AW-ELM, for the M-PR to recognize finger motions. This section proposes a new dimensionality reduction using extreme learning machine that will be applied in the M-PR for finger motion recognition. It is called spectral regression extreme learning machine (SR-ELM). SR-ELM is used to reduce the dimension of the features. In addition, SR-ELM projects the features that are normally scattered into the projected features that are separated properly according to their classes. Interestingly, SR-ELM is a kind of unsupervised method on the side of extreme learning machines, but it is a supervised method on the side of the dimensionality reduction.

This section is started with the background of SR-ELM and followed by the basic concepts of ELM and SR-ELM. The experiments on myoelectric pattern recognition for finger motion classification were conducted afterward. Not limited to the myoelectric signal, the experiments on UCI machine learning datasets were also performed to examine the performance of SR-ELM in broader applications. The conclusion will end the discussion of SR-ELM.

4.3.1 Background

The performance of myoelectric pattern recognition typically depends on the feature extraction and the classifiers (L.J. Hargrove *et al.*, 2007). L.J. Hargrove *et al.* (2007) and

others have proven that time domain feature and AR model parameters are good enough to extract features from the EMG signals. However, the extracted features are frequently scattered and large in dimension. This thesis proposes a new method to increase the class separability of the features to assist the classifier in doing its job in better way. Moreover, the method is also able to reduce the dimension of the features. The proposed method is called spectral regression extreme learning machine (SR-ELM), a new extreme learning machine for feature projection as well as for dimensionality reduction.

Extreme learning machine (ELM) is single hidden layer feed forward networks (SLFNs) that applies a random projection in the hidden layer. In other words, the hidden layer weight of ELM is determined randomly. Meanwhile, the output weight of ELM is calculated analytically using a least square method. It means no iterative training in ELM. As a result, ELM training is very fast compared to traditional SLFNs that use gradient descent algorithm. Interestingly, despite employing random projection in the hidden layer, ELM performance outperforms back propagation neural network in most cases, either for classification or regression problems (G.-B. Huang *et al.*, 2006; G. B. Huang *et al.*, 2012).

The ELM has succeeded after having been applied in many applications. As a classifier, it has been implemented in different application, such as in our published work on myoelectric pattern recognition (Khairul Anam *et al.*, 2013) and character recognition (Chacko *et al.*, 2012; Zheng *et al.*, 2013). In addition, it played an importance role in face recognition (Mohammed *et al.*, 2011), cancer detection (Saraswathi *et al.*, 2011), and protein structure prediction (Wang *et al.*, 2008). As for a regressor, ELM has proved its benefits in physical parameter estimation (Javed *et al.*, 2014) and electrical power system (Nizar *et al.*, 2008).

In addition to the classifier and approximator, ELM can be implemented in dimensionality reduction. G. Huang *et al.* (2014) have developed an unsupervised extreme learning for unsupervised dimensionality reduction (US-ELM). Its characteristic is similar to principal component analysis (PCA) that reduces the feature's dimension with an unknown label. In fact, if the label is available, the dimensionality reduction method can work better than without label. For this reason, linear discriminant analysis (LDA) has been proposed to consider the label. In many cases, LDA performs better than PCA except in a small number of data (Martínez & Kak, 2001).

To the best of the author's knowledge, no one has developed ELM for supervised dimensionality reduction. This section aims to develop a new ELM for supervised dimensionality reduction applied on myoelectric pattern recognition. This section employs spectral regression (Deng Cai *et al.*, 2007) to calculate the output weight of ELM instead of least square method as in the original ELM. Spectral regression is a spectral analysis of the Laplacian graph solved by least squares regression. It produces eigenvectors to project the input space to the output space. SR-ELM is similar to unsupervised ELM proposed by G. Huang *et al.* (2014) that utilizes the obtained eigenvector to project the hidden layer output to the output layer. The difference is on the calculation of the eigenvector. In this section, the known label is incorporated while, in US-ELM, it is not.

This section provides **two main contributions**. Firstly, it proposes a new and first ELM for supervised dimensionality reduction, i.e. SR-ELM. Secondly, it presents a new type of linear discriminant analysis (LDA) for myoelectric pattern recognition system and for general pattern recognition cases as will be shown in the experiments.

4.3.2 Extreme learning machine

For N arbitrary distinct samples $\{(x_i, t_i)\}_{i=1}^N \in \mathbf{R}^n$ x $\mathbf{R}^m$, the output of SLFNs with L hidden nodes is

$$f(\mathbf{x}_i) = \mathbf{h}(\mathbf{x}_i)\boldsymbol{\beta} = t_i, \quad i = 1, ..., N \qquad 4.22$$

where $\mathbf{h}(\mathbf{x}_i) \in \mathbf{R}^{NxL}$ and $\boldsymbol{\beta} \in \mathbf{R}^{Lxm}$. To solve the output weights, ELM minimize the sum of squared losses of prediction error as follows:

$$\text{Minimize}: L_{ELM} = \tfrac{1}{2}\|\boldsymbol{\beta}\|^2 + C\tfrac{1}{2}\sum_{i=1}^N \|e\|^2$$
$$\text{Subject to}: \mathbf{h}(\mathbf{x}_i)\boldsymbol{\beta} = t_i^T - e_i^T \qquad i = 1, ..., N \qquad 4.23$$

If the constraint is substituted into the objective function, the objective function becomes:

$$\text{Minimize}: L_{ELM} = \tfrac{1}{2}\|\boldsymbol{\beta}\|^2 + C\tfrac{1}{2}\sum_{i=1}^N \|\mathbf{T} - \mathbf{H}\boldsymbol{\beta}\|^2 \qquad 4.24$$

where $\mathbf{H} = [\mathbf{h}(\mathbf{x}_1), ..., \mathbf{h}(\mathbf{x}_N)^T]^T \in \mathbf{R}^{NxL}$ and $\mathbf{T} \in \mathbf{R}^{Nxm}$. Gradient of Eq. **4.24** with respect to β to zero gives:

$$\nabla L_{ELM} = \boldsymbol{\beta} + C\mathbf{H}^T(\mathbf{T} - \mathbf{H}\boldsymbol{\beta}) = 0 \qquad 4.25$$

Eq. **4.25** gives two solutions of $\boldsymbol{\beta}$ subject to the **H**. If **H** has more rows than columns:

$$\beta = \left(\mathbf{H}^T\mathbf{H} + \frac{I_L}{C} \right)^{-1} \mathbf{H}^T\mathbf{T} \qquad 4.26$$

where I_L is an identity matrix of dimension L. On the contrary, if $\mathbf{H}$ has more columns than rows, then

$$\beta = \mathbf{H}^T \left(\mathbf{H}\mathbf{H}^T + \frac{I_N}{C} \right)^{-1} \mathbf{T} \qquad 4.27$$

where I_N is an identity matrix of dimension N.

4.3.3 Spectral regression extreme learning machine (SR-ELM)

To modify ELM for a dimensionality reduction, the proposed method considers unknown labels of ELM. In other words, the proposed method employs unsupervised extreme machine learning as explained in (G. Huang *et al.*, 2014). Therefore, the objective function in Eq. **4.23** is modified as:

$$\text{Minimize} \ : L_{ELM} = \tfrac{1}{2}\|\beta\|^2 + \lambda\,\tfrac{1}{2}\mathrm{Tr}(\mathbf{F}^T\mathbf{L}\mathbf{F})$$
$$\text{Subject to} : \boldsymbol{f}_i = \mathbf{h}(\mathbf{x}_i)\boldsymbol{\beta} \qquad i = 1,...,N \qquad 4.28$$

where L is a graph Laplacian. Substitution of the constraint to the objective function will give:

$$\text{Minimize} \ : L_{ELM} = \tfrac{1}{2}\|\beta\|^2 + \lambda\,\tfrac{1}{2}\mathrm{Tr}(\boldsymbol{\beta}^T\mathbf{H}^T\mathbf{L}\boldsymbol{\beta}\mathbf{H})$$
$$\text{Subject to} \ : \boldsymbol{\beta}^T\mathbf{H}^T\mathbf{L}\boldsymbol{\beta}\mathbf{H} = \mathbf{I}_m \qquad 4.29$$

As proven in (G. Huang *et al.*, 2014), the optimal solution of Eq. **4.29** is the solution of the generalized eigenvalue problem:

$$\left(\mathbf{I}_L + \lambda\mathbf{H}^T\mathbf{L}\mathbf{H} \right)\mathbf{u} = \gamma\mathbf{H}^T\mathbf{L}\mathbf{H}\mathbf{u} \qquad 4.30$$

The spectral graph analysis assumes that the map of a graph to real line y, as a linear function:

$$\mathbf{y}=\mathbf{H}\mathbf{u} \qquad 4.31$$

As a result, Eq. **4.30** can be formulated as:

$$\left(\mathbf{I}_L + \lambda\mathbf{H}^T\mathbf{L}\mathbf{H} \right)\mathbf{u} = \gamma\mathbf{H}^T\mathbf{L}\mathbf{y} \qquad 4.32$$

According to the spectral regression theory (Deng Cai *et al.*, 2007; D. Cai *et al.*, 2008), the optimal y can be obtained by minimizing:

$$\sum_{i,j}\left(y_i - y_j\right)2\mathbf{W}_{ij} = 2\mathbf{y}^T\mathbf{L}\mathbf{y} \qquad 4.33$$

where L = D – W is a graph Laplacian. D is a diagonal matrix whose elements are $D_{ii} = \sum_j W_{ji}$, and W is a symmetric N x N matrix which is a pairwise similarity between two data points. N is the number of samples. They can also be optimized by solving the maximum eigenvalue problem (Deng Cai *et al.*, 2007):

$$\mathbf{W}\mathbf{y} = \lambda\mathbf{D}\mathbf{y} \qquad 4.34$$

In addition, the spectral regression algorithm can include label consisting *c* classes. The solution for **u** will contain **c-1** solutions.

In summary, the solution to **4.34** is done by two steps. Firstly, solve the eigenvalue problem. Secondly, find **u** with satisfies **Hu** = **y** using:

$$\mathbf{u} = \arg\min_u\left(\sum_{i=1}^{N}\left(\mathbf{u}^T h(x_i) - y_i\right)^2 + \alpha\sum_{j=1}^{L}u_j\right) \qquad 4.35$$

where α is regression parameters and u_j is the component of **u**. Finally

$$\boldsymbol{\beta} = \left[\mathbf{u}_1, \mathbf{u}_2, ..., \mathbf{u}_{c-1}\right] \in \mathrm{R}^L \qquad 4.36$$

Theoretically, the integration of ELM and SR, called SR-ELM, results in another variation of LDA. The ELM projects the input feature to a random feature. Then, the spectral regression projects the random feature to the reduced and meaningful features for the classifier. In the structure of ELM, the SR provides values for the output weights. Interesting characteristic of SR-ELM is, it is an unsupervised method on the side of ELM structure, but it is a supervised one on the side of dimensionality reduction.

4.3.4   Experiments and results

In this section, the work applied SR-ELM on two datasets. Firstly, SR-ELM is used to reduce the dimension of features from EMG signals for finger motion recognition. Secondly, SR-ELM is applied to public datasets from UCI Machine Learning Repository.

4.3.4.1   Experiments on myoelectric finger motion recognition

This section tested the performance of SR-ELM in the myoelectric pattern recognition system for classifying ten finger movements. Figure 4.11 describes the myoelectric pattern recognition used in this experiment.

EMG datasets used in this experiment were from data collection in section 4.2.4.1. EMG signals were recorded using 2000 kHz sampling frequency. The signals were

acquired from two electrodes located on the forearm of the subjects. Eight subjects, six males and two females participated in the experiment.
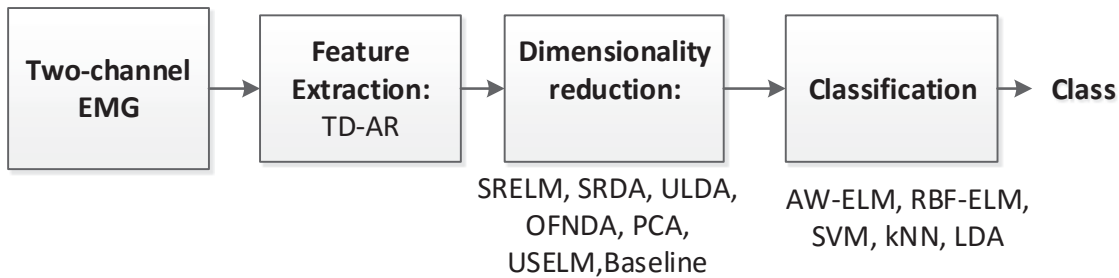
Figure 4.11 The myoelectric finger motion recognition for testing SR-ELM

In this research, the work summed two EMG signals from two channels to get a new EMG signal. Thus, there are three EMG channels now. From these EMG channels, the myoelectric pattern recognition (M-PR) extracted time domain features (TD). It involved zero waveform lengths (WL) (3 features), slope sign changes (SSC) (3 features), number of zero crossings (ZCC) (3 features), sample skewness (SS) (3 features) and mean absolute value (MAV) (3 features). In addition, some parameters from Hjorth-time domain parameters (HTD) (9 features) and 6-order autoregressive (AR) model parameters (18 features) were included. The total number of features extracted was 42. However, later, more features will be added to observe the performance of SR-ELM dealing with a wide range of features. For segmentation, the myoelectric pattern recognition (M-PR) system applied disjoint windowing with window length of 100 ms every 100 ms because it is compatible with the hardware that will be used in the real-time experiment.

SR-ELM reduces the dimension of the features from 42 to *c-1* features in which *c* is the number of classes. Then, the performance of SR-ELM will be compared with other dimensionality reduction methods such as uncorrelated linear discriminant analysis (ULDA) (Ye *et al.*, 2006), spectral regression dimensionality reduction (SRDA) and orthogonal fuzzy discriminant analysis (OFNDA) (R. N. Khushaba *et al.*, 2010). In addition, principal component analysis (PCA) and unsupervised extreme learning machine (US-ELM) will be involved. The trial without dimensionality reduction is also considered in the comparison (Baseline).

Furthermore, various classifiers will utilize projected features of SR-ELM to identify individual and combined finger movements. Those classifiers are AW-ELM (adaptive wavelet ELM), SVM (support vector machine), kNN (k-nearest neighbour) and LDA. Different numbers of classes will be tested starting from five up to ten classes. The ten classes consist of five individual finger movements, i.e. thumb (T), index (I), middle (M),

ring (R), little (L). The other movements are combined finger movements consisted of thumb-index (T–I), thumb-middle (T–M), thumb-ring (T–R), thumb-little (T–L) and the hand close (HC). The parameters of classifiers are presented in Table 4.14.

Table 4.14 The parameters of classifier involved in the experiment

Classifier	C	γ	d	#nodes	k
AW-ELM	-	-	-	100	-
RBF-ELM	2^0	2^{-5}	-	-	-
SVM	2^8	2^7	-	-	-
kNN	-	-	-	-	10

4.3.4.1.1 Parameter optimization

The parameter optimization of SR-ELM affects the performance of the system. SR-ELM contains two main parameters, i.e. the number of hidden nodes (a part of the ELM parameter) and alpha α (a part of the regression coefficient of the spectral regression). As in many feedforward neural networks, the number of hidden nodes is a trivial parameter that is not easy to determine. No general rule can be utilized to choose the optimal number of the hidden nodes. Therefore, the number of hidden nodes was varied, and the optimal one was selected by considering the accuracy and the reduction time. In this experiment, AW-ELM was employed as a classifier. In addition, the post-processing method is not used in the M-PR system.

Figure 4.12 presents the experimental result of the optimal node searching. As shown by the intersection of two red lines in Figure 4.12, approximately, 1000-node in the hidden layer is the optimum number. As for alpha (α), Figure 4.13 is used to obtain the relation of the number of nodes and alpha α. The figures show that as long as the number of nodes is a big number, then any value of alpha can be selected. However, the optimal value can be chosen by varying the value of alpha from 0.01 up to 15. Finally, 0.05 is the best value for the M-PR system in this section.
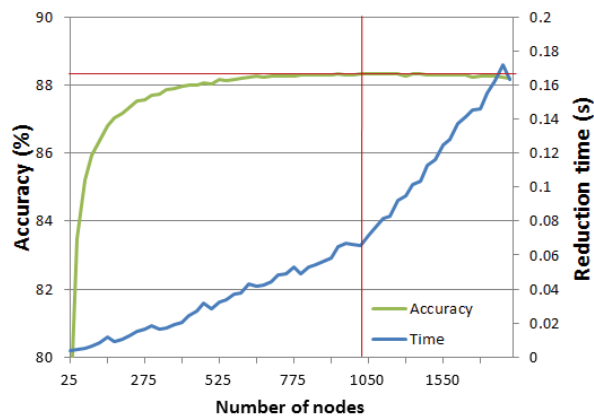
Figure 4.12 The experiment result for searching the optimal number of nodes
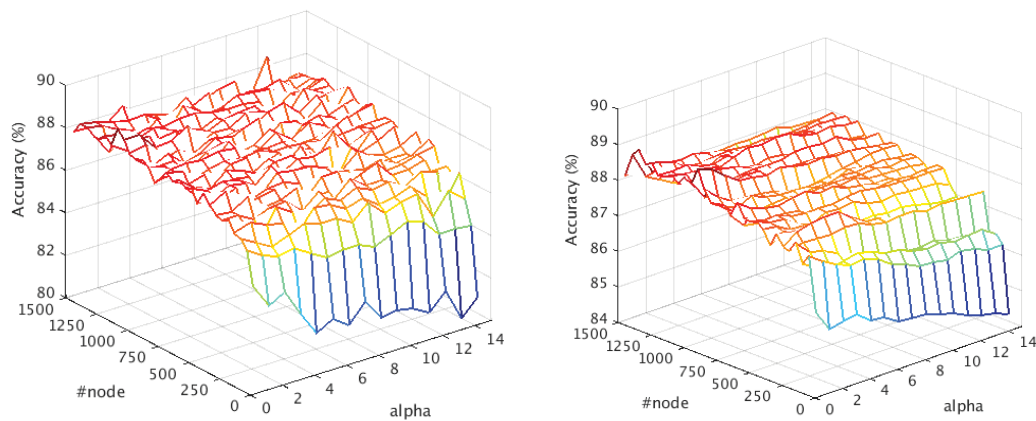
Figure 4.13 The relation of the number of nodes and alpha (α) using classifier AW-ELM (LEFT) and RBF-ELM (RIGHT)

4.3.4.1.2 The experiment on the class number

This section tested the performance of SR-ELM in reducing feature dimension for different classes, ranging from five up to ten classes. Table 4.15 presents the classes involved in the experiment.

Table 4.15 Various classes involved in the experiment

#Classes	Classes
5	T, I, M, R, L
6	T, I, M, R, L, T-I
7	T, I, M, R, L,T-I, T-M
8	T, I, M, R, L, T-I, T-M, T-R
9	T, I, M, R, L, T-I, T-M, T-R, T-L
10	T, I, M, R, L, T-I, T-M, T-R, T-L, HC

The SR-ELM's performance is compared to other well-known methods grouped into two groups: supervised and unsupervised dimensionality reduction. The supervised dimensionality reductions consist of ULDA (uncorrelated linear dimensionality reduction), SRDA (spectral regression dimensionality reduction), OFNDA (orthogonal fuzzy neighbourhood dimensionality reduction), while the unsupervised dimensionality reductions consist of PCA (principle component analysis), USELM (unsupervised extreme learning machine) and Baseline (without dimensionality reduction method). In addition, all experiments employed AW-ELM as a classifier. Figure 4.14 presents the experimental result.
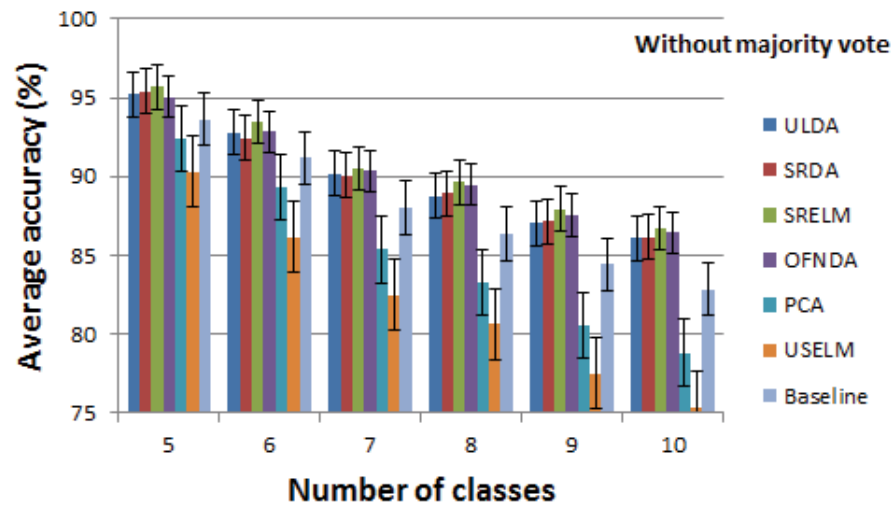
Figure 4.14 The performance of SR-ELM and others across eight subjects without using a majority vote

As shown in Figure 4.14, the accuracy of the system is decreasing as the number of classes is increasing. This trend happens to all methods. The characteristic of SR-ELM is comparable to the state-of-the-art of linear discriminant analysis. All supervised dimensionality reductions such as ULDA, SRDA, SR-ELM, and OFNDA attain similar accuracy in all class numbers. However, SR-ELM is better than all methods tested in the system that does not use the post-processing method, which is the majority vote. Its accuracy ranges from 95.67 % to 86.73 % for 5 to 10 classes of movement, as seen in Figure 4.14. However, when the system utilized the majority vote, the performance of SR-ELM and other methods is comparable (see Figure 4.15) with accuracy ranging from 98.64 % to 94.16 % for 5 to 10 motion classes.
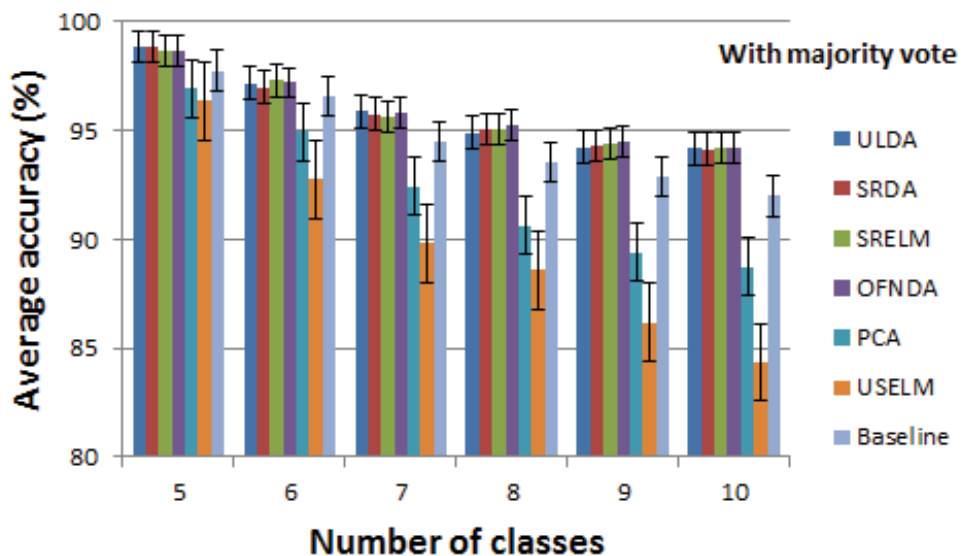
Figure 4.15 The performance of SR-ELM and others across eight subjects with a majority vote

111

SR-ELM and SRDA employ same spectral regression. They are different in treating the spectral regression (SR). SRDA uses SR to find the eigenvectors for the projection while SR-LEM utilizes SR to obtain the weight output of the extreme learning machine. Another difference of both is SR-ELM involves a random projection as additional to the SR projection. Experimentally, the random projection could improve the performance of the SRDA, as seen in Figure 4.14. Figure 4.14 shows that SR-ELM (green bars) is more accurate than SRDA and even better than other methods across five different classes. It indicates that SR-ELM enhances the performance of SRDA. However, when the classifiers employed the majority vote, the improvement of the SR-ELM is not seen significantly. Despite having better performance, SR-ELM takes more processing time than SRDA, as can be seen in Figure 4.16. However, its processing time is still reasonable and less than ULDA's processing time.
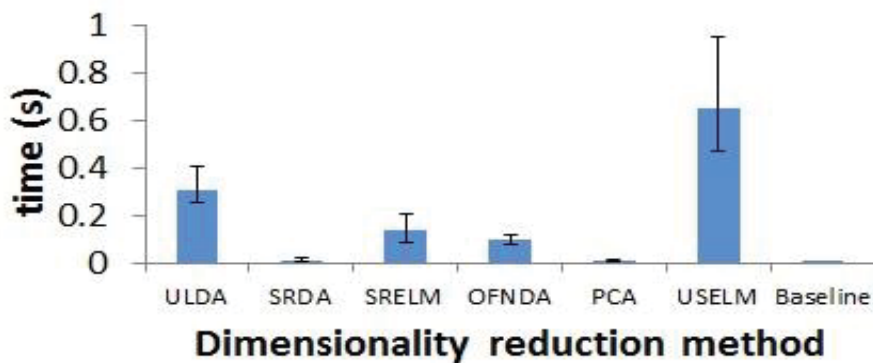
Figure 4.16 Processing time consumed by some dimensionality reduction methods

4.3.4.1.3 Classifier experiments

Various types of classifiers were involved to test the performance of SR-ELM. Figure 4.17 display the result. Figure 4.17 indicates that SR-ELM works well across five classifiers when the pattern recognition did not use the majority vote. The accuracy of SR-ELM is the best over classifiers except SVM. However, when the classifiers utilize the majority vote (see Figure 4.18) to refine the classification result, the influence of SR-ELM is not noticeable. In the myoelectric pattern recognition system, involving the majority vote could improve the performance, but it can increase the delay time (T. Farrell & Weir, 2008).
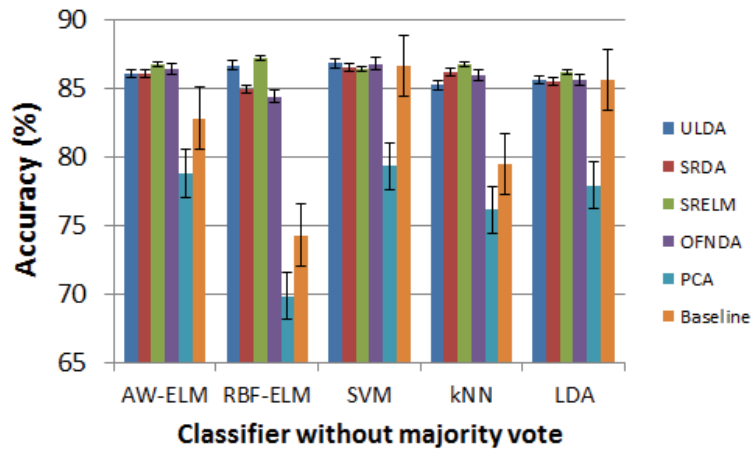
Figure 4.17 SR-ELM performance on different classifiers without majority vote across eight subjects
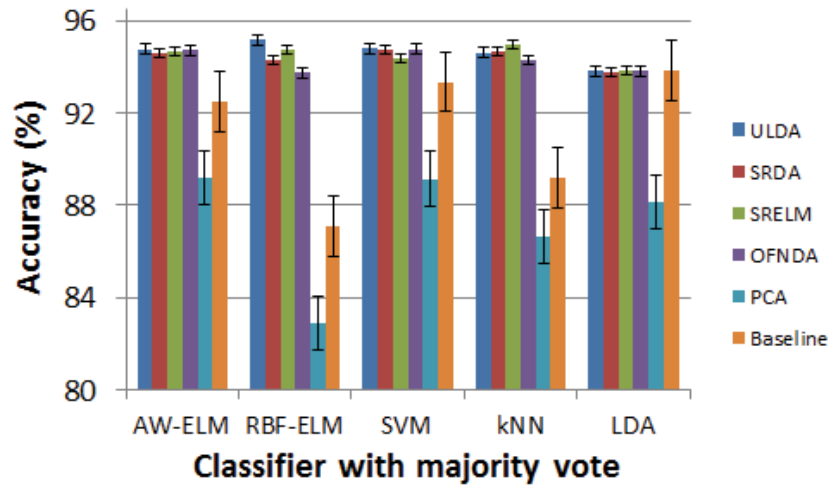
Figure 4.18 SR-ELM performance on different classifiers plus majority vote across eight subjects

An analysis of variance (ANOVA) test was also conducted to find the exact comparison of SR-ELM and other methods. Figure 4.19 presents the ANOVA test for p set at 0.05 using 10 classes with majority vote. The results indicate that there is a significant difference between SR-ELM and SRDA ($p<0.05$). However, the difference between SR-ELM and other LDA models like ULDA and OFNDA is not significant ($p>0.05$). This statistic analysis highlights the improvement of SR-ELM over SRDA.
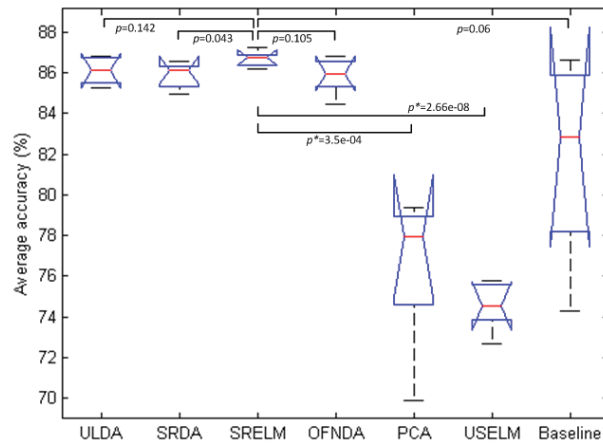
Figure 4.19 Anova test of SR-ELM and other methods across eight subjects using 10 classes with majority vote

The performance of the dimensionality reduction can be investigated from a scatter plot of the data. Figure 4.20 describes the scatter plot of three first features of the original feature set before being projected. The picture indicates that the data are scattered completely. The projection method such as LDA and SR-ELM could improve the class separability of the data, as shown in Figure 4.21 and Figure 4.22.
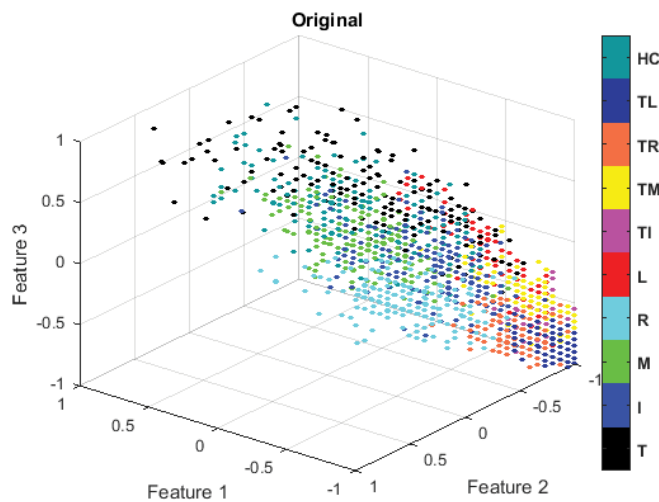
Figure 4.20 Scatter plot of the original features before projected

Figure 4.21 presents the scatter plot of ULDA and OFNDA. Both methods could enhance the class separability of features by grouping the data according to the class. Similarly, Figure 4.22 describing the scatter plot of the features using SRDA and SR-ELM indicates that SRDA and SR-ELM could improve the class separability of the features, compared with Figure 4.20. Furthermore, the comparison of the scatter plot of SRDA and SR-ELM is presented in Figure 4.22. The figure shows that feature projected using SR-ELM are slightly better than SRDA.

114
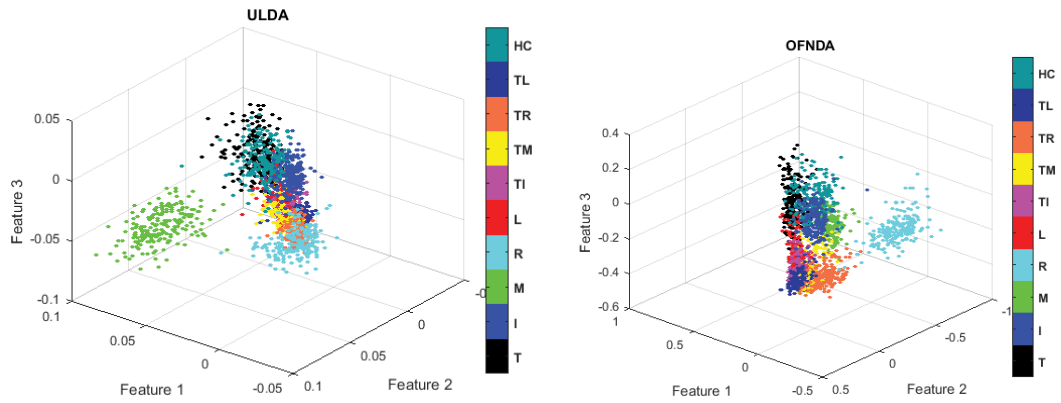
Figure 4.21 Scatter plot of the projected features using ULDA (LEFT) and OFNDA (RIGHT)
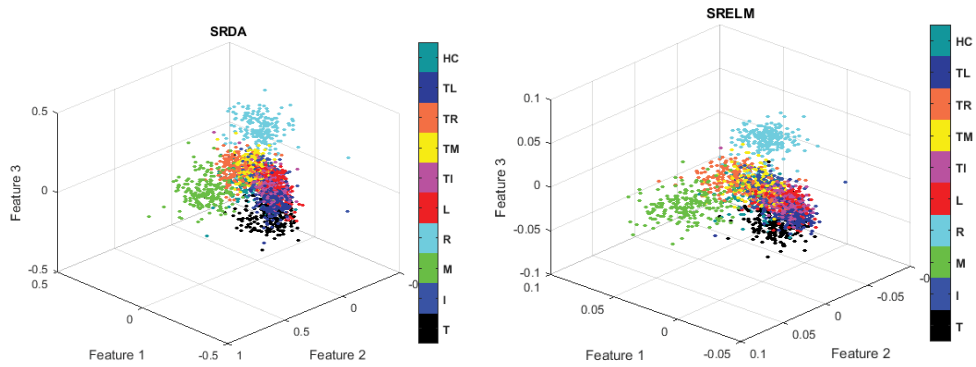
Figure 4.22 Scatter plot of the projected features using SRDA (LEFT) and SR-ELM (RIGHT)

4.3.4.1.4   Feature experiment

This section examined the performance of SR-ELM to reduce the features from EMG signals from various features.

Table 4.16 describes the various features used in the experiment.

Table 4.16 Various features used in the experiment

Name	#features	Features	Group
F1	12	SSC,ZC, WL, MAV	Small dimension
F2	15	SSC,ZC,WL,MAV, MAVS	
F3	24	SSC,ZC,WL,MAV, SKW, HJORTH	Medium dimension
F4	36	SSC,ZC,WL, MAV, MAVS, RMS,6AR	
F5	42	SSC,ZC,WL, MAV,SKW,HJORTH,6AR	
F6	48	SSC,ZC,WL,SKW,MAV,MAVS, HJORTH,RMS,6AR	
F7	195	Power autoregressive	Large dimension

Furthermore, several classifiers were employed along with the majority vote with *n* =4. They are AW-ELM (adaptive wavelet extreme learning machine), RBF-ELM (radial basis extreme learning machine), SVM (support vector machine), and LDA (linear

115

discriminant analysis). This experiments conducted 3-fold cross validation. Table 4.17 to Table 4.20 present the experimental results.

Table 4.17 The accuracy achieved employing AWELM on the feature test using 3-fold cross validation

Feature set	# features	Accuracy (100%)						
		ULDA	SRDA	SR-ELM	OFNDA	PCA	USELM	BASELINE
F1	12	88.88	88.35	**90.50**	86.15	87.59	80.52	89.51
F2	15	89.73	88.88	**91.38**	90.77	81.84	78.73	89.47
F3	24	93.55	93.31	**94.01**	93.49	90.44	87.91	92.99
F4	36	93.84	93.66	93.73	**93.90**	85.36	79.54	91.45
F5	42	**94.32**	94.15	94.22	94.20	88.60	84.45	92.21
F6	48	94.82	94.80	94.71	**94.85**	88.98	85.14	92.54
F7	195	63.99	94.02	92.52	**94.85**	88.98	85.14	92.54

Table 4.17 provides the experimental results when using AW-ELM as a classifier, to classify ten finger motions from the features reduced using various dimensionality reduction methods. SR-ELM achieved the highest accuracy for the feature set F1 up to F3. For the feature set F4 - F6, the accuracy of the system is not the highest but it is very close to the highest one. Another interesting fact is revealed when comparing SRDA and SR-ELM. In all features, SR-ELM attained better accuracy than SRDA except on the feature set F6 and F7. Especially on the feature set F7 whose dimension is vast, the difference of SRDA and SR-ELM is noticeable. Moreover, SR-ELM is better than unsupervised dimensionality reduction, PCA, and US-ELM. The comparison of SR-ELM and Baseline shows that the SR-ELM could reduce the dimension of data and at the same time could increase the class separability of the features. It is proven by looking at the accuracy of the Baseline, which is lower than SR-ELM except on the feature set F7. It seems that SR-ELM does not perform well on a large dimension of data.

In addition to AW-ELM, LDA also classified the ten finger movements along with various dimensionality reduction methods. Table 4.18 presents the experimental results. The table shows that SR-ELM is the most accurate method across six features sets: F1 to F6. However, SR-ELM is worse than SRDA when projecting the feature set F7, but it is still better than ULDA and OFNDA. This new fact confirms the previous assumption about SR-ELM that the accuracy is slightly low when it works on the large dimension of features. In general, compared to PCA, US-ELM and the Baseline, SR-ELM attained better accuracy.

Table 4.18 The accuracy achieved employing LDA on the feature test using 3-fold cross validation

Feature set	# features	Accuracy (100%)						
		ULDA	SRDA	SR-ELM	OFNDA	PCA	USELM	BASELINE
F1	12	85.70	84.17	**88.01**	82.07	82.83	73.12	85.70
F2	15	86.89	85.05	**88.81**	86.89	78.19	70.48	86.89
F3	24	92.53	92.34	**93.34**	92.53	88.48	82.37	92.53
F4	36	92.95	92.69	**93.64**	92.95	84.64	75.21	92.95
F5	42	93.33	93.25	**94.05**	93.33	87.65	80.85	93.33
F6	48	94.16	93.87	**94.59**	94.16	88.13	81.16	94.16
F7	195	92.10	**93.36**	92.77	92.10	91.33	87.24	92.10

By Looking at Table 4.19, Table 4.20, and facts mentioned in the previous discussion in this section, it could be concluded that SR-ELM is very useful for reducing the feature with low up to medium dimension. Compared to SRDA, the performance of SR-ELM is less but it is still high compared to unsupervised dimensionality reduction (PCA and USELM) and the baseline.

Table 4.19 The accuracy achieved employing RBF-ELM on the feature test using 3-fold cross validation

Feature set	# features	Accuracy (100%)						
		ULDA	SRDA	SR-ELM	OFNDA	PCA	USERLM	BASELINE
F1	12	90.63	87.33	**91.14**	85.50	80.24	81.15	80.79
F2	15	91.83	89.19	**92.15**	89.11	78.07	79.77	80.24
F3	24	94.39	93.06	**94.43**	92.25	87.15	88.46	87.81
F4	36	**94.67**	93.75	94.29	93.41	78.59	80.45	83.15
F5	42	**94.76**	93.83	94.52	93.25	82.43	85.14	86.57
F6	48	**95.47**	94.59	94.78	94.40	83.49	85.86	87.30
F7	195	92.47	**93.11**	92.98	17.62	87.64	87.34	88.01

Table 4.20 The accuracy achieved employing SVM on the feature test using 3-fold cross validation

Feature set	# features	Accuracy (100%)						
		ULDA	SRDA	SR-ELM	OFNDA	PCA	USERLM	BASELINE
F1	12	89.32	87.29	**89.55**	89.17	85.84	75.64	84.88
F2	15	**90.60**	88.09	90.39	90.50	81.62	73.71	85.60
F3	24	93.52	93.39	**93.57**	93.55	90.39	84.49	91.89
F4	36	**94.21**	93.94	93.93	94.18	84.93	77.81	91.78
F5	42	**94.30**	94.26	94.29	94.28	88.66	82.42	92.85
F6	48	95.21	94.83	94.58	**95.16**	89.53	83.10	93.29
F7	195	92.40	93.81	92.70	92.35	91.36	87.67	92.36

4.3.4.2   On UCI dataset

This section examined SR-ELM to reduce the dimension of features on the datasets in the UCI machine learning library. This section examined five datasets with various dimension and different numbers of data, as presented in Table 4.21.

Table 4.21 Various datasets used in the experiments from UCI Library

Datasets	Group	#data	#features	#classes
Iris	Small size and small dimension	150	4	3
Glass		214	9	6
Vehicle	Medium size and medium dimension	846	18	4
Segmentation	Large size and large dimension	2310	20	7
Satimage		6435	36	6

There are six dimensionality reduction methods involved. They consist of supervised and unsupervised methods. The supervised methods are ULDA (uncorrelated linear discriminant analysis), SRDA (spectral regression discriminant analysis), the proposed SR-ELM (spectral regression extreme learning machine) and OFNDA (orthogonal fuzzy neighbourhood discriminant analysis). In addition, two unsupervised methods employed are PCA (principle component analysis) and USELM (unsupervised extreme learning machine). In addition to those methods, the original features without projection method called BASELINE are involved.

As for the classifier, the myoelectric pattern recognition (M-PR) system classified the projected features into *c-1* classes using seven different classifiers. They are AW-ELM (the proposed classifier discussed in **section 4.2)**, RBF-ELM (the kernel-based ELM), LIBSVM, LDA and kNN. Table 4.22 to Table 4.26 present the classification results.

Table 4.22 presents the accuracy attained when the system employed AW-ELM as the classifier along with various dimensionality reduction methods. When working together with AW-ELM, SR-ELM is very good in reducing the features with large dimension with an accuracy of about 96 % and 88 % in Segmentation and Satimage datasets, respectively. This fact contrasts with the findings in the myoelectric pattern recognition discussed previously. Therefore, it can be concluded that the ability of SR-ELM is different, application-to-application as some datasets are working better without the need of the dimensionality reduction. Furthermore, in two datasets, Glass and Vehicle, the accuracy of the system using any reduction method is less than Baseline. It means both datasets do not need any dimensionality reduction when working together with AW-ELM.

Table 4.22 The accuracy attained using AW-ELM

Datasets	Average Accuracy (%)						
	ULDA	SRDA	SR-ELM	OFNDA	PCA	USELM	BASELINE
Iris	80.67	94.67	84.67	**96.67**	93.33	80.67	94.67
Glass	53.37	64.41	63.08	55.54	66.28	63.05	**66.29**
Vehilce	76.24	70.33	77.30	73.89	54.83	57.11	**81.68**
Segmentation	53.51	93.81	**96.19**	-	93.12	93.68	92.64
Satimage	-	84.18	**88.34**	-	87.38	82.02	87.38

"-" means the method does work properly because of singularity problem

In addition to AW-ELM, the experiment involved another ELM classifier, radial basis function extreme learning machine (RBF-ELM). Table 4.23 provides the classification results. In general, any method shows a good accuracy in one dataset but exhibits a low accuracy in other datasets. That happens on SR-ELM as well with general observation that it works better in datasets that need the feature reduction.

Table 4.23 The accuracy attained using RBF-ELM using 3-fold and 5-fold cross validation for satimage and other than satimage, respectively

Datasets	Average Accuracy (%)						
	ULDA	SRDA	SR-ELM	OFNDA	PCA	USERLM	BASELINE
Iris	82.67	97.33	84.67	**98.00**	94.67	79.33	96.67
Glass	57.98	66.83	64.62	64.50	69.14	62.27	**68.43**
Vehilce	76.00	75.41	78.02	76.12	54.72	45.99	**84.17**
Segmentation	88.48	96.71	91.26	-	97.06	85.24	**97.53**
Satimage	-	85.45	89.28	-	**90.02**	84.06	88.95

"-" means the method does work properly because of singularity problem

In Table 4.24, PCA is comparable to the supervised dimensionality reduction. This contrasts with the results in the myoelectric signal in which PCA is not as good as the LDA and its extension.

Table 4.24 The accuracy attained using LIBSVM using 3-fold and 5-fold cross validation for satimage and other than satimage, respectively

Datasets	Average Accuracy (%)						
	ULDA	SRDA	SR-ELM	OFNDA	PCA	USERLM	BASELINE
Iris	83.33	96.67	94.00	96.67	96.67	81.33	**96.00**
Glass	35.52	58.87	42.08	47.72	58.90	35.53	**60.82**
Vehilce	76.12	78.02	78.25	77.42	58.63	44.80	**70.80**
Segmentation	84.72	**94.20**	91.13	-	93.16	78.96	95.93
Satimage	-	85.13	83.68	-	89.53	74.31	**89.91**

"-" means the method does work properly because of singularity problem

Table 4.25 and Table 4.26 present the experimental results for the system that employed LDA and kNN as a classifier, respectively. Compared with other supervised

methods, the combinations of SR-ELM+LDA or SR-ELM+kNN give better performances. The comparison with unsupervised methods shows that SR-ELM and PCA are comparable, but SE-RLM is better than USERLM. SR-ELM and US-ELM are an extension of extreme learning machine for dimensionality reduction. The difference is that SR-ELM considers classes while US-ELM does not. It can be concluded that for ELM family, the taking of classes into consideration improves the performance of the method. However, the accuracy gap is not as large as in the myoelectric pattern recognition discussed before.

Table 4.25 The accuracy attained using LDA using 3-fold and 5-fold cross validation for satimage and other than satimage, respectively

Datasets	Average Accuracy (%)						
	ULDA	SRDA	SR-ELM	OFNDA	PCA	USERLM	BASELINE
Iris	98.00	**98.00**	97.33	**98.00**	97.33	80.67	98.00
Glass	63.05	58.37	62.38	**63.62**	47.12	49.59	61.26
Vehilce	77.79	77.06	**79.31**	77.31	43.98	46.34	77.90
Segmentation	91.52	91.69	92.73	-	84.07	85.41	**94.98**
Satimage	-	82.89	**85.67**	-	82.04	79.11	82.70

"-" means the method does work properly because of singularity problem

Table 4.26 The accuracy attained using kNN using 3-fold and 5-fold cross validation for satimage and other than satimage, respectively

Datasets	Average Accuracy (%)						
	ULDA	SRDA	SR-ELM	OFNDA	PCA	USERLM	BASELINE
Iris	94.67	96.00	96.00	**98.00**	95.33	84.67	96.00
Glass	63.01	61.69	**65.64**	60.69	64.49	64.52	63.08
Vehilce	76.13	75.89	**78.01**	77.29	57.45	55.80	70.44
Segmentation	95.41	95.76	**96.67**	-	93.85	93.59	94.81
Satimage	-	85.59	87.20	-	88.59	81.99	**88.66**

"-" means the method does work properly because of singularity problem

Another interesting fact exists when comparing SRDA and SR-ELM in all tables. In summary, SR-ELM is better than SRDA when the pattern recognition system employed AW-ELM, LDA and kNN as a classifier. As for RBF-ELM and LIBSVM, SRDA is better than SR-ELM.

4.3.5 Conclusion

This section proposes a new extreme learning machine and at the same time, a new dimensionality reduction called SR-ELM for finger movement classification. The experiment results on myoelectric pattern recognitions system show that SR-ELM is comparable to ULDA and OFNDA and better than SRDA. However, the processing time

of SR-ELM is much slower than that of SRDA, a bit slower than OFNDA and faster than ULDA. Moreover, SR-ELM can also work well on different classifiers and various numbers of classes with an average accuracy ranging from **95.67 %** to **86.73 %** for 5 to 10 classes of movement across eight subjects using two EMG channels. It is noted that the system did not implement the majority vote. When applying majority vote, the accuracy ranged from **98.64 %** to **94.16 %** for 5 to 10 motion classes.

The experimental results on UCI datasets showed that SR-ELM exhibits good performance when it works together with AW-ELM, LDA and kNN. As for RBF-ELM and LIBSVM, the performance of SR-ELM is comparable to other methods.

4.4 Evaluation of swarm based extreme learning machine (S-ELM) for myoelectric finger recognition

The experiment results in Chapter 3 and the previous sections (section 4.2 and 4.3), show that kernel-based ELM especially RBF-ELM is a powerful classifier. It is the most accurate classifier among the node-based ELM, SVM, LS-SVM, LDA, and kNN. However, the performance of kernel-based ELM greatly depends on its parameters. The parameter selection is a crucial issue in the RBF-ELM. Trying all possible candidates of the parameters will not be a good option. The optimization can be a wise option to deal with this issue. In this section, particle swarm optimization (PSO) will optimize the parameters of three different kernels. The background will be discussed first. The basic concept of the kernel-based ELM and PSO will come after that. Then, the hybridization of the kernel-based ELM and PSO will be presented. The experiments will be provided afterward. This section will be ended by the conclusion.

4.4.1 Background

ELM is a great improvement of feed-forward neural networks, which very considerably reduce the training time by omitting the iterative learning process. In ELM, the hidden node weights and biases are determined randomly, while the output weights are calculated analytically. Therefore, the training time is very fast compared to the traditional neural networks. ELM method has been used for a wide range of application (Cao *et al.*, 2010). Nevertheless, the hidden node parameters, the input weights, and biases, which are determined arbitrarily, result in a non-optimal system. Some efforts dealing with the optimization problem in ELM have been done. Self-adaptive

evolutionary ELM (SAE-ELM) (Cao *et al.*, 2012), and particle swarm optimization ELM (PSO-ELM) (Xu & Shu, 2006) are a number of methods developed to optimize the hidden node parameters.

ELM is not merely working on the node style. A kernel system can be incorporated in ELM by replacing the node processing structure with a kernel function. This kernel based ELM can be considered as a variance of least square support vector machine (LS-SVM) without the output bias (Zong *et al.*, 2011). Similar to the node-based ELM, the kernel-based ELM faces the optimization problem too. The efficacy of the kernel-based ELM greatly depends on the optimum combination of the kernel parameters (G. B. Huang *et al.*, 2012). The popular grid search algorithm that is simple was used to search the optimal kernel (Khairul Anam *et al.*, 2013). However, the exhaustive grid search on a large number of the parameter space may result in a very time-consuming process.

A popular particle swarm optimization (PSO) algorithm can be a promising solution for optimizing the kernel parameters in the kernel-based ELM. To the best of the author's knowledge, the integration of PSO and ELM only exists in the node-based ELM. This thesis extends the use of PSO into the kernel-based ELM.

4.4.2   Kernel-based extreme learning machine

ELM is a learning algorithm for single layer feedforward networks (SLFNs). In classical SLFNs, network parameters are tuned while in ELM, most of these parameters are analytically determined. Hidden parameters can be independently calculated from the training data, and output parameters can be determined by the pseudo-inverse method. As a result, the learning of ELM can be carried out fast compared to the other learning algorithms (G. B. Huang *et al.*, 2012).

As described in **Chapter 2 section 2.5.4.3**, the output of ELM is defined by:

$$f(\mathbf{x}) = \mathbf{g}(\mathbf{x})\mathbf{G}^T \left(\frac{\mathbf{I}}{C} + \mathbf{G}\mathbf{G}^T \right)^{-1} \mathbf{T} \qquad 4.37$$

where $\mathbf{g(x)}$ is the feature mapping in the hidden layer, $\mathbf{T}$ is the target and C is the regulation parameter of ELM. The feature mapping in the hidden layer of ELM can be replaced by a kernel function. Therefore, the formulation of the kernel based ELM is defined by:

$$f(\mathbf{x}) = \begin{bmatrix} K(\mathbf{x}, \mathbf{x}_1) \\ \vdots \\ K(\mathbf{x}, \mathbf{x}_N) \end{bmatrix}^T \left(\frac{\mathbf{I}}{C} + \mathbf{\Omega}_{ELM} \right)^{-1} \mathbf{T} \qquad 4.38$$

where

122

$$\Omega_{ELM} = \mathbf{G}\mathbf{G}^T : \Omega_{ELM\ i,j} = g(\mathbf{x}_i) . g(\mathbf{x}_j) = K(\mathbf{x}_i, \mathbf{x}_j)$$ 4.39

and K is a kernel function as shown in Eq. **4.40 - 4.42**.

$$\text{Radial basis function: } K(\mathbf{x}_i, \mathbf{x}_j) = \exp(-\gamma \|x_i - x_j\|)$$ 4.40

$$\text{Linear: } K(\mathbf{x}_i, \mathbf{x}_j) = \mathbf{x}_i . \mathbf{x}_j$$ 4.41

$$\text{Polynomial: } K(\mathbf{x}_i, \mathbf{x}_j) = (\mathbf{x}_i . \mathbf{x}_j + a)^d$$ 4.42

4.4.3 Particle swarm optimization (PSO)

Particle swarm optimization (PSO) is a population-based stochastic optimization algorithm that has been applied widely in many optimization areas (Ling *et al.*, 2008). PSO is inspired by the social behaviours of animals like fish schooling and bird flocking (Ling *et al.*, 2008). The particle swarm does not use selection. It means that all population members survive from the beginning until the end (Kennedy, 2010). In the PSO, a swarm of interacting particles moves in an n-dimensional search space of the problem's possible solution. Four elements that are a position $\vec{x}_i$, a velocity $\vec{v}_i$, the best previous (local) position $\vec{p}_i$ and the best global position $\vec{g}_i$ represent a particle in the swarm. Some generations are generated to update the particle's positions and velocities. The particles explore the promising domain to find the best solutions, which spread throughout the swarm. The parameter adaptations are given by:

$$\vec{x}_i^q(t + 1) = \vec{x}_i^q(t) + \vec{v}_i^q(t + 1)$$ 4.43

$$\vec{v}_i^q(t + 1) = \varphi\vec{v}_i^q(t) + c_1 . r_1 . \left(\vec{p}_i^q(t) - \vec{x}_i^q(t)\right) \\ + c_2 . r_2 . \left(\vec{g}_i^q(t) - \vec{x}_i^q(t)\right)$$ 4.44

where

$$\vec{p}_i^q = \begin{bmatrix} \vec{p}_1^q & \cdots & \vec{p}_k^q \end{bmatrix}$$
$$\vec{g}_i^q = \begin{bmatrix} \vec{g}_1^q & \cdots & \vec{g}_k^q \end{bmatrix}$$
$$i = 1, \dots, k$$
$$q = 1, \dots, d$$

In the Eq. **4.43** and **4.44**, t represents the generation, k denotes the number of the particles in the swarm, d denotes the number of dimension. φ is an inertia weight factor, and c_1 and c_2 are acceleration constants that are weighted by r_1 and r_2, random function in the range of [0-1]. Based on (de Souza *et al.*, 2006), the total number of c_1 and c_2

should exceed 4 to assure the convergence. The velocity is constrained to $[-v_{max}, v_{max}]$ to limit the swarm particles in the search space.

4.4.4 Optimization of the parameters of the kernel based ELM using PSO

The objective of the optimization using PSO is to find the optimal parameters of the kernel-based ELM. The optimization was implemented in three kernels, and it forms three hybridizations of PSO and ELM, i.e., a swarm-based radial basis function ELM (SRBF-ELM), a swarm-based linear ELM (SLIN-ELM) and swarm-based polynomial ELM (SPOLY-ELM). According to Eq. **4.40 - 4.42**, the SRBF-ELM contains two parameters: C and γ, the SLIN-ELM contains one parameter which is C, and the SPOLY-ELM consists of three parameters: C, a and d. The value ranges of the parameters of the PSO are C $\in [2^{-5}, 2^5]$, $\gamma \in [2^{-4}, 2^{10}]$, $a \in [2^{-4}, 2^{10}]$ and $d \in [1, 50]$. In this work, the c_1 and c_2 are set at 2.05 while φ is 0.9. In addition, the optimization was done until 150 generations with 30 particles in each generation. A 3-fold cross validation was employed to measure the error. Therefore, the fitness function of particle $\vec{x}_i$ is defined by

$$f(\vec{x}) = E_n(\vec{x}) \qquad 4.45$$

where E_n is the error in each validation process. Figure 4.23 shows the pseudo-code of PSO for optimization of the ELM parameters.

```
Begin
     t → 1                      // iteration
     Initialize xᵢ              // xᵢ : position (swarm particle)
     Evaluate f(xᵢ)             // f(xᵢ): fitness function Eq. 4.45
     Initialize vᵢ              // vᵢ : velocity
     x̃ = x                      // x̃ : personal best position
     x̂ = x̃                      // x̂ : global best position
     While (condition satisfied) do
          t → t+1
          update position of particle x(i)    // Eq. 4.43
          update velocity v(t)                     // Eq. 4.44
          if v(t)> vmax, v(t)=vmax end
          if v(t)< -vmax, v(t)=-vmax end
          Evaluate f(x(t))
          update x̃ if new x̃ better than previuos x̃
          update x̂ if new x̂ better than previuos x̂
     end
end
```

Figure 4.23 The pseudo code of PSO for the optimization of the kernel-based ELM parameters

4.4.5 Experimental setup

The proposed recognition system consists of two stages, i.e., a tuning of ELM parameters and the classification stage using optimized parameters, as shown in Figure 4.24.
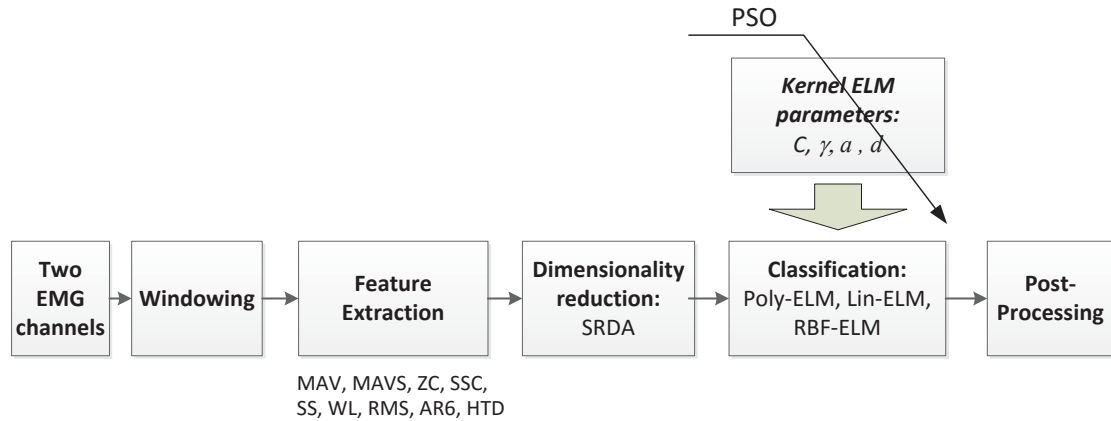
Figure 4.24 The myoelectric pattern recognition using integration PSO and the kernelized ELM

The EMG signal used in this experiment is the same data as in **section 4.2.4.1**. Then the filtering and windowing were applied to the collected data before being extracted using a time domain (TD) and autoregressive (AR) features. The features were extracted from the time domain feature set which consists of waveform length (WL), slope sign changes (SSC), number of zero crossings (ZCC), sample skewness (SS), the parameters of Hjorth time domain parameters (HTD) and auto regressive (AR) model parameters were included. Furthermore, SRDA is used to reduce the feature dimension.

Afterwards, the optimization process was done using PSO where the goal is to find the best ELM parameters which minimize the classification error. Based on the parameters obtained in the tuning stages, the offline classification was carried out. The classification outputs were refined by using a majority vote. Some analyses were performed to validate the result.

The optimized kernel-based ELMs were used to recognize ten classes of the individual and combined finger movements. They consisted of the flexion of individuated fingers. They consisted of Thumb (T), Index (I), Middle (M), Ring (R), Little (L) and the pinching of combined Thumb–Index (T–I), Thumb–Middle (T–M), Thumb–Ring (T–R), Thumb–Little (T–L), and the hand close (HC). The four-fold cross validation was used to validate the classification results. Simulation was done in the MATLAB 8.3 environment running on 2.8 GHz PC.

4.4.6   Experiments and Results

The first experiment conducted was plotting of the fitness function to investigate the convergence of the optimization process. Three experiments were performed in three different kernels. The discussion will be presented in **section 4.4.6.1**. Afterward, the investigation of the classification results according to the optimal parameters is presented. **Section 4.4.6.2** will describe the results as well as the analysis.

4.4.6.1   *The fitness function*

This section evaluates the convergence of the PSO for different kernels across eight subjects using 3-fold cross validation. As shown in Figure 4.25, all fitness outputs converge to the optimum value. SPOLY-ELM achieves the minimum error compared to other kernels. On the other hand, the SLIN-ELM shows different trends. Its fitness becomes constant quicker than the other two, but it keeps staying at the highest error compared to the others. Meanwhile, the SRBF-ELM shows a moderate behaviour. Although the SPOLY-ELM attained the lowest accuracy, the actual performance should be done by applying the optimal parameter to the testing session. Table 4.27 shows the optimal parameters obtained by PSO.
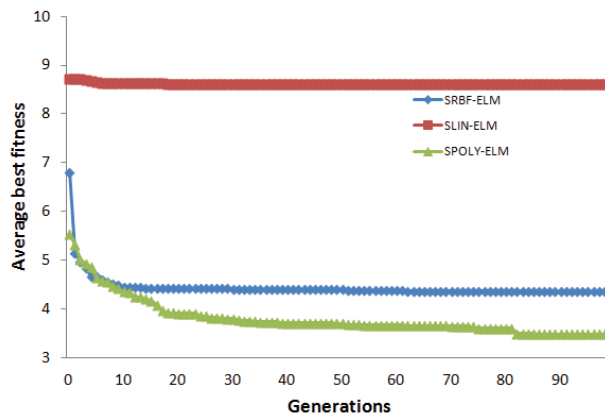
Figure 4.25 The average fitness function for different kernels across eight subjects using 3-fold cross validation

Table 4.27 The optimal parameter optimized by a swarm technique

Type of ELM	Optimal Parameters			
	C	γ	a	d
SLIN-ELM	1.56	-	-	-
SRBF-ELM	24.75	0.82	-	-
SPOLY-ELM	14.75	-	430.27	4.38

4.4.6.2   The classification performance over eight subjects

The next experiment is the evaluation of the classification performance using the optimal parameters optimized by PSO. Figure 4.26 depicts the accuracy of all systems over eight subjects. The figure shows that SRBF-ELM outperforms the other two systems especially compared to SLIN-ELM but not too much compared to SPLOY-ELM. SRBF-ELM is better than SPOLY-ELM in all subjects except subject S2. Table 4.28 provides overall accuracy of the system. It is clear that by averaging the accuracy over eight subjects as shown in Table 4.28, SRBF-ELM achieved the highest accuracy.
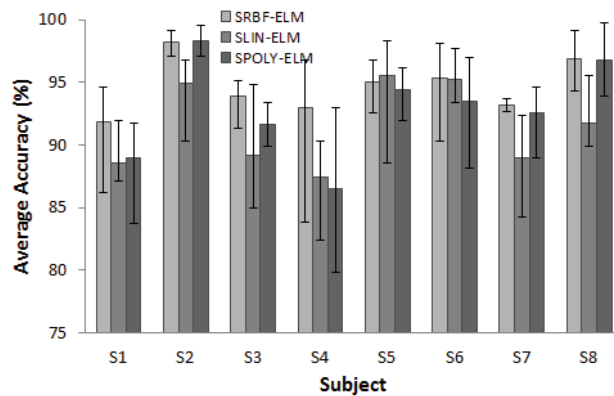
Figure 4.26 The classification accuracy of the optimized ELM averaged from eight subjects

Table 4.28 The average classification accuracy across eights subject

Type	Average Accuracy (%)
SRBF-ELM	94.62 ± 3.70
SLIN-ELM	91.43 ± 5.61
SPOLY-ELM	94.16 ± 3.70

4.4.6.3   The performance on the classified movements

The performance of the systems in recognizing the finger movements is also investigated. As described in Figure 4.27, SRBF-ELM outperforms SLIN-ELM and has similar performance to SPOLY-ELM. Moreover, all systems recognize individual motions better than combined motions. The figure shows that the accuracy of individual motions is mostly higher than the combined motions except the little finger (L). It is an interesting phenomenon that the little finger which is an individual digit, yet it is the most difficult motion to recognize.
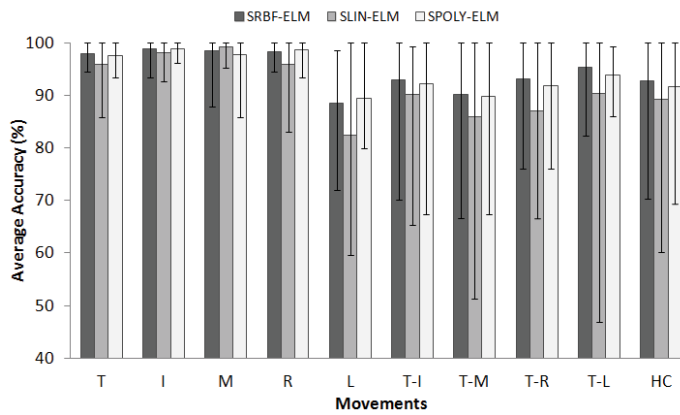
Figure 4.27 The classification accuracy of the optimized ELM for different finger movements

Besides two previous experiments, the statistical test using analysis of variance (ANOVA with significance values set at 0.05) was performed. The result is described in Table 4.29. The p-values in Table 4.29 indicate that there is no significant performance between SRBF-ELM and SPLOY-ELM ($p>0.05$). Thus, both systems have the same performance statistically. Meanwhile, the performance of SRBF-ELM and SLIN-ELM are significantly different ($p<0.05$). In addition, SPOLY-ELM and SLIN ELM are not significantly different ($p>0.05$).

Table 4.29 *p*-values resulting from a-pair wise comparison of classification accuracy

	SPOLY-ELM	SLIN-ELM
SRBF-ELM	0.72	0.04
SPOLY-ELM		0.09

4.4.7 Conclusion

This section proposes the hybridization of PSO and ELM for myoelectric finger motion recognition. Among three hybridizations, SRBF-ELM outperforms SLIN-ELM but is not too much different compared to SPOLY-LIN. This is also indicated by the *p*-values in which SRBF-ELM and SPOLY-ELM have similar performance. Moreover, PSO is able to optimize the three systems by giving the accuracy of more than 90% with the highest accuracy being about **94 %**.

However, Figure 4.25 shows that the PSO in SLIN-ELM and SRBF-ELM converges in the early stage of the searching stages and then saturates in the later stage. This fact indicates that PSO possibly becomes trapped in local optima. This phenomena confirms the fact expressed by Ling *et al.* (2008). Some methods have been proposed to overcome this problem (Chia-Feng, 2004; Ling *et al.*, 2008). Therefore, the next section will

investigate and implement the new PSO for optimizing the parameters of the kernel-based ELM. This new system will be discussed in the next section.

4.5 Evaluation of swarm-wavelet extreme learning machine (SW-ELM) for myoelectric finger recognition

This section proposes a new hybridization of PSO and ELM. The research utilizes the wavelet-PSO to tackle the local optima issue in the PSO. The experiment only involved one kernel, which is radial basis function (RBF) kernel as it is the most accurate kernel for finger motion classification in this research. It is called SW-RBF-ELM. The structure of this section is as follows. The first subsection will discuss the basic theory of wavelet-PSO. Then, the experimental setup is presented. The experimental results on the healthy subjects are discussed in detail. Additional experiment on the amputee subjects is also provided. Finally, this section is ended by the conclusion.

4.5.1 PSO with wavelet mutation

The theory of PSO is presented in Section 4.4.3. This section is discussing the PSO with wavelet mutation. The wavelet mutation in PSO was proposed by Ling *et al*. (Ling *et al*., 2008). A mutation chance is driven by a mutation probability $p_m \in [0\ 1]$. If $x_i(t)$ is selected to be mutated, then a new position is given by:

$$\vec{x}_i(t) = \begin{cases} \vec{x}_i(t) + \sigma\left(par_{max}^i - \vec{x}_i(t)\right) & if\ \sigma > 0 \\ \vec{x}_i(t) + \sigma\left(\vec{x}_i(t) - par_{min}^i\right) & if\ \sigma \leq 0 \end{cases} \qquad 4.46$$

where par_{max} and par_{min} are the maximum and minimum position, respectively. As for σ, it is the Morlet wavelet function defined by:

$$\sigma = \frac{1}{\sqrt{a}} e^{-\left(\frac{\alpha}{a}\right)/2} cos\left(5\left(\frac{\alpha}{a}\right)\right) \qquad 4.47$$

The variable "*a*" in the Morlet wavelet is determined by the following equation:

$$a = e^{-\ln(g)\left(1-\frac{t}{T}\right)^{\xi} + \ln(g)} \qquad 4.48$$

The objective of the optimization using the wavelet-PSO is to find the optimum parameters of the kernel-based ELM that minimize the classification error of the finger motion recognition. A 3-fold cross validation was employed to measure the error. Moreover, the fitness function of particle $\vec{x}$ is defined by

$$f(\vec{x}) = \frac{1}{N_v} \sum_{n=1}^{N_v} E_n(\vec{x})$$
4.49

where N_v is the number of cross validation, E_n is the error in each validation process.

The fitness function of Eq. **4.49** is different from the previous one, Eq. **4.45**. In the previous experiment, the optimization was conducted in each trial of the validation process. Calculating errors in each validation means that the work will perform all pattern recognition steps. As a result, the optimization process takes a lot of time. In this section, the optimization did not use the error in each validation step. Rather, it employed the average of the validation process as a fitness function. The pseudo code of the wavelet mutation for optimizing the parameters of the kernel based ELM is presented in Figure 4.28.

```
Begin
    t → 1                  // iteration number
    Initialize x(t)        // x(t) : position, a particle swarm
    Evaluate f(x)          // f(x): fitness function Eq. 4.45
    Initialize v           // v : velocity
    x̃ = x                  // x̃ : personal best position
    x̂ = x̃                  // x̂ : global best position
    While (condition satisfied) do
        i → i+1
        update position of particle x(i)      // Eq. 4.43
        update velocity v(i)                  // Eq. 4.44
        if v(i)> vmax, v(i)=vmax end
        if v(i)< -vmax, v(i)=-vmax end

        perform wavelet mutation operation with pm
        Updating x(i)                         // Eq. 4.46

        Evaluate f(x(i)) // f(x): fitness function Eq. 4.45
        update x̃ if new x̃ better than previuos x̃
        update x̂ if new x̂ better than previuos x̂
    end
end
```

Figure 4.28 The pseudo code for PSO with wavelet mutation for optimizing the parameters of ELM

4.5.2 The experimental setup
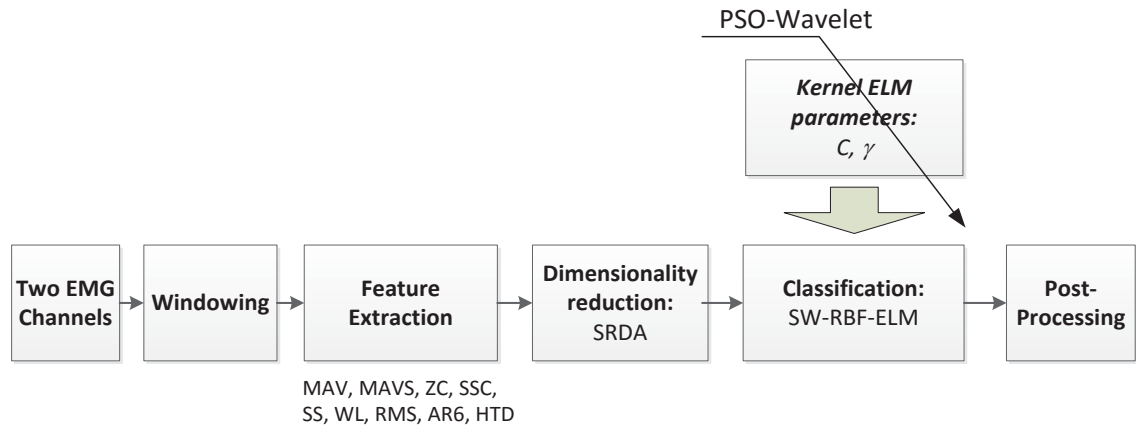
Figure 4.29 The experimental setup of the PSO-wavelet mutation for ELM parameters optimization

Figure 4.29 shows the block diagram of the experiment conducted in this section. It is similar to that in **section 4.4.5**. The experiments utilized the same data and the same methods as in **section 4.2.4** except for the classifier. In this section, the optimization process involves radial basis function (RBF) kernel only. This section focuses on the efficacy of the wavelet mutation on PSO, so it is enough to use one kernel only. Besides, the previous work (see Chapter 3) shows that RBF kernel outperformed other kernels. The hybridization of PSO, wavelet and ELM is called SW-RBF-ELM (swarm-wavelet based RBF-ELM).

Some parameters should be determined in the beginning of the experiment. Two parameters of RBF-ELM are C and γ (see Eq. **4.38** and **4.40**). They are in the range of $[2^{-7}, 2^{10}]$, and $[2^{-7}, 2^{10}]$ for C and γ, respectively. Then, the parameters of PSO (see Eq. **4.43** and **4.44**) are set as follows. Parameter c_1 and c_2 are set at 2.05, and φ is 0.9. Parameters r_1 and r_2 are random functions in the range of [0-1]. In addition, the optimization was done until 150 generations with 30 particles in each generation. As for the parameter of the wavelet, the work in this section will vary the value of the wavelet parameters, as seen in Eq. **4.46** and **4.47** except for α; it is determined randomly, according to (Ling *et al.*, 2008).

To test the efficacy of the proposed system, some experiments will be conducted. They are:

- The experiment on the influence of the mutation probability p_m
- The experiment on the shape parameter ξ (Eq. **4.48**)
- The experiment on the parameter g (Eq. **4.48**)
- The experiment on the pattern recognition performance

4.5.3　Experiments and Results

4.5.3.1　Mutation probability p_m

This section tested the influence of the mutation probability p_m to the SW-RBF-ELM performance. The p_m value is varied from 0 to 0.6. The parameter $p_m = 0$ means no wavelet mutation in the PSO. Besides, ξ is equal to 0.2 and g is equal to 10000. The experimental results are presented in Figure 4.30 and Table 4.30.

Figure 4.30 indicates that on the parameter $p_m = 0$, the fitness value of the PSO is larger than that with p_m more than 0, even when it is the largest value. The lower the fitness value, the better the system, so the PSO with wavelet mutation is better than without wavelet mutation. Therefore, the wavelet mutation can enhance the optimization process. Moreover, in general, the figure also shows that the more the mutation probability, the less the fitness value. However, the $p_m = 0.5$ is the optimum value among the tested values.
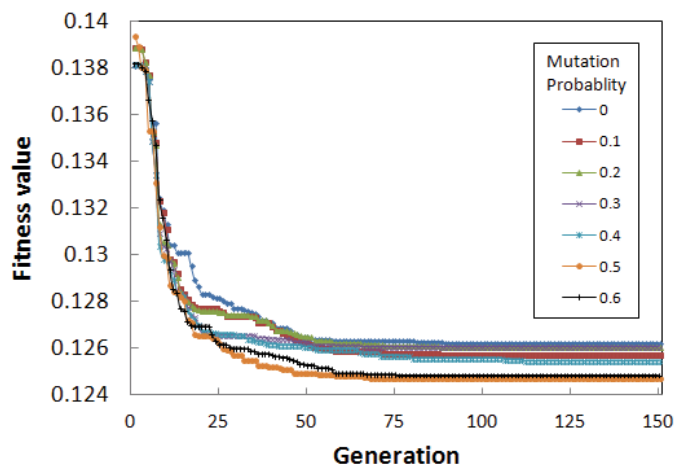
Figure 4.30 The fitness values for variable p_m when ξ=0.2 and g=10000 over eight subjects

Table 4.30 give more information regarding the mutation probability p_m across different subjects. In Table 4.30, the underlined value indicates the minimum value in each subject. This table emphasizes the fact in Figure 4.30 that $p_m = 0.5$ is the most accurate PSO across seven subjects, out of eight. Although the accuracy of the parameter p_m=0.6 is the highest, it occurred on five subjects only. Another interesting fact is also found in the Table. The mutation wavelet does not provide a benefit to the optimization process on two subjects, S5 and S8 because the accuracy of the system with wavelet mutation and without is very similar. This fact shows that the wavelet mutation in the PSO does not fully ensure the improvement in the classification performance. However, there is a high probability that the optimization process will be improved. Finally, the parameter $p_m = 0.5$ is selected for the rest of the experiment.

132

Table 4.30 The accuracy of SW-RBF-ELM when ξ=0.2 and g=10000

Subject	Mutation parameter (Accuracy in %)						
	0	**0.1**	**0.2**	**0.3**	**0.4**	**0.5**	**0.6**
S1	92.278	92.417	92.417	**92.869**	**92.869**	**92.869**	**92.869**
S2	98.098	98.098	98.028	98.028	98.028	**98.129**	98.098
S3	95.070	95.070	95.070	95.139	95.139	95.440	**95.546**
S4	93.240	93.238	93.238	**93.344**	**93.344**	**93.344**	93.310
S5	**96.731**	96.660	96.660	96.731	96.660	**96.731**	**96.731**
S6	97.088	97.215	97.215	97.215	97.215	**97.250**	**97.250**
S7	93.898	94.106	94.106	93.967	94.005	**94.038**	94.004
S8	**97.880**	**97.880**	**97.880**	**97.880**	**97.880**	**97.880**	**97.880**
Average	95.535	95.585	95.577	95.647	95.643	95.710	**95.711**

*The underlined value is the highest one

The big number of the parameter p_m increases the searching space of the optimization in PSO. If the number of element in a particle is small, it is preferable to increase the value of the parameter. Figure 4.30 implies that the big number of p_m tends to give good optimization performance. This phenomena matches with the fact suggested by Ling *et al*. (Ling *et al.*, 2008). They recommended a big number of p_m in between 0.5 – 0.8 for a small number of elements in a particle. In this research, the number of elements is two.

To examine the benefit of wavelet mutation statistically, an analysis of variance (ANOVA) test was conducted on the fitness value of the PSO without wavelet mutation and with wavelet mutation p_m = 0.5. The confidence level p is set at 0.05. ANOVA test produced $p = 3.69 \times 10^{-7}$. This result concludes that the enhancement produced by wavelet mutation is statistically significant.

4.5.3.2 Shape-parameter ξ

This section varied the value of shape parameter ξ in Eq. **4.48**. The shape parameter is varied among 0.1, 0.2, 0.3, 0.5, 2 and 5. The value of the parameter p_m is 0.5 following the result in **section 4.5.3.1**. Furthermore, g is equal to 10000. The experimental result is presented in Figure 4.31 and Table 4.31.

Figure 4.31 indicates that ξ = 2 converged earlier than the others did. The final fitness value of it is the second worst after ξ = 5. On the other hand, the small value of ξ gave a good optimization process. These facts imply that the high value of ξ is not a good option for optimization of SW-RBF-ELM. The best optimization process is shown when ξ = 0.2.
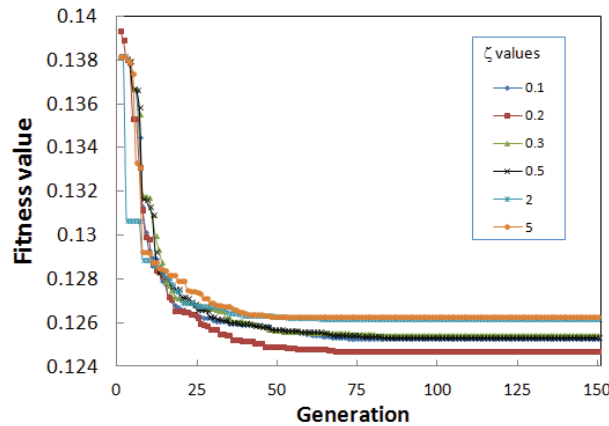
Figure 4.31 The fitness values for variable ξ when $p_m = 0.5$ and g = 10000

Table 4.31 draws different finding from Figure 4.31. The table shows that SW-RBF-ELM with $\zeta = 0.1$ achieved the highest average accuracy, not $\zeta = 0.2$. Besides, it attains the highest accuracy across four subjects, which is similar to $\zeta = 0.2$. By considering the fitness value and the average accuracy performed, $\zeta = 0.2$ is selected as the optimal shape parameter.

Table 4.31 The accuracy of SW-RBF-ELM when p_m=0.5 and g=10000

Subject	ζ (Accuracy in %)					
	0.1	**0.2**	**0.3**	**0.5**	**2**	**5**
S1	92.869	92.869	92.869	92.869	92.869	92.869
S2	98.028	**98.129**	98.028	98.098	98.028	98.028
S3	**95.893**	95.440	**95.893**	95.139	95.070	95.139
S4	93.310	**93.344**	93.310	**93.344**	93.240	93.309
S5	**96.731**	**96.731**	96.660	**96.731**	96.660	**96.731**
S6	**97.321**	97.250	97.250	97.250	97.215	97.123
S7	**94.106**	94.038	94.002	94.004	93.898	93.898
S8	97.845	**97.880**	**97.880**	97.845	97.845	97.845
Average	**95.763**	95.710	95.737	95.660	95.603	95.618

*The underlined value is the highest one

4.5.3.3   Parameter g

The previous two experiments have selected two optimum parameters, $p_m = 0.5$ and $\zeta = 0.2$. This section tries to get the optimum g parameter. The parameter g (Eq. 4.48) is varied from 100, 1000, 10000 and 100000. The experimental result is presented in Figure 4.32.
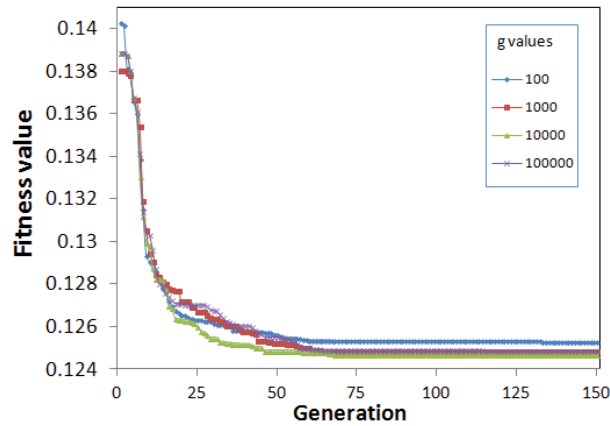
Figure 4.32 The fitness values for variation of the parameter g when p_m=0.5 and ξ=0.2

Figure 4.32 depicts the fitness values of four different g values. This figure indicates that the big number of g value give better accuracy than the small one. However, the best fitness value is not $g = 100,000$. The $g = 10,000$ exhibits the best performance. Therefore, there is no general rule for selecting g value. It is required to perform experimental procedure to find the best g value. This fact is supported by the accuracy of SW-RBF-ELM in Table 4.32. On average, the lower g attained the lower accuracy. Although the accuracy of the parameter $g = 10000$ is the lowest one on average across eight subjects, it is the highest in the over half of the subjects, which is five out of eight.

Table 4.32 The accuracy of SW-RBF-ELM when p_m=0.5 and $\zeta = 0.2$

Subject	Parameter g (Accuracy in %)			
	100	1000	10000	100000
S1	**92.869**	**92.869**	92.834	92.800
S2	98.028	98.098	**98.129**	**98.129**
S3	95.732	**95.893**	95.440	95.546
S4	93.347	93.310	**93.344**	93.238
S5	**96.731**	96.660	**96.731**	**96.731**
S6	**97.250**	97.215	**97.250**	97.215
S7	94.038	94.004	94.038	**94.106**
S8	97.845	97.845	**97.880**	**97.880**
Average	95.730	95.737	95.706	95.706

*The underlined value is the highest one

4.5.3.4 *Pattern recognition performance across subjects*

The previous sections conducted some experiments to determine the optimum parameters of the wavelet. They are p_m=0.5, $\zeta = 0.2$ and $g = 10000$. This section applied those values to SW-RBF-ELM and did analysis on the results especially on the

comparison between PSO with wavelet mutation and without mutation. The result is shown in Figure 4.33.
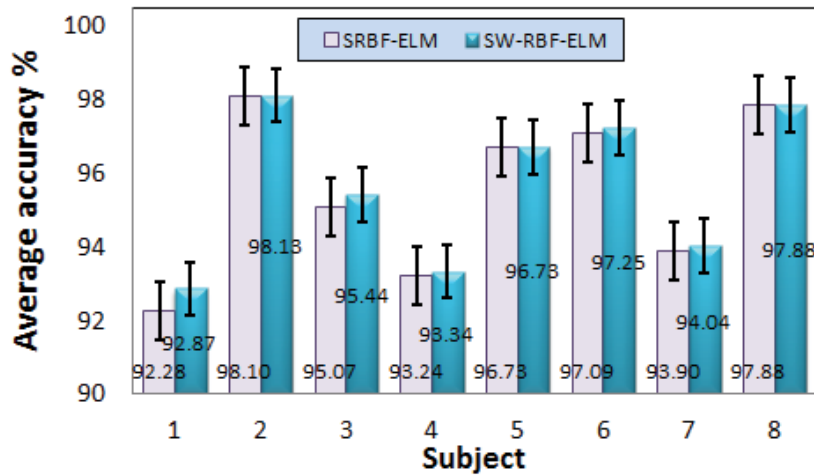
Figure 4.33 The accuracy of RBF-ELM with mutation and without mutation using 3-fold cross validation

Figure 4.33 depicts the average accuracy of RBF-ELM that is optimized by PSO with wavelet mutation (SW-RBF-ELM) and without mutation (SRBF-ELM). The figure indicates that SW-RBF-ELM achieves better accuracy than SRBF-ELM. SRBF-ELM is as accurate as SW-RBF-ELM in one subject only, which is subject S8. Therefore, the probability of the improvement of the performance using wavelet mutation is 7/8 x 100 % = 87.5 %. On average, SW-RBF-ELM attained an accuracy of 95.62 % while SRBF-ELM achieved the accuracy of 95.54 %.

4.5.3.5   *Pattern recognition performance on the movement*

This section investigates the performance of both systems, SRBF-ELM and SW-RBF-ELM, in classifying finger movements. The myoelectric pattern recognition classifies ten finger movements. They include thumb (T), index (I), middle (M), ring (R), and little (L) finger movements. The other movements are thumb–index (TI), thumb–middle (TM), thumb–ring (TR), thumb–little (TL), and the hand close (HC) movements. Figure 4.34 presents the classification results of SRBF-ELM (without wavelet mutation) and SW-RBF-ELM (with wavelet mutation).
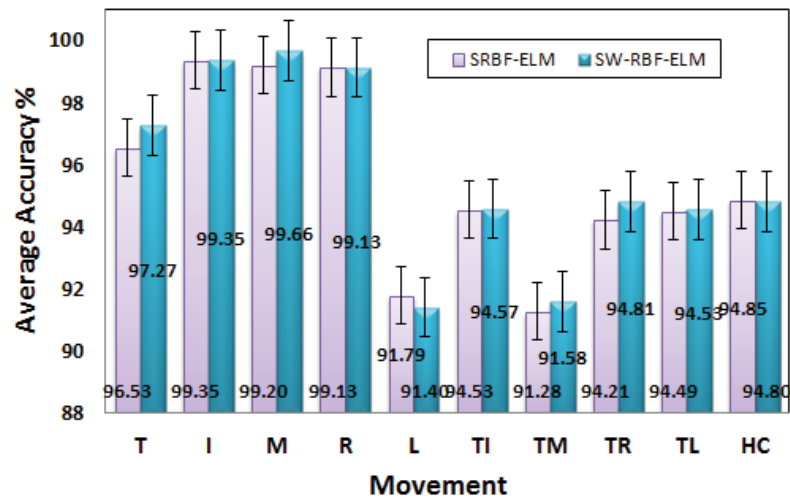
Figure 4.34 The accuracy of the finger movement classification across eight subjects using 3-fold cross validation

Figure 4.34 shows that SW-RBF-ELM is better than SRBF-ELM in classifying two individual finger movements (T, and M), and four combined movements (TI, TM, TR, and TL). On the other hand, SRBF-ELM is better than SW-RBF-ELM in two movements only: L and HC. As for finger movement I and R, both systems exhibited the similar performance. Overall, the SW-RBF-ELM is better than SRBF-ELM. In other words, the wavelet mutation in PSO enhances the classification performance of the pattern recognition system. However, the analysis of variance test (ANOVA) set $p = 0.05$ yields p is equal to 0.96. Therefore, the improvement is statistically not significant. This result confronts the ANOVA test outcomes in **section 4.5.3.1** that proved the significance of the existence of the wavelet in PSO. These two results can be accommodated by saying that the enhancement of wavelet mutation in the optimization process is statistically significant, but it is statically not significant in the classification performance.

Another fact found in Figure 4.34 is that SRBF-ELM and SW-RBF-ELM exhibit relatively bad performance in classifying all combined movements and little finger movement. The phenomena can be investigated through the confusion matrix in Table 4.33 and Figure 4.35. Table 4.33 shows that the SW-RBF-ELM mostly misclassified the little finger movement (L) to thumb-index motion (TI) by accuracy of 2.19 %. Besides, the system also misclassifies L to movement R and TL. As for the combined movement, SW-RBF-ELM generally misclassified them to the individual movement they belong to. For instance, the movement TL is mostly misclassified to the movement L by accuracy 2.65 %. Nevertheless, it did not occur in all combined movements.

137

Table 4.33 The confusion matrix of the classification result of SW-RBF-ELM

		Classified									
		T	I	M	R	L	TI	TM	TR	TL	HC
Intended	T	97.27	0.00	0.04	0.00	0.52	0.65	0.00	0.61	0.00	0.91
	I	0.04	99.35	0.00	0.00	0.00	0.48	0.13	0.00	0.00	0.00
	M	0.00	0.00	99.66	0.00	0.00	0.00	0.34	0.00	0.00	0.00
	R	0.00	0.00	0.09	99.13	0.17	0.00	0.00	0.61	0.00	0.00
	L	0.00	1.19	0.00	1.84	91.40	2.19	0.79	0.53	1.89	0.18
	TI	0.56	1.91	0.04	0.00	1.48	94.57	1.00	0.13	0.30	0.00
	TM	0.00	0.74	0.22	0.26	1.48	4.30	91.58	1.22	0.22	0.00
	TR	1.27	0.17	0.00	0.17	0.38	0.55	1.44	94.81	0.55	0.68
	TL	0.30	0.00	0.22	0.13	2.65	1.13	0.00	1.04	94.53	0.00
	HC	0.75	0.35	0.00	0.00	1.27	0.17	1.96	0.70	0.00	94.80
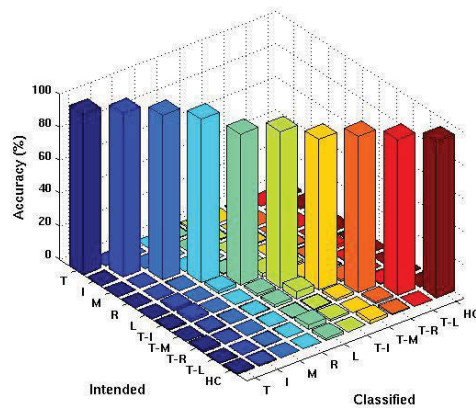
Figure 4.35 The confusion matrix plot of the classification result of SW-RBF-ELM

4.5.4   Experiment on the amputee database

This section tested the performance of SW-RBF-ELM and SRBF-ELM to classify 12 finger movements on the EMG signals collected from the amputee subjects. The data collection is presented in Chapter 3 **section 3.2.1.1**. The finger motion classes consist of a thumb abduction (Ta), thumb flexion (Tf), index flexion (If), and middle flexion (Mf). Then ring flexion (Rf), and little flexion (Lf). Moreover, it involved thumb extension (Te), index extension (Ie), middle extension (Me), ring extension (Re), little extension (Le), little and ring flexion (LRf), index, middle and ring flexion (IMRf), and middle, ring and little flexion (IMRLf).

The myoelectric pattern recognition used in this experiments is the same as the system used in section 4.5.2 and   Figure 4.29. For wavelet parameters, the values of the parameters are $p_m = 0.1$, $\zeta = 2$ and g = 10000, following the our work (Khairul Anam & Al-Jumaily, 2014c). Figure 4.36 depicts the experimental results of SRBF-ELM and SW-RBF-ELM on five amputee subjects.

138
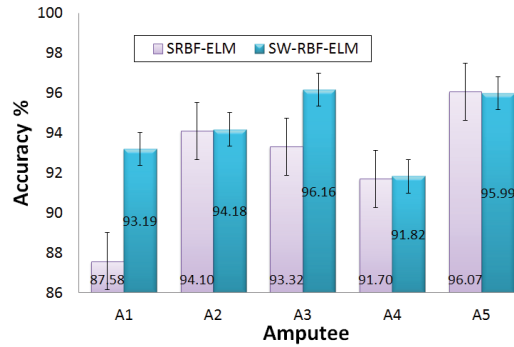
Figure 4.36 Average classification accuracy of three different ELM methods

Figure 4.36 shows that the SW-RBF-ELM achieved better performance than SRBF-ELM across five amputees except on amputee A5. On the amputee A5, SRBF-ELM is better than SW-RBF-ELM. Overall, SW-RBF-ELM outperformed SRBF-ELM. Probably, the optimization process in the PSO influences the superiority of SW-RBF-ELM over SRBF-ELM. Figure 4.37 gives clearer information about this assumption. It is shown in Figure 4.37 that after 30th generation, the PSO did not change the fitness value. Meanwhile, the wavelet mutation helped the PSO to avoid the local optima.
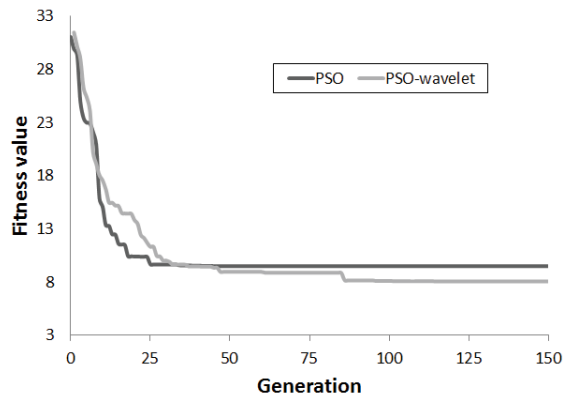
Figure 4.37 The fitness value of PSO and wavelet-PSO across five amputees

Furthermore, a statistical test on the accuracy using one-way ANOVA (p set at 0.05) was also done. The performance of the SW-RBF-ELM is significantly different from swarm ELM ($p = 0.036$). The SW-RBF-ELM achieved the average accuracy of 94.27 %, while SRBF-ELM produced the average accuracy of 92.55 %.

In addition, the classification performance in regards to the finger motion was observed. As shown in Figure 4.38, the SRBF-ELM was able to classify the flexion motions with the average accuracy more than 90%. In contrast, the extension motions were classified with the average accuracy less than 90%. Similarly, the SW-RBF-ELM recognized the flexion motions better than the extension motions, but with the average accuracy that is better than the SRBF-ELM.

139
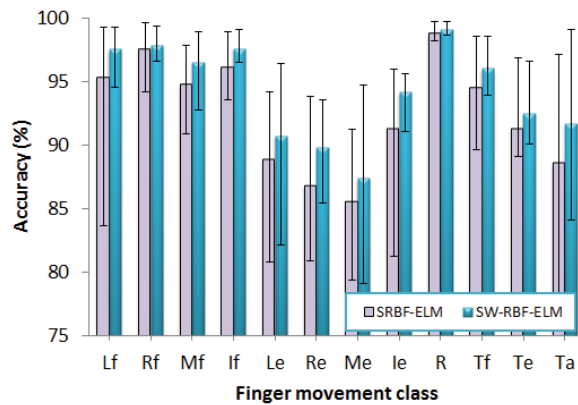
Figure 4.38 The accuracy of different finger motions across five amputees

The confusion matrix in Table 4.34 provides information about the misclassified finger motions. According to the Figure 4.38, SW-RBF- ELM poorly classified the Little extension (Le), Middle extension (Me), and Ring extension (Re). Me was mostly misclassified to Thumb abduction (Ta) and Middle flexion (Mf). Furthermore, the system mostly misclassified the little extension (Le) to Re and vice versa. Even though the misclassified motions were present, arguably the SW-RBF-ELM has succeeded to recognize different finger motions on five amputee subjects with accuracy of about 94%.

Table 4.34 The confusion matrix of the classification results of swarm-wavelet elm averaged for five amputees (Units : %)

		Intended Task											
		Lf	Rf	Mf	If	Le	Re	Me	Ie	R	Tf	Te	Ta
Classified Task	Lf	98.2	0.5	0.1	0.0	0.0	0.0	0.1	0.3	0.0	0.4	0.0	0.3
	Rf	0.8	98.4	0.6	0.0	0.0	0.0	0.1	0.0	0.0	0.0	0.0	0.0
	Mf	0.2	0.7	95.8	0.3	0.3	0.8	0.9	0.6	0.0	0.0	0.3	0.2
	If	0.2	0.1	0.1	97.7	0.3	0.3	0.2	0.1	0.0	0.7	0.1	0.3
	Le	0.0	0.0	0.4	0.3	90.1	4.6	1.8	0.2	0.0	0.6	1.0	0.9
	Re	0.1	0.0	0.7	0.2	3.8	89.8	2.1	0.2	0.0	0.6	0.7	1.7
	Me	0.2	0.0	1.3	0.3	2.4	3.1	88.6	1.3	0.0	0.4	0.7	1.8
	Ie	0.1	0.0	0.7	0.3	0.2	0.2	1.0	94.8	0.1	0.2	1.7	0.8
	R	0.1	0.0	0.0	0.2	0.1	0.0	0.0	0.1	99.1	0.3	0.0	0.0
	Tf	0.1	0.0	0.0	1.3	0.9	0.5	0.2	0.2	0.1	96.0	0.4	0.2
	Te	0.0	0.1	0.3	0.1	1.2	0.9	0.7	2.0	0.0	0.7	92.8	1.1
	Ta	0.0	0.0	0.3	0.4	1.2	2.3	1.1	0.3	0.0	0.2	1.2	93.0

To conclude, the proposed pattern-recognition system, which employs PSO mutated using a wavelet function to optimize the kernel based ELM (SW-RBF-ELM), was able to recognize eleven imagined finger motions on five transradial amputees with the high accuracy of 94.27 % even though it employed only two EMG channels. The proposed system performed better than standard PSO-ELM (SRBF-ELM).

4.5.5 Conclusion

This section proposed an improvement in the optimization process of PSO by injecting wavelet function to the PSO. The goal is to increase the searching space of the PSO to avoid the local optima that normally occurs in the PSO process. A swarm wavelet radial basis function ELM (SW-RBF-ELM) was proposed in addition to a swarm radial basis function ELM (SRBF-ELM). The former is the one that involves wavelet function and the latter is the one that does not. The experimental results show that the wavelet mutation improves the optimization process of the PSO. Consequently, the wavelet mutation in PSO also enhance the classification performance of the system. The experiments have been done on the healthy subjects and amputees. On the healthy subjects, the accuracy of SW-RBF-ELM is 95.62 % while SRBF-ELM is 95.53 %. The improvement of wavelet mutation on the amputees is more significant than that on the healthy subjects. On the amputees, the SW-RBF-ELM achieved the average accuracy of 94.27 %, while SRBF-ELM produced the average accuracy of 92.55 %.

4.6 Summary

This chapter proposes two new ELMs and two hybridizations of ELM and PSO. The first ELM is adaptive wavelet extreme learning machine (AW-ELM). The experimental results on EMG datasets for finger motion recognition shows that the performance of AW-ELM is good with the average accuracy of about 94 %. It is comparable to some well-known classifiers such as SVM, LDA, and kNN. Furthermore, the performance of AW-ELM is comparable to RBF-ELM, the most accurate kernel-based ELM. Although AW-ELM and RBF-ELM are comparable, the performance of RBF-ELM is better than AW-ELM. The experiments on UCI machine learning repository show that AW-ELM could work on a wide range of datasets.

Another new ELM that is proposed in this thesis is spectral regression extreme learning machine (SR-ELM). SR-ELM is an ELM for dimensionality reduction method that reduces and projects the features to new features that has smaller dimension but better class separability. The advantage of SR-ELM is that it has a good separation performance. The experimental results on the EMG dataset and benchmark datasets exhibit its benefits. Moreover, the experimental results on UCI datasets show that SR-ELM achieves the best performance when working together with AW-ELM, LDA and kNN. As for RBF-ELM and LIBSVM, the performance of SR-ELM is comparable to other methods. The

shortcoming of SR-ELM is on the processing time. The processing time of SR-ELM is slower than SRDA but faster than ULDA.

In addition to the new type of ELMs, this chapter provides two optimizations of the parameters of the kernel-based ELM. The first optimization was using particle swarm optimization (PSO). Three different kernels were involved including linear (SLin-ELM), polynomial (SPoly-ELM) and radial basis function kernels (SRBF-ELM). The experimental results show that SRBF-ELM is the most accurate system with the accuracy of about 94 %.

The experimental results show that the PSO tends to be trapped on the local optima. Therefore, the advanced PSO should be incorporated into the system. In this research, the wavelet-PSO was utilized to overcome the local optima issue. The benefit of the wavelet-PSO is not significant when working on the able-bodied subjects, but it is significant when it is applied to the amputees.

Another improvement in the fitness function is made as well. The previous experiments compute the fitness function from the error in each cross-validation output. In the new experiment, the fitness function was calculated from the average error of the cross-validations. Using this mechanism, the accuracy of SRBF-ELM improved to the accuracy of 95.53 %. As for the hybridization of wavelet-PSO and ELM (SW-RBF-ELM), it attained the accuracy of 95.64% on the healthy subjects.

In summary, all proposed systems show its benefits and advantages. Next, the system proposed should be applied to the real-time application. The real-time application considers not only the accuracy but also the processing time. Another thing is the robustness issue that should be taken into account. The next chapter will present the real-time application of the methods that have been designed in this chapter. In addition, the next chapter will propose some methods to improve the robustness of the myoelectric pattern recognition for finger motion classification.

CHAPTER 5

Toward robust myoelectric pattern recognition for real-time finger movement classification

5.1 Introduction

This chapter presents implementations of the myoelectric pattern recognition (M-PR) or EMG-based pattern recognition (EMG-based PR) that have been developed in the previous two chapters (chapter 3 and 4) in the real-time application. This chapter consists of three sections. The first section will provide the implementation of myoelectric pattern recognition in the real-time environment, as presented in **section 5.2**. The second section will propose a new classifier that can reject the untrained movements. The shortcoming of the system developed in section 5.2 is that the system is trained only with a limited number of movements compared to the movements that human can do. Therefore, there should be a mechanism to reject the untrained movement. The discussion will be presented in **section 5.3**. Finally, **section 5.4** proposes the way to deal with the degradation of the classification performance in the day-to-day use.

This chapter provides **three main contributions of the thesis**. The first contribution is the real-time M-PR for finger motion classification. The second one is the improvement of the real-time M-PR by introducing a rejection mechanism to reject the movements that are involved in the training stage. The last one is an adaptive real-time M-PR to anticipate the changes that may happen during the day-to-day activities.

5.2 Evaluation of real-time myoelectric finger motion recognition using two EMG channels

This section presents real-time implementation of the myoelectric pattern recognitions (M-PR) that have been developed in Chapter 3 and 4. The major change made in this section compared to those made in Chapter 3 and 4 is on the involvement of the transient

state of EMG signal along with the steady state. Involving the transient state in the system will decrease the accuracy, but it can increase the robustness of the M-PR. The discussion will be started with the introduction, and then followed by the methodology used in the real-time experiments. The next section will discuss the offline and the online experiment. The conclusion will end the discussion.

5.2.1   Background

The electromyography signal has been used widely to control hand rehabilitation devices such as the exoskeleton hand and the prosthetic hand. Furthermore, many attempts have been made to decode the hand movements as control sources of the hand robot (Micera *et al.*, 2010; Oskoei & Huosheng, 2008; Sang Wook *et al.*, 2011).   In addition to the hand movement, the finger movement has been taken into consideration in an effort to develop a dexterous control system (R. N Khushaba *et al.*, 2012; Tenore *et al.*, 2009). One of the major researches in the finger movement is finger movement recognition. Tenore *et al.* (2009) decoded ten classes of individual finger movements by using up to 32 EMG channels with accuracy about 90%. In addition, Al-Timemy *et al.* (2013) classified 15 individual finger movements and achieved 98 % accuracy by using six sEMG channels.

The use of few numbers of electrodes in the finger motion recognition system without compromising the decoding performance is a challenging task. Tsenov *et al.* (2006) used two sEMG channels for four finger movements i.e. the thumb, index, middle finger and hand closure with the best accuracy of nearly 93 % in offline classification (Tsenov *et al.*, 2006). Moreover, R. N Khushaba *et al.* (2012) classified ten classes of individual and combined finger movements which consisted of five individual finger movements by using two sEMG channels. The work could achieve 92% and 90 % accuracy for the offline and online classification, respectively.

To the best of the author's knowledge, most reports show the efficacy of myoelectric pattern recognition using few EMG channels in the laboratory environment, yet they are not proven yet for real-time application. This chapter proposes some methods that are intended to close the gap between the success of laboratory experiments and the real-time application. This section is the initial step of the project.

There are some issues that have to be addressed when doing real-time myoelectric pattern recognition. The major issue is the robustness of the recognition system. Many aspects influence the robustness of the EMG-based pattern recognition (EMG-based PR)

including electrode shifts, the limb position, muscle fatigue, and the improvement on the muscle function. This chapter proposes methods to deal with the robustness issues. The robustness of the myoelectric pattern recognition (M-PR) system can be attained by considering the transient and steady state of the EMG signal, even though it will decrease the classification accuracy. Involving both states in the training can improve the robustness of EMG-based PR.

5.2.2 Methodology

In this thesis, the real-time myoelectric pattern recognition (real-time M-PR) system consists of two main components: the hardware and software, as shown in Table 5.1. Both components will be involved in the stages of the real-time M-PR system. In general, all the stages of real-time pattern recognition based EMG are shown in Figure 5.1. In the experiment, the system collects the data from a subject. Then, the collected data is used to train the system. The output of the offline classification is the trained classifier and the eigenvectors for features projection. Instantly, the online classification is conducted after completing the offline classification. The result of the online classification is presented on the computer screen located in front of the subject.

Table 5.1 The hardware and software needed for real-time application

Component	Description	Picture
Hardware	Personal Computer Intel Core i5 3.1 GHz with 4 GB RAM equipped with Windows 7 operating system	
	EMG acquisition device, the FlexComp Infiniti™ System from Thought Technology with frequency sampling 2000 Hz.	
	Two EMG sensors: MyoScan™ T9503M Sensors from Though technology	
	Two electrodes	
Software	Matlab	
	API library from Though Technology connecting the Flexcomp to Matlab	
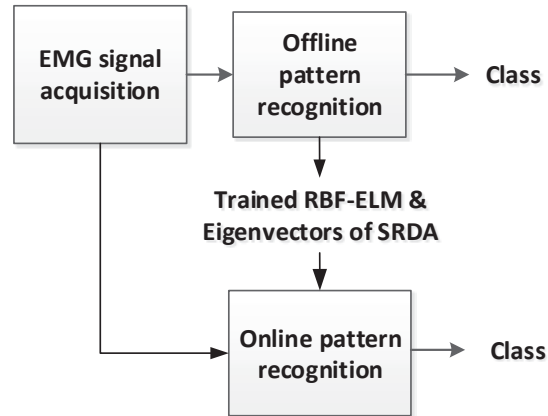
Figure 5.1 Stages of online myoelectric pattern recognition system

5.2.2.1　Data acquisition

In the experiment, eight subjects are involved in the offline and online experiments. The data for the offline classification is same as the data used in Section 4.2.4.1. As for the online classification, the EMG data were collected from two females and six males who were normally limbed with no muscle disorder. During the experiment, the subject's arm was supported and fixed at a certain position as described in Figure 5.2 to avoid the effect of position movement on EMG signals. In the data collection, a couple of digital filters used during the data collection and online experiments. They were a band pass filter between 20 and 500 Hz and a notch filter to remove the 50 Hz line interference. Then the EMG signals were down- sampled to 1000 Hz.

Figure 5.2 The electrodes placement

The offline and online experiment involved ten finger movements as explained in Section 4.2.4.1 Figure 4.6. They consisted of the individual and combined finger movements consisting of the flexion of individuated fingers, i.e., Thumb (T), Index (I), Middle (M), Ring (R), Little (L) and the pinching of combined Thumb–Index (T–I), Thumb–Middle (T–M), Thumb–Ring (T–R), Thumb–Little (T–L), and the hand close (HC).

5.2.2.2   Feature extraction

In this section, the features are extracted from a time domain feature set which consists of waveform length (WL), slope sign changes (SSC), number of zero crossings (ZCC), and sample skewness (SS). In addition, some parameters from Hjorth time domain parameters (HTD) and auto regressive (AR) Model Parameters were included as used in (R. N Khushaba *et al.*, 2012).

The AR model parameters have been proven to be stable and robust to the electrode location shift and the change of signal level (Tkach *et al.*, 2010). Moreover, aforementioned time domain features were windowed by using disjoint window instead of sliding window to keep computational cost low. A 100-ms window and a 100-ms increment were used to form a system that is suitable for the real-time application.

5.2.2.3   Dimensionality reduction

Chapter 4 section 4.4 have tested different types of dimensionality reduction method including the proposed SR-ELM. In this experiment, the M-PR system will use one of the tested methods based on the speed. All methods are reasonable for real-time application. However, the M-PR system selects the fastest one that is spectral regression dimensionality reduction (SRDA).

5.2.2.4   Classification

Chapter 4 presented various types of myoelectric pattern recognition (M-PR) for finger movement recognition employing different types of components. In the classifier side, this thesis has developed two different classifiers. The first one is the node-based ELM, which is adaptive wavelet extreme learning machine (AW-ELM) and the second one is the kernel-based ELM optimized using particle swarm optimization (PSO). This chapter selects the optimized kernel-based ELM especially radial basis function ELM. In this chapter, the term of RBF-ELM is used instead of SRBF-ELM or SW-RBF-ELM for the sake of simplicity. All classifiers that have been developed are comparable to each other. However, in this real-time experiment, the work has to select one of them due to difficulty in using different classifiers for long duration experiments on many subjects. In addition, RBF-ELM has two important parameters, C and γ. This work used the optimized RBF-ELM with the $\gamma=2^{-5}$ and $C=2^0$.

5.2.2.4.1   Offline experiment

The offline classification was performed based on signals collected through data acquisition, as explained in Section 4.2.4.1. The main purpose of doing the offline

classification is to train the myoelectric pattern recognition especially for the feature projection and classification. Before training the system for the online classification, this section will investigate the possibility of adding a new channel from the summation of two channels collected in the data acquisition. In both the offline and online stage, the signals were extracted in 100 ms windows length incremented every 100 ms.

5.2.2.4.2 Online experiment

In the online stage, the subject performed similar activities as in the offline classification. The difference is the repetition, which is only four times instead of six. Furthermore, no more training exists in the system. All data are for testing only which is carried out online and real-time. Another difference is the recognition system is performed each 100 ms and then the result is displayed on the screen. The detailed procedure for the online experiment is depicted in Figure 5.3.
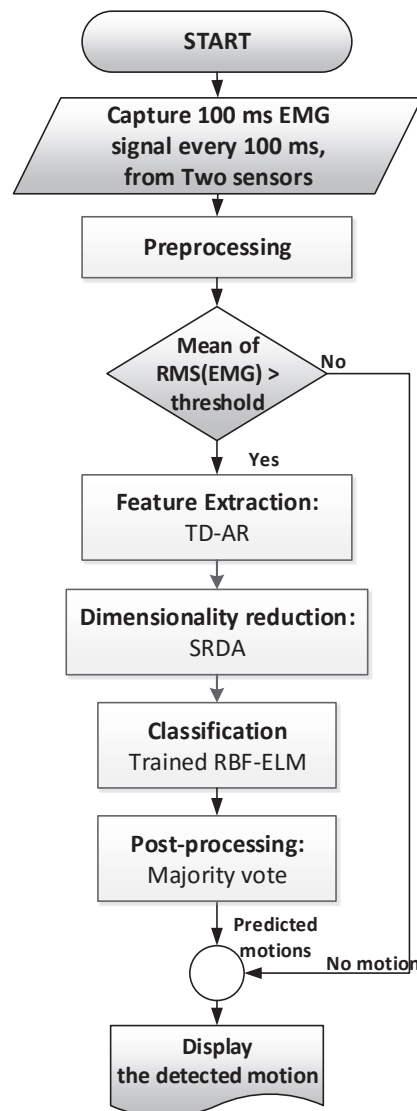
Figure 5.3 Procedure for the online classification

As shown in Figure 5.3, the online experiment detects the intention of the user to move the finger by calculating the root mean square value of EMG signals from all channels. Then, the calculated value is compared with the threshold value. If the value is less than the threshold, the system will produce no motion. Otherwise, the pattern recognition system will begin to work.

5.2.2.5 Post-processing

In the online experiment, a majority vote was used to refine the classification results. The number of previous votes is four to comply with the acceptable controller delay of the myoelectric controller (<300 ms) based on Eq. **3.1**.

5.2.3   Experiment 1: offline classification

Before conducting the online experiment, the offline classification is performed to learn and investigate the optimal setting of the myoelectric pattern recognition system for the online experiment. Firstly, the efficacy of adding a new channel from integration of two EMG channels was observed. Before conducting the offline classification, the EMG signals were collected from the subject's forearm using a customized software created in Matlab. The appearance of the software is shown in Figure 5.4
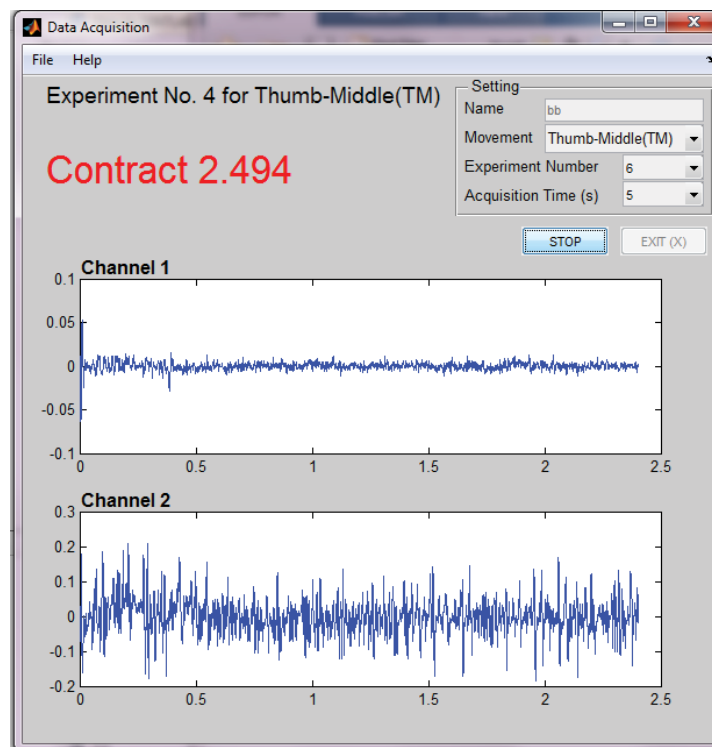
Figure 5.4 The Interface for EMG signal acquisition

After collecting data, the offline classification is conducted using a menu displayed in Figure 5.5. A user needs to specify where the EMG signals are stored. If all steps are done, then the offline classification runs by clicking the start button on the figure.
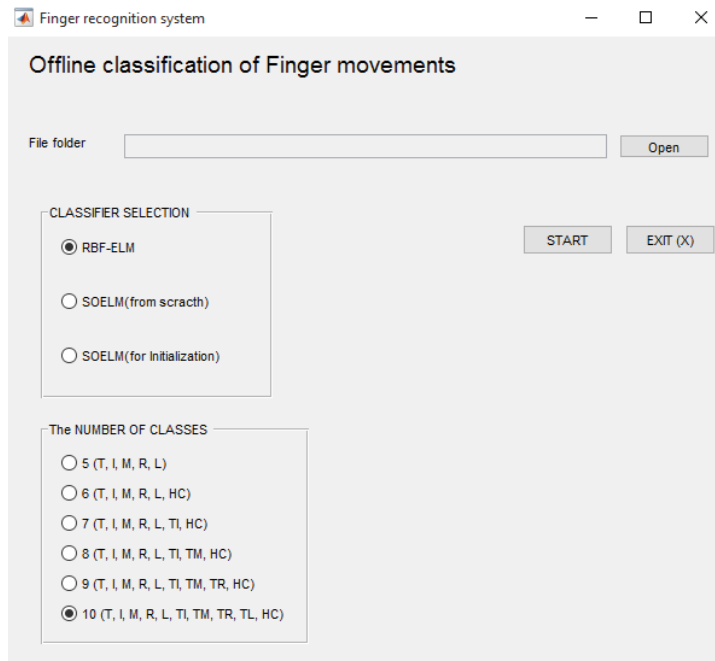
Figure 5.5 The offline classification menu done after data collection

5.2.3.1 Adding new virtual channel

The first experiment is a new channel experiment. In this stage, the performance of the classification system using only two original signals (channel 1 = ch1, channel 2 = ch2) was compared to the original signals plus the new additional channel from the summation of both the channels (ch1, ch2, ch1+ch2). The classification utilized 3-fold cross validation. Figure 5.6 presents the classification results.
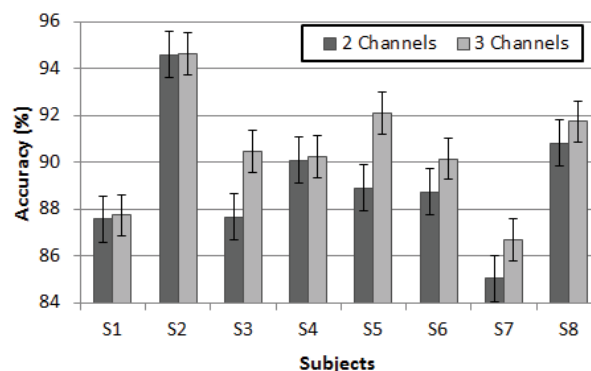
Figure 5.6 The accuracy of the system using two and three channels

Figure 5.6 shows that both configurations achieved good accuracies across eight subjects. However, the additional signal of the summation of two channels gives better

150

average accuracy than two channels only. It occurs in all subjects. However, the difference is not significant, as shown by the one-way ANOVA test results in Table 5.2. By setting p at 0.05, the accuracy difference between two is statistically not significant because p-values are above 0.05. Although the improvement is insignificant statistically, the work on the online experiment employed the third channel to improve the robustness of the pattern recognition system.

Table 5.2 One-way ANOVA test between two-channel and three-channel experiment

	p-value							
	S1	**S2**	**S3**	**S4**	**S5**	**S6**	**S7**	**S8**
2Ch vs 3Ch	0.95	0.97	0.20	0.96	0.50	0.14	0.41	0.21

5.2.3.2 Classification performance

Figure 5.7 presents the offline classification results across eight subjects. This figure shows that the myoelectric pattern recognition (M-PR) system could recognize the individual finger well, except on the little finger motion (L). Furthermore, the performance of M-PR system on the individual finger motions is better than the combined finger except in little finger movement (L). The average classification accuracy for offline classification is 90.46 %.

The offline classification produces an optimal M-PR system for finger motion recognition in the online experiment. The optimal M-PR system consists of the trained RBF-ELM and the eigenvectors of SRDA. The M-PR software stores them and then loads them when conducting the real-time application.
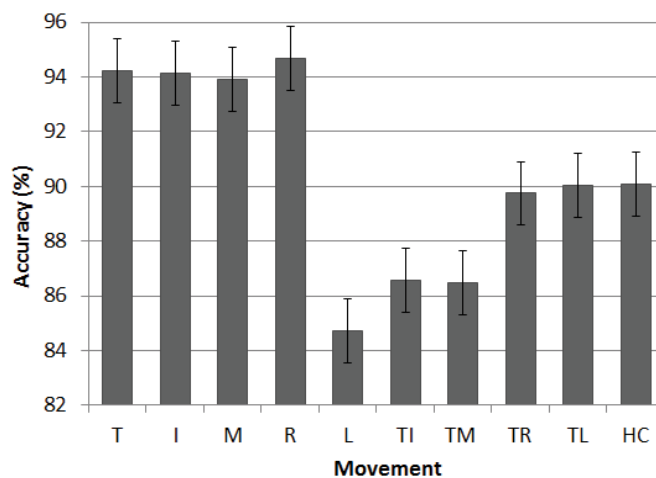
Figure 5.7 The accuracy of the myoelectric pattern recognition in the offline classification

5.2.4   Experiment 2: online classification

5.2.4.1   *Experimental environment*

This section presents the online classification. Figure 5.8 presents the environment utilized during the online experiment. Two EMG sensors are located on the forearm of the user. The EMG acquisition device captures the EMG signals every 100 ms and then processes it to yield the predicted movement. The predicted movement will be displayed on the screen computer. Before starting the online classification, the user should load the trained system produced in the offline classification. Therefore, offline classification is very important to the success of the online classification.
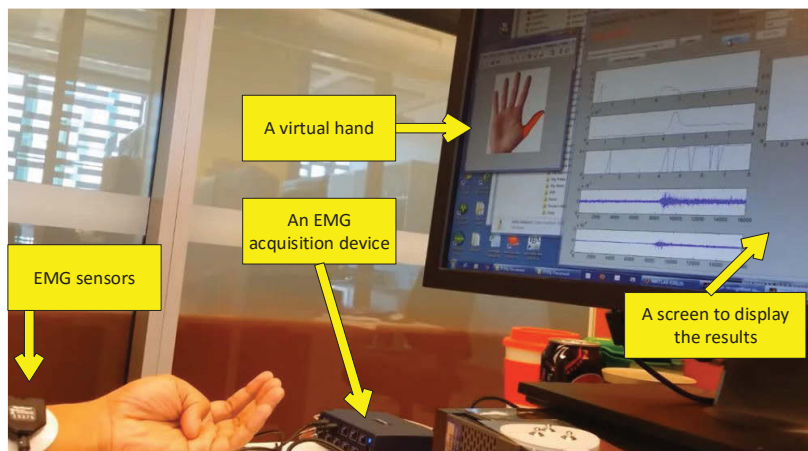
Figure 5.8 The experimental environment for the online myoelectric pattern recognition

In this experiment, the online classification should be conducted after offline classification straight way. The reason is to avoid muscle fatigue of the user because of a long period of the experiment. The second reason is to prevent the electrode shift. Electrode shift affects the online classification performance. Certainly, this procedure is not suitable for daily life activities. The end of this chapter will discuss this and propose a new method to overcome such defects in the real-time application (see **section 5.4**).

5.2.4.2   *Analysis of subjects*

Each subject conducted ten different finger movements consisting of five individual motions, four combinations of two fingers and one hand close movement. Each finger movement was repeated four times. Figure 5.9 depicts the results of the online experiment.

Figure 5.9 shows that the myoelectric pattern recognition (M-PR) system could work on various subjects with an average accuracy of about 89%. The accuracy is lower than the offline experiment (90.46 %). Furthermore, the offline classification is better than the

online one on five subjects, out of eight. Interestingly, on three subjects, which are S5, S7, and S8 (three dot circles in Figure 5.9) , the online classification achieved better accuracy than the offline one. In regards to the subject discussion, the online M-PR got the worst accuracy on subject S2 and then on subject S1. On the other hand, the M-PR system achieved the best performance when it recognized the EMG signal from subject S8 and then S5. In general, the online classification results verify the reliability of the online M-PR.
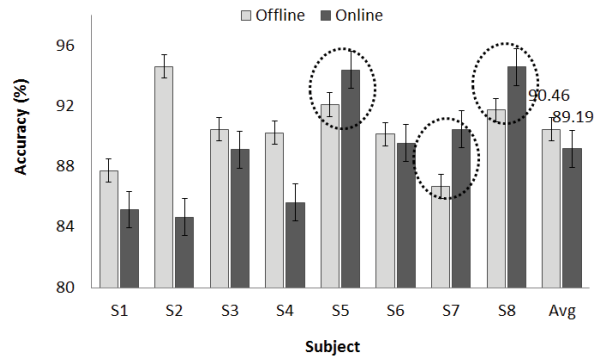
Figure 5.9 The average accuracy of the online experiment from four trials.

5.2.4.3 *Analysis of the movement*

Figure 5.10 exhibits the accuracy of the movements in the online classification. The figure presents all four trials and the average of it (black colour). The thumb-index finger movement (TI) is the most difficult movement to recognize. The accuracy of the movement is the worst. Besides, during four trials, the accuracy is not stable. The second most unstable movement is the little finger movement (L). Most of the combination movements exhibited unstable performance across four trials except the hand-close (HC) movement. On the other hand, all individual movements show a stable performance on four trials except the little finger movement (L).
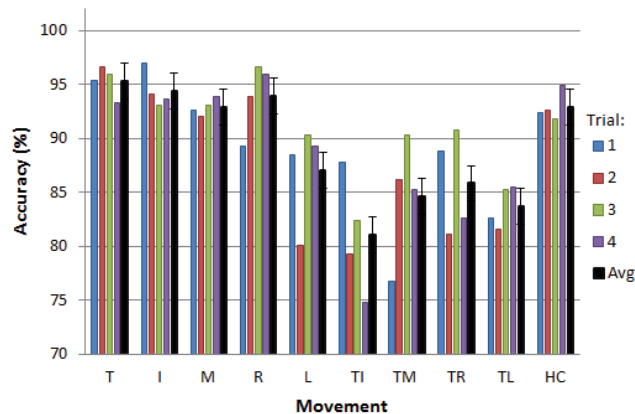
Figure 5.10 The accuracy of the online MPR in various finger movements across eight subjects

153

Comparison between the offline and online classification is presented in Figure 5.11. In general, the figure indicates that the behaviour of offline and online is similar. In both classifications, the individual movements are better than combined movements except in the hand close (HC) movement. The difference exists in the worst movements. In the offline classification, the most difficult movement to recognize is the little finger movement (L) and TI is the second, while in the online classification it is the opposite of the offline. The movement TI is the worst and then followed by L. Overall, the online classification has succeeded in classifying ten finger movements as what have achieved in the offline classification.
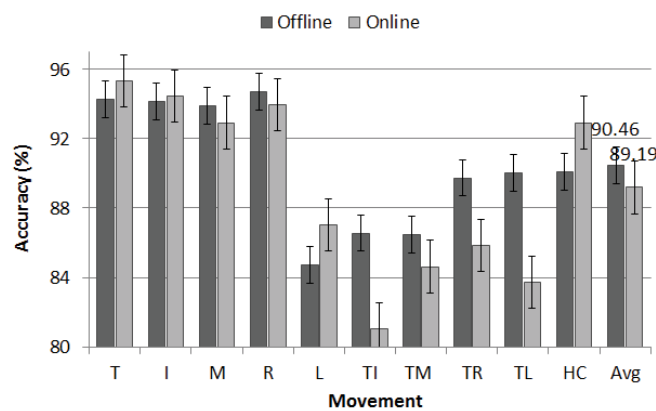
Figure 5.11 The performance comparison between offline and online classification across eight subjects

Table 5.3 presents the average confusion matrix of the online classification performance across eight subjects. This table indicates that the thumb-index finger movement (TI) was misclassified to the thumb (T), little finger (L) and thumb-little finger (TL) movements. Meanwhile, the L movement was mostly misclassified to T, I, TM and TL movements.

Table 5.3 Confusion matrix of the online classification

		Target Movement									
		T	**I**	**M**	**R**	**L**	**TI**	**TM**	**TR**	**TL**	**HC**
	T	95.34	1.47	0.00	0.00	0.32	1.28	0.13	0.00	0.32	1.15
	I	0.45	94.45	0.00	0.00	0.38	2.87	0.06	0.00	1.28	0.51
	M	0.32	0.13	92.92	2.04	0.32	0.26	3.06	0.00	0.19	0.77
	R	0.38	0.13	0.00	93.94	3.76	0.19	0.00	0.89	0.70	0.00
Actual movement	**L**	1.72	1.34	0.19	0.96	87.05	0.57	3.83	0.70	2.87	0.77
	TI	3.25	1.85	0.06	0.32	4.78	81.06	2.93	0.00	4.91	0.83
	TM	0.00	0.06	5.93	0.26	4.78	2.04	84.63	0.83	0.64	0.83
	TR	0.77	0.51	0.06	2.42	1.28	1.72	3.19	85.84	3.57	0.64
	TL	1.72	3.13	0.19	0.19	5.04	1.79	1.28	2.49	83.74	0.45
	HC	2.04	0.89	0.64	0.64	0.06	1.85	0.26	0.57	0.13	92.92

To evaluate the performance of the M-PR in recognizing ten finger motions, this thesis also considers the performance of the M-PR over time, as shown in Figure 5.12. The total of root mean square (RMS) of two channels is used to detect the moving intention of a user. Figure 5.12 shows the output of the system (the fifth row) will be zero if the total of RMS from two channels is less than the threshold. Otherwise, the system produced a predicted movement.
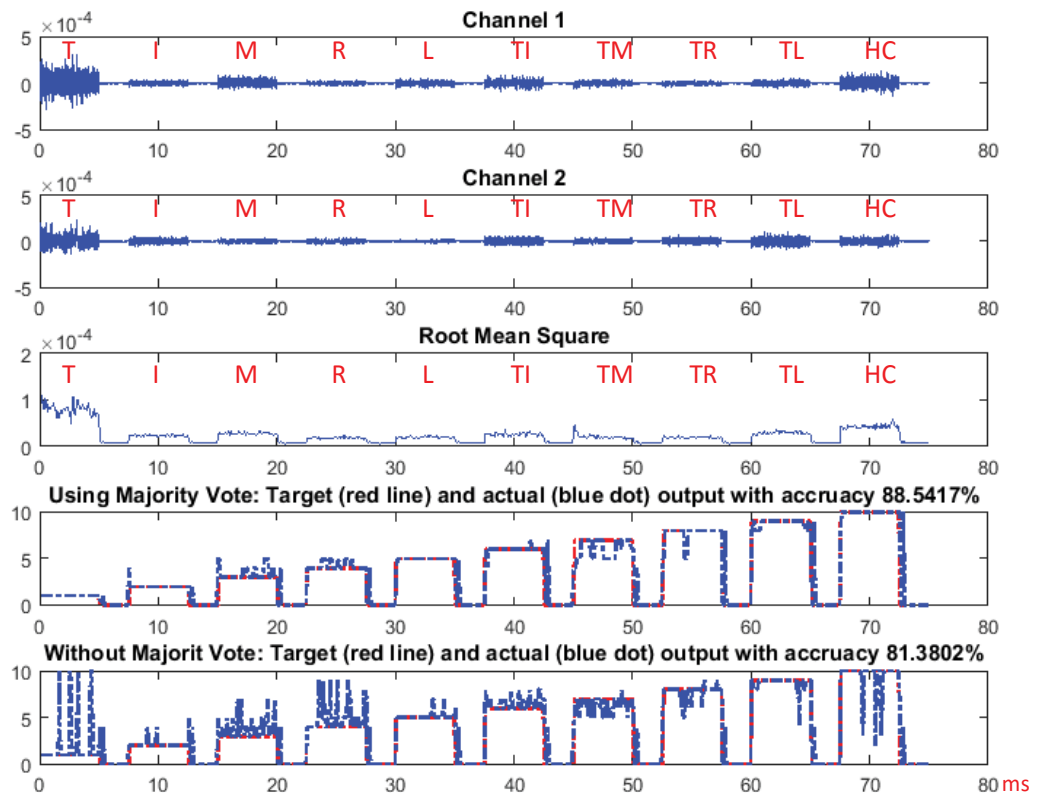
Figure 5.12 The performance of the online classification across time on subject S6.

Figure 5.12 also provides a comparison of the existence of a majority vote (the fourth row) and the absence of it (the fifth row). It is noticeable that the majority vote could smooth the output of the system. This performance is needed when the output is used to drive a hand rehabilitation device. The absence of majority vote will reduce the comfort of the users because the movement of the robot is not stable. By contrast, the existence of majority vote improves the stability of the output and finally it will enhance the user's comfort. Indeed, the existence of the majority vote increases the time delay. However, as long as it can be maintained lower than 300 ms, it will not matter. The reader is recommended to watch the video about the online experiment reported in this thesis through the following link:

https://www.youtube.com/watch?v=DCj-y8JxRLY

5.2.4.4 Processing time

This section investigates the delay time produced by the system to comply with the acceptable delay time of myoelectric controller. The calculation of the delay time follows the equation proposed by T. Farrell and Weir (2008), as defined in Eq. **3.1**. Table 5.4 presents the results.

Table 5.4 The controller delay of the online experiment

Class	Window length (ms)	Window Increment (ms)	Filter (ms)	Extraction & reduction (ms)	ELM (ms)	Vote (n=4) (ms)	Total (Eq. 3.1) (ms)
T	100	100	3.9	7.6	0.5	0.1	262.1
I	100	100	3.5	7.2	0.5	0.1	261.3
M	100	100	3.5	7.3	0.5	0.1	261.4
R	100	100	3.6	7.4	0.5	0.1	261.6
L	100	100	3.7	7.6	0.6	0.1	262
T-I	100	100	3.5	7.3	0.5	0.1	261.4
T-M	100	100	3.6	7.5	0.5	0.1	261.7
T-R	100	100	3.6	7.6	0.6	0.1	261.9
T-L	100	100	3.5	7.3	0.5	0.1	261.4
HC	100	100	3.5	7.3	0.5	0.1	261.4
Avg	**100**	**100**	**3.6**	**7.4**	**0.5**	**0.1**	**261.62**

Table 5.4 shows that the delay time of the system is about 261 ms. This time length is lower than the acceptable controller delay recommended by Kevin Englehart *et al.* (2001). However, it is longer than the optimal delay time proposed by T. Farrell and Weir (2008) in which 175 ms (for average users). The optimal delay time of T. Farrell and Weir (2008) can complied by reducing the number of votes in the majority vote. However, it will decrease the performance of the online classification, as discussed in **5.2.4.3**.

5.2.5 Conclusion

This thesis developed real-time myoelectric pattern recognition (real time M-PR) for the finger motion detection. There are eight subjects involved. The subjects conducted the offline and online classification in sequence without long delay and without taking off the electrodes. It means that the electrode positions in offline and online experiments are exactly same. The offline classification is done to train the parameters of the components in the M-PR system such as the eigenvectors of dimensionality reduction SRDA and the weights of the classifier. Once those parameters are set, the online

experiment was performed based on those parameters and no change in them occurred during the online experiment.

Furthermore, the both experiments considered the transient and steady state of the signal. Although the inclusion of transient state can reduce the classification performance, it can increase the robustness of the system on real-time application. The experimental results show that the online classification accuracy is not too much different from the offline classification. The classification accuracy is 90.46 % and 89.19 % on the offline and online classification, respectively.

As for the controller delay time, the M-PR system took about 261 ms to produce a movement. This length time is less than the acceptable controller delay proposed by Kevin Englehart *et al.* (2001). Therefore, the developed M-PR system is reliable for the next project which is moving the hand rehabilitation device.

The implementation of the M-PR in the hand rehabilitation device should consider some issues. Firstly, the system should be able to tackle the movements that are not included in the training stage or it is called untrained movements. In fact, the untrained movements in the real-time application are far larger in number than the trained movements. The second issue is in regard to day-to-day activity. The M-PR should be able to work not only on the day of training but also for the days after it. In fact, the performance of the M-PR degrades along with the passing of time. The reason is that the environment has changed from the day of the training. As a result, the M-PR system is not able to cope with changes in the environment. Electrode shifts, improvement in the muscle functionality are some examples of what possibly happens.

The next section will address these two issues to increase the acceptance rate of the myoelectric controller in the real-time or clinical application.

5.3 Evaluation of myoelectric finger motion recognition with motion rejection for an exoskeleton hand

This section provides two major contributions. Firstly, the myoelectric pattern recognition (M-PR) with rejection mechanism is introduced. The rejection mechanism helps M-PR to deal with the movements that are not included in the training stage. Inevitably, it will improve the accuracy and the robustness of the M-PR. Secondly, this section introduces a new myoelectric controller for the exoskeleton hand. The novelty lies on the capability of dealing with the individual and the combined finger movements.

157

The structure of this section is as follows. The first and the second sections will discuss the introduction and methodology used in the experiments. The experimental results come after that. The conclusion will end this section.

5.3.1 Background

The myoelectric finger motion detection can recognize the trained movement, but it fails to recognize untrained movement. The untrained movement means the movement that is not included in the training stage. In the real-time application, the trained movements are limited, yet the untrained movements are very large. As a result, the performance of myoelectric pattern recognition (M-PR) is affected when it works in the real-time or clinical application.

To cope with the untrained movements, this thesis proposes a classifier with a rejection mechanism called RBF-ELM-R, radial basis function extreme learning with rejection. RBF-ELM-R is equipped with a mechanism to detect the untrained movements and reject them. In other words, the system will consider the rejected movement as no action or rest.

In this section, the proposed method will be used to drive an exoskeleton hand. To the best of the author's knowledge, the implementation of a myoelectric controller in the exoskeleton hand is limited to the threshold controller. The threshold controller drives the exoskeleton hand based on the state of the EMG signal. If the value of EMG signal is more than the threshold value, then the controller will move the exoskeleton hand. Otherwise, the exoskeleton hand is in a rest position. A "hand of hope", a commercial exoskeleton hand from rehab-robotics, employs the threshold controller to detect user intension to move all fingers simultaneously or just stay in a rest position. The control method of the "hand-of-hope" is developed by Ho *et al.* (2011). Similar controller was also applied to another exoskeleton hand (Mulas *et al.*, 2005).

A more advanced method was proposed by Wege and Zimmermann (2007) when they employed a blind separation to decompose individual finger movements using ten EMG channels. This thesis proposes a myoelectric control system that can move five individual fingers and five-finger combinations using only two channels.

5.3.2 Methodology

This section presents the proposed myoelectric control for the exoskeleton hand that can move or flex five individual fingers and five combined finger movements. The work employed an exoskeleton hand developed by Rahman and Al-Jumaily (2012). The control system diagram is depicted in Figure 5.13. As shown in Figure 5.13, a root mean square

(RMS) is used to detect the user's intention to initiate movement. Besides, RMS is used to measure the level of the movement contraction and then utilize it to move electric motors of the exoskeleton hand proportionally.
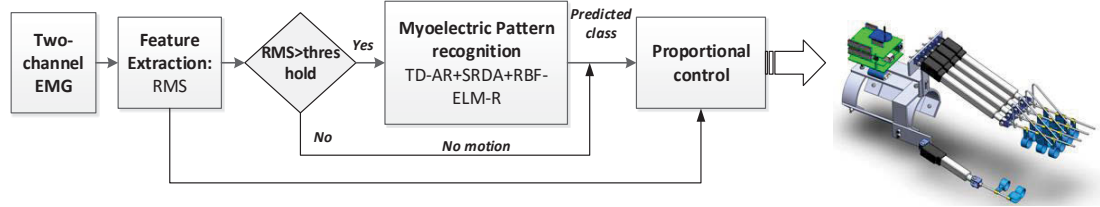
Figure 5.13 Myoelectric control system developed to control the exoskeleton hand

The control system of the exoskeleton hand consists of two main parts: myoelectric pattern recognition and proportional controller. In this section, the thesis proposes myoelectric pattern recognition with motion rejection (M-PR-R). Section 5.2 has discussed the performance of RBF-ELM for online classification. This section provides the RBF-ELM that is equipped with a rejection mechanism (E. J. Scheme *et al.*, 2013). The algorithm of the motion rejection mechanism is shown in Figure 5.14.

As presented in Figure 5.14, the rejection mechanism utilized entropy as confidence measurement. The lower the entropy is, the more confidence the output is. The formulation of entropy is defined by:

$$E(n) = -\sum_{j}^{N} o_j(n) ln\big(o_j(n)\big)$$

5.1

The second main component of the myoelectric controller used in these projects is the proportional controller. The proportional controller translates the predicted class produced by the myoelectric pattern recognition into motor action. The action is given proportionally according to the RMS of the amplitude of the EMG signals. The algorithm for the proportional controller is described in Figure 5.15.

The exoskeleton hand used in this experiment was developed by Rahman and Al-Jumaily (2012). The exoskeleton hand is able to flex the finger actively at the metacarpophalangeal (MCP) joint and passively in the proximal interphalangeal (PIP) and distal interphalangeal (DIP) joint. The Arduino microcontroller board is used to drive the five linear DC motors, as described in Figure 5.16.
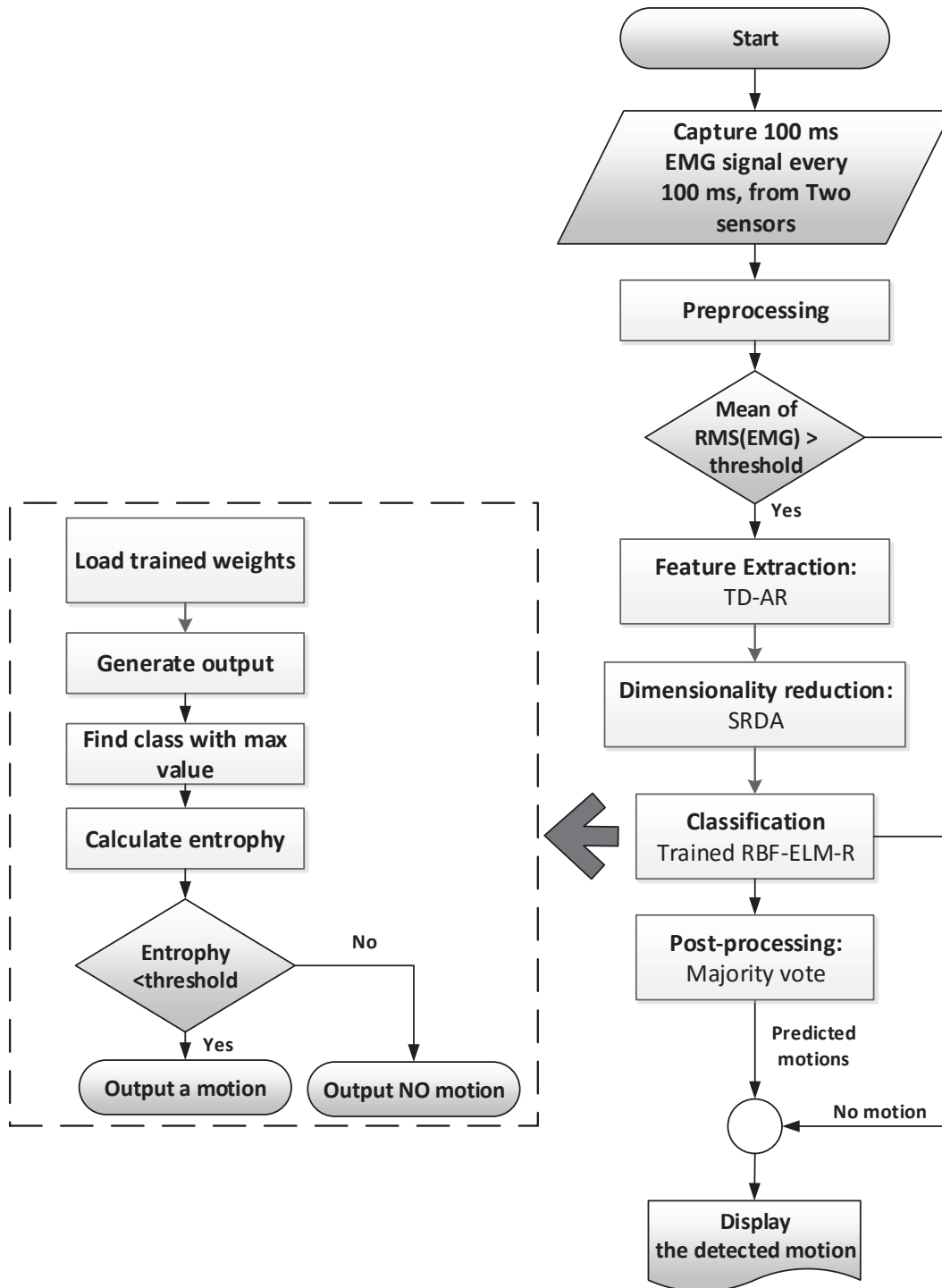
Figure 5.14 Myoelectric finger movement recognition using RBF-ELM with rejection mechanism
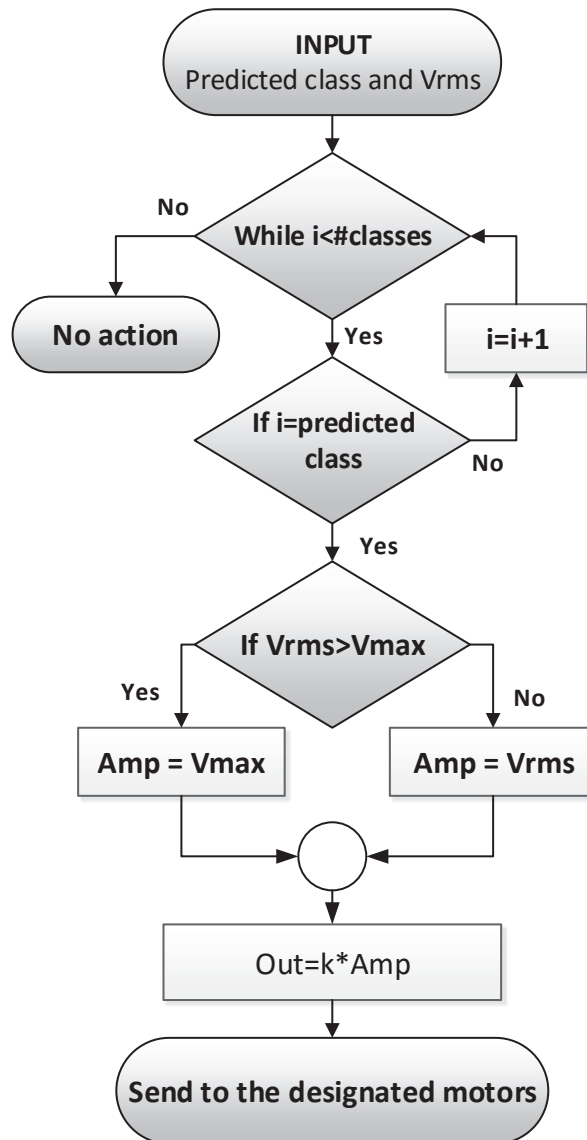
Figure 5.15 Proportional controller for the exoskeleton hand
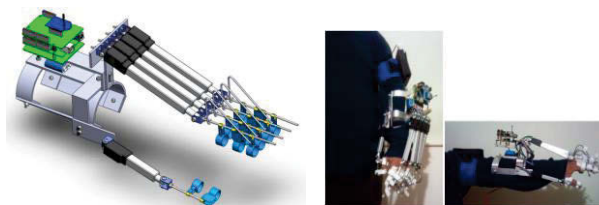
Figure 5.16 The exoskeleton hand used in the experiment

5.3.3   Experiments and results

5.3.3.1   Offline experiment

In the offline experiment, the thesis investigates the efficacy of the rejection mechanism in RBF-ELM and its implication on the performance of the myoelectric pattern recognition system. The threshold values of the motion detection were varied from

0 to 1 by increments of 0.1. In addition to varying the threshold values, the composition of the number of trained classes and untrained classes was changed. In the experiments, the data consists of ten movements or classes. If five classes are used in the training, the others are used to test the rejection capability of the system. As a result, if the M-PR is trained using nine classes, then only one untrained classes is used in the testing.

Afterward, the thesis investigates the performance of the system that utilizes the rejection mechanism and compares it with the system without the rejection mechanism. The offline experiments were conducted using 3-fold cross validation. The EMG signals collected in section **5.2.2.1** were used in the experiments. The data was collected from eight able-bodied subjects. Figure 5.17 and Table 5.5 provides the results.

Figure 5.17 and Table 5.5 indicate that M-PR with small threshold values achieved high accuracy. In addition, the system that is trained using five classes and then tested using five untrained classes achieved poor accuracy. Another interesting fact provided in Table 5.5 is that the system without rejection mechanism (RBF-ELM) and with rejection mechanism (RBF-ELM-R) experience poor performance when the untrained classes were imposed into the system. The accuracy of RBF-ELM on 10 trained classes was 87 %. However, the accuracy dropped to 65.9 % when one untrained class was introduced to the system (see the dark-grey background in Table 5.5). Fortunately, the system with rejection motion (RBF-ELM-R) could improve the dropped accuracy due to the existence of the untrained classes on RBF-ELM by 10 %, when using threshold 1.0. The similar improvement also occurs in all cases, but the enhancement gets less by increasing the number of untrained classes in the testing.
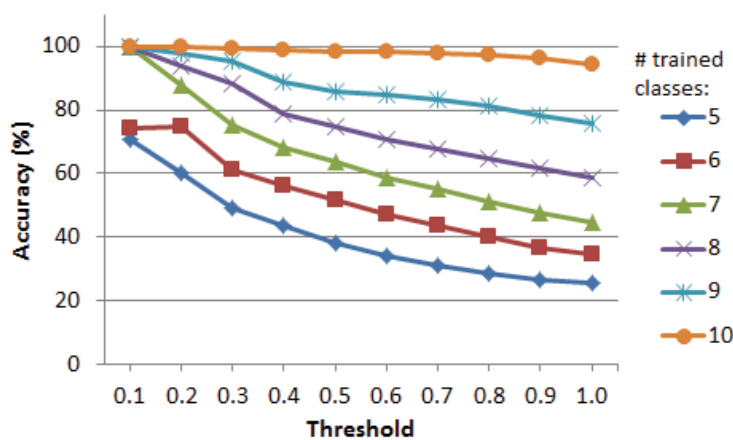
Figure 5.17 The variation of rejection threshold on the system performance without majority vote

Table 5.5 The accuracy achieved by varying the threshold of the rejection mechanism across eight subjects using 3-fold cross validation without using the majority vote

#classes		Rejection with threshold (accuracy %)										No Rejec-tion
Trained	Untrained	0.1	0.2	0.3	0.4	0.5	0.6	0.7	0.8	0.9	1.0	
5	5	71.0	60.1	49.3	43.8	38.1	34.1	31.2	28.4	26.5	25.4	23.8
6	4	74.5	74.6	61.2	56.2	51.6	47.4	43.7	40.1	36.6	34.6	30.8
7	3	NA	87.7	75.4	68.5	63.7	58.6	55.0	51.2	47.6	44.7	39.5
8	2	NA	94.1	88.5	79.0	75.0	70.8	67.8	64.6	61.7	58.7	51.1
9	1	NA	97.8	95.4	89.1	85.9	84.8	83.4	81.2	78.5	75.9	65.9
10	0	NA	NA	99.6	99.0	98.6	98.4	98.1	97.4	96.2	94.6	87.0

NA : Not Applicable

In addition to Table 5.5, Table 5.6 describes the accuracy when the rejection mechanism is combined with the majority vote. It seems that the majority vote decreases the accuracy of the system with the rejection mechanism especially for low threshold value. The rejection rate of the low threshold value is high so that the majority vote does not have enough data to vote the correct outputs. Therefore, for good performance, the threshold selection should be selected properly.

Table 5.6 The accuracy achieved by varying the threshold of the rejection mechanism across eight subjects using 3-fold cross validation using the majority vote

#classes		Rejection with threshold (accuracy %)										No Rejec-tion
Trained	Untrained	0.1	0.2	0.3	0.4	0.5	0.6	0.7	0.8	0.9	1.0	
5	5	43.1	55.7	46.8	42.0	36.7	33.1	30.4	28.0	26.3	25.2	23.6
6	4	46.6	64.2	56.7	53.2	49.2	45.5	42.4	39.3	36.2	34.4	30.8
7	3	NA	62.0	67.2	63.5	60.1	56.0	53.1	50.1	47.2	44.7	40.1
8	2	NA	50.2	74.0	71.4	69.6	66.9	64.9	62.5	60.6	58.4	52.3
9	1	NA	59.1	70.7	77.7	78.4	79.3	79.2	78.1	76.5	75.2	68.1
10	0	NA	NA	63.2	81.6	87.6	90.5	92.1	92.7	93.0	92.9	90.5

Table 5.7 The rejection rate of threshold experiments on eight subjects using 3-fold cross validation

# trained classes	Untrained classes (%)	Threshold (rejection rate %)									
		0.1	0.2	0.3	0.4	0.5	0.6	0.7	0.8	0.9	1.0
5	75.0	89.6	80.1	64.7	56.0	47.4	38.8	32.0	24.2	15.6	10.7
6	60.1	99.5	88.9	71.9	62.1	52.6	43.1	35.5	26.9	17.4	11.9
7	45.1	100	95.3	80.9	70.1	60.2	49.0	40.5	32.4	23.2	15.8
8	29.9	100.0	98.1	86.5	73.4	63.2	52.7	43.5	36.0	27.9	20.4
9	14.9	100.0	99.3	91.3	77.6	66.6	56.4	46.3	38.5	30.7	23.4
10	0.0	100.0	100	94.2	81.0	69.6	58.4	47.5	38.8	31.6	23.9

Figure 5.17 indicates that the smaller the threshold value is, the most accurate the system is. However, the rejection rate of the system should be considered to determine the optimal threshold value in order to avoid wrong rejection. Table 5.7 can be used to find the optimal threshold value for each case. In the experiment that used five trained classes, percentage of the untrained data is 75 %. It means the system with rejection mechanism could reject the output by a rejection rate around or less than this value. Therefore, threshold ranging 0.2 - 0.4 can be the optimal solution for this case. Similarly, if the same procedure is applied, the grey background in Table 5.7 presents the possible threshold values for different cases.

Looking back at Table 5.5 and Table 5.6, the data presented proves that the motion rejection in the myoelectric control improves the performance of the system. Figure 5.18 shows a detailed comparison between the two systems, RBF-ELM and RBF-ELM-R on the 10-classes experiment. The figure clearly indicates that RBF-ELM-R outperforms RBF-ELM on all subjects without exception. RBF-ELM attained accuracy of around 90 % while RBF-ELM-R is around 92 %. The superiority of RBF-ELM-R over RBF-ELM is more obvious when one-way ANOVA test is conducted on them. By setting p at 0.05, the p value is 0.034, which is less than 0.05. Therefore, the enhancement made by RBF-ELM-R is statistically significant.
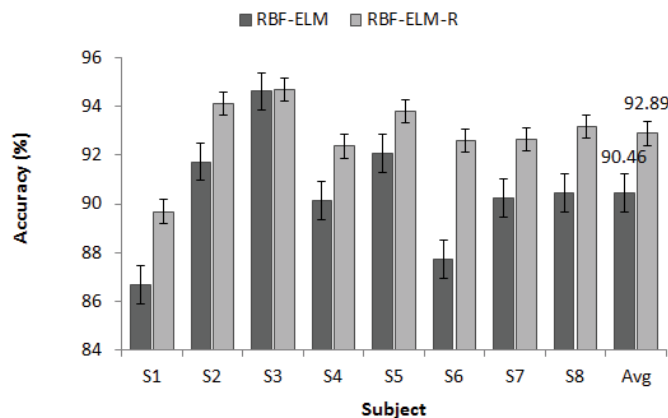
Figure 5.18 The accuracy achieved by RBF-ELM and RBF-ELM-R (threshold = 1.0) across 8 subjects suing 3-fold cross validation using majority vote

5.3.3.2 *Online experiment*

The result of the offline experiments concludes that the system with rejection mechanism could enhance the classification performance especially when the untrained movements are introduced in testing stage. The experiments in this section utilize the result of the real-time application to control the exoskeleton hand. In the online

experiment, an able-bodied user wore the exoskeleton hand on the left hand. On the right hand, there were two EMG sensor placed on the forearm, as shown in Figure 5.19.

Figure 5.19 exhibits the example of the real-time experiments on the exoskeleton hand on the healthy subject. The figure only provides six movements. In the experiment, ten movements were tested as well. To get a better understanding of the system, the reader could watch the videos regarding the experiment in this section online on YouTube. Here is the link to access those videos:

- https://www.youtube.com/watch?v=Bou7URGQQ_4 for 10-classes experiment
- https://www.youtube.com/watch?v=pPTft3SmtlM for 6-classes experiments
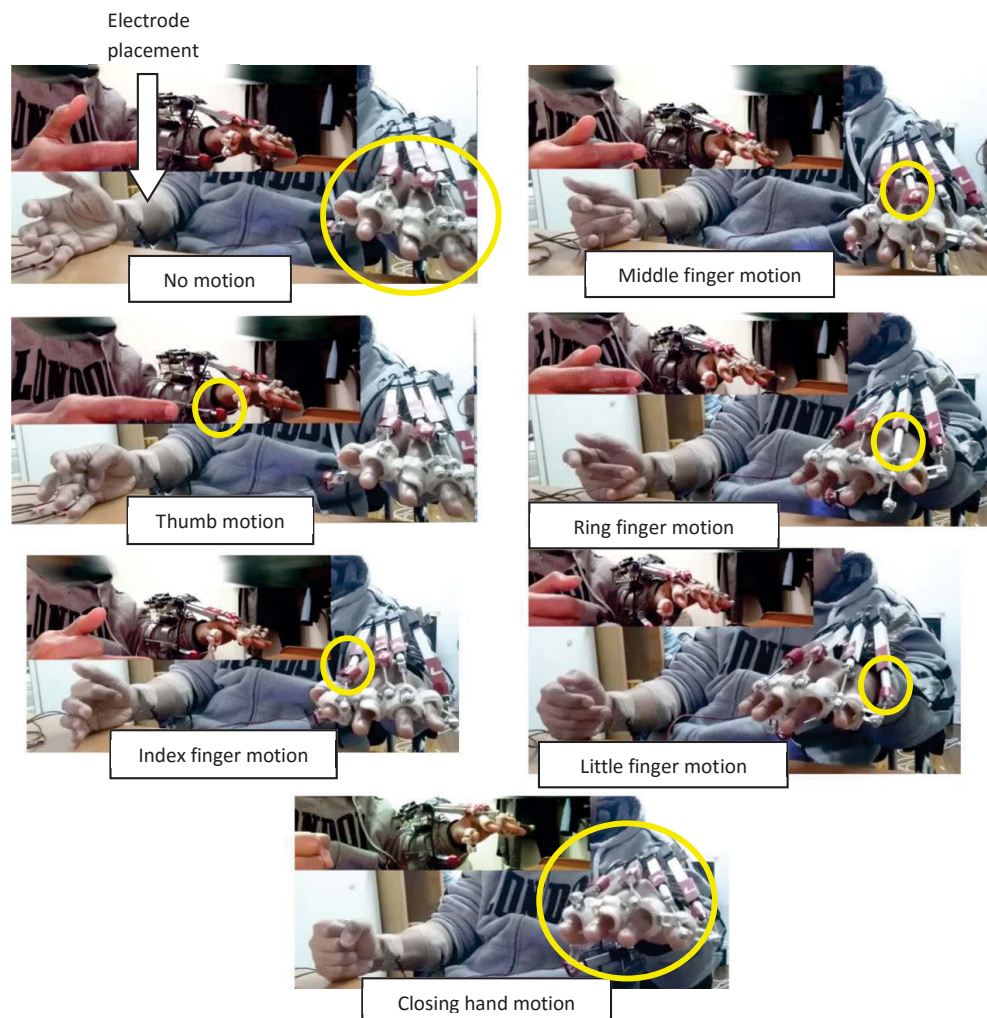
Figure 5.19 An example of online experiment on the implementation of myoelectric pattern recognition with motion rejection on the exoskeleton hand

In this experiment, the subject performed 10 subsequent movements from the thumb, index finger until the hand-close movement. The duration of each movement is 5 seconds

with a rest state in between lasting 5 seconds as well. The subject repeated the experiment four times. The performance of the system is presented in Table 5.8.

Table 5.8 The accuracy of the real-time experiment using 10 trained classes

Trials	Online accuracy (%)	
	RBF-ELM	RBF-ELM-R
1	89.06	90.46
2	89.45	89.75
3	90.23	90.06
4	88.15	88.64
Average	**89.22**	**89.73**

The experiment results in Table 5.8 show that the average accuracy of the real-time application across four trials is 89.22 % and 89.72 % using RBF-ELM and RBF-ELM-R, respectively. The timing diagram of an experiment is presented in Figure 5.20.
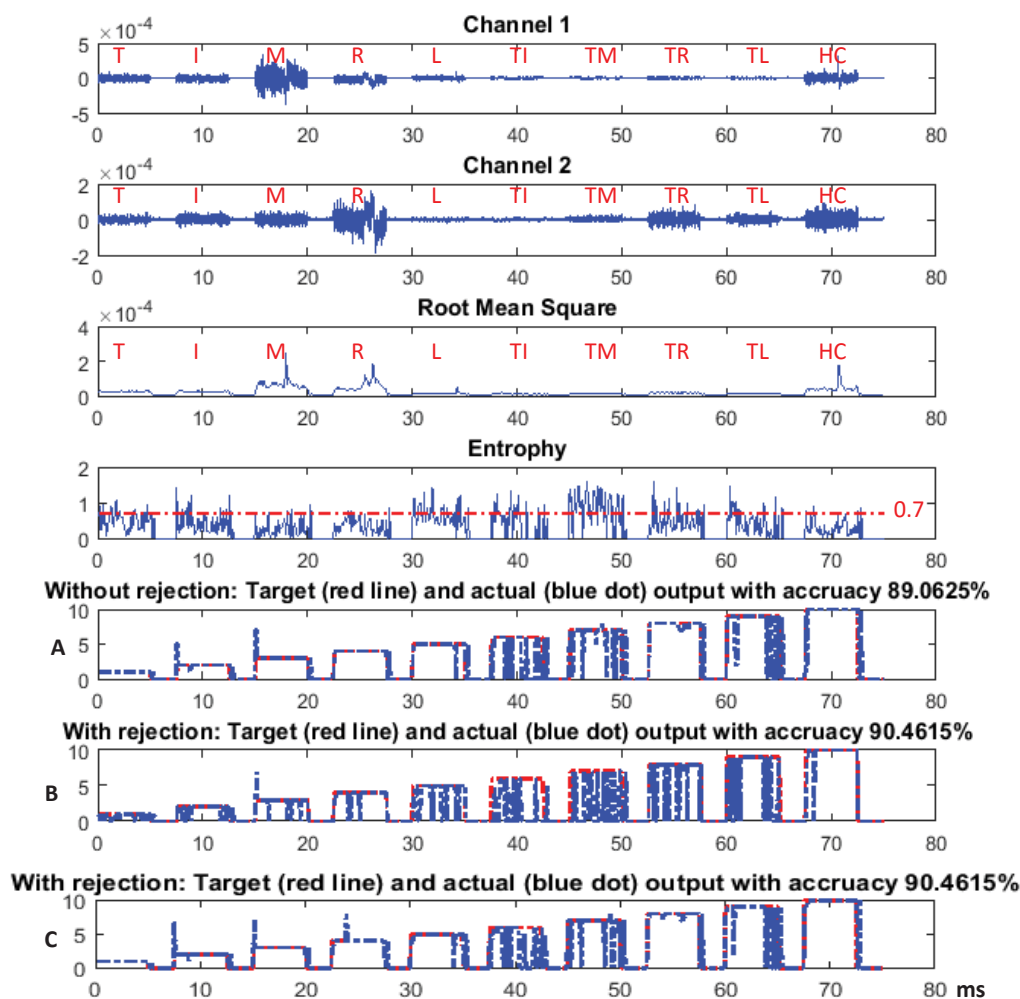
Figure 5.20 An example of real-time experiment over time using threshold 0.7 on 10-classes experiment

Figure 5.20 presents the outputs of myoelectric pattern recognition using three different scenarios. The first scenario is the output of RBF-ELM, the system that does not use the rejection mechanism. It is shown in the figure by the letter A. The second scenario is the output of RBF-ELM-R with rejection threshold 0.7. It is shown by the letter B in the figure. The last scenario, which is shown by the letter C, is the output of RBF-ELM-R with rejection threshold 0.7 but it employed different concepts of "no motion" from the previous RBF-ELM-R.

The rejection motion in RBF-ELM-R can be applied in two ways. Firstly, no motion means that the output of the system is the rest state. Therefore, whenever the system rejects a motion, the system forces the output to the rest state by neglecting the current movement. As a result, the output changes from one state to a rest state back and forth frequently, as shown in Figure 5.20 part B. This action will be inconvenient for the user.

The second implementation of "no motion" is that instead of the rest state, the output is the last movement produced before the implementation of the rejection mechanism. This scenario provides smoother output than the first scenario, as shown in Figure 5.20 part C. For this reason, the second scenario is a good choice for controlling the exoskeleton hand.

The advantage of the second scenario is also exhibited in Figure 5.21. Figure 5.21 describes the online experiments using five classes in the training. Then, in the online experiment, the system is tested with the data including the five classes in the training stage and the additional five classes that were not included in the training stage. The figure shows that the second scenario, that considers "no motion" as the previous movement instead of the rest state, exhibits reasonable performance for real-time application, as shown in Figure 5.21 part C. Part C of the figure is much smoother than part B.

However, there is a drawback when using "no motion" as the previous state. When the previous state is the wrong movement, then the "no motion" produces the wrong movement as well. For example, see Figure 5.21 part C, the thumb-middle finger movement (TM) is a motion that was not included in the training stage. When it is imposed on the system, the system outputs the L movement. In fact, the correct output should be no movement.

Regarding the accuracy of the experiment on five trained classes and untrained classes, Table 5.9 shows that the rejection mechanism could minimize the performance degradation of the real-time myoelectric pattern recognition (M-PR). The M-PR using

RBF-ELM-R could achieve the accuracy of about 80% while the one using RBF-ELM attained the accuracy of about 59 %.

Table 5.9 The accuracy of the real-time experiment using five trained classes and five untrained classes

Trials	Online accuracy (%)	
	RBF-ELM	**RBF-ELM-R**
1	59.38	82.01
2	60.55	79.07
3	60.29	81.45
4	58.33	78.35
Average	**59.64**	**80.22**
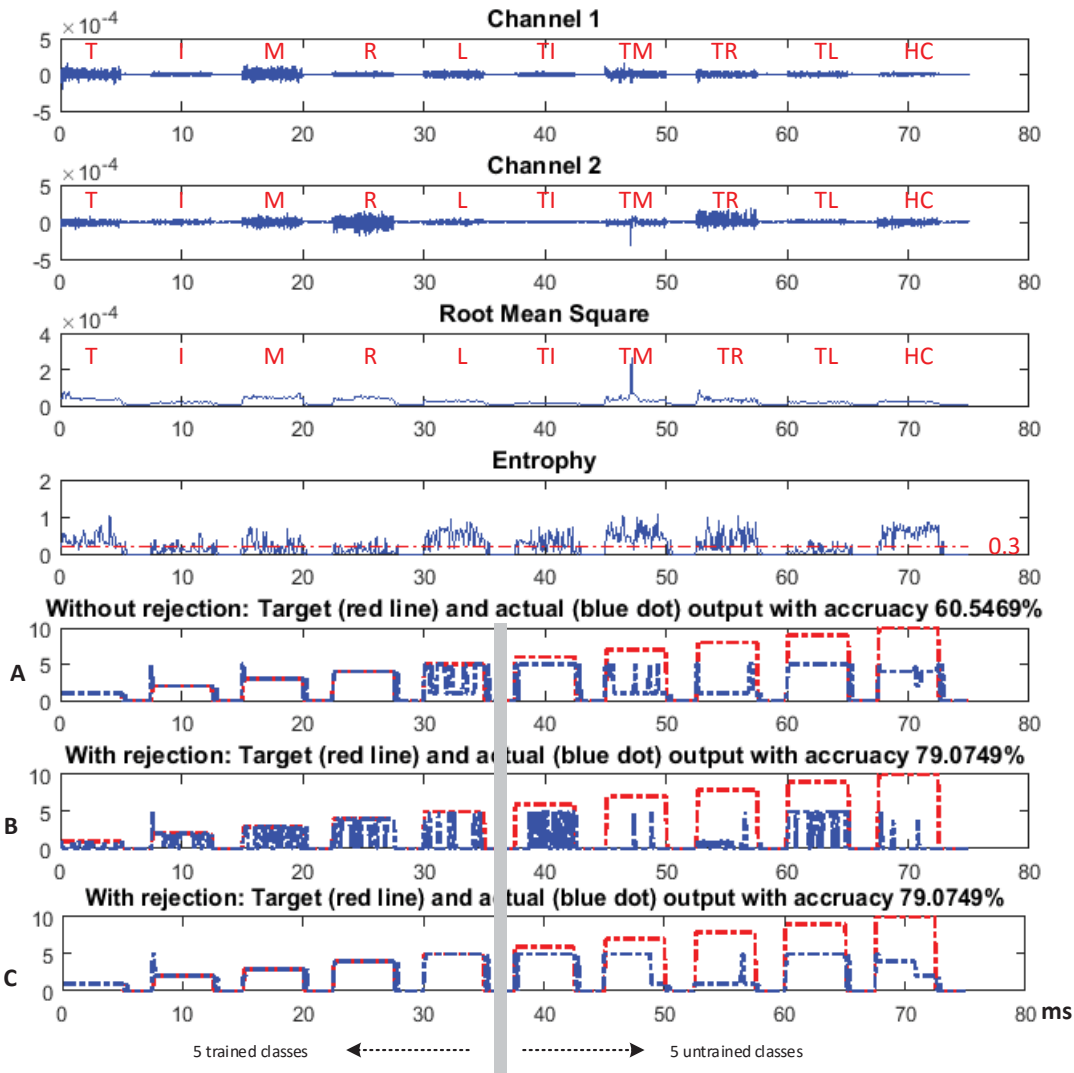
Figure 5.21 The real-time experiment results over time using threshold 0.3 using 5 trained classes and 5 untrained classes.

5.3.4 Conclusion

This section proposes myoelectric pattern recognition (M-PR) with motion rejection using radial basis function extreme leaning machine. In short, it is named RBF-ELM-R. The existence of the motion rejection mechanism improves the performance of the recognition system in both offline and online experiment. In the offline experiment of 10 classes, the accuracy is around 90 % and 92 % for RBF-ELM and RBF-ELM-R, respectively. In the online experiment, the accuracy is about 89.22 % and 89.73 % for RBF-ELM and RBF-ELM-R, respectively.

The efficacy of RBF-ELM-R is more noticeable if the classes that are not included in the training stage are involved in the test stage. In the online experiment, when using five classes in the training stage and then in the testing stage, another five classes are involved, the accuracy is about 59 % and 80 % for RBF-ELM and RBF-ELM-R, respectively. In addition, the implementation of RBF-ELM-R in the exoskeleton hand system shows its efficacy in the real-time application.

Nevertheless, the efficacy of the proposed system should be tested in day-to-day application. The users do not use a hand rehabilitation device once; often they employ it for days as long as they need it. Therefore, such a promising system should be able to overcome many issues regarding daily uses. The next section will discuss this issue.

5.4 Evaluation of online sequential extreme learning (OS-ELM-R) for robust myoelectric finger recognition

The rejection mechanism in myoelectric pattern recognition improves the robustness of the system. Another robustness issue emerges when implementing the hand rehabilitation device for longer time use. The performance will decrease due to changes in the EMG characteristic. This section proposes the way to adapt to these changes. The first section will discuss the introduction. The methodology will come next. The experimental results will be presented to describe the efficacy of the proposed system. Finally, the conclusion will end this section.

5.4.1 Introduction

For daily use, myoelectric pattern recognition should be able to deal with all situations that are possibly faced in the future, such as electrode shift and improvement in the muscle activity after several training sessions. Young et al. (Young *et al.*, 2012) found that a 2

cm-electrode shift can increase classification errors up to 25 – 30 % of eight EMG channels. They suggested tight procedures so as to design a robust myoelectric pattern recognition system. Of course, such procedures, somehow, are not comfortable and not convenient for people, the therapist and the patient.

Such problems can also be solved by incorporating all data that involve all conditions possibly faced in the training session. However, this idea results in a cumbersome training process and will not be convenient for users (R N Khushaba *et al.*, 2014). Moreover, all conditions cannot be covered in the beginning due to variation of the user's pattern over time. The variations can be influenced by the muscle fatigue, humidity, electrode displacement, and other potential causes.

To anticipate such variation, Nishikawa *et al.* (Nishikawa *et al.*, 2000) proposed supervised adaptation technique using a feed-forward neural network. In the proposed method, the new data is appended to the training data according to the user's intention. Furthermore, the method could also eliminate the redundant or harmful data. A similar approach to Nishikawa's work has been proposed by Chen *et al.* (Chen *et al.*, 2013) who developed self-enhanced linear and quadratic discriminant analysis (SLDA and SQDA). These methods retrain the classifiers using testing data in addition to training data. Interestingly, the methods use predicted labels/classes to adjust the classifier's internal parameters. In other words, adaptation is conducted in an unsupervised manner.

Sensinger *et al.* (Sensinger *et al.*, 2009) suggested that the supervised adaptation mechanism should be considered to be applied in a clinically feasible pattern recognition system. Following the suggestion, Gijsberts *et al.* (Gijsberts *et al.*, 2014) occasionally retrain the classifier using a modest amount of training data, instead of adding new data to original data. Different from previous researchers who employed batch learning classifiers, they utilized incremental learning classifier called incremental ridge regression with random Fourier features (iRFFRR). iRFFRR is a combination of incremental ridge regression and random Fourier features, which is an approximation of the Gaussian kernel machine. The main issue of a kernel machine is in the processing speed which is slow especially for large data.

This thesis proposes a new supervised adaptation mechanism using an online sequential extreme learning machine (Liang *et al.*, 2006) with motion rejection as the classifier. This new online classifier is called OS-ELM-R. The adaptation is conducted manually by the user or the therapist at the beginning of a new session using a small

number of a new training data. A new session means a session that has different experimental setups from the previous one. Briefly, the proposed method combines the ideas of Nishikawa and Gijsberts. The proposed method will be applied to the finger classification problems. Interestingly, the number of channels used is only two.

5.4.2 Methodology

5.4.2.1 Online sequential extreme learning machine (OS-ELM)

Online sequential extreme learning machine (OS-ELM) is formed on the basis of ELM. In ELM, for N arbitrary distinct samples $\{(x_i, t_i)\}_{i=1}^{N} \in \mathbf{R^n} \times \mathbf{R}^m$, the output of a single hidden layer feed-forward network (SLFN) with L hidden nodes is:

$$f(x_i) = \sum_{j=1}^{L} \beta_j G(a_j, b_j, x_i) = \mathbf{h}(\mathbf{x}_i)\boldsymbol{\beta} = t_i, \qquad i = 1, .. N \qquad 5.2$$

where f is an output of ELM, G is a hidden layer output, $\mathbf{h}(\mathbf{x}_i) \in \mathrm{R}^{NxL}$ is a matrix of hidden layer output and $\boldsymbol{\beta} \in R^{Lxm}$ is a matrix of output weight.

OS-ELM consists of two phases, an initialization phase and a sequential phase. In the initialization phase, a small chunk of training data $\{(x_i, t_i)\}_{i=1}^{N_0}$ is taken from the whole training dataset. In addition, $N_0 \geq L$.

INITIALIZATION LEARNING PHASE

The procedures in this phase are as follows:

1. Assign the hidden node parameters, such as weight a and bias b, randomly.
2. Calculate the initial hidden layer output matrix $\mathbf{H}_0$.

$$\mathbf{H}_0 = \begin{bmatrix} G(a_1, b_1, x_1) & \cdots & G(a_L, b_L, x_1) \\ \vdots & \cdots & \vdots \\ G(a_1, b_1, x_{N_0}) & \cdots & G(a_L, b_L, x_{N_0}) \end{bmatrix} \qquad 5.3$$

3. Calculate the initial output weight $\boldsymbol{\beta}^{(0)}$
4. Using the target $\mathbf{T}_0 = \begin{bmatrix} t_1, \dots, t_{N_0} \end{bmatrix}^{\mathrm{T}}_{N_0 xm}$, the goal of ELM is to minimize:

$$\|\mathbf{H}_0\boldsymbol{\beta} - \mathbf{T}_0\| \qquad 5.4$$

The solution is

$$\boldsymbol{\beta}^{(0)} = \mathbf{M}_0\mathbf{H}_0^{\mathrm{T}}\mathbf{T}_0 \qquad 5.5$$

where

$$\mathbf{M}_0 = (\mathbf{H}_0^{\mathrm{T}}\mathbf{H}_0)^{-1} \qquad 5.6$$

and

$$\mathbf{K}_0 = \mathbf{H}_0^{\mathrm{T}}\mathbf{H}_0 = \mathbf{M}_0^{-1} \qquad 5.7$$

This phase is set as k=0 as the initial sequent.

SEQUENTIAL LEARNING PHASE

The second phase is the sequential learning phase. A new observation for (k+1)th chunk of data will involve:

$$N_{k+1} = \left\{ \left(\mathbf{x}_i, \mathbf{t}_i \right) \right\}_{i=\left(\sum_{j=0}^{k} N_j \right)+1}^{\sum_{j=0}^{k+1} N_j} \tag{5.8}$$

Procedures involved in this phase are as follows.

1. Calculate the output matrix of the partial hidden layer $\mathbf{H}_{k+1}$.

$$\mathbf{H}_{k+1} = \begin{bmatrix} G\left(a_1, b_1, x_{\left(\sum_{j=0}^{k} N_j\right)+1}\right) & \cdots & G\left(a_L, b_L, x_{\left(\sum_{j=0}^{k} N_j\right)+1}\right) \\ \vdots & \cdots & \vdots \\ G\left(a_1, b_1, x_{\sum_{j=0}^{k+1} N_j}\right) & \cdots & G\left(a_L, b_L, x_{\sum_{j=0}^{k+1} N_j}\right) \end{bmatrix}_{N_{k+1} \text{x} L} \tag{5.9}$$

2. Compute the output weight

The target is:

$$\mathbf{T}_{k+1} = \begin{bmatrix} \mathbf{t}_{\left(\sum_{j=0}^{k} N_j\right)+1} & ,...., & \mathbf{t}_{\sum_{j=0}^{k+1} N_j} \end{bmatrix}^{T}_{N_{k+1} \text{x} m} \tag{5.10}$$

$$\mathbf{K}_{k+1} = \mathbf{K}_k + \mathbf{H}_{k+1}^{T} \mathbf{H}_{k+1} \tag{5.11}$$

$$\boldsymbol{\beta}^{(k+1)} = \boldsymbol{\beta}^{(k)} + \mathbf{K}_{k+1}^{-1} \mathbf{H}_{k+1}^{T} \left(\mathbf{T}_{k+1} - \mathbf{H}_{k+1} \boldsymbol{\beta}^{(k)} \right) \tag{5.12}$$

The inverse of K_{k+1}^{-1} should be avoided in the recursive process.

$$\begin{aligned} \mathbf{K}_{k+1}^{-1} &= \left(\mathbf{K}_k + \mathbf{H}_{k+1}^{T} \mathbf{H}_{k+1} \right)^{-1} \\ &= \mathbf{K}^{-1} - \mathbf{K}^{-1} \mathbf{H}_{k+1}^{T} \left(\mathbf{I} + \mathbf{H}_{k+1} \mathbf{K}_k^{-1} \right)^{-1} \mathbf{H}_{k+1} \mathbf{K}_k^{-1} \end{aligned} \tag{5.13}$$

And

$$\mathbf{M}_{k+1} = \mathbf{K}_{k+1}^{-1} \tag{5.14}$$

So, 5.14 can be modified by:

$$\mathbf{M}_{k+1} = \mathbf{M}_k - \mathbf{M}_k \mathbf{H}_{k+1}^{T} \left(\mathbf{I} + \mathbf{H}_{k+1} \mathbf{M}_k \mathbf{H}_{k+1}^{T} \right)^{-1} \mathbf{H}_{k+1} \mathbf{M}_k \tag{5.15}$$

$$\boldsymbol{\beta}^{(k+1)} = \boldsymbol{\beta}^{(k)} + \mathbf{M}_{k+1} \mathbf{H}_{k+1}^{T} \left(\mathbf{T}_{k+1} - \mathbf{H}_{k+1} \boldsymbol{\beta}^{(k)} \right) \tag{5.16}$$

Set k=k+1 and go to (a) in this phase.

5.4.2.2 Online sequential extreme learning machine with motion rejection (OS-ELM-R) for real-time application

OS-ELM consists of two main stages: an initialization phase and sequential leaning phase. These two steps are conducted during the offline classification. OS-ELM differs from all previous classifiers that are used in this thesis in the way data treated and passed to the classifiers. In OS-ELM, data is presented block by block, so the training stage is conducted in a sequential manner. In addition, OS-ELM can be trained using small number of data. New data can be imposed to the OS-ELM whenever data is available. The M-PR system can take benefit from this way of learning by conducting sequential learning phase before doing the online classification using small number of data. This thesis injects the rejection mechanism to OS-ELM. It is named OS-ELM-R. The implementation of OS-ELM-R in the online classification is shown in Figure 5.22. As a note, the experiments employed SRDA instead of SR-ELM for feature projection due to the quick processing time of SRDA.

5.4.2.3 Experimental procedure

In this section, the experiment consists of three stages. They are the offline, adaptation and online experiment. In the **offline stage**, the experiments is conducted to investigate the optimal OS-ELM by finding the optimal number of the hidden layer unit. Then, the performance of the optimal OS-ELM to classify the finger movements in various numbers of classes was observed. Finally, the comparison of the performance of OS-ELM with other well-known classifiers is presented. In the offline experiment, the EMG signals collected in section **5.2.2.1** were employed. The data collected from eight normal subjects consists of ten finger movements.

The next stage is an **adaptation stage**. The adaptation stage is performed before doing real-classification when the environment of the experiment changes. For instance, when the electrode position has changed or when the real-time experiment is done in different days of the offline classification. The adaptation stage needs a small number of new data from the current situation.

The last stage is the **online stage** or real-time implementation. The online stage can be done anytime by calling up the trained system produced in the adaptation stage. The procedure of the online classification is shown Figure 5.22. The process of online classification is similar to the online classification in section 5.3.2. The difference is on the use of OS-ELM-R instead of using RBF-ELM-R.
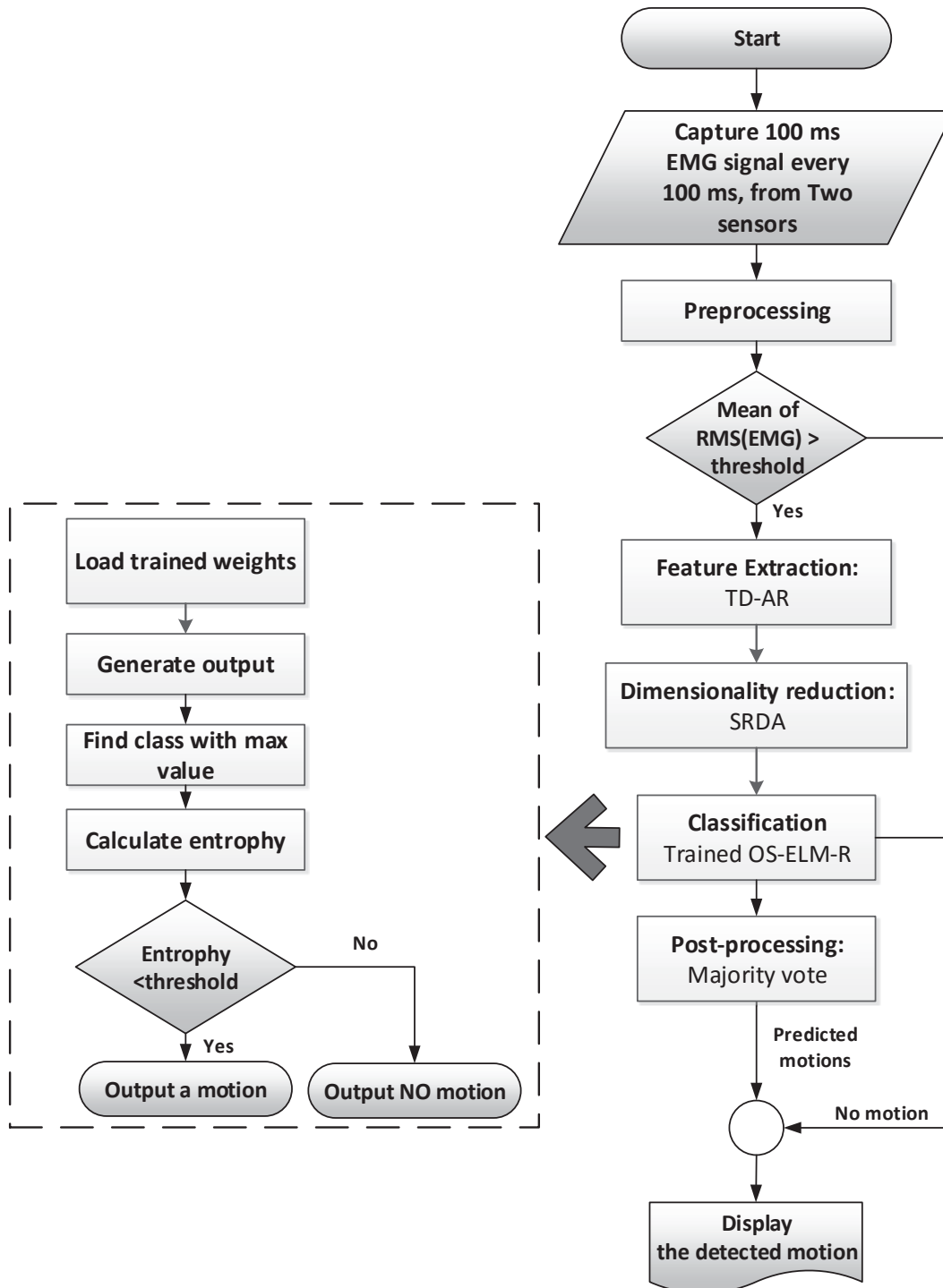
Figure 5.22 Online myoelectric pattern recognition for finger motion recognition using OSELM-R

5.4.3 Experiments and results

5.4.3.1 Offline experiment

This section investigates the reliability of OS-ELM for recognizing finger movement using two EMG channels. The components of the myoelectric pattern recognition (M-PR) in the offline experiment are completely the same as those in previous experiments,

as provided in **section 5.2.2**. The offline experiment was performed using 3-fold cross validation. The experiment was started by finding the optimal number of hidden layer unit in OS-ELM.

The precise method that can be used to determine the optimum number of the hidden node is hard to get except trial-and-error method. Therefore, in this experiment, the number of hidden nodes was varied from 50 to 150. Figure 5.23 provides the result. The figure indicates that the hidden node numbers less than 110 produce smaller errors than the numbers above it. Besides, the smallest error was achieved when the number of the hidden nodes is 110. Therefore, 110 is selected as the optimum number of the hidden node.
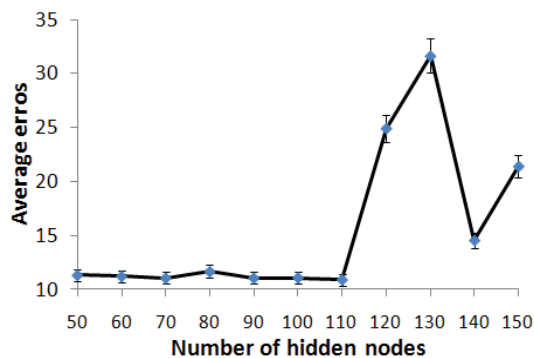
Figure 5.23 Average errors on the node experiments across eight subjects using 3-fold validation

Another offline experiment conducted in this section is an experiment to investigate the performances of the OS-ELM in the myoelectric pattern recognition using different class numbers. The result depicted in Figure 5.24 shows that the system employing OS-ELM can work across different classes. Interestingly, the fewer class number does not guarantee good accuracy. As can be seen in Figure 5.24, nine and ten classes perform better than six up to eight classes do.
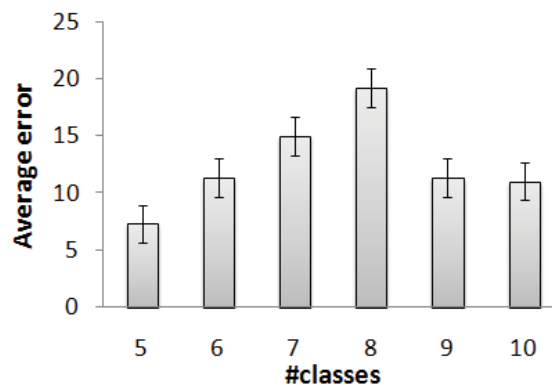
Figure 5.24 Average errors on the class number experiments across eight subjects using 3-fold validation

To understand and evaluate the real performance of OS-ELM in the M-PR for finger motion recognition, this section compares the performance of OS-ELM with other classifiers such as SVM (support vector machine), RBF-ELM (radial basis function ELM) and AW-ELM (adaptive wavelet ELM). Figure 5.25 presents the experimental result. The figure indicates that the performance of OS-ELM is comparable to other tested classifiers across eight subjects. All classifiers achieved similar accuracy around 89 % except RBF-ELM that attained around 90 %. The one-way ANOVA showed the $p = 0.984$. If the confident level is set at $p = 0.05$, then the performance difference among classifiers are not significant. Hence, the incremental method used in OS-ELM does not affect its performance.
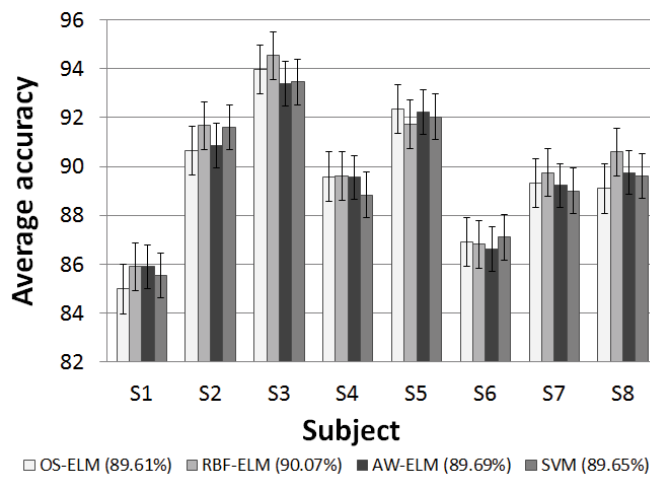
Figure 5.25 The overall performance of the OS-ELM compared with other classifiers across eight subjects using 3-fold cross validation

The last offline experiment is an experiment to investigate the efficacy of motion rejection in OS-ELM. In other words, the performance of OS-ELM is compared to OS-ELM-R to investigate the influence the rejection mechanism in the performance of OS-ELM. The results are presented in Figure 5.26 and Table 5.10.

Figure 5.26 presents the accuracy (TOP) and rejection rate (BOTTOM) of M-PR with different threshold values. The figure shows that the accuracy decreases along with the increasing of the threshold. In other words, a small threshold value exhibits better performance than higher threshold. However, the threshold value that is very small could reject too many data. For example, Figure 5.26 (BOTTOM) presents the rejection rate of the 10-classes experiment for threshold less than 0.6, which is 100 %. It means the system rejects all data used in the experiment, so the system does not produce any output (not applicable). Therefore, the selection of threshold value is not trivial. However, Figure

5.26 (bottom) indicates that the threshold values more than 1 are a possible solution for various cases.
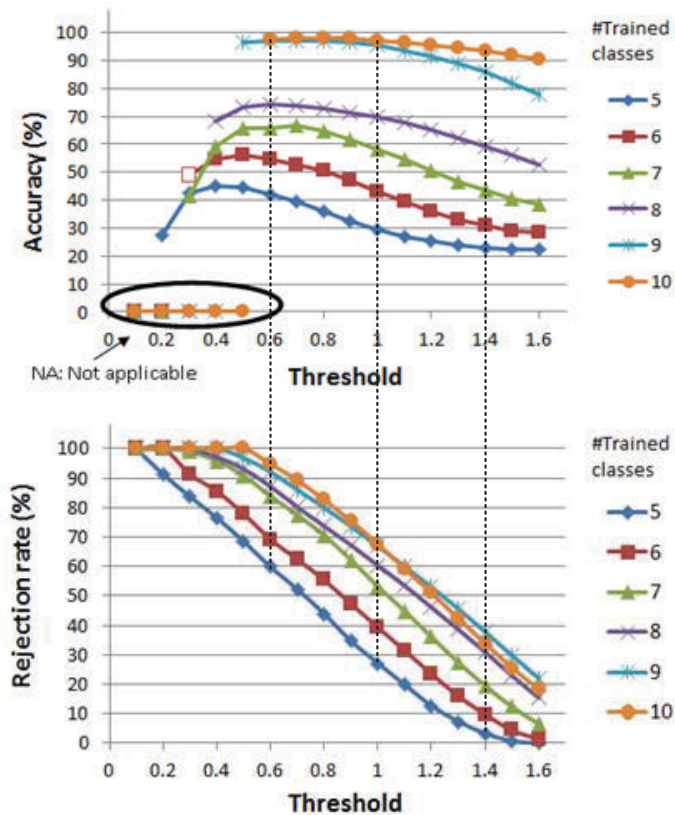
Figure 5.26 The performance of the M-PR with rejection using 3-fold cross validation without a majority vote: the accuracy (TOP) and the rejection rate (BOTTOM)

In addition to the threshold selection, the comparison between the system with and without motion rejection is discussed as well, as shown in Table 5.10. Table 5.10 exhibits the improvement of the rejection mechanism in the myoelectric pattern recognition. In the case of 10-classes experiment, the rejection mechanism could improve the accuracy from around 86% to around 91 % and around 89% to around 92 % without the majority vote and with the majority vote, respectively. Another interesting fact in Table 5.10 is related to the efficacy of the majority vote when the rejection mechanism is employed. The existence of the majority vote is not significant. This results support the fact that occurred in Table 5.5 and Table 5.6. The majority vote does not give a significant improvement on the system with the rejection mechanism, even it reduces the performance of the system. However, in this section, the system with the majority vote is better than the system without a majority vote. Maybe, the type of classifier is the cause of this contradictory results. The prior system employed the batch classifier while the later utilized the sequential classifier.

Table 5.10 The comparison of OS-ELM with and without rejection rate using 3-fold cross validation across eight subjects

#trained class	Rejection rate (%)	Accuracy without Majority vote (%)		Accuracy with Majority vote (%)	
		Threshold 1.6	No rejection	Threshold 1.6	No rejection
5	0.05	21.92	21.91	22.05	22.04
6	1.39	29.24	28.73	29.58	29.11
7	6.52	41.69	39.38	42.24	40.03
8	15.40	56.87	50.81	57.48	51.93
9	21.98	78.64	65.46	79.46	67.67
10	18.34	91.89	86.12	92.33	89.69

5.4.3.2   *Online experiment*

5.4.3.2.1   The first day experiment

After doing the offline experiments, eventually, the optimum parameters for the online classification are obtained. The hidden node number is 100 and threshold value is 1.7. In the online experiment, the work tested the M-PR system on three different days. In the first day, data acquisition is collected from a subject. Afterward, the offline classification employs the collected data to train the OS-ELM and RBF-ELM. The experiment involved only two classifiers because both classifiers represent different data representation. The former utilizes a chunk-by-chunk style while the later employs the batch style. The subject performed four trials for each movement and took a rest for 5 s between two movements. Figure 5.27 depicts the results.
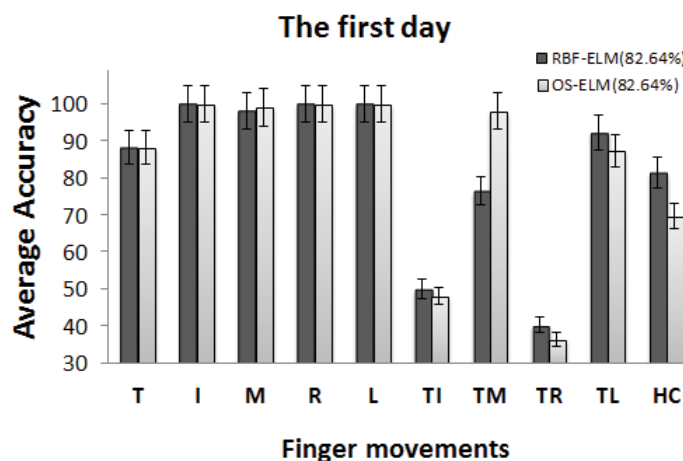
Figure 5.27 The classification results of M-PR using OS-ELM and RBF-ELM

Figure 5.27 shows that, on the first day of data collection, OS-ELM and RBF-ELM exhibit the same average accuracy, which is about 82.64%. However, the accuracy for each movement is not the same. OS-ELM is as good as RBF-ELM in recognizing the

178

individual movements (T, I, M, R, L). As for the combined finger movements, OS-ELM outperformed RBF-ELM on the thumb-middle finger movements. For the other movements, RBF-ELM outperformed OS-ELM. In general, the M-PR system using incremental method such as OS-ELM is comparable to batch method.

Next, the discussion of the performance of the M-PR using OS-ELM and OS-ELM-R over time is presented, as shown in Figure 5.28. The experimental procedure for the result in Figure 5.28 is different from Figure 5.27. The result in Figure 5.28 involved a rest state and the rest state became part of a movement that should be recognized using the threshold value in the RMS. Meanwhile, the rest state was not involved in Figure 5.27. As seen in Figure 5.28, the figure provides the fact that OS-ELM-R outperforms OS-ELM by accuracy of 89.32 % and 91.19 %, respectively. Furthermore, both systems had a difficulty to differentiate the rest state and the R movement because the RMS value of it is similar to the RMS value of the rest.
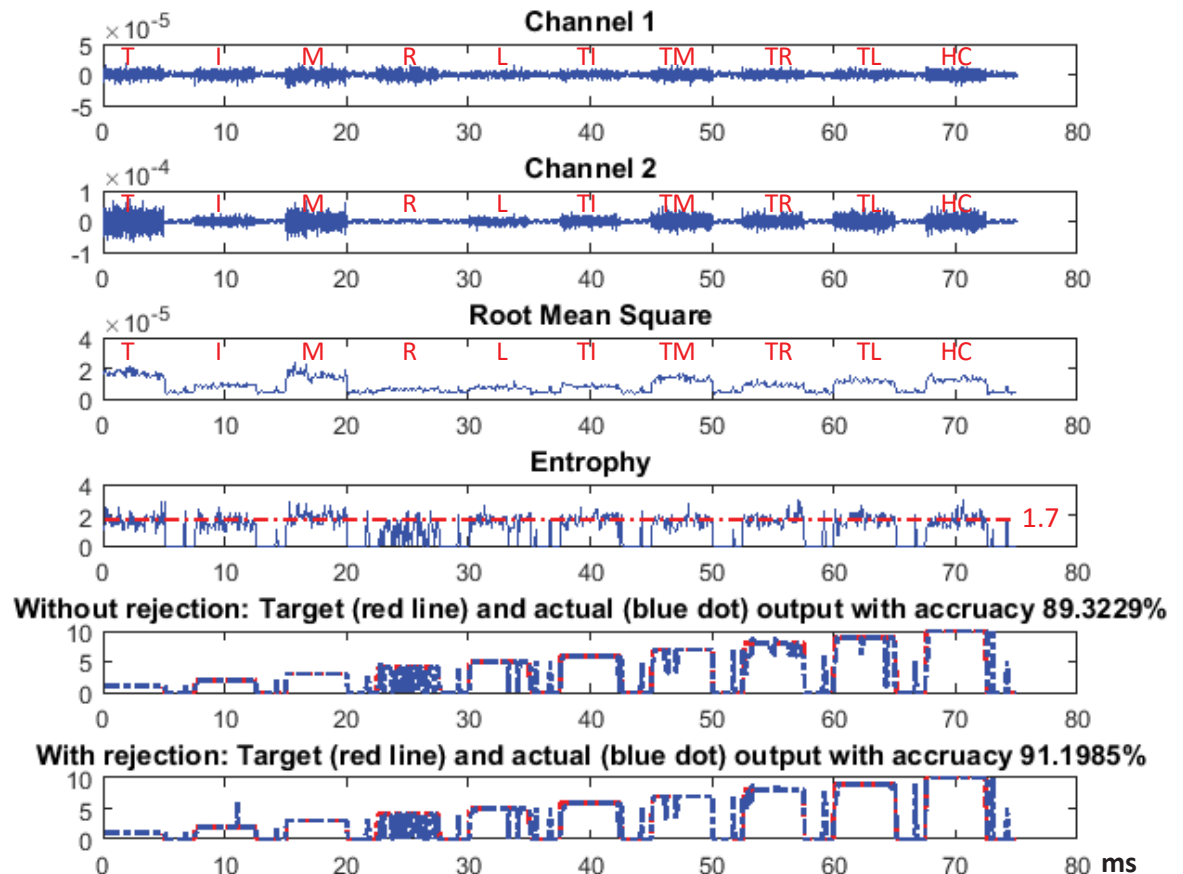
Figure 5.28 Online classification of OS-ELM and OS-ELM-R for recognition of 10 finger motions on one subject on one trial

179

5.4.3.2.2   Daily basis experiments

The primary benefit of utilizing OS-ELM is to provide an adaptation mechanism to deal with problems appearing in the daily uses. For that aim, the thesis investigates the performance of the proposed system on the different days from the offline classification. The results are presented in Figure 5.29.
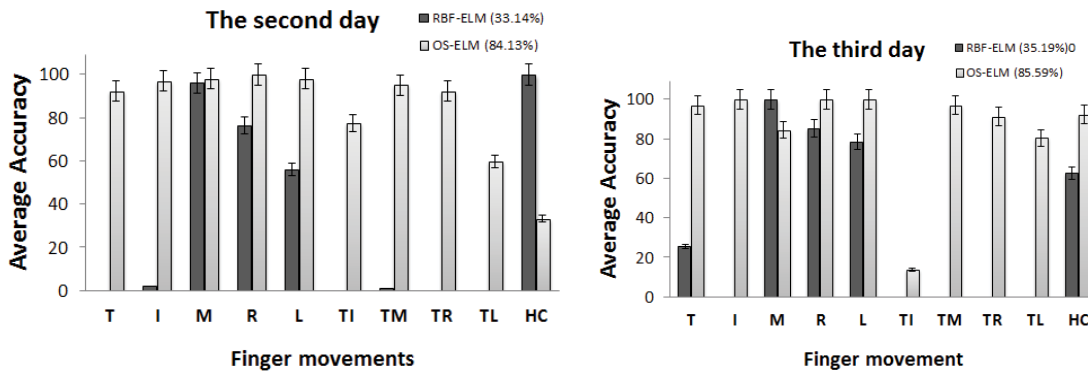
Figure 5.29 Daily classification performance of OS-ELM and RBF-ELM

In the previous discussion, it has been concluded that, on the first day (see the Figure 5.27), the system with OS-ELM and RBF-ELM has the same performance. Both systems achieved accuracy around 82 %. Figure 5.29 presents the comparison of both systems on the second and third days. On the second day, the system with OS-ELM achieved better accuracy than the day before, while RBF-ELM attained accuracy that is worse than the day before. Similar phenomena occurred on the third day. These facts indicate that the pattern recognition with OS-ELM has stable performance. The adaptation mechanism of OS-ELM helps M-PR to adapt to the new environment.

The complete classification that involves the rest state into consideration is presented in Figure 5.30 and Figure 5.31. The last and second last rows describe the output of OS-ELM-R and OS-ELM, respectively. If Figure 5.28 representing the first-day experiment is compared to Figure 5.30 representing the second day experiment, then it is found that the performance of OS-ELM increases. Again, the experiment result on the third-day shows another improvement, as in Figure 5.31. The output of the third day is smoother than the previous days. In summary, the OS-ELM or OS-ELM-R benefits the myoelectric pattern recognition (M-PR) and improves the stability of (M-PR).
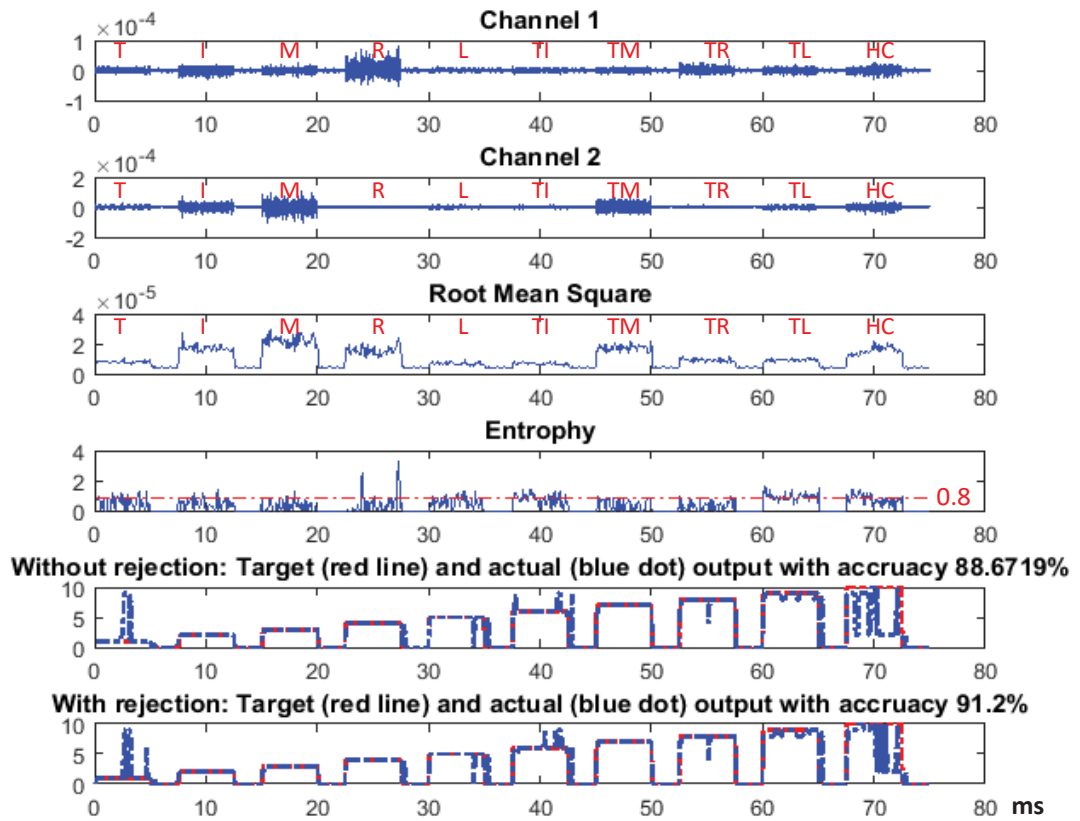
Figure 5.30 An example of online classification result of OS-ELM and OS-ELM-R in reconizing 10 finger motions for the second day
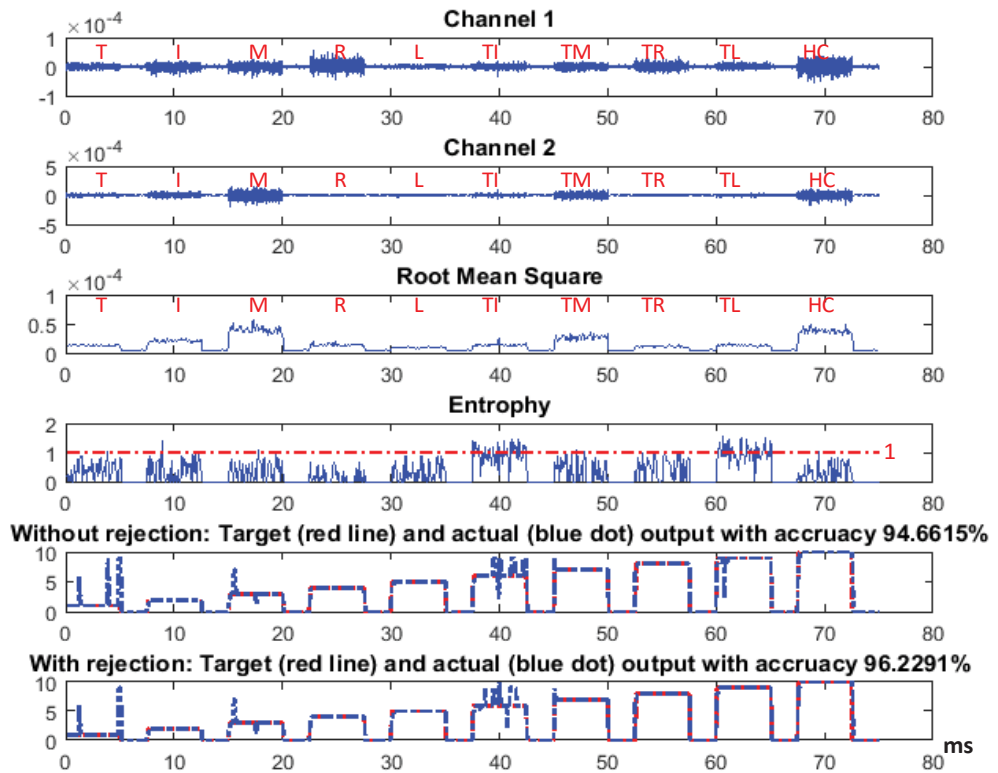
Figure 5.31 An example of online classification result of OS-ELM and OS-ELM-R in reconizing 10 finger motions for the third day

181

5.4.4   Conclusion

This thesis aims to develop myoelectric pattern recognition (M-PR) that is robust and can work over time for long term usage. The mechanism adaptation of OS-ELM enables M-PR to adapt to the changes that possibly occur during long usage of the EMG-based hand rehabilitation device. The thesis also developed OS-ELM with rejection mechanism named OS-ELM-R. The comparison of OS-ELM and RBF-ELM across different day experiments show that the adaptation mechanism improves the robustness of the system. The M-PR with OS-ELM has stable performance, and even the accuracy is improved. The average accuracy is around 82%, 84% and 85 % on the first, second and third days, respectively. Meanwhile, the performance of the M-PR with RBF-ELM decreased across three different days. The average accuracy is about 82 %, 33% and 35 % on the first, second and third days, respectively.

Furthermore, the rejection mechanism improves the robustness of the M-PR because it can anticipate the existence of the untrained movement in the clinical application. The experimental results, offline and online prove the efficacy of the rejection mechanism in the myoelectric finger motion recognition. In the offline experiment for the 10-class experiment, the accuracy is 81 and 90 % for OS-ELM and OS-ELM-R. In the online experiment, the accuracy is around 89 % and 91 % for OS-ELM and OS-ELM-R on the first-day experiment.

5.5   Summary

This chapter addresses the real-time application of myoelectric pattern recognition (M-PR) for finger movement detection. There are three different applications conducted. The first application is the online classification of M-PR for finger movement recognition, as discussed in **section 5.2**. The virtual hand simulation displayed on the screen of a personal computer was used to demonstrate the classification performance. The classification accuracy is 90.46 % and 89.19 % on the offline and online classification, respectively. Interestingly, the experiment included the transient state in which many researchers avoided because it can downgrade the classification performance. In fact, the transient state of EMG signals should be incorporated to enhance the robustness of the system.

Then, **section 5.3** addressed the implementation of the previous section on the exoskeleton hand robot. Not only that, a mechanism to reject the movement that is not involved in training session was also discussed. Again, the rejection mechanism improves

the robustness of the M-PR system. For long use, the M-PR system should deal with the changes that possibly exist in the environment such as electrode system, the improvement of muscle function. For that reason, the thesis proposed a new M-PR using OS-ELM in **section 5.4**. It is an incremental classifier that can be updated to the new situation using a small number of data. The experimental results showed that the M-PR with OS-ELM had stable performance over three different days and in addition, the performance had improved.

These experimental results provide optimism for implementation of the proposed system to be tested on the disabled person following a stroke. In this thesis, the proposed system was applied to an able-bodied subject. The proposed system consists of a control system that can recognize the intended finger movement of the patient. Based on this information, the control system will drive the corresponding finger exoskeleton and at the same time, the user's finger will be actuated. The advantage of the proposed system over the existing system is on the number of movements that can be dealt with. The system can move individual fingers while other cannot. Inevitably, this feature will improve the rehabilitation process of the disabled person.

This page is intentionally left blank

CHAPTER 6

Summary, conclusion and future research

In this chapter, the summary of this thesis and major finding of the research conducted in this thesis are given. Afterward, the future works following on from the research in the same field are described.

6.1 Thesis summary

The main aim of this research is to introduce novel myoelectric controllers for hand rehabilitation devices that can deal with problems occurring in real-time application. To achieve the main goal, this research has proposed various methods and algorithms, and examined them in real-time application.

In **Chapter 3**, novel myoelectric pattern recognition (M-PR) for finger motion recognition that can work well on amputees and non-amputees was proposed. Different feature extraction methods were examined. Furthermore, the experiments involved various methods and different components of M-PR. Three dimensionality reduction methods were incorporated including linear discriminant analysis (LDA), spectral regression discriminant analysis (SRDA), and orthogonal fuzzy neighbourhood discriminant analysis (OFNDA). The research has investigated different extreme learning machine algorithms including kernel-based ELM and node-based ELM. The kernel based ELM consists of radial basis function ELM (RBF-ELM), polynomial ELM (Poly-ELM) and linear ELM (Lin-ELM), while the node based ELM is composed of sigmoid ELM (Sig-ELM) and radial basis ELM (Rad-ELM). In addition, some well-knows classifiers were involved including support vector machine (SVM), linear discriminant analysis (LDA) and k-nearest neighbour (kNN).

Some possible configurations of those methods were investigated to find the optimal M-PR for finger motion recognition. The experimental results show that RBF-ELM along with TD-AR and SRDA achieved the best classification performance. The M-PR

achieved good accuracy in amputees and non-amputees with an accuracy of about 99 % and 98%, respectively, using six EMG channels. In addition, the experimental results using two EMG channels show that RBF-ELM achieves the highest accuracy on both subjects with an accuracy of 92.73 % across five amputees and of 97.11 % across nine able-bodied subjects. Therefore, the research has succeeded in developing a highly accurate M-PR for complex finger-motion recognitions using radial basis function ELM (RBF-ELM).

The first section of **Chapter 4** proposes a new ELM classifier named adaptive wavelet extreme learning machine (AW-ELM). Wavelet extreme learning machine (W-ELM) and AW-ELM are special types of wavelet neural network (WNN) that avoid iterative training to determine the weights. In W-ELM and AW-ELM, the weights of the hidden nodes are randomly determined, while the weights of the output are calculated analytically. For that reason, the training time of W-ELM and AW-ELM are very fast compared to WNN. AW-ELM differs from W-ELM in the wavelet activation function. In W-ELM, the wavelet shape does not change during the process. On the contrary, in AW-ELM, the wavelet shape changes according to the input characteristic. The mechanism of the changing of the wavelet shape enables AW-ELM to avoid the initialization stage that is needed in WNN or W-ELM, to set the wavelet shape in the range of input. The experimental results on myoelectric pattern recognition for finger motion classification using two EMG channels show that the improvement made by AW-ELM is significant. In addition, AW-ELM attained the accuracy of about 94 % and the result is comparable to other well-known classifiers such as RBF-ELM, SVM, LDA, and kNN. The experimental results on the UCI machine learning datasets indicate that AW-ELM could work on a wide range of datasets from small size to large size data and in general, the performance is comparable to other well-known classifiers.

In the second section of **Chapter 4**, the thesis presents a novel dimensionality reduction named spectral regression-extreme learning machine (SR-ELM) to improve the class separability of the features. To the best of the author's knowledge, SR-ELM is the first ELM for supervised dimensionality reduction. The experimental results on myoelectric finger motion classification show that SR-ELM + AW-ELM achieved accuracy from 98.64 % to 94.16 % for 5 to 10 motion classes. One-way ANOVA test showed that the performance of SR-ELM is comparable to ULDA (uncorrelated linear discriminant analysis) and OFNDA (orthogonal fuzzy neighbourhood discriminant

analysis), but it is better than SRDA (spectral regression discriminant analysis). The experimental results on UCI machine learning datasets showed that SR-ELM exhibits good performance when it works together with AW-ELM, LDA, and kNN. As for RBF-ELM and LIBSVM, the performance of SR-ELM is comparable to other methods.

The experimental results in Chapter 3 shows that ELM needs parameter optimizations to work optimally, especially in the kernel based ELM. For that purpose, in the second section of **Chapter 4**, a hybridization of particle swarm optimization (PSO) and the kernel based ELM was introduced. This hybridization resulted in three different classifiers: swarm radial basis ELM (SRBF-ELM), swarm polynomial ELM (SPoly-ELM) and swarm linear ELM (SLin-ELM). The experimental results show that SRBF-ELM and SPoly-ELM have similar performance. As for SRBF-ELM and SLin-ELM, SRBF-ELM is better than SLin-ELM. Interestingly, the performance of SPloy-ELM and SLin-ELM are not significantly different. The most accurate classifier is SBRF-ELM that attained an accuracy of 94.62 % across eight subjects using 3-fold cross validation. In addition, the experimental results show that there is a possibility of PSO becoming trapped on local optima.

The third section of **Chapter 4** presents the next experiment conducted in this thesis in relation to overcoming the likeliness of PSO to become trapped in local optima. Many attempts have been proposed to overcome the local optima issue in PSO. One of them is to mutate PSO using wavelet, as proposed by Ling *et. al.* (Ling *et al.*, 2008). Therefore, the thesis proposed swarm wavelet radial basis function (SW-RBF-ELM). In this experiment, fitness function was obtained from the average errors of the cross-validation results, which was different from the previous experiment in which fitness function was obtained from the error of each cross-validation. This new mechanism shortens the searching time of PSO. The experimental results showed that the accuracy of SRBF-ELM improved when using this new mechanism from 94.62 % to 95.54 %. As for SW-RBF-ELM, its performance was 95.62 % across eight subjects using 3-fold cross validation. The one-way ANOVA test result shows that improvement made by SW-RBF-ELM is not significant. However, the comparison of the fitness value of SBRF-ELM and SW-RBF-ELM indicated that the improvement made by SW-RBF-ELM is significant.

Chapter 5 provides some efforts to improve the robustness of the myoelectric pattern recognition (M-PR) in the real-time application. The second section of Chapter 5 presents the real-time application of myoelectric pattern recognition (M-PR). In the real-time

experiment, the M-PR considered the transient and steady state of the EMG signals. Majority researchers avoid the transient state in the experiment because it can downgrade the classification performance. However, including the transient state in the training stage will improve the robustness of M-PR in the real-time application. This thesis has proposed many methods to improve the performance of M-PR for finger motion classification. Nevertheless, this thesis employed the configuration of TD-AR for feature extraction, SRDA for feature projection and the optimized RBF-ELM for classifiers. The experimental results show that the M-PR could attain an accuracy of 90.46 % and 89.19 % on the offline and online classification, respectively. In the delay time, the M-PR took 261 ms to produce an output. This delay time is less than the acceptable delay time of myoelectric controller (300 ms).

In the third section of Chapter 5, the M-PR produced in the previous section was employed to control an exoskeleton hand. To improve the robustness of the M-PR, RBF-ELM was equipped with a rejection mechanism. The aim of this mechanism is to neglect any movement that is not included in the training stage. The offline classification results show that RBF-ELM with rejection mechanism (RBF-ELM-R) could attain an accuracy of around 94 % while RBF-ELM achieved around 90%. In addition, the M-PR with RBF-ELM-R along with proportional controller has succeeded in controlling an exoskeleton hand with an accuracy of 89.7 % on an able-bodied subject.

The last section of Chapter 5 proposed M-PR that has an adaptation mechanism to anticipate changes on EMG signal characteristic, especially for long use. The adaptation mechanism was performed by online sequential extreme learning machine (OS-ELM). OS-ELM enables M-PR to be updated using a small number of data. Therefore, before doing the online experiment, if the experimental environment has changed, a small number of data is collected and then used to retrain the M-PR. The experimental results show that, in day-to-day experiments, the M-PR with OS-ELM has more stable performance than that with RBF-ELM. For example, in one subject, OS-ELM could achieve an accuracy of around 82 % on the first day, around 84 on the second day and 85 % on the third day. On the contrary, RBF-ELM achieved the accuracy of around 82% on the first day, and the accuracy dropped to around 32 % and 35 % on the second and third day, respectively. These results exhibit the benefit of adaptation mechanism to enhance the robustness of M-PR in the real-time application.

The experimental results of M-PRs developed in this thesis are summarized in Table 6.1.

Table 6.1 The summary of the M-PR developed in this thesis

M-PR	#Ch	#Finger motion		#Subject	#Features	Dim. reduction+ Classifier	Avg. Accuracy (%)	Mode	Signal State
		Trained	**Un-trained**						
Chapter 3	6	12 Id and 3 Cm		9H	16	SRDA+ RBF-ELM	99.5	OF	Tr
	6	12 Id		5A	16	SRDA+ RBF-ELM	98.55	OF	Tr
Chapter 4	2	5 id and 5 Cm		8H	16	SRDA+ AW-ELM	94.84	OF	Tr
	2	5 id and 5 Cm		8H	16	SRDA+ RBF-ELM	94.59	OF	Tr
	2	5 id and 5 Cm		8H	16	SR-ELM+ AW-ELM	94.71	OF	Tr
	2	5 id and 5 Cm		8H	16	SR-ELM+ RBF-ELM	94.78	OF	Tr
	2	5 id and 5 Cm		8H	16	SRDA+ RBF-ELM	95.53	OF	Tr
	2	5 id and 5 Cm		8H	16	SRDA+ SW-RBF-ELM	95.62	OF	Tr
Chapter 5	2	5 id and 5 Cm		8H	16	SRDA+ RBF-ELM	90.46	OF	St + Tr
	2	5 id and 5 Cm		8H	16	SRDA+ RBF-ELM	89.19	OL	St + Tr
	2	5 id and 5 Cm		1H	16	SRDA+ RBF-ELM-R	92.89	OF	St + Tr
	2	5 id and 5 Cm		1H	16	SRDA+ RBF-ELM-R	89.73	OL	St + Tr
	2	5 id trained	5cm	1H	16	SRDA+ RBF-ELM	59.64	OL	St + Tr
	2	5 id trained	5cm	1H	16	SRDA+ RBF-ELM-R	80.22	OL	St + Tr
	2	5 id and 5 Cm		1H	16	SRDA+ OS-ELM	89.69	OL	St + Tr
	2	5 id and 5 Cm		1H	16	SRDA+ OS-ELM-R	92.33	OL	St + Tr
	2	5 id	5cm	1H	16	SRDA+ OS-ELM	22.04	OL	St + Tr
	2	5 id	5cm	1H	16	SRDA+ OS-ELM-R	22.05	OL	St + Tr

Ch = Number of channels, Id = Individual finger movements, Cm = Combined Finger movements, H = Healthy Subjects, A = Amputees, OF= Offline classification, OL = Online Classification, Tr = Trainsient state, St = Steady state

6.2   Recommendation for future research

The following issues are recommended for future research.

- Employing AW-ELM in the real-time experiment and introducing sequential learning of AW-ELM for adaptive myoelectric pattern recognition.

- In the real-time experiment, myoelectric pattern recognition (M-PR) employed two EMG channels and attained accuracy around 89 %. A few more EMG channels may be added to improve the performance in the real-time application.

- The delay time of the myoelectric controller is around 261 ms. It is less than the acceptable delay time (300 ms). However, it is more than the optimal delay time (175 ms for average users). In the future work, the delay time should be shortened to improve the comfort of the user,

- The efficacy of the myoelectric controller developed here should be investigated for broader users including able-bodied and paralyzed users.

- The exoskeleton hand used in this research does not have sensory feedback. For future research, any hand devices used in the experiment should have sensory feedback to improve the performance and the robustness of the myoelectric controller.

- The implementation of the proposed myoelectric controller on the hand prosthetic should be investigated as well.

- In this thesis, to update the M-PR for long use, the user should provide small data. It means that the data for updating M-PR should be provided. The reason is the M-PR should be retrained with the good data. In other words, M-PR could not select the data by itself. In the future research, a mechanism that can select and sort the good and the bad data should be developed. Therefore, the adaptation mechanism will be fully automated.

- The feature learning on EMG signals should be investigated to improve the performance of the myoelectric pattern recognition system.

- The classification accuracy or error have been used as the main metric to measure the efficacy of the M-PR in both laboratory environment and clinical application. In fact, in the clinical application, many parameters should be considered to measure the performance of the M-PR. In the future, this issue should be addressed to enhance the performance of the M-PR and finally

increase the acceptance rate of the usage of the rehabilitation device among the disabled people.

6.3   Conclusion

In this thesis, eight contributions were proposed including some new algorithms, novel myoelectric pattern recognition systems, and a novel myoelectric controller for an exoskeleton hand.

This thesis proposed some novel systems for finger motion recognitions. The first system is myoelectric pattern recognition (M-PR) system that could work well in amputee and non-amputees for complex finger-motion recognitions. The latest publication in this area [2] shows that for complex finger motion, there was a big performance gap of myoelectric pattern recognition on amputee and non-amputees. This research exhibits its contribution by proposing an M-PR system that works well in both subjects using a combination of time domain and autoregressive features (TD-AR), SRDA and RBF-ELM. The second M-PR is a real-time M-PR. The real-time M-PR developed in this thesis considers the transient state of the EMG signals. In many M-PRs, the transient state is avoided and removed. In fact, the inclusion of the transient state will increase the robustness of the real-time experiments even though it will decrease the accuracy of the M-PR. For the real-time application, robustness and accuracy should be considered.

The third M-PR system proposed is M-PR with motion rejection for real-time experiments. This M-PR employed RBF-ELM with motion rejection or RBF-ELM-R. This RBF-ELM-R increases the robustness of the M-PR. The fourth M-PR system proposed is the M-PR that can adapt to changes in the environment that affect the EMG signal characteristic. The main component that enables adaptation in the M-PR is online sequential extreme learning machine (OS-ELM). The efficacy of OS-ELM is very noticeable by empowering the M-PR to have an experimentally demonstrated stable performance over three different days.

Furthermore, **this thesis proposed four new algorithms** that are dealing with two electromyography (EMG) channels. The first two methods are to optimize the parameters of the kernel based ELM, which are swarm radial basis function extreme learning machine (SRBF-ELM) and swarm wavelet radial basis function extreme learning machine (SW-RBF-ELM). These two methods have been proven to be able to optimize kernel based ELMs. Another algorithm proposed in this thesis is adaptive wavelet

extreme learning machine (AW-ELM). AW-ELM is a classifier that can change the shape of the wavelet activation function according to the condition of the input. Compared to WNN, AW-ELM is faster, yet it has comparable performance to well-known classifiers such as SVM, LDA, and kNN. Compared to W-ELM, AW-ELM does not need an initialization to cover the range of input, as is needed in W-ELM. AW-ELM has been tested on the EMG dataset for myoelectric finger motion recognition. In addition, it has been tested on the UCI machine learning datasets. The experimental results indicate the benefit of AW-ELM.

Another algorithm regarding the feature projection or dimensionality reduction methods was also proposed. It is named spectral regression extreme learning machine (SR-ELM). SR-ELM is a novel extreme learning machine for supervised dimensionality reduction. The experimental results on EMG dataset for finger motion recognitions and UCI machine learning datasets show that SR-ELM could work on various applications with good performance.

The last contribution is a new myoelectric controller for exoskeleton hands. The literature informs that the majority of the exoskeleton hand employ EMG signal for simple motions such opening hand and closing hand. This thesis proposed a myoelectric controller that enables the exoskeleton hand to move the individual movement as well as the combined finger motions. The proposed myoelectric controller consists of M-PR plus proportional controller. The M-PR consists of TD-AR, SRDA, and RBF-ELM-R, while the proportional controller consists of a proportional controller for the linear motor of the hand. The experimental result shows the efficacy of the controller for controlling the exoskeleton hand by an accuracy of around 89 % from four trials on one subject.

Overall, all experiments conducted in this thesis have been presented in various high-quality conference and have been published online. This indicates that the contributions have been widely acknowledged internationally.

APPENDIX A: ETHICAL APPROVAL

UNIVERSITY OF TECHNOLOGY SYDNEY

UTS HUMAN RESEARCH ETHICS COMMITTEE

ANNUAL REPORT / EXTENSION REQUEST

This report is to be completed every twelve months following the date of ethics approval, and at the completion of your research project. To cross the check boxes, double click on the check box and tick checked (under default value). Type your responses into the box which expand to accommodate your answers. If you have any queries on how to complete this report, please contact the Research Ethics Officer (Ph.: 02/9514 9772).

Project Title:	**EMG Pattern Recognition**

UTS HREC Approval Number: 2009-181A

Current status of project: (Double click on box and mark 'checked')

☐ **Not yet commenced** (you have not commenced recruitment or data collection)	Estimated commencement date:
☒ **In Progress** (You have commenced research **or** have put the research on hold)	Estimated completion date: Dec 2017
☐ **Completed** (You have completed data collection and first stage analysis of data)	Approximate completion date:
☐ **Discontinued** (You have withdrawn **or** stopped the research due to insufficient or suspension of funding, **or** have stopped the research for another reason)	Approximate discontinued date:

Position	Name (include title)	Contact number	Email	Period of involvement
Chief Investigator/ Supervisor	Dr. Adel Al-Jumaily	X7939	Adel.Al-Jumaily@uts.edu.au	Since the beginning of project
Co-investigator	Dr. Ahmed Al-Ani	X2420	ahmed@eng.uts.edu.au	Since the beginning of project
(Student)	Mr. Khairul Anam	7143		Starting May 2013
	Mis Yee Mon Aung	X9230		Starting from Dec 2010
	Mr Yashar Maali	X9230		Starting from Dec 2010
	Tanvir Anwar	X7143		Starting July 2014

(Note: copy this section as required to accommodate the number of investigators)

Page **1** of **3**

193

1. **Are you requesting an extension to your project?** *Please tick Yes or No. If yes, please justify why you require an extension to your HREC approval. Your request will be reviewed by the UTS HREC Chairperson.*
   Please note: Extensions are for 1 year. A maximum of 2 extension requests can be given per project before a new ethics application is required.

(a) Yes ☒ No ☐

This ongoing project that involve many PhD students

2. **Have there been any changes to your research project since ethics approval was granted or since your last progress report?**
Please tick Yes or No to the options below. If yes, please outline and explain the reasons for any changes that have occurred in any of the following areas in the boxes provided:
(Note: major changes may require an amendment application form. Please contact the Research Ethics Officer on 02/9514 9772 or email Research.Ethics@uts.edu.au if you are unsure)

(a) Participating investigators

Yes ☒ No ☐

One new student will be involved (Tanvir Anwar). One Co-investigator has been removed (Dr. Rami N. Khushaba) since he left the University.

(b) Procedures or methodology

Yes ☐ No ☒

(c) Data collection instruments (surveys/questionnaires/interview questions)

Yes ☐ No ☒

(d) Has an amendment application been submitted for any of these changes? *Note: changes to personnel do not require an amendment application.*

Yes ☐ No ☒

3. **Did any of the following events occur?** *Please tick Yes or No. If yes, please give details of the event, and how it was resolved or addressed.*

(a) Unforeseen ethical or other difficulties during your research

Yes ☐ No ☒

(b) Adverse effects for your subjects /participants

Yes ☐ No ☒

(c) Complaints received from participants or other persons involved in the research

Yes ☐ No ☒

4. **How and where have you stored the data you have collected?** *Please give details (e.g. coded on computer, files, etc.)*

Coded on computer

5. **What steps have you taken to ensure the confidentiality of your participants?**
    Please give details (e.g. de-identified data, password protected, locked filing cabinet, limited access to data, etc.)

Limited access to information

6. **Are you planning to publish or have you published the results of your research?**
    Please tick Yes or No. If yes, please provide the reference and attach a copy of any articles or abstracts.

Yes ☒ No ☐

Plan to publish

7. **Additional Comments?** *Please add any further information you feel may be relevant.*

DECLARATION

I declare that the information I have given above is true and that my research has contravened neither the *National Statement on Ethical Conduct in Research Involving Humans (2007);;* the Commonwealth Privacy Act (1998); NSW Privacy and Personal Information Protection Act (1998); nor the UTS policy, directives and guidelines relating to the ethical conduct of research.

I also declare that I have respected the personality, rights, wishes, beliefs, consent and freedom of the individual subject in the conduct of my research and that I have notified the UTS Human Research Ethics Committee of any ethically relevant variation in this research.

Production Note:
Signature removed prior to publication.

Digitally signed by Adel Al-Jumaily
DN: cn=Adel Al-Jumaily, o=UTS,
ou=EMMS, email=Adel.Al-
Jumaily@uts.edu.au, c=AU
Date: 2014.02.15 09:14:40 +10'00'

Date: _14_/_07__/2014___

Chief Investigator/Supervisor

_Adel Al-Jumaily , Associate Professor____
Name & Title

_____   Date: ____/____/____
Student (if applicable)

_____
Name & Title

INSTRUCTIONS ON HOW TO SUBMIT

All reports must be submitted by email to Research.Ethics@uts.edu.au. A printed copy of the report is only required if the electronic copy is not signed.

Printed reports can be sent to:

Internal mail address:

Research Ethics Officer
Research & Innovation Office
Level 14, Building 1

Postal address:

Research Ethics Officer
Research & Innovation Office
University of Technology, Sydney, PO Box 123
Broadway NSW 2007

Page **3** of **3**

195

This page is intentionally left blank

Bibliography

Abdi, H., & Williams, L. J. (2010). Principal component analysis. *Wiley Interdisciplinary Reviews: Computational Statistics, 2*(4), 433-459.

Akdoğan, E., & Adli, M. A. (2011). The design and control of a therapeutic exercise robot for lower limb rehabilitation: Physiotherabot. *Mechatronics, 21*(3), 509-522.

Al-Timemy, A. H., Bugmann, G., Escudero, J., & Outram, N. (2013). Classification of Finger Movements for the Dexterous Hand Prosthesis Control With Surface Electromyography. *IEEE Journal of Biomedical and Health Informatics, 17*(3), 608-618.

Anam, K., & Al-jumaily, A. (2013). Real-time Classification of Finger Movements using Two-channel Surface Electromyography.

Anam, K., & Al-Jumaily, A. (2014a). *Adaptive Wavelet Extreme Learning Machine (AW-ELM) for Index Finger Recognition Using Two-Channel Electromyography.* Paper presented at the Neural Information Processing.

Anam, K., & Al-Jumaily, A. (2014b, 17-20 Feb. 2014). *Swarm-based extreme learning machine for finger movement recognition.* Paper presented at the Proc. Middle East Conf. Biomedical Engineering (MECBME).

Anam, K., & Al-Jumaily, A. (2014c, 26-30 Aug. 2014). *Swarm-wavelet based extreme learning machine for finger movement classification on transradial amputees.* Paper presented at the The 36th Annual International Conference of the IEEE Engineering in Medicine and Biology Society (EMBC).

Anam, K., & Al-Jumaily, A. (2015, 22-24 April 2015). *A novel extreme learning machine for dimensionality reduction on finger movement classification using sEMG.* Paper presented at the The 7th International IEEE/EMBS Conference on Neural Engineering (NER), , Montpellier, France.

Anam, K., & Al-Jumaily, A. (2015, 25-29 Aug. 2015). *A robust myoelectric pattern recognition using online sequential extreme learning machine for finger movement*

classification. Paper presented at the The 37th Annual International Conference of the IEEE Engineering in Medicine and Biology Society (EMBC), Chicago, USA.

Anam, K., & Al-Jumaily, A. A. (2012). Active exoskeleton control systems: State of the art. *Procedia Engineering, 41*, 988-994.

Anam, K., Al-Jumaily, A., & Maali, Y. (2014). Index Finger Motion Recognition using Self-Advise Support Vector Machine. *International Journal on Smart Sensing and Intelligent Systems, 7*(2), 644-657.

Anam, K., Khushaba, R., & Al-Jumaily, A. (2013, Aug). *Two-channel surface electromyography for individual and combined finger movements*. Paper presented at the Proc. 35th Ann. Int. Conf. IEEE Engineering Medicine and Biology Society (EMBC).

Battye, C., Nightingale, A., & Whillis, J. (1955). The use of myo-electric currents in the operation of prostheses. *Journal of Bone & Joint Surgery, British Volume, 37*(3), 506-510.

Boostani, R., & Moradi, M. H. (2003). Evaluation of the forearm EMG signal features for the control of a prosthetic hand. *Physiol Meas, 24*(2), 309.

Brault, M. W. (2008). *Americans With Disabilities: 2005*. Retrieved from

Buchanan, T. S., Lloyd, D. G., Manal, K., & Besier, T. F. (2004). Neuromusculoskeletal Modeling: Estimation of Muscle Forces and Joint Moments and Movements From Measurements of Neural Command. *Journal of Applied Biomechanics, 20*(4), 367-395.

Cai, D., He, X., & Han, J. (2007). *Spectral regression: A unified approach for sparse subspace learning*. Paper presented at the The Seventh IEEE International Conference on Data Mining (ICDM).

Cai, D., He, X., & Han, J. (2008). SRDA: An efficient algorithm for large-scale discriminant analysis. *IEEE Trans. Knowl. Data Eng., 20*(1), 1-12.

Cao, J., Lin, Z., & Huang, G.-b. (2010). Composite function wavelet neural networks with extreme learning machine. *Neurocomputing, 73*(7), 1405-1416.

198

Cao, J., Lin, Z., & Huang, G.-B. (2012). Self-adaptive evolutionary extreme learning machine. *Neural processing letters, 36*(3), 285-305.

Chacko, B. P., Krishnan, V. V., Raju, G., & Anto, P. B. (2012). Handwritten character recognition using wavelet energy and extreme learning machine. *International Journal of Machine Learning and Cybernetics, 3*(2), 149-161.

Chan, A. D., & Englehart, K. B. (2005). Continuous myoelectric control for powered prostheses using hidden Markov models. *IEEE Transactions on Biomedical Engineering, 52*(1), 121-124.

Chan, A. D. C., & Green, G. C. (2007, M0100). *Myoelectric control development toolbox.* Paper presented at the Proceeding of the 30th Conference of Canadian Medical and Biological Engineering Society (CMBES).

Chang, C.-C., & Lin, C.-J. (2011). LIBSVM: a library for support vector machines. *ACM Transaction on Intelligent System and Techology (TIST), 2*(3), 27.

Chen, X., Zhang, D., & Zhu, X. (2013). Application of a self-enhancing classification method to electromyography pattern recognition for multifunctional prosthesis control. *Journal of NeuroEngineering and Rehabilitation, 10*(1), 44.

Chia-Feng, J. (2004). A hybrid of genetic algorithm and particle swarm optimization for recurrent network design. *IEEE Transactions on Systems, Man, and Cybernetics, Part B: Cybernetics, 34*(2), 997-1006.

Cipriani, C., Antfolk, C., Controzzi, M., Lundborg, G., Rosen, B., Carrozza, M. C., & Sebelius, F. (2011). Online Myoelectric Control of a Dexterous Hand Prosthesis by Transradial Amputees. *IEEE Trans. Neural Sys. Rehabil. Eng., 19*(3), 260-270.

Criswell, E. (2010). *Cram's introduction to surface electromyography. 2nd ed*: Jones & Bartlett Publishers.

De Luca, C. (2006). Electromyography *Encyclopedia of Medical Devices and Instrumentation*: John Wiley & Sons, Inc.

De Luca, C. J. (2002). Surface electromyography: Detection and recording. *DelSys Incorporated, 10*, 2011.

de Souza, B. F., de Carvalho, A., Calvo, R., & Ishii, R. P. (2006). *Multiclass SVM model selection using particle swarm optimization.* Paper presented at the The Sixth International Conference on Hybrid Intelligent System HIS'06.

Doyle, J. R., & Botte, M. J. (2002). *Surgical Anatomy of the Hand and Upper Extremity*. Philadelphia, PA, USA: Wolters Kluwer.

Englehart, K., Hudgin, B., & Parker, P. A. (2001). A wavelet-based continuous classification scheme for multifunction myoelectric control. *IEEE Transactions on Biomedical Engineering, 48*(3), 302-311.

Englehart, K., & Hudgins, B. (2003). A robust, real-time control scheme for multifunction myoelectric control. *IEEE Transactions on Biomedical Engineering, 50*(7), 848-854.

Englehart, K., Hudgins, B., & Chan, A. D. (2003). Continuous multifunction myoelectric control using pattern recognition. *Technology and Disability, 15*(2), 95-103.

Englehart, K., Hudgins, B., Parker, P. A., & Stevenson, M. (1999). Classification of the myoelectric signal using time-frequency based representations. *Medical engineering & physics, 21*(6–7), 431-438.

Ewing, I. (2010). Disability, Ageing And Carers, Australia: Summary Of Findings, 2009. In A. B. o. Statistics (Ed.), (pp. 40). Canberra: Australian Bureau of Statistics.

Farina, D., Ning, J., Rehbaum, H., Holobar, A., Graimann, B., Dietl, H., & Aszmann, O. C. (2014). The Extraction of Neural Information from the Surface EMG for the Control of Upper-Limb Prostheses: Emerging Avenues and Challenges. *IEEE Transactions on Neural Systems and Rehabilitation Engineering, 22*(4), 797-809.

Farmer, M., & Macleod, F. (2011). Involving Disabled People in Social Research : Guidance by the Office for Disability Issues (pp. 7): The Office for Disability Issues UK.

Farrell, T., & Weir, R. F. (2008). *Analysis window induced controller delay for multifunctional prostheses.* Paper presented at the Proceeding of MyoElectric Controls/Powered Prosthetics Symposium.

Farrell, T. R., & Weir, R. F. (2007). The optimal controller delay for myoelectric prostheses. *IEEE Transactions Neural Systems and Rehabilation Engineering, 15*(1), 111-118.

Fletcher, R. (2013). *Practical methods of optimization*: John Wiley & Sons.

Fougner, A., Stavdahl, O., Kyberd, P. J., Losier, Y. G., & Parker, P. A. (2012). Control of upper limb prostheses: terminology and proportional myoelectric control—a review. *IEEE Transactions on Neural Systems and Rehabilitation Engineering, 20*(5), 663-677.

Fukunaga, K. (2013). *Introduction to statistical pattern recognition*: Academic press.

Gijsberts, A., Bohra, R., González, D. S., Werner, A., Nowak, M., Caputo, B., . . . Castellini, C. (2014). Stable myoelectric control of a hand prosthesis using non-linear incremental learning. *Frontiers in neurorobotics, 8*.

Gopura, R., Bandara, D., Gunasekara, J., & Jayawardane, T. (2013). Recent Trends in EMG-Based Control Methods for Assistive Robots.

Hargrove, L. J., Englehart, K., & Hudgins, B. (2007). A comparison of surface and intramuscular myoelectric signal classification. *IEEE Transactions on Biomedical Engineering, 54*(5), 847-853.

Hargrove, L. J., Scheme, E. J., Englehart, K. B., & Hudgins, B. S. (2010). Multiple Binary Classifications via Linear Discriminant Analysis for Improved Controllability of a Powered Prosthesis. *IEEE Transactions Neural Systems and Rehabilation Engineering, 18*(1), 49-57.

Heo, P., Gu, G. M., Lee, S.-j., Rhee, K., & Kim, J. (2012). Current hand exoskeleton technologies for rehabilitation and assistive engineering. *International Journal of Precision Engineering and Manufacturing, 13*(5), 807-824.

Hinton, G. E., & Salakhutdinov, R. R. (2006). Reducing the dimensionality of data with neural networks. *Science, 313*(5786), 504-507.

Hiraiwa, A., Shimohara, K., & Tokunaga, Y. (1989). *EMG pattern analysis and classification by neural network.* Paper presented at the IEEE International Conference on Systems, Man and Cybernetics.

Ho, N. S. K., Tong, K. Y., Hu, X. L., Fung, K. L., Wei, X. J., Rong, W., & Susanto, E. A. (2011, June 29 2011-July 1 2011). *An EMG-driven exoskeleton hand robotic training device on chronic stroke subjects: Task training system for stroke rehabilitation.* Paper presented at the Proc. IEEE Int. Conf. Rehabilitation Robotics (ICORR).

Hu, X. L., Tong, K. Y., Wei, X. J., Rong, W., Susanto, E. A., & Ho, S. K. (2013). The effects of post-stroke upper-limb training with an electromyography (EMG)-driven hand robot. *Journal of Electromyography and Kinesiology, 23*(5), 1065-1074.

Huang, G.-B., Zhu, Q.-Y., & Siew, C.-K. (2006). Extreme learning machine: Theory and applications. *Neurocomputing, 70*(1–3), 489-501.

Huang, G., Song, S., Gupta, J. N., & Wu, C. (2014). Semi-supervised and unsupervised extreme learning machines.

Huang, G. B., Zhou, H., Ding, X., & Zhang, R. (2012). Extreme learning machine for regression and multiclass classification. *IEEE Trans. Syst. Man Cybern. B, Cybern., 42*(2), 513-529.

Hudgins, B., Parker, P., & Scott, R. N. (1993). A new strategy for multifunction myoelectric control. *IEEE Transactions on Biomedical Engineering, 40*(1), 82-94.

Jacobson, S. C., Knutti, D. F., Johnson, R. T., & Sears, H. H. (1982). Development of the Utah Artificial Arm. *IEEE Transactions on Biomedical Engineering, BME-29*(4), 249-269.

Javed, K., Gouriveau, R., & Zerhouni, N. (2014). SW-ELM: A summation wavelet extreme learning machine algorithm with a priori parameter initialization. *Neurocomputing, 123*(0), 299-307.

Kennedy, J. (2010). Particle swarm optimization *Encyclopedia of Machine Learning* (pp. 760-766): Springer.

Khushaba, R. (2010). *Application of Biosignal-Driven Intelligent Systems for Multifunction Prosthesis Control.* University of Technology, Sydney.

Khushaba, R. N., Al-Ani, A., & Al-Jumaily, A. (2010). Orthogonal Fuzzy Neighborhood Discriminant Analysis for Multifunction Myoelectric Hand Control. *IEEE Transactions on Biomedical Engineering, 57*(6), 1410-1419.

Khushaba, R. N., Kodagoda, S., Takruri, M., & Dissanayake, G. (2012). Toward improved control of prosthetic fingers using surface electromyogram (EMG) signals. *Expert Syst. with Applicat., 39*(12), 10731-10738.

Khushaba, R. N., Takruri, M., Miro, J. V., & Kodagoda, S. (2014). Towards limb position invariant myoelectric pattern recognition using time-dependent spectral features. *Neural networks, 55*, 42-58.

Kontoudis, G. P., Liarokapis, M. V., Zisimatos, A. G., Mavrogiannis, C. I., & Kyriakopoulos, K. J. (2014). Open-Source, Anthropomorphic, Underactuated Robot Hands with a Selectively Lockable Differential Mechanism: Towards Affordable Prostheses.

Lenzi, T., De Rossi, S. M. M., Vitiello, N., & Carrozza, M. C. (2012). Intention-Based EMG Control for Powered Exoskeletons. *IEEE Transactions on Biomedical Engineering, 59*(8), 2180-2190.

Li, G., Schultz, A. E., & Kuiken, T. A. (2010). Quantifying pattern recognition—Based myoelectric control of multifunctional transradial prostheses. *IEEE Transactions Neural Systems and Rehabilation Engineering, 18*(2), 185-192.

Liang, N.-Y., Huang, G.-B., Saratchandran, P., & Sundararajan, N. (2006). A fast and accurate online sequential learning algorithm for feedforward networks. *IEEE Transactions on Neural Networks, 17*(6), 1411-1423.

Lin, C.-J., & Tsai, H.-M. (2008). FPGA implementation of a wavelet neural network with particle swarm optimization learning. *Mathematical and Computer Modelling, 47*(9–10), 982-996.

Ling, S. H., Iu, H., Leung, F. H.-F., & Chan, K. Y. (2008). Improved hybrid particle swarm optimized wavelet neural network for modeling the development of fluid dispensing for electronic packaging. *IEEE Transactions on Industrial Electronics, 55*(9), 3447-3460.

Ling , S. H., Iu , H. H., Chan, K. Y., Lam, H. K., Yeung, B. C., & Leung, F. H. (2008). Hybrid particle swarm optimization with wavelet mutation and its industrial applications. *IEEE Transactions on Systems, Man, and Cybernetics-PART B: Cybernetics, 38*(3), 743-763.

Marieb, E. N. (2009). *Essentials of Human Anatomy & Physiology*: Pearson Benjamin Cummings.

Martínez, A. M., & Kak, A. C. (2001). Pca versus lda. *IEEE Transactions on Pattern Analysis and Machine Intelligence, 23*(2), 228-233.

Micera, S., Carpaneto, J., & Raspopovic, S. (2010). Control of Hand Prostheses Using Peripheral Information. *IEEE Rev. Biomed. Eng., 3*, 48-68.

Mohammed, A. A., Minhas, R., Jonathan Wu, Q., & Sid-Ahmed, M. A. (2011). Human face recognition based on multidimensional PCA and extreme learning machine. *Pattern recognition, 44*(10), 2588-2597.

Moritani, T., Stegeman, D., & Merletti, R. (2005). Basic Physiology and Biophysics of EMG Signal Generation *Electromyography* (pp. 1-25): John Wiley & Sons, Inc.

Mouzé-Amady, M., & Horwat, F. (1996). Evaluation of Hjorth parameters in forearm surface EMG analysis during an occupational repetitive task. *Electroencephalography and Clinical Neurophysiology/Electromyography and Motor Control, 101*(2), 181-183.

Mulas, M., Folgheraiter, M., & Gini, G. (2005, 28 June-1 July 2005). *An EMG-controlled exoskeleton for hand rehabilitation.* Paper presented at the Proc. 9th Int. Conf. Rehabilitation Robotics ICORR.

Muscolino, J. E. (2014). *Kinesiology: the skeletal system and muscle function*: Elsevier Health Sciences.

Ngeo, J., Tamei, T., Shibata, Orlando, M. F. F., Behera, L., Saxena, A., & Dutta, A. (2013). *Control of an Optimal Finger Exoskeleton based on Continuous Joint Angle Estimation from EMG signals*. Paper presented at the 35th Annual International Conference of the IEEE EMBS.

Ning, J., Dosen, S., Muller, K., & Farina, D. (2012). Myoelectric Control of Artificial Limbs?? Is There a Need to Change Focus? [In the Spotlight]. *Signal Processing Magazine, IEEE, 29*(5), 152-150.

Nishikawa, D., Yu, W., Maruishi, M., Watanabe, I., Yokoi, H., Mano, Y., & Kakazu, Y. (2000). On-line Learning Based Electromyogram to Forearm Motion Classifier with Motor Skill Evaluation. *JSME International Journal Series C, 43*(4), 906-915.

Nizar, A. H., Dong, Z. Y., & Wang, Y. (2008). Power Utility Nontechnical Loss Analysis With Extreme Learning Machine Method. *IEEE Transactions on Power Systems, 23*(3), 946-955.

Nordin, M., & Frankel, V. H. (2012). *Basic biomechanics of the musculoskeletal system (4th edition)*: Lippincott Williams & Wilkins.

Oskoei, M. A., & Huosheng, H. (2007). Myoelectric control systems—A survey. *Biomed. Signal Process. and Control, 2*(4), 275-294.

Oskoei, M. A., & Huosheng, H. (2008). Support Vector Machine-Based Classification Scheme for Myoelectric Control Applied to Upper Limb. *IEEE Transactions on Biomedical Engineering, 55*(8), 1956-1965.

Pao, Y.-H., Park, G.-H., & Sobajic, D. J. (1994). Learning and generalization characteristics of the random vector functional-link net. *Neurocomputing, 6*(2), 163-180.

Pao, Y.-H., & Takefji, Y. (1992). Functional-link net computing. *IEEE Computer Journal, 25*(5), 76-79.

Phinyomark, A., Phukpattaranont, P., & Limsakul, C. (2012). Feature reduction and selection for EMG signal classification. *Expert Systems with Applications, 39*(8), 7420-7431.

Popov, B. (1965). The bio-electrically controlled prosthesis. *Journal of Bone & Joint Surgery, British Volume, 47*, 421-424.

Rahman, M. A., & Al-Jumaily, A. (2012). Design and Development of a Hand Exoskeleton for Rehabilitation Following Stroke. *Proc. Eng., 41*(0), 1028-1034.

Roche, A. D., Rehbaum, H., Farina, D., & Aszmann, O. C. (2014). Prosthetic Myoelectric Control Strategies: A Clinical Perspective. *Current Surgery Reports, 2*(3), 1-11.

Salih, D. M., Noor, S. B. M., Marhaban, M. H., & Ahmad, R. M. K. R. (2013, 23-26 June 2013). *Wavelet network based online sequential extreme learning machine for dynamic system modeling.* Paper presented at the Control Conference (ASCC), 2013 9th Asian.

Sang Wook, L., Wilson, K. M., Lock, B. A., & Kamper, D. G. (2011). Subject-Specific Myoelectric Pattern Classification of Functional Hand Movements for Stroke Survivors. *IEEE Trans. Neural Sys. Rehabil. Eng., 19*(5), 558-566.

Saraswathi, S., Sundaram, S., Sundararajan, N., Zimmermann, M., & Nilsen-Hamilton, M. (2011). ICGA-PSO-ELM Approach for Accurate Multiclass Cancer Classification Resulting in Reduced Gene Sets in Which Genes Encoding Secreted Proteins Are Highly Represented. *IEEE/ACM Transactions on Computational Biology and Bioinformatics, 8*(2), 452-463.

Scheme, E., & Englehart, K. (2011). Electromyogram pattern recognition for control of powered upper-limb prostheses: State of the art and challenges for clinical use. *Journal of rehabilitation research and development, 48*(6), 643.

Scheme, E. J., Englehart, K. B., & Hudgins, B. S. (2011). Selective Classification for Improved Robustness of Myoelectric Control Under Nonideal Conditions. *Biomedical Engineering, IEEE Transactions on, 58*(6), 1698-1705. doi:10.1109/tbme.2011.2113182

Scheme, E. J., Hudgins, B. S., & Englehart, K. B. (2013). Confidence-Based Rejection for Improved Pattern Recognition Myoelectric Control. *IEEE Trans. Biomed. Eng., 60*(6), 1563-1570. doi:10.1109/TBME.2013.2238939

Schlogl, A., & Brunner, C. (2008). BioSig: a free and open source software library for BCI research. *Computer, 41*(10), 44-50.

Sensinger, J. W., Lock, B. A., & Kuiken, T. A. (2009). Adaptive pattern recognition of myoelectric signals: exploration of conceptual framework and practical algorithms. *IEEE Transactions on Neural Systems and Rehabilitation Engineering, 17*(3), 270-278.

Simon, A. M., Stern, K., & Hargrove, L. J. (2011, Aug. 30 2011-Sept. 3 2011). *A comparison of proportional control methods for pattern recognition control.* Paper presented at the The 2011 Annual International Conference of the IEEE Engineering in Medicine and Biology Society EMBC.

Smith, L. H., Hargrove, L. J., Lock, B. A., & Kuiken, T. A. (2011). Determining the optimal window length for pattern recognition-based myoelectric control: balancing the competing effects of classification error and controller delay. *IEEE Transactions Neural Systems and Rehabilation Engineering, 19*(2), 186-192.

Subasi, A., Yilmaz, M., & Ozcalik, H. R. (2006). Classification of EMG signals using wavelet neural network. *Journal of Neuroscience Methods, 156*(1), 360-367.

Suzuki, R., & Suematsu, T. (1969). Pattern Recognition of Multichannel Myoelectric Signals by Learning Method. *医用電子と生体工学, 7*(1), 47-50.

Tenore, F. V. G., Ramos, A., Fahmy, A., Acharya, S., Etienne-Cummings, R., & Thakor, N. V. (2009). Decoding of individuated finger movements using surface electromyography. *IEEE Transactions on Biomedical Engineering, 56*(5), 1427-1434.

Tkach, D., Huang, H., & Kuiken, T. A. (2010). Study of stability of time-domain features for electromyographic pattern recognition. *IEEE Trans. Neural Sys. Rehabil. Eng., 7*(1), 21.

Tong, K., Ho, S., Pang, P., Hu, X., Tam, W., Fung, K., . . . Chen, M. (2010). *An intention driven hand functions task training robotic system.* Paper presented at the The 2010 Annual International Conference of the IEEE Engineering in Medicine and Biology Society (EMBC).

TouchBionics. (2007). The Big Picture: Bionic Hand. *Spectrum, IEEE, 44*(10), 22-22. doi:10.1109/MSPEC.2007.4337661

TouchBionics. (Accessed in 2015). Retrieved from http://www.touchbionics.com/products/active-prostheses/i-limb-ultra

Tsenov, G., Zeghbib, A. H., Palis, F., Shoylev, N., & Mladenov, V. (2006, 25-27 Sept. 2006). *Neural Networks for Online Classification of Hand and Finger Movements Using Surface EMG signals.* Paper presented at the 8th Seminar on Neural Network Application in Electrical Engineering (NEUREL).

Uchida, N., Hiraiwa, A., Sonehara, N., & Shimohara, K. (1992). *EMG pattern recognition by neural networks for multi fingers control.* Paper presented at the 14th Annual International Conference of IEEE EMBS.

Wang, G., Zhao, Y., & Wang, D. (2008). A protein secondary structure prediction framework based on the extreme learning machine. *Neurocomputing, 72*(1), 262-268.

Wege, A., & Zimmermann, A. (2007, 15-18 Dec. 2007). *Electromyography sensor based control for a hand exoskeleton.* Paper presented at the Proc. IEEE Int. Conf. Robotics and Biomimetics, ROBIO

WHO. (2001). The UN Standard Rules on the Equalization of Opportunities for Persons with Disabilities. *II. Main Report, WHO/DAR/01.2*, 290.

Xu, Y., & Shu, Y. (2006). Evolutionary extreme learning machine–based on particle swarm optimization *Advances in Neural Networks-ISNN 2006* (pp. 644-652): Springer.

Ye, J., Janardan, R., Li, Q., & Park, H. (2006). Feature reduction via generalized uncorrelated linear discriminant analysis. *IEEE Transactions on Knowledge and Data Engineering, 18*(10), 1312-1322.

Young, A. J., Hargrove, L. J., & Kuiken, T. A. (2012). Improving Myoelectric Pattern Recognition Robustness to Electrode Shift by Changing Interelectrode Distance and Electrode Configuration. *IEEE Transactions on Biomedical Engineering, 59*(3), 645-652.

Zecca, M., Micera, S., Carrozza, M., & Dario, P. (2002). Control of multifunctional prosthetic hands by processing the electromyographic signal. *Critical Reviews in Biomedical Engineering, 30*(4-6), 459.

Zhang, R., Lan, Y., Huang, G.-B., Xu, Z.-B., & Soh, Y. C. (2013). Dynamic Extreme Learning Machine and Its Approximation Capability. *IEEE Transactions on Cybernetics, 43*(6), 2054-2065.

Zheng, W., Qian, Y., & Lu, H. (2013). Text categorization based on regularization extreme learning machine. *Neural Computing and Applications, 22*(3-4), 447-456.

Zhou, B., Shi, A., Cai, F., & Zhang, Y. (2004). Wavelet neural networks for nonlinear time series analysis *Advances in Neural Networks-ISNN 2004* (pp. 430-435): Springer.

Zhu, Q.-Y., Qin, A. K., Suganthan, P. N., & Huang, G.-B. (2005). Evolutionary extreme learning machine. *Pattern recognition, 38*(10), 1759-1763.

Zong, W., Zhou, H., Huang, G.-B., & Lin, Z. (2011). Face recognition based on kernelized extreme learning machine *Autonomous and Intelligent Systems* (pp. 263-272): Springer.